Old Dominion University

ODU Digital Commons

Spring 2013

Computational Dynamics for the Flexible Multi-Body System

Yu Liu
Old Dominion University

COMPUTATIONAL DYNAMICS FOR THE FLEXIBLE MULTI-BODY SYSTEM

by

Yu Liu
B.S. June 2002, Chang'an University, China
M.S. March 2005, Shanghai Jiao Tong University, China

A Dissertation Submitted to the Faculty of
Old Dominion University in Partial Fulfillment of the
Requirements for the Degree of

DOCTOR OF PHILOSOPHY

MECHANICAL ENGINEERING

OLD DOMINION UNIVERSITY
May 2013

Approved by:

_____
Gene Hou (Director)

_____
Duc Nguyen (Member)

_____
Miltiadis Kotinis (Member)

_____
Jennifer Michaeli (Member)

ABSTRACT

COMPUTATIONAL DYNAMICS FOR THE FLEXIBLE MULTI-BODY SYSTEM

Yu Liu
Old Dominion University, 2013
Director: Dr. Gene J. W. Hou

Research in computational dynamics has tremendously developed in the recent years because of the demand for analysis and simulation of various multi-body systems in the growing bio-medical, mechanical and aerospace industries. These multi-body systems are made of individual bodies that are interconnected via mechanical joints. Mathematically, these joints that connect the bodies can be described as constraint equations imposed upon the motions of the involved free bodies. This process will result in an equation of motion expressed in the form of a differential-algebraic equation (DAE). This is one of the main difficulties when dealing with the multi-body system because these constraints must be satisfied all the time.

The main objective of this dissertation is to develop an efficient and accurate solution algorithm to solve the DAE resulting from flexible multi-body dynamics. The principle of virtual work and D'Alembert's principle are used in this dissertation to formulate the equation of motion for a general three dimensional (3D) multi-body dynamic system that involves rigid as well as flexible bodies. The elastic mode shapes and modal coordinates are used to convert the time-variant integrals associated with elastic deformations in the mass matrix into time-invariant ones. In addition, the transient stress distribution is obtained directly in terms of the linear combination of the modal element stress and corresponding modal coordinates solved from DAE. Euler parameters and the matrix exponential method are used to calculate the time-dependent transformation matrix for a general 3D problem. The projection method with constraints correction is proposed in this dissertation to solve the DAE modeling the motion of a

constrained multi-body dynamic system. The mixed order technique with the additional Euler parameters method is proposed to solve a general 3D flexible multi-body system. Two examples are studied in this dissertation: a planar slider-crank mechanism and a 3D flexible moving craft in irregular waves.

The planar slider-crank mechanism is used in this dissertation to demonstrate the application of the integrals calculated as time-invariants and the proposed projection method with displacement and velocity constraints correction. The flexibility of the connecting rod of the slider-crank mechanism is included in the formulation. The numerical results obtained by the projection method will be compared with those by the commonly used coordinate partitioning method. The results show the validation and efficiency of the proposed constraints correction method.

For the 3D flexible craft dynamics, the pressure distribution reconstruction algorithm is carried out to construct the hydrodynamics pressure on the wetted surface based upon the test pressure data. Then the nodal pressure loads are converted to the equivalent nodal force as the external loads for the flexible craft. Both Euler parameters and angular velocities are treated as the generalized coordinates in the equation of motion to model the rotation motion of the craft. Hence, the second order of Euler parameters is not incorporated in the equation of motion. It means that only constraints on first order time derivation of Euler parameter are needed. The results from the proposed Euler parameter methods are compared with the matrix exponential based Newmark method. It shows that the proposed Euler parameter method is non-sensitive to the time steps and has good accuracy. Finally, the least square error optimization method is used to find the Von Mises stress at each node. Thus, the time history nodal stress can be obtained directly from the modal element stress and modal coordinates solved from DAE. Hence, it doesn't need to rerun the dynamic analysis under the nodal displacement to obtain the node stress.

ACKNOWLEDGMENTS

I would like to express my sincere gratitude to my advisor Dr. Gene J. W. Hou for his tremendous support and for always being available to help during this research. He always challenged me to prove that the results were correct instead of just taking it for granted. He also taught me how to check the code: "You should assume that the code is wrong at first, otherwise, you will never find the errors". He always told me that I should solve the engineering problem independently through the training of the Ph.D study: breaking down the complex problem into a series of simple problems.

I also express my gratitude to Dr. Duc T. Nguyen, Dr. Miltiadis Kotinis and Dr. Jennifer Michaeli. I learned a lot from Dr. Nguyen's several courses: engineering optimization, finite element method and parallel computation. I always remember Dr. Nguyen's enthusiasm in teaching: taking off his shoe to give an example of mode shape and kneeling down on the floor to write on the blackboard. I appreciate Dr. Kotinis's advice in my thesis direction. Dr. Kotinis always told me to just stop by his office or write an e-mail to him whenever I needed his help. Dr. Kotinis also put a lot of effort in correcting grammar errors and expressions word by word in my dissertation. I cherished the opportunity to work with Dr. Michaeli for nearly two years. Dr. Michaeli helped me collect some important literature in design standards of planing craft.

I really appreciate the help from Peng Cheng's family to accommodate me during my time at the campus.

This thesis is dedicated to my parents and parents in law, my wife Fang Li and my son Brian Liu for their unselfish sacrifice, enormous patience and full support throughout the completion of my Ph. D degree.

ABBREVIATIONS AND NOTATION

DAE: Differential and Algebraic Equation   ODE: Ordinary Differential Equation

EOM: Equation of Motion   DOF: Degree of Freedom

CG: Center of Gravity   LCG: Longitudinal Center of Gravity

ABS: American Bureau of Shipping   DNV: Det Norske Vertas

LR: Lloyd's Register   2D: Two Dimensional

3D: Three Dimensional   FFT: Fast Fourier Transform

IFFT: Inverse Fast Fourier Transform   DFT: Discrete Fourier Transform

PSD: Power Spectra Density

$\mathbf{r}$: Position vector in global coordinate $\mathbf{r'}$: Position vector in local coordinate

$\mathbf{e}$: Elastic deformation $\mathbf{r'_e}$: Total Position Vector in local coordinate

$\mathbf{R}$: Position Vector of the Origin of Local Coordinate in Global Coordinate

$\mathbf{\Pi'}$: Angular Vector of the Origin of Local Coordinate

A : Transformation matrix ω' : Local angular velocity

$\tilde{\omega}'$: Skew matrix of local angular velocity N : Shape function matrix

$\mathbf{q_e}$: Elastic displacement at all nodes L: Linear operator

ψ : Mode shape matrix $\mathbf{a}$: Modal coordinate

$\mathbf{q}$: Generalized system coordinates δ : Delta operator

U : The strain energy λ : Lame constant, or Lagrange multiplier

σ_{ij} : Stress K_{ff} : The global stiffness matrix

M: Generalized mass matrix f: Generalized force term

$\mathbf{q}$: Generalized system coordinate C_q : The constraint Jacobian matrix

τ_{ij} : The stress tensor ε_{ij} : The strain tensor

I_e : Integral of elastic deformation $I_{r'}$: Integral of local vector

$I_{\bar{r}\bar{r}}$: Linear moment of inertia $\mathbf{p} = \{e_0 \quad e_1 \quad e_2 \quad e_3\}^T$: Euler parameter

$\mathbf{c} = (c_1 \quad c_2 \quad c_3)^T$:The unit rotation axis χ : An angular displacement

$\mathbf{q_I}$: Independent coordinates $\mathbf{q_d}$: Dependent coordinates

P: The projection matrix $\Delta\mathbf{q}$: The change of system coordinates

T_{si}: Starting time at transducer

$\overline{T}_1$: Corresponding time at 1st transducer

$\overline{T}_2$: Corresponding time at 2nd transducer

S: Distance along transverse section

S_{b1}: Bonds of 1st transducer

S_{b2}: Bonds of 2nd transducer

ξ, η, ζ : Area coordinates for triangular

TABLE OF CONTENTS

LIST OF TABLES

LIST OF FIGURES

CHAPTER 1

INTRODUCTION

1.1 Background

A flexible multi-body system is composed of a series of flexible and rigid bodies connecting with each other through different joints or force elements to fulfill the specified function. Many engineering systems such as vehicles, robots, and space structures are made up of multi-bodies. The functional performance of these systems depends highly on the design and the characteristics of the bodies involved and the joint conditions between them. In order to determine the performance of the system accurately, one has two choices: the first is to formulate the mathematical model in as much detail as possible; the second is to improve the reliability and efficiency of the method utilized to solve the governing equation of motion that describes the physical system.

Strictly speaking, all bodies that constitute a multi-body system are elastic. In most applications, the flexible bodies are considered rigid for computational simplicity. However, considering the ever-increasing demand for higher operating speeds and lighter structures, the rigid body assumption is no longer accurate enough to describe the performance of a system. Therefore, the elastic deformation of the body must be taken into account in order to accurately evaluate the system performance.

The governing equation of motion of a flexible multi-body system is usually formulated as a differential algebraic equation (DAE) due to the kinematic constraints. The DAEs can't be directly solved by the classical solution procedure for an ordinary differential equation (ODE). In the last few years, a significant amount of research in multi-body dynamics has aimed to increase either the application sophistication or the computational efficiency. This dissertation investigates two areas in order to improve the computational efficiency in solving such DAEs. One is to look at the numerical integration of elasticity-dependent inertia terms in the mass matrix. The other is the numerical method that deals with the constraints correction and 3D rotation description.

Two examples are studied here to illustrate and validate the proposed methods: a two dimensional (2D) slider-crank mechanism and a three dimensional (3D) flexible marine craft under wave-induced hydrodynamic pressure.

1.2 Literature Survey on the Flexible Multi-body Dynamics

The flexible multi-body dynamics emerged as a new research field in the early 1970s [1-6] as the result of the need to simulate the mechanical systems more accurately by taking elastic deformation into account. In contrast to the rigid multi-body dynamics, the flexible multi-body dynamics describes the dynamic deformation of a flexible body. One reason is that the number of coordinates required to describe the flexible body can be very large compared to a rigid body; the latter requires only six coordinates, even in the 3D space. Another reason is that the elastic deformation may cause a strong nonlinear coupling between the rigid and the flexible deformations.

Comprehensive reviews of the past, current, and future for the flexible multi-body dynamics were done by Schiehlen, Shabana and Wasfy. Schiehlen [7] summarized the development of flexible multi-body dynamics, such as historical remarks, textbooks and proceedings, dynamic analysis software, and future concerns. Shabana [8] reviewed the kinematic approaches used to describe the motion of the flexible body, the analytical methods for formulating the governing equation of motion of the flexible multi-body system, different numerical methods, and interesting research topics for the flexible multi-body dynamics. Wasfy [9] reviewed 877 references about different aspects of the flexible multi-body dynamics. He gave an entire picture of the flexible multi-body dynamics: modeling of the flexible components and constraints, solution techniques, control strategies, coupled problems, design and experimental studies.

In the flexible multi-body dynamics, it is critical to determine the coordinate system or frame in describing the kinematic configurations of the system that may undergo large translation and rotation. Many different frames have been used in the past: floating frame [10-12], co-rotational frame [13, 14], convected coordinate system [15], and absolute nodal coordinate [16]. One widely used method is the floating frame based on the assumption that the elastic deformation is small. In the floating frame methods, the total motion of the flexible body can be viewed as a combination of the rigid body motion and the relatively elastic deformation. The rigid motions, including translation and orientation, are represented in the global coordinate by the motion of the origin of the floating frame. The elastic deformation is described in the body-fixed coordinate in terms of the nodal displacement. Then, the elastic deformation is expressed in the global

coordinates through the transformation matrix from the body-fixed coordinate to the global coordinate. It can be noted that this kinematic configuration description is identical to that of a rigid body system when the elastic deformation is equal to zero.

Although the floating frame method is straightforward, it has its own issue to deal with [17]. One of the critical issues is the selection of the body-fixed coordinate. It should be mentioned that the dynamic responses are independent of the selection of the body-fixed coordinate. The purpose of selecting a body-fixed coordinate is to simplify the computation. In the rigid body dynamics, the body-fixed coordinate can be placed at the center of gravity of the body in order to decouple the rigid translation and the orientation motion. However, for the flexible body, this coupling cannot be eliminated even though the body-fixed coordinate is located at the center of gravity due to the elastic deformation. Many attempts [18-23] have been made in the past forty years in order to select a proper body-fixed coordinate system to weaken the coupling between the reference motion and the elastic deformation. Some of these [20-21] are the body-fixed frames, in which the floating frame is attached to a fixed point in the body. The others [22, 23] are floating frames moving with respect to the elastic body, in which the floating frame satisfies the condition that the relative kinetic energy with respect to the body is minimal.

In the flexible multi-body dynamics, the first problem encountered is how to express the elastic deformation, because theoretically infinite coordinates are needed to describe the position of any arbitrary point in a flexible body. This issue can be resolved by using approximation techniques, such as the Rayleigh-Ritz method or the finite element method to reduce the infinite coordinates to an acceptable set of coordinates. In the Rayleigh-Ritz method, the elastic deformation can be approximated using a finite set of known trial functions that satisfy the boundary conditions. One of the main problems associated with the Rayleigh-Ritz method is the difficulty in finding these trial functions for a complex structure. The finite element method can overcome such a difficulty. In the finite element method, the flexile bodies are discretized into small regions called elements that are connected at points called nodes. The displacement at the nodes can be obtained from the finite element analysis. On the other hand, the displacement at any location besides these nodes within an element can be interpolated using the shape functions, which are usually polynomials. Moreover, the mode superposition technique

[24, 25] can be used to approximate the elastic deformation in terms of a linear combination of the mode shapes. The mode shapes and natural frequencies used in the mode superposition technique can be obtained either from modal analysis or from the modal identification technique based upon experiment. By so doing, the numbers of the system generalized coordinates for the flexible body will be considerably reduced from the infinite to the numbers of the mode shapes. However, the accuracy of the elastic deformation is heavily dependent on the selection of a set of suitable mode shapes. It is neither necessary nor realistic to select all the mode shapes because some mode shapes have a negligible effect on the elastic deformation. In addition, the high frequency mode shapes, which carry only a small amount of energy, are not necessary for global deformation, but they are needed for the local deformation effect. Some researchers [26-28] have attempted to select the proper mode shapes to approximate not only the elastic global deformations but also the local elastic deformation due to the applied loads and the kinematic joints.

The second problem is how to calculate the inertia integrals in the mass matrix and the generalized force vector of the governing equation of motion because they are time variants in terms of the elastic deformations and the local angular velocities. The solution of the final ordinary differential equations (ODEs) requires substantial computational resources because these integrals are calculated every time the ODE solver is called. Fortunately, these integrals can be calculated in advance using the mode superposition technique with the help of the shape functions. In other words, these integrals can be calculated as constants based upon shape functions, mode shapes and geometry information provided by a finite element code. Hence, the governing equation of motion that describes the system is totally independent of the finite element code used to compute the mode shapes of the flexible body. The main idea for this method is to move the modal coordinates from these integrals explicitly. In this way, substantial reductions in computational cost will be achieved. Chapter 3 introduces this technique in detail for the various types of finite elements.

The inertia integrals can be obtained in advance using a lumped or consistent mass approach. Yoo and Haug [29, 30] used a lumped mass method to calculate the inertia integrals as time-invariants for the articulated structures dynamics. Pan and Haug

[31] presented a lumped inertia matrix approach that can optimize the calculation of the flexible multi-body dynamics. Pan [32] incorporated the nodal rotary inertias in flexible multi-body dynamics to consider the stress-stiffening effects. Cardona and Geradin [23] used a co-rotational technique to calculate the inertia integrals for the super-elements. Thus, the dynamic analysis and the finite element analysis are fully uncoupled.

The kinematic configurations of the flexible multi-body system can be described either by the system generalized coordinates or by the degrees of freedom of the system [33]. The system generalized coordinates are not independent due to the constraints between different bodies. However, the degrees of freedom are totally independent of each other. Hence, the governing equation of motion for the flexible multi-body system can be obtained based upon these two different descriptions with the help of the principle of virtual work or the Lagrange method. In the first case, the equation of motion is formulated by using a set of Cartesian coordinates that describe the locations and orientations of the bodies in the global coordinate system and a set of modal coordinates that describe the elastic deformations. The kinematic constraints between different bodies can be represented by a set of nonlinear algebraic equations. These kinematic constraints can be incorporated into the equation of motion with the help of Lagrange multipliers. The governing equation of motion for the flexible multi-body system is a set of highly nonlinear DAEs. The derivation of this method is general and straightforward, in which the additional bodies and constraints can be added easily without destroying the format of the governing equation of the existing system. In the second case, relative or joint coordinates are used to formulate the equations of motion in terms of the system degrees of freedom. This method is more desirable in a tree topology system as it employs a minimum number of coordinates to describe the system. The basic difference between these two methods is how to deal with the constraints.

Once the governing equations of motion describing the flexible multi-body system have been established, a proper numerical algorithm is needed. These highly nonlinear DAEs cannot be directly solved by classical integrator schemes. The solution strategy in the flexible multi-body dynamics used in the early days was the linear theory of elastodynamics [8, 29], in which the rigid body motion and the elastic deformation are not solved simultaneously. It has been based upon the pervasive assumption that the

elastic deformations have a negligible effect on the rigid body motion. Thus, the solution is divided into two steps; the first step is to solve the equation related to the rigid coordinates by eliminating the elastic deformations. The second step is to solve the equation related to the elastic coordinates by imposing the coupling terms calculated based upon the results from the first step. However, the accuracy and stability is not guaranteed, especially for the system under the high speed and light weight circumstance. Hence, it is critical to find a proper numerical algorithm for the flexible multi-body dynamics to obtain accurate results. The widely used numerical algorithms are the augmented methods [34], the recursive methods [35-38], and other methods based upon these two methods [39-42]. In the augmented method, the system generalized coordinates and Lagrange multipliers in the DAEs are solved simultaneously, e.g., the projection method [43, 44] introduced in Chapter 3. However, for the recursive method, the Lagrange multipliers are eliminated first by introducing independent and dependent coordinates through the constraint equations. The resultant ODEs will be in terms of the system degrees of freedom only. In other words, a minimum set of coordinates is only needed in the recursive method. The coordinate partitioning method [45], which divided the system coordinates into dependent and independent, is be introduced in Chapter 3.

At the same time, an implicit and an explicit solution can be used in integration marching for both the augmented and the recursive methods. In the implicit solution, the system generalized coordinates that simultaneously satisfy the governing equation of motion and the constraints equations are sought based upon the information obtained in the previous and current steps in order to minimize error. It should be noted that the Newton-Raphson method will be used to solve the nonlinear constraints equation in order to satisfy the prescribed error tolerance. One of the advantages of the implicit solution is that the time step can be larger compared to the explicit solution because it is unconditionally stable. In the explicit solution, the system coordinates that simultaneously satisfy the governing equation of motion and the constraints equations are sought only based upon the information in the previous step. Hence, it is easier to solve the final equations in the explicit solution. However, one issue for the explicit solution is how to determine the size of time step to achieve a stable and convergent solution.

1.3 Literature Survey on Pressure Loads Prediction on the Craft Hull Surface

One of the challenges that designers face in the early design phase for a craft is to determine the hydrodynamic pressure loads. These hydrodynamic pressure loads between the hull and the water have a negative effect on the overall performance of the craft including ride quality, personnel comfort, habitability and safety, equipment reliability, as well as the craft itself. In addition, these hydrodynamic pressure loads are related to the sea-state, craft speed, and the geometry of the craft itself. Generally, designers have to make a compromise between the strength and the weight to ensure performance of a craft.

Three approaches are currently available for predicting the pressure loads. The first approach is the standard specified by classification societies such as the American Bureau of Shipping (ABS) [46], Det Norske Veritas (DNV) [47] or Lloyd's Register (LR) [48]. The advantages of this approach are that it is simple and less time-consuming. However, the shortcoming is its emphasis on safety, which leads to a suboptimal design in terms of weight. The second approach is a semi-empirical method, in which the design pressure loads on the hull surface are calculated using the acceleration information from either model or full-scale tests. These semi-empirical methods are both simple and easy to implement; however, they are less accurate. The main assumption of the semi-empirical methods is that the pressure loads are static and uniform; therefore, these methods are not appropriate for time domain simulations. The standards of the classification societies are based upon these semi-empirical methods with some improvements. The third approach is the model or full-scale test. This is the most insightful option for the designer. However, it can be extremely expensive, and the pressure is measured, and thus is known, only at specific points.

The prediction of the lifting and the resistant pressure loads for the high speed craft design has received considerable attention by many researchers. The lifting load is the main source that causes structural damage. The resistant load is the main reason to determine the characteristics of the propulsor. The hull-water impact has been studied using experimental methods. In 1960, Heller and Jasper [49] did pioneering work on load prediction for the craft structural design. Prior to this, the structural design of craft under 100 ft had merely relied on the designer's experience. They first attempted to calculate the hydrodynamic pressure loads on the hull surface directly using a semi-empirical

algorithm based upon the vertical acceleration at the longitudinal center of gravity from the full-scale test data obtained at high speeds in rough water.

In 1964, Savitsky [50] formulated a semi-empirical iterative method for predicting the lift, trim angle, resistance and porpoising stability for a prismatic planing craft in calm water based upon a large amount of test data combined with a theoretical method. In 1976, Savitsky and Brown [51] extended this method to incorporate the statistical measures of vertical acceleration and the resistance for a planing craft in regular and irregular waves based on the model tests done by Fridsma [52, 53]. Savitsky has made a great contribution towards better understanding and prediction of the hydrodynamic loads for planing craft design. In 1993, Savitsky and Koelbel [54] gave a comprehensive review of seakeeping analysis and load prediction for a planing craft, including a description of design features that result in good seakeeping performance. In 2007, Savitsky et al. [55] quantified the drag resistance force caused by the whisker spray in an analytical procedure and identified the area, flow direction, and location of whisker spray in terms of the hull geometry and the operating conditions.

In 1975, Spencer [56] proposed a methodology to predict the impact pressure on the hull surface for the structural design of the aluminum crewboats based upon the work done by several researchers. He used the work done by Savitsky for determining the craft's running trim angle, the method developed by Fridsma for predicting vertical accelerations at the LCG, and the technique from Heller and Jasper for calculating the impact pressure distributions on the hull. In the methodology, impact pressure load is a function of dimension, proportion, displacement (weight) and speed of the craft. In 1980, Spencer and Henrickson [57] simplified Spencer's original methodology to compile a "cookbook" method to predict impact pressure that was intended primarily for the use by the U.S. Coast Guard.

In 1978, Allen and Jones [58] developed a method for predicting the impact pressure loads on the hull of a craft based upon the test data of a 65 ft crewboat and a 75 ft slender planning hull done by the U.S. Navy. They stated that the impact pressure loads are non-uniform across the hull surface. The highest pressures are usually located at the first quarter point aft of the bow. However, the lower pressures are over a greater portion of the hull.

In 1998, Grimsley [59] summarized seven semi-empirical/theoretical methods, including Heller and Jasper, Spencer, Danahy, Angeli, Henrickson and Spencer, Koelbel and Allen and Jones, and three classification society rules: ABS, DNR and LR, for the pressure design load predicting. Grimsley also compared the results of these methods with full-scale test data for seven monohulls ranging in length from 20 to 100 ft with speeds of 20 to 46 knots.

In 2000 and 2001, Koelbel [60, 61] gave a comprehensive and critical review of the semi-empirical methods for predicting pressure loads. He stated that these semi-empirical methods yielded large variations between the different formulas for predicting the design acceleration, even for the same dimensional craft. These semi-empirical methods involve uncertainties and ambiguities for designer in predicting the seakeeping characteristics and the design loads. Another serious issue in these methods is that the value of the predicted pressure load is constant and uniform, which is the extreme load that the craft may encounter during its lifetime. Although the non-uniform pressure loads are considered in the Allen and Jones method, they are just static constant and time-independent. However, the hydrodynamic pressure loads of a craft are transient in the time and space domain. When a uniform pressure load is applied to the structure design for a craft, it will lead to the use of large safety factors. Hence, it will result in an over-designed craft.

In 2003, the American Bureau of Shipping (ABS) [62] recognized that time domain predicting hull pressure loads is an effective way to structure analysis of a high speed craft. Direct time-domain simulation involving short-term predictions based upon the time domain pressure loads is recommended as a minimum requirement for strength assessment on the monohull craft in order to get a detailed analysis.

In 2004, Rosen [63] systematically summarized the load and response of a craft in waves, widely used design methods, experimental analysis and theoretical analysis for the hull-water impact in his PhD thesis. He and his colleagues presented a direct approach for calculating the impact pressure loads based upon large amounts of the model and full scale tests for the craft in different sea states. Hydrodynamic pressure loads between hull and water are calculated using a non-linear time-domain strip method.

In 2007 and 2009, Chiu et al. [64, 65] carried out a series of model tests in regular and irregular head waves in the towing tank to capture the motion, acceleration at LCG, wave-induced loads for the high-speed patrol ship, and found frequency response functions of pressure loads using third order and fifth-order Volterra models for regular and irregular waves respectively. They also conducted the statistical analysis of the response data and concluded that the response data follows the Rayleigh distribution.

Besides the above experimental and semi-empirical studies of the hydrodynamic loads on a craft, numerical simulation techniques for predicting the hydrodynamic loads in order to estimate the performance are another efficient way, which have been studied by many researchers. Three widely used numerical methods are: the vortex lattice method (VLM) [66, 67] first utilized for lifting wings in aerodynamics, the boundary element method [68-71], and the finite element method [72, 73].

During the period between 2008 and 2010, Ghassemi et al. [74-78] published several papers that presented the investigation of a combined method for determining the hydrodynamic characteristics of different hull forms in calm water, in which the induced pressure resistance is integrated using the boundary element method (BEM), the frictional resistance calculation is based upon the boundary layer theory, and the spray resistance is determined using Savitsky's method. It should be noted that the work done by Ghassemi is for calm water conditions; thus, the nonlinear characteristics of the pressure loads are neglected.

Recently, Faltinsen and Sun [79-81] investigated the performance of a craft in regular incident waves in head seas numerically. A 2D+t nonlinear theory is presented to perform the time domain simulations of the porpoising and the wave-induced motions and the acceleration of a prismatic planing boat in incident waves. A boundary element method is employed to solve the initial boundary value problems in 2D cross-planes.

Based upon the aforementioned methodologies, the assumptions for the pressure distribution algorithm proposed by Rosen are used in this dissertation to determine the pressure loads at each transverse section. The pressure loads are converted into the equivalent nodal force in order to simplify the dynamic analysis. The dynamic response of a flexible craft under reconstructed pressure loads is conducted to obtain more detailed stress information compared to rigid dynamics.

1.4 Motivation

A craft experiences wave-induced hydrodynamic impact when it operates in a complex sea-state at high speed. These wave-induced hydrodynamic pressure loads are known to cause structural damage. Hence, the proper understanding and the accurate prediction of the wave-induced hydrodynamic pressure loads on the craft are critical in order to achieve a design with good seakeeping and habitability characteristics.

As already mentioned, semi-empirical methods are not appropriate for a time domain analysis because they assume that the pressure load is static and uniform. Hence, a better method for predicting the impact pressure loads is necessary for the design of a high-speed craft. In this dissertation, a pressure distribution reconstruction algorithm is developed based upon the output of pressure transducers in order to predict the time-dependent hydrodynamic pressure at any point on the wetted surface of the craft.

Generally, the simulation of the flexible planing craft dynamics under the hydrodynamic pressure loads is carried out in the explicit finite element software, such as LS_DYNA, or CFD. In LS_DYNA, the instantaneous fluid structure interaction between the hull surface and water is modeled using the contact parameters [82]. However, the values of the contact parameters should be determined by the users themselves. Hence, the analysis results are dependent on the user's experience. On the other hand, the explicit finite element analysis is computationally intensive. Hence, computational efficiency in flexible multi-body dynamics is one of the critical concerns in this dissertation.

In this dissertation, the final DAEs describing the motions of a flexible craft are solved in Matlab using two numerical algorithms: Newmark's method and the mixed order technique with the additional Euler parameters. In this work, the commercial finite element code is utilized only as a pre-processor to provide the geometry information and the mode shapes. The inertia integrals that represent the dynamic coupling between the rigid motion and elastic deformation in the DAEs can be calculated in terms of the mode shapes right at the beginning of the solution process. This process results in significant savings regarding the computational cost because the integrals are constants and need to be calculated only once regardless of the number of times the ODE solver is called.

1.5 Study Plan

This dissertation focuses on the derivation and the solution procedure for the flexible multi-body dynamics. A 2D slider-crank mechanism and a 3D moving craft are used as examples to facilitate the discussion. The main research tasks are as follows.

The first task is to determine how to calculate the time-dependent elastic inertia integrals. Mode superposition technique is used to approximate the elastic deformation in terms of a linear combination of the modes shapes. Hence, the integrals can be obtained in advance as constants with the help of shape functions by moving the modal coordinates out of the integration explicitly.

The second task is how to determine the hydrodynamic pressure loads between the hull surface and the water for the high speed craft in irregular waves. The linear pressure distribution reconstruction algorithm is used to obtain the momentary pressure loads at any arbitrary location using the filtered data measured at the limited number of transducers. Thus, the equivalent nodal force in time domain is calculated as the externally applied forces for the 3D flexible craft based upon the node pressures.

The third task is to determine how to solve the differential algebraic equations efficiently. For the planar slider-crank mechanism, the coordinates partitioning method and the projection method with constraints correction will be used. For the 3D moving craft, Newmark's method based on the matrix exponential function and the mixed order techniques with the additional Euler parameters is used to obtain the motion of the craft subjected to the large rotation.

The flow chart of the research method for the flexible craft dynamics is shown in Fig. 1.1. It can be easily observed that the whole process is divided into three parts.

The first part is the test data processing and pressure distribution reconstruction. The raw pressure test data is filtered by eliminating the noise at high frequency without changing the trend of the data. Fast Fourier Transform (FFT), low-pass Butterworth filter and demeaning method are used for the raw test data filtering. Thus, the maximum pressure peaks are found based upon all the filtering test data so as to determine when and how the impact event occurred. As a result, the starting points and wave velocities along each transverse section can be determined. Finally, the momentary pressure distributions at any arbitrary point (x, y, z) can be obtained using the pressure

reconstruction algorithm, in which 3D coordinate (x,y,z) is converted to 2D coordinate (x,S) based on the assumption that the shape of the hull surface is U or V type.

The second part is to conduct the modal analysis using a commercial finite element code, such as MSC/Nastran. One can then calculate the time-invariant inertia integrals and time-dependent equivalent external loads based on the geometry information and modal shapes provided by the modal analysis. It should be noted that the commercial finite element code is utilized only as a pre-processor.

The third part is to solve the final DAEs representing the flexible multi-body system mathematically and display the results. One can get the kinematic motion and the strain and stress distribution on the craft for future design consideration.

Pre-Processor   Finite Element Analysis   Post-Processor
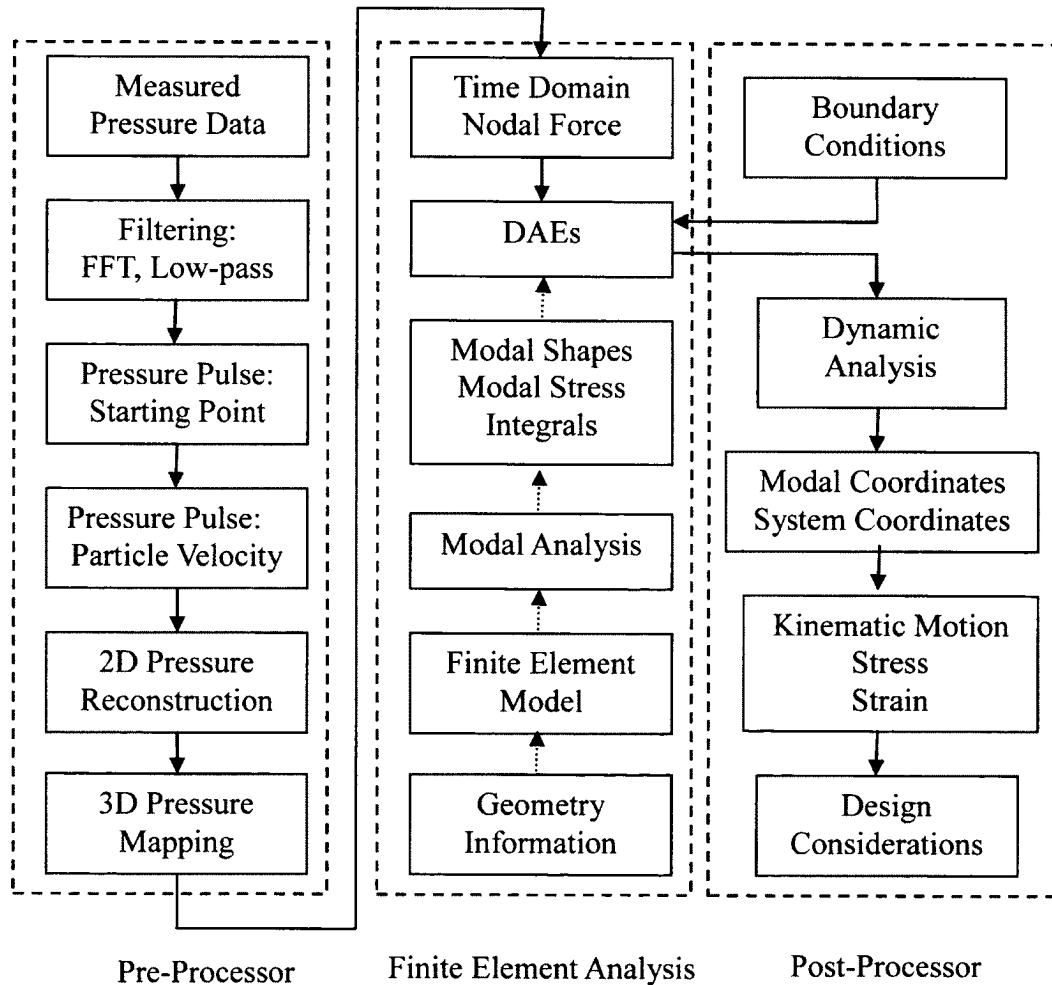
Figure 1.1 Flow chart of research method

1.6 Scope of the Study

The subsequent chapters of the dissertation are organized as follows.

In Chapter 2, the generalized governing equation of motion for a flexible multi-body system is derived based on the principle of virtual work and D'Alembert's principle in terms of the absolute Cartesian coordinates. The nonlinear constraints between different bodies are introduced into the equation of motion with the help of Lagrange Multipliers. The floating frame is used to describe the kinematic configurations of the flexible multi-body system, in which the elastic deformations are approximated in terms of the linear combination of mode shapes obtained from the finite element modal analysis.

In Chapter 3, three numerical issues related to the computational efficiency in solving the flexible multi-body system are discussed in detail. The integrals of coupling terms in the mass matrix, the transformation matrix and the methods of solving DAEs are discussed. The integral terms that represent the dynamic coupling between the rigid motion and elastic deformation are calculated as constants in advance by expressing in the explicit format of the modal coordinates. The transformation matrix A can be calculated in five different methods based upon available information of the input data: direction cosines, Euler angles, Rodriguez parameters, Euler parameters and matrix exponential function. The relationships between these different methods are also derived. The Euler parameters method is widely used because it never encounters singularity as the three-parameter Euler angles method does. Two different numerical methods: the coordinate partitioning method and the projection method are used to solve the DAEs.

In Chapter 4, a 2D planar slide-crank mechanism with rigid/ flexible connecting rod is studied in detail to verify the two numerical methods introduced in Chapter 3, namely, the numerical integrals in the mass matrix and the DAEs solution procedure. For the rigid case, the direct method is set as the benchmark to check the coordinate partitioning method and the projection method with constraints correction. It validates the projection method with constraints correction. Two different locations are selected as the origin of the body-fixed coordinate. The results show that it is computationally efficient if the origin of the connecting rod is located at the center of gravity. The results are also compared with the flexible crank-slide mechanisms in terms of solution accuracy and efficiency.

In Chapter 5, a numerical method is presented to reconstruct the pressure distribution over the wetted surface of the craft based upon the data measured by several pressure transducers. The high frequency noise in the measured data is first filtered out by using the FFT and a low-pass filter. The pressure distribution reconstruction algorithm proposed by Rosen for a planar domain is carried out based on the filtered pressure data. The pressure reconstruction for the 3D finite element model of the craft is then calculated by converting the 3D coordinate (x, y, z) to 2D coordinate (x, S) based on the assumption that the given hull surface is either a U or a V type.

In Chapter 6, the dynamic response of a flexible craft subject to the reconstructed pressure load is simulated based on the derivations and the methods discussed in Chapter 2 and 3. In particular, the 3D pressure distribution generated in Chapter 5 is first converted into equivalent nodal force for dynamic analysis. Furthermore, a mixed order technique with additional Euler parameters is proposed in this chapter in order to handle the large angular rotation incurred in the 3D craft motion. The results from the proposed algorithm are compared to that from the Newmark method, in which the transformation matrix is calculated using the matrix exponential function. At last, the dynamic element stress distribution is calculated based upon the modal element stress using the least mean square error technique.

In Chapter 7, research conclusions and suggestions for future investigations are provided.

CHAPTER 2

EQUATION OF MOTION FOR A FLEXIBLE MULTI-BODY

SYSTEM

Mechanical systems can be considered as a collection of bodies or components, connecting with each other through various joints to fulfill a specific function. Mechanical systems have been widely used for different purposes in modern society. Some are comparatively simple, such as slider–crank mechanisms, while others are much more complex, such as vehicles. Both, however, can be denoted as the collection of four basic elements: *body*, the component in the system; *joint*, the constraint between bodies; *force element*, the spring and actuator counting for interactions between bodies; *external excitation*, the force or the moment.

In this chapter, the governing differential equation of motion pertaining to a mechanical system is derived in detail. To this end, many methods can be used, including the Newton-Euler method and the Newton-Lagrange method. It is, however, the principle of virtual work that is used in this study.

The organization of this chapter is in following order.

The equation of motion for a single flexible body is first derived in detail in Section 2.1. The result will be easily extended to a flexible multi-body system in Section 2.2 because the flexible multi-body system is made of many flexible bodies connected with joints. The kinematic constraints that describe the joints between flexible bodies are included in the equation of motion through the use of Lagrange multipliers. For the computational simplicity, the modal coordinates are introduced in Section 2.3 to approximate the elastic deformation in the equation of motion. Finally, the equation of motion for a rigid multi-body system is obtained directly in Section 2.4, which is considered as a special case for the flexible multi-body system.

2.1 Equation of Motion for a Single Flexible Body

The schematic diagram for a single flexible body is shown in Fig. 2.1. The body occupies the domain, Ω. The frame $x - y - z$ is the global coordinate system with the origin at O. The frame $x' - y' - z'$ is the body-fixed coordinate system with the origin fixed at O'. The position vector r' and the linear elastic deformation e of any point in the body can be conveniently defined with respect to the body-fixed coordinate system. The body force f_b is distributed throughout the body. The traction forces T are applied over part of the boundary, S_1 while the prescribed displacement filed is over part of boundary, S_2.
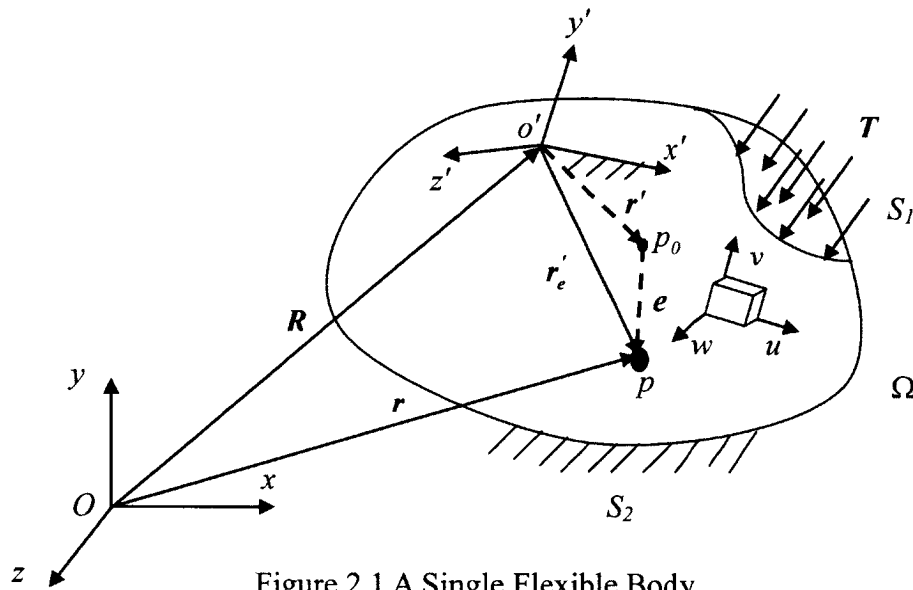
Figure 2.1 A Single Flexible Body

The configuration of a multi-body system is identified by a set of variables called the system generalized coordinates that completely define the location and orientation of each body in the system. The least of those generalized coordinates is called the Degrees of Freedom (DOFs). Once this set of generalized coordinates is identified, they can be used to describe the global position of an arbitrary point on the body.

The movement of any arbitrary point in a single flexible body can be viewed as a combination of the rigid body motion and the relative elastic deformation. The rigid-body motion is measured by the relative motion between the body-fixed coordinate system and the global coordinate system, whereas the elastic deformation is measured by the motion

of the point with respect to the body-fixed coordinate system. Thus, the position vector r of any point p_0 in the body can be defined in the global coordinate system as:

$$r(t) = R(t) + A(t)r'_e(t) \tag{2.1}$$

where $R(t)$ is the time-dependent position vector of the origin of the body-fixed coordinate described in global coordinate system, and $A(t)$ is the transformation matrix from the body-fixed coordinate system to the global coordinate system. The transformation matrix A can be described in terms of cosine directions, Euler angles, Euler parameters, Rodriguez parameters, or the Matrix exponential function depending on the information available. Calculation of the transformation matrix based upon different methods will be discussed in detail in Chapter 3.

The vector $r'_e(t)$ is the summation of rigid position vector r' and the elastic deformation e of the point in the body-fixed coordinate system, which can be written as follows:

$$r'_e(t) = r' + e(t) = \begin{Bmatrix} x' \\ y' \\ z' \end{Bmatrix} + \begin{Bmatrix} u(t) \\ v(t) \\ w(t) \end{Bmatrix} \tag{2.2}$$

where r' is the position vector of point p_0, whereas e is the translational elastic deformation of the same point. The position vector r' does not change with time.

To obtain the velocity of point p_0 in the global coordinate system, one can differentiate Eq. 2.1 with respect to time. Thus, the first order derivation of r relative to time is as follows:

$$\dot{r} = \dot{R} + \dot{A}r'_e + A\dot{r}'_e = \dot{R} + A\tilde{\omega}'r'_e + A\dot{e} = \dot{R} - A\tilde{r}'_e\omega' + A\dot{e}$$

$$= \begin{bmatrix} I & -A\tilde{r}'_e & AN \end{bmatrix} \begin{Bmatrix} \dot{R} \\ \omega' \\ \dot{q}_e \end{Bmatrix} \equiv L\dot{q} \tag{2.3}$$

where q_e is the elastic deformation vector, ω' the vector of the local angular velocity of the flexible body, is given by $\omega' = \begin{Bmatrix} \omega'_x & \omega'_y & \omega'_z \end{Bmatrix}^T$, and $\tilde{\omega}'$ is a skew matrix, which is defined as:

$$\tilde{\omega}' = \begin{bmatrix} 0 & -\omega'_z & \omega'_y \\ \omega'_z & 0 & -\omega'_x \\ -\omega'_y & \omega'_x & 0 \end{bmatrix} \tag{2.4}$$

Note that, for the convenience of derivation, the elastic displacement e is approximated by interpolation as

$$e = Nq_e,$$

where N is a $3 \times n_e$ matrix shape function of position with n_e being the number of the elastic deformation coordinates. In other words, n_e is the dimension of q_e. Since N is known as it is selected by the user, this interpolation helps to reduce the degrees of freedom of the elastic displacement from infinite to finite.

The velocity derivative in Eq. 2.3 produces a virtual displacement as follows:

$$\delta r = \begin{bmatrix} I & -A\tilde{r}'_e & AN \end{bmatrix} \begin{Bmatrix} \delta R \\ \delta\Pi' \\ \delta q_e \end{Bmatrix} = L\delta q \tag{2.5}$$

where δ is the delta operator, which represents a small arbitrary change in variable. δr is called virtual displacement and Π' is the local angular displacement, $\delta q = \{\delta R \quad \delta\Pi' \quad \delta q_e\}^T$. The virtual displacement [83] is defined as an infinitesimal change in the configuration that does not violate any of the kinematic constraints imposed on the motion of the system. The virtual displacement is imposed while the time is held fixed.

Similarly, one can differentiate Eq. 2.3 to obtain the second order derivation of the position vector r relative to time as follows:

$$\ddot{r} = L\ddot{q} + \dot{L}\dot{q} = \begin{bmatrix} I & -A\tilde{r}'_e & AN \end{bmatrix} \begin{Bmatrix} \ddot{R} \\ \alpha' \\ \ddot{q}_e \end{Bmatrix} + \begin{bmatrix} 0 & -A\tilde{\omega}'\tilde{r}'_e - A\tilde{e} & A\tilde{\omega}'N \end{bmatrix} \begin{Bmatrix} \dot{R} \\ \omega' \\ \dot{q}_e \end{Bmatrix}$$

$$= \begin{bmatrix} I & -A\tilde{r}'_e & AN \end{bmatrix} \begin{Bmatrix} \ddot{R} \\ \alpha' \\ \ddot{q}_e \end{Bmatrix} - (A\tilde{\omega}'\tilde{r}'_e + A\tilde{e})\omega' + A\tilde{\omega}'N\dot{q}_e = L\ddot{q} + A\tilde{\omega}'\tilde{\omega}'r'_e + 2A\tilde{\omega}'\dot{e} \tag{2.6}$$

where the angular acceleration $\alpha' = \{\dot{\omega}'_x \quad \dot{\omega}'_y \quad \dot{\omega}'_z\}^T$.

With the help of D'Alembert principle, the inertia force can be equally considered

as the external force acting on the flexible body. Thus, the virtual work done by all the forces for a single flexible body is given as follows [84]:

$$\delta W = \int_{\Omega}[f_{bi}(t) - \rho\ddot{r}_i(t)]^T \delta r_i dv + \iint_{S_I} T_i^{(v)^T}(t)\delta r_i dA \tag{2.7}$$

It is noted that $\delta r_i = 0$ on S_2 where the displacement is known. The surface integral in Eq. 2.7 can then be extended to cover the entire surface of the flexible body $S = S_I \cup S_2$,

$$\delta W = \int_{\Omega}[f_{bi}(t) - \rho\ddot{r}_i(t)]\delta r_i dv + \iint_S T_i^{(v)}(t)\delta r_i dA \tag{2.8}$$

With the help of Cauchy's Stress Formula [84], the surface traction force can be written as follows:

$$T_i^{(v)} = \tau_{ij}v_j \tag{2.9}$$

where τ_{ij} is the stress tensor, v_j is the unit vector outward normal to the surface of the body in terms of the local coordinate system. $i, j=1, 2, 3$. Based upon Gauss' Divergence Theorem [84], the surface integral can be converted to the volume domain as follows:

$$\int_{\Omega}\tau_{jk,i}dv = \iint_S \tau_{jk}v_i dA \tag{2.10}$$

Substituting Eqs. 2.9 and 2.10 into the right hand side of Eq. 2.8, one has

$$\iint_S T_i^{(v)}\delta r_i dA = \iint_S \tau_{ij}v_j\delta r_i dA = \int_{\Omega}(\tau_{ij}\delta r_i)_{,j} dv$$

$$= \int_{\Omega}(\tau_{ij,j}\delta r_i)dv + \int_{\Omega}\tau_{ij}(\delta r_i)_{,j} dv = \int_{\Omega}(\tau_{ij,j}\delta r_i)dv + \int_{\Omega}\tau_{ij}\delta r_{i,j}dv$$

Then Eq. 2.8 can be written as:

$$\delta W = \int_{\Omega}[f_{bi}(t) - \rho\ddot{r}_i(t)]\ \delta r_i dv + \int_{\Omega}(\tau_{ij,j}\delta r_i)dv + \int_{\Omega}\tau_{ij}\delta r_{i,j}dv$$

$$= \int_{\Omega}[\tau_{ij,j} + f_{bi}(t) - \rho\ddot{r}_i(t)]\ \delta r_i dv + \int_{\Omega}\tau_{ij}\delta r_{i,j}dv \tag{2.11}$$

The last term $\tau_{ij}\delta r_{i,j}$ can be spanned in terms of displacement, based upon the small strain assumption, as follows:

$$\tau_{ij}\delta r_{i,j} = \tau_{ij}\cdot\delta\left[\frac{1}{2}(r_{i,j} + r_{j,i}) + \frac{1}{2}(r_{i,j} - r_{j,i})\right] = \tau_{ij}\cdot(\delta\varepsilon_{ij} + \delta\omega_{ij}) \tag{2.12}$$

where $\varepsilon_{ij} = \frac{1}{2}(r_{i,j} + r_{j,i})$ is the strain tensor and $\omega_{ij} = \frac{1}{2}(r_{i,j} - r_{j,i})$ is the rotation tensor.

Since the product of the skew of the rotation tensor ω_{ij} and the stress tensor τ_{ij} is zero, Eq. 2.12 becomes:

$$\tau_{ij}\delta r_{i,j} = \tau_{ij}\delta\varepsilon_{ij} \tag{2.13}$$

Substituting Eq. 2.13 into Eq. 2.11, one has:

$$\int_{\Omega}[f_{bi}(t)-\rho\ddot{r}_i(t)]\delta r_i dv + \oiint_S T_i^{(v)}\delta r_i dA = \int_{\Omega}[\tau_{ij,j}+f_{bi}(t)-\rho\ddot{r}_i(t)]\delta r_i dv + \int_{\Omega}\tau_{ij}\delta\varepsilon_{ij} dv \tag{2.14}$$

It is noted that the balance of forces at any arbitrary point in a body satisfies the condition

$\tau_{ij,j} + f_{bi}(t) - \rho\ddot{r}_i(t) = 0$ [84]. Hence, the first integral on the right-hand side of Eq. 2.14 is

dropped out. As a result, one has the principle of virtual work for a single flexible body as

follows:

$$\int_{\Omega}[f_{bi}(t)-\rho\ddot{r}_i(t)]\delta r_i dv + \oiint_S T_i^{(v)}\delta r_i dA = \int_{\Omega}\tau_{ij}\delta\varepsilon_{ij} dv \tag{2.15}$$

The left hand side of the above equation can be considered as the external virtual work

done by the generalized external force and the right hand side as the internal virtual work

due to the elastic deformation. Based upon Eq. 2.15, one can formulate the equation of

motion for a single flexible body. The calculation of each term in Eq. 2.15 is discussed in

detail in the following subsections.

2.1.1 Strain Energy, $\delta U = \int_{\Omega}\tau_{ij}\delta\varepsilon_{ij} dv$

The right hand side of Eq. 2.15, $\int_{\Omega}\tau_{ij}\delta\varepsilon_{ij} dv \equiv \delta U$, is the strain energy stored in the

body due to the elastic deformation. Since the distance between any two arbitrary points

in a rigid body remains constant, it is known that the strain energy is equal to zero for a

rigid body. However, the strain energy is time dependent for a flexible body.

In order to calculate the strain energy, the stress τ and strain ε should be obtained

first. The strain can be calculated based upon the strain-displacement relationship [85],

once the elastic displacement is obtained. The relationship is as follows:

$$\varepsilon = \begin{Bmatrix} \varepsilon_{xx} \\ \varepsilon_{yy} \\ \varepsilon_{zz} \\ \gamma_{yz} \\ \gamma_{xz} \\ \gamma_{xy} \end{Bmatrix} = \begin{Bmatrix} \dfrac{\partial u}{\partial x} \\[4pt] \dfrac{\partial v}{\partial y} \\[4pt] \dfrac{\partial w}{\partial z} \\[4pt] \dfrac{\partial w}{\partial y} + \dfrac{\partial v}{\partial z} \\[4pt] \dfrac{\partial w}{\partial x} + \dfrac{\partial u}{\partial z} \\[4pt] \dfrac{\partial v}{\partial x} + \dfrac{\partial u}{\partial y} \end{Bmatrix} = \begin{bmatrix} \dfrac{\partial}{\partial x} & 0 & 0 \\[4pt] 0 & \dfrac{\partial}{\partial y} & 0 \\[4pt] 0 & 0 & \dfrac{\partial}{\partial z} \\[4pt] 0 & \dfrac{\partial}{\partial z} & \dfrac{\partial}{\partial y} \\[4pt] \dfrac{\partial}{\partial z} & 0 & \dfrac{\partial}{\partial x} \\[4pt] \dfrac{\partial}{\partial y} & \dfrac{\partial}{\partial x} & 0 \end{bmatrix} \begin{Bmatrix} u \\ v \\ w \end{Bmatrix} \equiv [\partial]e \tag{2.16}$$

where $[\partial]$ is defined here as the operator matrix.

According to the general form of Hooke's law [84], the constitute equation for the stress-strain relationship is given as follows:

$$\tau_{ij} = \lambda \delta_{ij} \varepsilon_{ll} + 2G\varepsilon_{ij} \tag{2.17}$$

where $\lambda = \dfrac{Ev}{(1+v)(1-2v)}$ and $G = \dfrac{E}{2(1+v)}$ are the so-called Lame constants, in which E

is the Young's modulus, v is the poisson's ratio, and $\delta_{ij} = \begin{cases} 0 & i \neq j \\ 1 & i = j \end{cases}$ is the Kronecker

delta symbol. $i, j = 1, 2, 3$. Specifically, Eq. 2.17 gives the stress-strain relationship as:

$$\sigma = \begin{Bmatrix} \sigma_{xx} \\ \sigma_{yy} \\ \sigma_{zz} \\ \tau_{yz} \\ \tau_{xz} \\ \tau_{xy} \end{Bmatrix} = \begin{Bmatrix} (\lambda + 2G)\varepsilon_{xx} + \lambda\varepsilon_{yy} + \lambda\varepsilon_{zz} \\ \lambda\varepsilon_{xx} + (\lambda + 2G)\varepsilon_{yy} + \lambda\varepsilon_{zz} \\ \lambda\varepsilon_{xx} + \lambda\varepsilon_{yy} + (\lambda + 2G)\varepsilon_{zz} \\ 2G\gamma_{yz} \\ 2G\gamma_{xz} \\ 2G\gamma_{xy} \end{Bmatrix}$$

$$= \begin{bmatrix} (\lambda + 2G) & 1 & 1 & 0 & 0 & 0 \\ 1 & (\lambda + 2G) & 1 & 0 & 0 & 0 \\ 1 & 1 & (\lambda + 2G) & 0 & 0 & 0 \\ 0 & 0 & 0 & 2G & 0 & 0 \\ 0 & 0 & 0 & 0 & 2G & 0 \\ 0 & 0 & 0 & 0 & 0 & 2G \end{bmatrix} \begin{Bmatrix} \varepsilon_{xx} \\ \varepsilon_{yy} \\ \varepsilon_{zz} \\ \gamma_{yz} \\ \gamma_{xz} \\ \gamma_{xy} \end{Bmatrix} \equiv D\varepsilon \tag{2.18}$$

where D is the stress-strain matrix.

The strain energy can be conveniently calculated based upon the finite element method; the elastic displacement can be approximated as a product of the shape functions and the nodal vector,

$$e = \{u \quad v \quad w\}^T = Nq_e \tag{2.19}$$

where N is the shape function matrix and q_e is the nodal displacement vector. Substituting Eq. 2.19 into Eq. 2.16, one has:

$$\varepsilon = [\partial](N \cdot q_e) \equiv Bq_e \tag{2.20}$$

where B is the strain-displacement matrix. Substituting Eqs. 2.18 and 2.20 into the elastic energy term, one has the strain energy stored in one element as:

$$\int_{\Omega_i} \sigma_i^T \delta\varepsilon_i dv = \int_{\Omega_i} (D\varepsilon_i)^T \delta\varepsilon_i dv = \int_{\Omega_i} (DBq_e^i)^T \delta Bq_e^i dv = q_e^{i^T} \int_{\Omega_i} B^T D^T B dv \delta q_e^i \equiv q_e^{i^T} K_e \delta q_e^i \tag{2.21}$$

where $K_e = \int_{\Omega_i} B^T D^T B dv$ is the element stiffness matrix, in which Ω_i is the volume of the ith element, and q_e^i is the nodal displacement vector evaluated at the ith element.

The strain energy due to the elastic deformation for the whole domain can then be obtained by summing up the energy stored in each element as follows:

$$\int_{\Omega} \sigma^T \delta\varepsilon dv = \sum_{i=1}^{NE} \int_{\Omega_i} (D\varepsilon_i)^T \delta\varepsilon_i dv = q_e^T K_{ff} \delta q_e \tag{2.22}$$

where K_{ff} is the global stiffness matrix, which is dependent on the element types and the element connections. NE is the total number of the elements, and q_e is the total elastic displacement vector of all nodes. Eq. 2.22 can be expressed in terms of the system generalized coordinate of a flexible body as follows:

$$\int_{\Omega} \sigma^T \delta\varepsilon dv = \begin{bmatrix} R^T & \pi^T & q_e^T \end{bmatrix} \begin{bmatrix} 0 & 0 & 0 \\ 0 & 0 & 0 \\ 0 & 0 & K_{ff} \end{bmatrix} \delta q \equiv q^T K \delta q$$

2.1.2 Virtual Work Done by the Body Force, $\int_{\Omega} f_b^T \delta r dv$

Gravity is the only body force considered in this study. Its magnitude is the product of the density of the material ρ and the gravitational acceleration g. The direction of the body force is dependent on the global coordinate system. The body force

is normally assumed to be constant in multi-body dynamics. Hence, one has:

$$\int_\Omega f_b^T \delta r dv = \int_\Omega f_b^T \cdot L \delta q dv = \int_\Omega f_b^T [I \quad -A\tilde{r}_e' \quad AN] \delta q dv$$

$$= [f_b^T V \quad -f_b^T A(I_{\tilde{r}} + I_{\tilde{e}})/\rho \quad f_b^T AI_N/\rho] \delta q = \begin{bmatrix} Vf_b \\ (I_{\tilde{r}} + I_{\tilde{e}})A^T f_b/\rho \\ I_N^T A^T f_b/\rho \end{bmatrix}^T \delta q \qquad (2.23)$$

where f_b^T is the body force, V is the volume of a single flexible body, $I_{\tilde{r}} = \int_\Omega \rho \tilde{r}' dv$ and

$I_{\tilde{e}} = \int_\Omega \rho \tilde{e} dv$ are linear moment for the original configuration of the body and the elastic

deformation, respectively, and $I_N = \int_\Omega \rho N dv$, the moment of the shape function.

It should be noted that the transformation matrix A is space-independent, so it can be placed outside of the integration.

2.1.3 Virtual Work Done by the Inertia Force, $\int_\Omega \rho \ddot{r}^T \delta r dv$ [86]

Substituting the virtual displacement, Eq. 2.5, and the acceleration terms, Eq. 2.6, into the virtual work done by the inertia force term, one has:

$$\int_\Omega \rho \ddot{r}^T \delta r dv = \ddot{q}^T \int_\Omega \rho L^T L dv \delta q + \int_\Omega \rho (A\tilde{\omega}'\tilde{\omega}'r_e' + 2A\tilde{\omega}'\dot{e})^T L dv \delta q \qquad (2.24)$$

The first integration on the right hand side of Eq. 2.24 can be calculated as:

$$\ddot{q}^T \int_\Omega \rho L^T L dv \delta q = \begin{Bmatrix} \ddot{R} \\ \ddot{\Pi}' \\ \ddot{q}_e \end{Bmatrix}^T \int_\Omega \rho \begin{bmatrix} I \\ (-A\tilde{r}_e')^T \\ (AN)^T \end{bmatrix} [I \quad -A\tilde{r}_e' \quad AN] dv \delta q$$

$$= \left(\begin{bmatrix} mI & -A(I_{\tilde{r}} + I_{\tilde{e}}) & AI_N \\ -[A(I_{\tilde{r}} + I_{\tilde{e}})]^T & -(I_{\tilde{r}\tilde{r}} + I_{\tilde{r}\tilde{e}} + I_{\tilde{e}\tilde{r}} + I_{\tilde{e}\tilde{e}}) & (I_{\tilde{r}N} + I_{\tilde{e}N}) \\ [AI_N]^T & [(I_{\tilde{r}N} + I_{\tilde{e}N})] & I_{N^T N} \end{bmatrix} \begin{Bmatrix} \ddot{R} \\ \ddot{\Pi}' \\ \ddot{q}_e \end{Bmatrix} \right)^T \delta q \qquad (2.25a)$$

where m is the mass of the body and the rest are integrals that are defined as:

$$I_{\tilde{r}\tilde{r}} + I_{\tilde{r}\tilde{e}} + I_{\tilde{e}\tilde{r}} + I_{\tilde{e}\tilde{e}} = \int_\Omega \rho \tilde{r}'\tilde{r}' dv + \int_\Omega \rho \tilde{r}'\tilde{e} dv + \int_\Omega \rho \tilde{e}\tilde{r}' dv + \int_\Omega \rho \tilde{e}\tilde{e} dv,$$

$$I_{\tilde{r}N} + I_{\tilde{e}N} = \int_\Omega \rho \tilde{r}'N dv + \int_\Omega \rho \tilde{e}N dv \text{ and } I_{N^T N} = \int_\Omega \rho N^T N dv.$$

The second integration on the right hand side of Eq. 2.24 can be calculated as:

$$\int_\Omega \rho (A\tilde{\omega}'\tilde{\omega}'r_e' + 2A\tilde{\omega}'\dot{e})^T L dv \delta q = \int_\Omega \rho (A\tilde{\omega}'\tilde{\omega}'r_e' + 2A\tilde{\omega}'\dot{e})^T [I \quad -A\tilde{r}_e' \quad AN] dv \delta q$$

$$= \left[\begin{array}{c} A\tilde{\omega}'\tilde{\omega}'(I_{r'} + I_{\tilde{e}}) + 2A\tilde{\omega}'I_{\tilde{e}} \\ -\tilde{\omega}'(I_{\tilde{r}\tilde{r}} + I_{\tilde{r}\tilde{e}} + I_{\tilde{e}\tilde{r}} + I_{\tilde{e}\tilde{e}})\omega' - 2(I_{\tilde{e}\tilde{r}} + I_{\tilde{e}\tilde{e}})^T \omega' \\ -(I_{\tilde{r}\tilde{\omega}'N} + I_{\tilde{e}\tilde{\omega}'N})^T \omega' + 2I_{\tilde{e}N}^T \omega' \end{array} \right]^T \delta q \qquad (2.25b)$$

where $I_{\tilde{e}} = \int_\Omega \rho \dot{e} dv$, $I_{\tilde{e}\tilde{r}} + I_{\tilde{e}\tilde{e}} = \int_\Omega \rho \tilde{e} \tilde{r}' dv + \int_\Omega \rho \tilde{e} \tilde{e} dv$,

$I_{\tilde{r}\tilde{\omega}'N} + I_{\tilde{e}\tilde{\omega}'N} = \int_\Omega \rho \tilde{r}' \tilde{\omega}' N dv + \int_\Omega \rho \tilde{e} \tilde{\omega}' N dv$ and $I_{\tilde{e}N} = \int_\Omega \rho \tilde{e} N dv$.

It is noted that $\tilde{a} = -\tilde{a}^T$, $\tilde{a}a = 0$, $a^T \tilde{b} = -b^T \tilde{a}$ and $\tilde{a}\tilde{b} = \tilde{b}\tilde{a} - ab^T + ba^T$ are used in Eq.2.25b.

Finally, the total virtual work done by the inertia force is summarized as follows:

$$\int_\Omega \rho \ddot{r}^T \delta r dv =$$

$$\left(\left[\begin{array}{ccc} mI & -A(I_{\tilde{r}} + I_{\tilde{e}}) & AI_N \\ -[A(I_{\tilde{r}} + I_{\tilde{e}})]^T & -(I_{\tilde{r}\tilde{r}} + I_{\tilde{r}\tilde{e}} + I_{\tilde{e}\tilde{r}} + I_{\tilde{e}\tilde{e}}) & (I_{\tilde{r}N} + I_{\tilde{e}N}) \\ [AI_N]^T & [(I_{\tilde{r}N} + I_{\tilde{e}N})] & I_{N^T N} \end{array} \right] \left\{ \begin{array}{c} \ddot{R} \\ \ddot{\Pi}' \\ \ddot{q}_e \end{array} \right\} + \left\{ \begin{array}{c} (I_{r'} + I_e)^T \tilde{\omega}'\tilde{\omega}'A^T - 2I_{\tilde{e}}^T \tilde{\omega}'A^T \\ \omega'^T(I_{\tilde{r}\tilde{r}} + I_{\tilde{r}\tilde{e}} + I_{\tilde{e}\tilde{r}} + I_{\tilde{e}\tilde{e}})\tilde{\omega}' - 2\omega'^T(I_{\tilde{e}\tilde{r}} + I_{\tilde{e}\tilde{e}}) \\ -\omega'^T(I_{\tilde{r}\tilde{\omega}'N} + I_{\tilde{e}\tilde{\omega}'N}) + 2\omega'^T I_{\tilde{e}N} \end{array} \right\} \right)^T \delta q \quad (2.26)$$

2.1.4 Virtual Work Done by the External Force, $\iint_S T_i^{(v)^T} \delta r_i dA$

A moving body may not often be subjected to any surface traction. However, it is common for it to be subjected to point loads. Moreover, the surface load can be converted equivalently to a point load by distributing the total surface traction to the corresponding node points enclosed by the surface of concern. Hence, without loss of generality, the external forces can be taken as point forces and moments.

The work done by the point load, F_i, and the point moment, T_i', acting on the body at point i can be calculated as follows:

$$\delta w^e = \sum_{i=1}^{N_p} \left(F_i^T \delta r_i + T_i'^T \delta \Pi' \right)$$

$$= \sum_{i=1}^{N_p} \left[F_i^T (\delta R - A\tilde{r}_{ei}' \delta \Pi' + A\delta e) + T_i'^T \delta \Pi' \right] = \sum_{i=1}^{N_p} \left[F_i^T \delta R - \left(F_i^T A\tilde{r}_{ei}' - T_i'^T \right) \delta \Pi' + F_i^T A\delta q_e \right]$$

$$= \sum_{i=1}^{N_p} F_i^T \cdot \delta R - \sum_{i=1}^{N_p} \left(F_i^T A\tilde{r}_{ei}' - T_i'^T \right) \delta \Pi' + \sum_{i=1}^{N_p} F_i^T A \cdot \delta q_e \equiv \left[F^T \quad T'^T \quad W'^T \right] \delta q = \left[\begin{array}{c} F \\ T' \\ W' \end{array} \right]^T \delta q \quad (2.27)$$

where F_i is defined in the global coordinate system and T_i' the body-fixed coordinate system, and N_p is the total number of nodes where the external forces and moments are applied. Furthermore, the following notations are in order: $F = \sum_{i=1}^{N_p}(F_i)$ is the total force

acting on the body, $T' = \sum_{i=1}^{N}(\tilde{r}_{ei}' A^T F_i + T_i')$ and $W' = \sum_{i=1}^{N}[A^T F_i]$ are equivalent external

moment and force, respectively, in the body-fixed coordinate system.

2.1.5 Equation of Motion for a Single Flexible Body

In the preceding subsections, the virtual work done by the internal elastic force, the body force, the inertia force, and the external force has been derived in detail. The corresponding terms defined by Eqs. 2.22~ 27 can be substituted into Eq. 2.15. One can then obtain the equation to represent the total virtual work of the system as

$$\left(\begin{bmatrix} mI & -A(I_{\tilde{r}}+I_{\tilde{e}}) & AI_N \\ -(I_{\bar{r}r}+I_{\bar{r}\tilde{e}}+I_{\bar{e}r}+I_{\bar{e}\tilde{e}}) & (I_{\bar{r}N}+I_{\tilde{e}N}) \\ sym. & I_{N^TN} \end{bmatrix}\begin{Bmatrix} \ddot{R} \\ \ddot{\Pi}' \\ \ddot{q}_e \end{Bmatrix} + \begin{bmatrix} (I_{\tilde{r}}+I_e)^T\tilde{\omega}'\tilde{\omega}'A^T - 2I_e^T\tilde{\omega}'A^T \\ \omega'^T(I_{\bar{r}r}+I_{\bar{r}\tilde{e}}+I_{\bar{e}r}+I_{\bar{e}\tilde{e}})\tilde{\omega}' - 2\omega'^T(I_{\tilde{e}r}+I_{\tilde{e}\tilde{e}}) \\ -\omega'^T(I_{\bar{r}\tilde{\omega}'N}+I_{\tilde{e}\tilde{\omega}'N})+2\omega'^T I_{\tilde{e}N} \end{bmatrix}\right)^T \delta q$$

$$-\begin{bmatrix} Vf_b \\ (I_{\tilde{r}}+I_{\tilde{e}})A^T f_b / \rho \\ I_N^T A^T f_b / \rho \end{bmatrix}^T \delta q + q^T K \delta q - \begin{bmatrix} F \\ T' \\ W' \end{bmatrix}^T \delta q = 0 \qquad (2.28)$$

The above equation can be written as follows:

$$(M\ddot{q}-f)^T \delta q = 0 \qquad (2.29)$$

where

$$M = \begin{bmatrix} mI & -A(I_{\tilde{r}}+I_{\tilde{e}}) & AI_N \\ -[A(I_{\tilde{r}}+I_{\tilde{e}})]^T & -(I_{\bar{r}r}+I_{\bar{r}\tilde{e}}+I_{\bar{e}r}+I_{\bar{e}\tilde{e}}) & (I_{\bar{r}N}+I_{\tilde{e}N}) \\ [AI_N]^T & [(I_{\bar{r}N}+I_{\tilde{e}N})] & I_{N^TN} \end{bmatrix} \qquad (2.30)$$

$$f = \begin{Bmatrix} Vf_b - A\tilde{\omega}'\tilde{\omega}'(I_{\tilde{r}}+I_e)-2A\tilde{\omega}'I_{\tilde{e}}+F \\ (I_{\tilde{r}}+I_{\tilde{e}})A^T f_b / \rho + \tilde{\omega}'(I_{\bar{r}r}+I_{\bar{r}\tilde{e}}+I_{\bar{e}r}+I_{\bar{e}\tilde{e}})\omega'+2(I_{\tilde{e}r}+I_{\tilde{e}\tilde{e}})^T\omega'+T' \\ -Kq_e + (AI_N)^T f_b / \rho + (I_{\bar{r}\tilde{\omega}'N}+I_{\tilde{e}\tilde{\omega}'N})^T\omega' - 2I_{\tilde{e}N}^T\omega'+W' \end{Bmatrix} \quad (2.31)$$

Since the virtual displacement is arbitrary, Eq. 2.29 yields the equation of motion for a single flexible body as follows:

$$M\ddot{q} - f = 0 \qquad (2.32)$$

The mass matrix and the generalized force vector in the equation of motion for a single flexible body, Eq. 2.32 can be symbolically expressed in the function of the elastic displacement q_e, the elastic velocity $\dot{q}_e$, angular velocity ω' and the transformation matrix A as follows:

$$\begin{bmatrix} M_{RR} & M_{R\theta}(q_e, A) & M_{Rq}(A) \\ M_{\theta R}(q_e, A) & M_{\theta\theta}(q_e) & M_{\theta q}(q_e) \\ M_{qR}(A) & M_{q\theta}(q_e) & M_{qq} \end{bmatrix} \begin{Bmatrix} \ddot{R} \\ \ddot{\theta} \\ \ddot{q}_e \end{Bmatrix} = \begin{Bmatrix} f_R(q_e, \dot{q}_e, \omega', A) \\ f_\theta(q_e, \dot{q}_e, \omega', A) \\ f_q(q_e, \dot{q}_e, \omega', A) \end{Bmatrix} \qquad (2.33)$$

where $M_{RR} = mI_3$, which is a constant diagonal matrix related to the translate motion, in which m is the mass of the body and I_3 is a 3×3 identify matrix.

$M_{R\theta}(q_e, A) = -A(I_{\bar{r}} + I_{\bar{e}})$ is the coupling term between the translation and the rotation. If the origin of the body-fixed coordinate is located at the Center of Gravity of the body, the term $I_{\bar{r}}$ will vanish, though the elastic term $I_{\bar{e}}$ will stay. Therefore, it implies that the translation and the rotation are always coupled for a flexible body in motion.

$M_{Rq}(A) = AI_N$ is the coupling term between the translation and the elastic deformation.

$M_{\theta\theta}(q_e) = -(I_{\bar{r}\bar{r}} + I_{\bar{r}\bar{e}} + I_{\bar{e}\bar{r}} + I_{\bar{e}\bar{e}})$ can be taken equivalently as the rotation "mass" of the deformable body. $M_{\theta q}(q_e) = I_{\bar{r}N} + I_{\bar{e}N}$ is the coupling term between the rotation and the elastic deformation. $M_{qq} = I_{N^T N}$ can be taken equivalently as the "mass" corresponding to the elastic deformation, which is constant and related to the shape functions.

$f_R(q_e, \dot{q}_e, \omega', A) = Vf_b - A\tilde{\omega}'\tilde{\omega}'(I_{\bar{r}} + I_e) - 2A\tilde{\omega}'I_{\bar{e}} + F$ is the translational generalized external force, where $F = \sum_{i=1}^{N_p}(F_i)$ is the equivalent total force acting on the body whereas

$f_\theta(q_e, \dot{q}_e, \omega', A) = (I_{\bar{r}} + I_{\bar{e}})A^T f_b / \rho + \tilde{\omega}'(I_{\bar{r}\bar{r}} + I_{\bar{r}\bar{e}} + I_{\bar{e}\bar{r}} + I_{\bar{e}\bar{e}})\omega' + 2(I_{\bar{e}\bar{r}} + I_{\bar{e}\bar{e}})^T \omega' + T'$

is the generalized moment related to the rotation, where $T' = \sum_{i=1}^{N}(\tilde{r}_{ei}' A^T F_i + T_i'^T)$.

$f_{q_e}(q_e, \dot{q}_e, \omega', A) = -Kq_e + (AI_N)^T f_b / \rho + (I_{\bar{r}\tilde{\omega}'N} + I_{\bar{e}\tilde{\omega}'N})^T \omega' - 2I_{\bar{e}N}^T \omega' + W'$ is the generalized elastic force, where $W' = \sum_{i=1}^{N_p}[(AN)^T F_i]$.

2.2 Equation of Motion for a Flexible Multi-body System

A flexible multi-body system is composed of a series of interconnected bodies. These bodies can be either flexible or rigid. They are connected through joints, such as the prismatic joint and the revolute joint. The equation of motion for any single flexible body in the flexible multi-body system can be expressed by Eq.3.20 as follows:

$$\left(M^i \ddot{q}^i - f^i\right)^T \delta q^i = 0 \tag{2.34}$$

where $i = 1, 2, \cdots, n_b$, n_b is the number of bodies, M^i is the mass matrix for the ith body in the flexible multi-body system, $q^i = \{R_i^T \quad \Pi_i'^T \quad q_{ei}^T\}^T$ is the generalized coordinates, and

$$f^i = \begin{Bmatrix} f_R^i \\ f_\theta^i \\ f_q^i \end{Bmatrix} \text{ is the generalized force term.}$$

These equations can be combined into a single matrix equation as follows:

$$\left(\begin{bmatrix} M^1 & & & & \\ & M^2 & & & 0 \\ & & \ddots & & \\ & & & M^i & \\ & 0 & & & \ddots \\ & & & & & M^{n_b} \end{bmatrix} \begin{Bmatrix} \ddot{q}^1 \\ \ddot{q}^2 \\ \vdots \\ \ddot{q}^i \\ \vdots \\ \ddot{q}^{n_b} \end{Bmatrix} - \begin{Bmatrix} f^1 \\ f^2 \\ \vdots \\ f^i \\ \vdots \\ f^{n_b} \end{Bmatrix}\right)^T \begin{Bmatrix} \delta q^1 \\ \delta q^2 \\ \vdots \\ \delta q^i \\ \vdots \\ \delta q^{n_b} \end{Bmatrix} = 0 \tag{2.35}$$

which can be collectively written as:

$$\left(M\ddot{q} - f\right)^T \delta q = 0 \tag{2.36}$$

where $q = \{R_1^T \quad \Pi_1^T \quad q_{e1}^T \quad R_2^T \quad \Pi_2^T \quad q_{e2}^T \quad \cdots \quad R_{n_b}^T \quad \Pi_{n_b}^T \quad q_{en_b}^T\}^T$ is the system generalized coordinate, the mass matrix M and the generalized force f are given as

$$M = \begin{bmatrix} M^1 & & & & \\ & M^2 & & & 0 \\ & & \ddots & & \\ & & & M^i & \\ & 0 & & & \ddots \\ & & & & & M^{n_b} \end{bmatrix}, \text{ and } f = \begin{Bmatrix} f^1 \\ f^2 \\ \vdots \\ f^i \\ \vdots \\ f^{n_b} \end{Bmatrix}. \tag{2.37}$$

Since the bodies in a flexible multi-body system are connected by joints or force elements, they cannot move freely due to the constraints. The kinematic constraint conditions that

describe the mechanical joint and the prescribed motion trajectories can be defined as a set of m algebraic relationships in terms of the system coordinates and time as follows:

$$C(t,q) = 0 \tag{2.38}$$

Note that Eq. 2.38 defines the holonomic constraints, which are the ones that will be considered in this study. For the workless constraints, the virtual work done by the constraints is as follows:

$$C_q(t,q)\delta q = 0 \tag{2.39}$$

where C_q is the constraint Jacobian matrix, defined as

$$C_q = \frac{\partial C}{\partial q} = \begin{bmatrix} \dfrac{\partial C_1}{\partial q_1} & \dfrac{\partial C_1}{\partial q_2} & \cdots & \dfrac{\partial C_1}{\partial q_n} \\ \dfrac{\partial C_2}{\partial q_1} & \dfrac{\partial C_2}{\partial q_2} & \cdots & \dfrac{\partial C_2}{\partial q_n} \\ \vdots & \vdots & \ddots & \vdots \\ \dfrac{\partial C_{nc}}{\partial q_1} & \dfrac{\partial C_{nc}}{\partial q_2} & \cdots & \dfrac{\partial C_{nc}}{\partial q_n} \end{bmatrix}_{m \times n} \tag{2.40}$$

The number of rows of the constraint Jacobian matrix in Eq. 2.40 is equal to that of the constraint equations m, and the number of columns is equal to that of the generalized system coordinates n.

With the help of Lagrange Multiplier vector, λ, one can add Eq. 2.38 into the total virtual equation Eq. 2.36 to form a single equation as follows:

$$(M\ddot{q} - f)^T \delta q + \lambda^T C_q \delta q = 0 \tag{2.41}$$

Rewriting the above equation, one has:

$$(M\ddot{q} - f)^T \delta q + \left[(\lambda^T C_q)^T \right]^T \delta q = (M\ddot{q} - f + C_q^T \lambda)^T \delta q = 0 \tag{2.42}$$

Since δq is an arbitrary admissible displacement vector, one has:

$$M\ddot{q} - f + C_q^T \lambda = 0 \tag{2.43}$$

The constraints on the velocity vectors due to joint conditions can also obtained by differentiating the displacement constraints with respect to time as:

$$C_q \dot{q} + C_t = 0 \tag{2.44}$$

After differentiating it with respect to time once more and rearranging the terms, one has a second order differential equation as:

$$C_{qt}\dot{q} + (C_q\dot{q})_{,q}\dot{q} + C_q\ddot{q} + C_{tt} + C_{tq}\dot{q} = 0 \tag{2.45}$$

Since $C_{tq} = C_{qt}$ one has:

$$C_q\ddot{q} = -(C_q\dot{q})_{,q}\dot{q} - 2C_{qt}\dot{q} - C_{tt} \equiv C_{qq} \tag{2.46}$$

which can be written as:

$$\begin{bmatrix} C_{q^1} & C_{q^2} & \cdots & C_{q^{n_b}} \end{bmatrix} \begin{bmatrix} \ddot{q}^1 \\ \ddot{q}^2 \\ \vdots \\ \ddot{q}^{n_b} \end{bmatrix} = C_{qq} \tag{2.47}$$

Combining Eqs. 2.43 and 2.47 to form a matrix equation:

$$\begin{bmatrix} M^1 & 0 & \cdots & 0 & C_{q^1}^T \\ 0 & M^2 & \cdots & 0 & C_{q^2}^T \\ \vdots & \vdots & \ddots & \vdots & \vdots \\ 0 & 0 & \cdots & M^{n_b} & C_{q^{n_b}}^T \\ C_{q^1} & C_{q^2} & \cdots & C_{q^{n_b}} & 0 \end{bmatrix} \begin{bmatrix} \ddot{q}^1 \\ \ddot{q}^2 \\ \vdots \\ \ddot{q}^{n_b} \\ \lambda \end{bmatrix} = \begin{Bmatrix} f^1 \\ f^2 \\ \vdots \\ f^{n_b} \\ C_{qq} \end{Bmatrix} \tag{2.48}$$

which can be simplified as:

$$\begin{bmatrix} M & C_q^T \\ C_q & 0 \end{bmatrix} \begin{Bmatrix} \ddot{q} \\ \lambda \end{Bmatrix} = \begin{Bmatrix} f \\ C_{qq} \end{Bmatrix} \tag{2.49}$$

which is subjected to the displacement constraint $C(t,q) = 0$ and velocity constraint $C_q\dot{q} + C_t = 0$, where M and f are defined in Eq. 2.37.

The above equations are a combination of differential as well as algebraic equations, which are called Differential Algebraic Equations (DAEs). The analytical solutions of DAEs are difficult to obtain because they are highly nonlinear. Furthermore, DAEs cannot be integrated directly like the ordinary differential equation (ODEs) due to the presence of the Lagrange multipliers. Hence, it is necessary to find a numerical method which is suitable to solve the highly nonlinear DAEs accurately and efficiently. Chapter 3 introduces a few available numerical algorithms to solve these DAEs in detail. In addition, the projection method with the constraints correction is proposed to deal with the constraint violation.

2.3 Equation of Motion for a Flexible Multi-body System Using Modal Coordinates

One challenge in the flexible multi-body dynamics is the numerical representation of the elastic deformation. Modal synthesis method has been widely used for structural dynamics. In this case, the elastic deformation can be represented by the linear combination of finite number of mode [31]. Generally speaking, the number of unknowns in the elastic nodal vector, q_e, can be very large for a complex structure. To simplify the computation, the q_e is often spanned in terms of the given mode shapes as

$$q_e = \Psi a = \sum_{i=1}^{Nm} \Psi_i a_i \tag{2.50}$$

where Ψ the modal matrix, is made of the given mode shapes. a is the amplitude coefficients of those mode shapes. The latter is called the modal coordinates. The modal coordinates measure the contribution of the corresponding mode shape to the total elastic deformation. It can be seen from Eq. 2.50 that the DOFs of the elastic nodal vector, q_e are equal to the number of mode shapes.

The velocity and the acceleration of the elastic deformation are then obtained as

$$\dot{q}_e = \Psi \dot{a} \tag{2.51}$$

$$\ddot{q}_e = \Psi \ddot{a} \tag{2.52}$$

Thus, the degrees of freedom of a single flexible body can be written in terms of modal coordinates as:

$$q = \begin{Bmatrix} R \\ \Pi' \\ q_e \end{Bmatrix} = I_\Psi \begin{Bmatrix} R \\ \Pi' \\ a \end{Bmatrix} = I_\Psi q_a \tag{2.53}$$

where $I_\Psi = \begin{bmatrix} I & 0 & 0 \\ 0 & I & 0 \\ 0 & 0 & \Psi \end{bmatrix}$, $q_a = \begin{Bmatrix} R \\ \Pi' \\ a \end{Bmatrix}$.

The virtual work equation (Eq. 2.36), $(M\ddot{q} - f)^T \delta q = 0$, can then be recast as:

$$(MI_\Psi \ddot{q}_a - f)^T I_\Psi \delta q_a = [I_\Psi^T (MI_\Psi \ddot{q}_a - f)]^T \delta q_a = (I_\Psi^T MI_\Psi \ddot{q}_a - I_\Psi^T f)^T \delta q_a = 0 \tag{2.54}$$

The above equation yields a simplified equation of motion as follows:

$$M_{\Psi\Psi} \ddot{q}_a = f_\Psi \tag{2.55}$$

where

$$M_{\Psi\Psi} = I_{\Psi}{}^{T} M I_{\Psi}$$

$$= \begin{bmatrix} M_{RR} & M_{R\theta} & M_{Rq}\Psi \\ M_{\theta R} & M_{\theta\theta} & M_{\theta q}\Psi \\ \Psi^{T}M_{qR} & \Psi^{T}M_{q\theta} & \Psi^{T}M_{qq}\Psi \end{bmatrix} \equiv \begin{bmatrix} M_{RR} & M_{R\theta}(a,A) & M_{Ra}(A) \\ M_{\theta R}(a,A) & M_{\theta\theta}(a) & M_{\theta a}(a) \\ M_{aR}(A) & M_{a\theta}(a) & M_{aa} \end{bmatrix}$$ (2.56)

and

$$f_{\Psi} = I_{\Psi}^{T}f = \begin{Bmatrix} f_{R} \\ f_{\theta} \\ \Psi^{T}f_{q_{e}} \end{Bmatrix} \equiv \begin{Bmatrix} f_{R}(a,\dot{a},\omega',A) \\ f_{\theta}(a,\dot{a},\omega',A) \\ f_{a}(a,\dot{a},\omega',A) \end{Bmatrix}$$ (2.57)

Specifically, one can calculate the components of the mass matrix and the force vector based on Eqs. 2.30 and 2.31. They are as follows:

$$M_{\Psi\Psi} = \begin{bmatrix} mI_{3} & -A(I_{\tilde{r}'} + I_{\tilde{e}}) & AI_{N}\Psi \\ & -(I_{\tilde{r}\tilde{r}} + I_{\tilde{r}\tilde{e}} + I_{\tilde{e}\tilde{r}} + I_{\tilde{e}\tilde{e}}) & I_{\tilde{r}N}\Psi + I_{\tilde{e}N}\Psi \\ & sym & \Psi^{T}I_{N^{T}N}\Psi \end{bmatrix}$$ (2.58)

and

$$f_{\Psi} = \begin{Bmatrix} Vf_{b} - A\tilde{\omega}'\tilde{\omega}'(I_{r'} + I_{e}) - 2A\tilde{\omega}'I_{\dot{e}} + \mathbf{F} \\ (I_{\tilde{r}'} + I_{\tilde{e}})A^{T}f_{b}/\rho + \tilde{\omega}'(I_{\tilde{r}\tilde{r}} + I_{\tilde{r}\tilde{e}} + I_{\tilde{e}\tilde{r}} + I_{\tilde{e}\tilde{e}})\omega' + 2(I_{\tilde{e}\tilde{r}} + I_{\tilde{e}\tilde{e}})^{T}\omega' + T' \\ -\Psi^{T}K\Psi\Psi + (AI_{N}\Psi)^{T}f_{b}/\rho + (I_{\tilde{r}\tilde{\omega}'N}\Psi + I_{\tilde{e}\tilde{\omega}'N}\Psi)^{T}\omega' - 2\Psi^{T}I_{\dot{e}N}^{T}\omega' + \Psi^{T}W' \end{Bmatrix}$$ (2.59)

where F, T', W' are defined in Eq. 2.27.

Notice that if the eigenvectors are selected to form Ψ from the results of modal analysis of the finite element method, the term $\Psi^{T}K\Psi$, becomes a diagonal matrix made of the corresponding eigenvalues, i.e., $\Psi^{T}K\Psi \equiv \Lambda$. As a result, the stiffness matrix K is not required to be explicitly known in dynamic analysis, as soon as the eigenvalues become available to form Λ. This simplification can certainly improve the computational efficiency. However, the major advantage of the modal synthesis method stems from the fact that it can alleviate the cumbersome computation of the many integrals present in the mass matrix and in the force vector. The corresponding integration process is introduced in detail in Chapter 3.

2.4 Equation of Motion for a Rigid Multi-body System

A rigid body in a multi-body system can translate and rotate, but it cannot change its shape, i.e., the distance between any two arbitrary points in a rigid body is assumed unchanged during its motion. This assumption is an approximation to reality since no component is perfectly rigid. However, for a vast number of applications, this is a sufficient assumption that simplifies the modeling of mechanical systems. A rigid multi-body system can be treated as a special case of a flexible multi-body system. In this case, the elastic deformation is set to be zero in the equation of motion for a flexible body. Similarly, the equation of motion for a constrained rigid multi-body system can be obtained directly by eliminating the elastic displacement in the equation of motion for a flexible multi-body system. Therefore, Eq. 2.49 is reduced to:

$$
\begin{bmatrix} M & C_{,q}^{T} \\ C_{,q} & 0 \end{bmatrix} \begin{Bmatrix} \ddot{q} \\ \lambda \end{Bmatrix} = \begin{Bmatrix} f \\ C_{,qq} \end{Bmatrix}
$$

where $q = \begin{Bmatrix} R_1^T & \Pi_1'^T & R_2^T & \Pi_2'^T & \cdots & R_{n_b}^T & \Pi_{n_b}'^T \end{Bmatrix}^T$ is the system generalized coordinates, which are not totally independent because of the constraints in Eq. 2.38. In this case, the mass matrix and the force vector are given by

$$
M = \begin{bmatrix} M^1 & 0 & 0 & 0 \\ 0 & M^2 & 0 & 0 \\ 0 & 0 & \ddots & 0 \\ 0 & 0 & 0 & M^{n_b} \end{bmatrix}, \text{ and } f = \begin{Bmatrix} f^1 \\ f^2 \\ \vdots \\ f^{n_b} \end{Bmatrix}
$$

Specifically, each of the mass sub-matrix, M^i, and the force vector, f^i can be spanned, respectively, as

$$
M^i = \begin{bmatrix} m^i & -(AI_{\bar{r}})^i \\ sym & -(I_{\bar{r}\bar{r}})^i \end{bmatrix} \equiv \begin{bmatrix} M_{RR}^i & M_{R\theta}^i \\ M_{\theta R}^i & M_{\theta\theta}^i \end{bmatrix} \text{ and } f^i = \begin{Bmatrix} (Vf_b - A\tilde{\omega}'\tilde{\omega}'I_{\bar{r}} + F)^i \\ (I_{\bar{r}}A^T f_b / \rho + \tilde{\omega}'I_{\bar{r}\bar{r}}\omega' + T')^i \end{Bmatrix} \equiv \begin{Bmatrix} f_R^i \\ f_\theta^i \end{Bmatrix}
$$

$i = 1, 2, \cdots, n_b$, the point load $F = \sum_{i=1}^{N} (F_i)$, and point moment $T' = \sum_{i=1}^{N} (\bar{r}_{ei}' A^T F_i + T_i')$.

CHAPTER 3

NUMERICAL METHODS FOR DYNAMIC ANALYSIS OF

A FLEXIBLE MULTI-BODY SYSTEM

It was shown in Chapter 2 that the equation of motion for a flexible multi-body system can be formed as a set of second order differential algebraic equations (DAEs). This set of DAEs is normally highly nonlinear and time dependent. Their analytical solutions are difficult to obtain. Hence, it is critical to find a proper numerical algorithm to solve the DAEs accurately and efficiently. Special attention needs to be placed on the transformation matrix and the integrals in the generalized mass matrix and the generalized force vector in DAEs. These terms are functions of the system generalized coordinates and, as a result, are time-dependent. Computing these terms efficiently presents a challenge in solving the DAEs pertaining to the multi-body dynamic system. This chapter will discuss some numerical strategies for the flexible multi-body dynamics.

The procedure to compute the integrals in the generalized mass matrix and the generalized force vector is first discussed in Section 3.1. Two different ways to deal with the integrals in this dissertation are called In-Loop calculation and Pre-ODE calculation. Then, the transformation matrix is discussed in Section 3.2. Five approaches are considered including Direction Cosines, Euler angles, Rodriguez parameters, Euler parameters and Matrix Exponential function. The relationships between these different approaches are derived in Section 3.3. Two commonly used numerical algorithms, the coordinate partitioning method and the projection method, are introduced in Sections 3.4 and 3.5, respectively. The optimization algorithm is proposed in the projection method to make sure the displacement and velocity constraints are satisfied. These two methods convert the DAEs pertaining to multi-body dynamics into ODEs for numerical integration. The coordinate partitioning method will identify the independent coordinates based upon the constraint equations, and only those independent coordinates will be kept in the final form of the ODEs. On the other hand, the projection method will keep the entire set of the system generalized coordinates in its final form of ODEs.

3.1 Integrals in Mass Matrix and Force Vector

The inertia integrals in the generalized mass matrix and the generalized force vector in the equation of motion involve the elastic displacement field, e, angular velocity, ω', and the position vector, r'. Those terms are described in reference to the body-fixed coordinate. Since e and ω' are time dependents and unknowns before the DAEs are solved, the update of the values of these integrals at every time instant becomes very cumbersome in a time-marching scheme. This section investigates two different approaches on computing these integrals. The first is called "In-Loop" method, in which these integrals are treated as time-dependent and evaluated at each time step called by the ODE solver. The second is called "Pre-ODE" method. This method uses the mode superposition technique to describe the elastic displacement in terms of the modal coordinate explicitly. Hence, the spatial integrals become time-invariant and to be integrated before the ODE solver calls. It implies that the integrals can be calculated only once as constants.

The integral term I_e, relating to the elastic displacement, is be used as an example in this subsection to demonstrate the use of the "In-Loop" and the "Pre-ODE" methods for the integration. All integrals appearing in the equation of motion can be found in the Appendices. Particularly, Appendices 1 and 2 pertain to the beam elements and Appendix 3 to the spatial triangular element.

3.1.1 In-Loop Integrals Calculation

In the framework of finite element analysis, the flexible displacement e_i defined in each element is approximated as:

$$e_i = N_i q_{ei} \tag{3.1}$$

where N is the matrix of shape functions, which is a space-dependent, though time-independent variable. The vector q_{ei} contains the nodal values of the elastic displacement. For an arbitrary element, one has:

$$I_{e_i} \equiv \int_{\Omega_i} \rho e_i dv = \int_{\Omega_i} \rho N_i q_{ei} dv = \int_{\Omega_i} \rho N_i dv q_{ei} \equiv I_{N_i} q_{ei}.$$

Summing up all the elements, one has:

$$I_e = \sum_{i=1}^{N_E} I_{e_i} = \sum_{i=1}^{N_E} \int_{\Omega_i} \rho e_i dv = \sum_{i=1}^{N_E} I_{N_i} q_{ei} \tag{3.2}$$

where N_E is the total number of elements. It should be noted that the formulation of I_{N_i} is the same for the same type of element.

In the above equation, the elastic nodal displacements q_{ei} are calculated based on the coefficients of the mode shapes,

$$q_{ei} = \psi_i a .$$

At each time step, the modal coordinates a are unknown until the ODEs have been solved. Therefore, the integrals, such as I_{e_i} must be placed in the loop of the ODE subroutine.

3.1.2 Pre-ODE Integrals Calculation

This section will present a process that can move the modal coordinates out of the integration route. As a result, the spatial integrals can be integrated prior to the time marching procedure. The detailed process is discussed below.

The integral term I_e in Eq. 3.2 is a linear function of the elastic displacement, q_{ei}, due to I_{N_i} is the constant for the same type of element. However, the summation of the term, $I_{N_i} q_e^i$, has to be done at any time step over N_E, the total number of elements. An alternative is to approximate the nodal displacement vector in terms of the linear combination of the mode shapes ψ as:

$$q_e = \psi a = \sum_{k=1}^{N_m} \psi_k a_k = \sum_{k=1}^{N_m} a_k N \psi_k \tag{3.3}$$

where N_m is the number of mode shapes used for the approximation, ψ is the mode shape matrix, and a_k is the corresponding modal coordinate. By doing so, for an arbitrary element i, one has:

$$\int_{\Omega_i} \rho e_i dv = \sum_{k=1}^{N_m} a_k \int_{\Omega_i} N \psi_{ik} dv = \sum_{k=1}^{N_m} a_k I_N \psi_{ik} \tag{3.4}$$

where ψ_{ik} is the kth mode shape, evaluated at the corresponding i^{th} element.

Consequently, the integral I_e of concern can be calculated as follows:

$$I_e = \int_\Omega \rho e dv = \sum_{i=1}^{N_E} \int_{\Omega_i} \rho e_i dv = \sum_{i=1}^{N_E} \sum_{k=1}^{N_m} a_k I_N \psi_{ik} = \sum_{k=1}^{N_m} a_k \cdot \sum_{i=1}^{N_E} I_N \psi_{ik} = \sum_{k=1}^{N_m} a_k \cdot I_{N\psi} \quad (3.5)$$

where $I_{N\psi} = \sum_{i=1}^{N_E} I_N \psi_{ik}$ is a matrix, which dimension is 3 by N_m. The mode shapes can be

obtained from any commercial finite element code prior to the dynamic analysis. Thus,

$I_{N\psi}$, a matrix can be evaluated and stored as an input data set, ready for dynamic analysis.

Multiplication and addition of $3 \times N_m$ times is required by Eq. 3.5, which is much less

than that of $27 \times N_E$. Thus, it is expected that numerically the "Pre-ODE" integration will

be faster than the "In-the-Loop" integration. Furthermore, the "Pre-ODE" integrated

matrix, $I_{N\psi}$, can be used repeatedly to compute other integrals. For example, the term $I_{\dot{e}}$

can be conveniently computed as

$$I_{\dot{e}} = \int_\Omega \rho \dot{e} dv = \sum_{i=1}^{N_E} \int_{\Omega_i} \rho \dot{e}_i dv = \sum_{i=1}^{N_E} \sum_{k=1}^{Nm} \dot{a}_k I_N \psi_{ik} = \sum_{k=1}^{Nm} \dot{a}_k \sum_{i=1}^{N_E} I_N \psi_{ik} = \sum_{k=1}^{Nm} \dot{a}_k I_{N\psi} \quad (3.6)$$

This matter represents another aspect of time-saving comparing to the "In-the-Loop"

integration in dynamic analysis. Furthermore, due to the nature of a skew matrix, the

integral $I_{\tilde{e}}$, can be directly evaluated from I_e. After careful examination, only 6 out of 19

integrals appearing in the equation of motion for a flexible body required "Pre-ODE"

integration. The six integrals required by the "Pre-ODE" integration and their extension

are shown in Table 3.1. The corresponding integrals required by "In-Loop" integration

are also shown in the same table for comparison. It should be noted that $I_{r'}$ and $I_{\tilde{r}}$ in

Table 3.1 become zero when the origin of the body-fixed coordinate system is located at

the center of gravity (CG) of the body. However, it is not true for the elastic term I_e even

though the local origin is placed at CG.

The planar slider-crank mechanism is used to demonstrate the accuracy and

efficiency of "Pre-ODE" method by comparing to "In-Loop" method. For the craft

dynamics, only "Pre-ODE" method is used.

The detail integral calculation can be found in the Appendices.

Table 3.1 "In-Loop" and "Pre-ODE" Integrals Calculation

"In-the-Loop" of ODE Integration		"Pre-ODE" Integration		
Terms	Dimension	Terms	Dimension	Direct Extension
K	$N_{dof} \times N_{dof}$	$\psi^T K \psi$	$N_m \times N_m$	Eigenvalues, Λ
I_N	$3 \times N_{dof}$	$I_{N\psi}$	$3 \times N_m$	$I_e, I_{\dot{e}}, I_{\tilde{e}}$
$I_{r'}, I_{\tilde{r}}$	$3 \times 1, 3 \times 3$	$I_{r'}$	$3 \times 1, 3 \times 3$	$I_{\tilde{r}}$
$I_{\tilde{r}r'}$	3×3	$I_{\tilde{r}r'}$	3×3	
$I_{\tilde{e}r'}$	3×3	$I_{\tilde{e}r'}$	$3 \times N_m$	$I_{\tilde{r}\tilde{e}}, I_{\tilde{e}\tilde{r}}, I_{\tilde{r}\omega'N\psi}, I_{\tilde{r}N\psi}$
$I_{\tilde{e}\tilde{e}}$	3×3	$I_{\tilde{e}\tilde{e}}$	$N_m \times N_m$	$I_{\tilde{e}\tilde{e}}, I_{\tilde{e}\omega'N\psi}$
$I_{\tilde{e}N}$	$3 \times N_{dof}$	$I_{\tilde{e}N\psi}$	$3 \times N_m$	
$I_{N^T N}$	$N_{dof} \times N_{dof}$	$I_{\psi^T N^T N\psi}$	$N_m \times N_m$	Identity matrix I
$I_e, I_{\tilde{e}}$	$3 \times 1, 3 \times 3$	See $I_{N\psi}$		
$I_{\dot{e}}$	3×1	$I_{N\psi}$		
$I_{\tilde{e}r'}, I_{\tilde{r}\tilde{e}}$	3×3	$I_{N\psi}$		
$I_{\tilde{e}\tilde{e}}$	3×3			
$I_{\tilde{r}\omega'N}$	$3 \times N_{dof}$			
$I_{\tilde{e}\omega'N}$	$3 \times N_{dof}$			
$I_{\tilde{r}N}$	$3 \times N_{dof}$			
$I_{\tilde{e}N}$	$3 \times N_{dof}$			

3.2 Transformation Matrix

The configuration of a body can be described by translation and rotation. The translational degrees of freedom (DOFs) can be expressed as a vector. However, it can't be extended to rotation. Consequently, the angular displacement can't be directly

integrated from the angular velocity. This poses a great challenge with respect to the computation of the transformation matrix for dynamic analysis of a body in space.

Many sets of parameters have been discussed in the literature [33,87] to describe the configuration change of a body subjected to rotary motion. They include direction cosines, Euler angles, Euler-Rodriguez parameters, Euler parameters and matrix exponential. The latter three are based upon the Euler theorem. All of these parameters can be used to describe the transformation matrix. These sets of parameters and the associated transformation matrix are discussed one-by-one in the following subsections.

3.2.1 Direction Cosines

The relationship between the components of the same vector projected onto different coordinate systems is used to define the transformation matrix A in this approach. Let two coordinate systems, $(\vec{e}_1 \quad \vec{e}_2 \quad \vec{e}_3)$ and $(\vec{e}_1' \quad \vec{e}_2' \quad \vec{e}_3')$ share the same origin as shown in Fig. 3.1. The same vector, $\vec{u}$, is projected onto these two coordinate systems with different components. The coordinate system $(\vec{e}_1 \quad \vec{e}_2 \quad \vec{e}_3)$ can be viewed as the reference coordinate system, while $(\vec{e}_1' \quad \vec{e}_2' \quad \vec{e}_3')$ the body-fixed coordinate system. The vector in the body-fixed coordinate system can be expressed as:

$$\vec{u} = u_1'\vec{e}_1' + u_2'\vec{e}_2' + u_3'\vec{e}_3'$$

(3.7)

The same vector can be expressed with respect to the reference coordinate system as:

$$\vec{u} = u_1\vec{e}_1 + u_2\vec{e}_2 + u_3\vec{e}_3$$

(3.8)
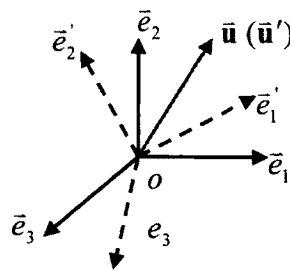
Figure 3.1 Rotations of the Coordinate Systems

Since it is the same vector viewed from different coordinate systems, the following relation is true:

$$u_1\bar{e}_1 + u_2\bar{e}_2 + u_3\bar{e}_3 = u_1'\bar{e}_1' + u_2'\bar{e}_2' + u_3'\bar{e}_3' \tag{3.9}$$

Taking the inner product of the above equation with respect to $\bar{e}_1$, one has an equation for u_1 in terms of u_1', u_2' and u_3' as:

$$u_1 = u_1'(\bar{e}_1' \cdot \bar{e}_1) + u_2'(\bar{e}_2' \cdot \bar{e}_1) + u_3'(\bar{e}_3' \cdot \bar{e}_1) \tag{3.10a}$$

Similarly, one can obtain the rest of the equations as:

$$u_2 = u_1'(\bar{e}_1' \cdot \bar{e}_2) + u_2'(\bar{e}_2' \cdot \bar{e}_2) + u_3'(\bar{e}_3' \cdot \bar{e}_2) \tag{3.10b}$$

$$u_3 = u_1'(\bar{e}_1' \cdot \bar{e}_3) + u_2'(\bar{e}_2' \cdot \bar{e}_3) + u_3'(\bar{e}_3' \cdot \bar{e}_3) \tag{3.10c}$$

In short, the equations can be expressed in a matrix format

$$\mathbf{u} = A\mathbf{u}' \tag{3.11}$$

where the transformation matrix, A is defined in terms of the direction cosine:

$$A = [a_{ij}] = \begin{bmatrix} a_{11} & a_{21} & a_{31} \\ a_{12} & a_{22} & a_{32} \\ a_{13} & a_{23} & a_{33} \end{bmatrix} \tag{3.12}$$

where $a_{ij} = \bar{e}_i' \cdot \bar{e}_j = \cos\theta_{ij}$, θ_{ij} is the angle between the axes $\bar{e}_i'$ and $\bar{e}_j$, $i, j = 1, 2, 3$

Therefore, in order to compute the transformation matrix A in the form of Eq. 3.12, one needs to know the angles between the axes or the relative directions of the body-fixed and the reference coordinate systems.

3.2.2 Euler Angles

The direction cosines are rarely used in describing the rotary motion of a body in space due to the difficulty in finding the angles between axes of the reference and the body-fixed coordinate systems. As an alternative, Euler angles describe the rotary motion of a body as a result of three successive rotations about known axes. Specifically, the body is first rotated by ϕ with respect to the $\bar{e}_3$ axis, then by θ with respect to the new $\bar{e}_1^1$ axis, and finally, by ψ with respect to the new $\bar{e}_3^2$ axis. The rotation scheme is shown in Fig. 3.2. It should be noted that the sequence of rotations is critical because the rotation is not commutative in 3D space.
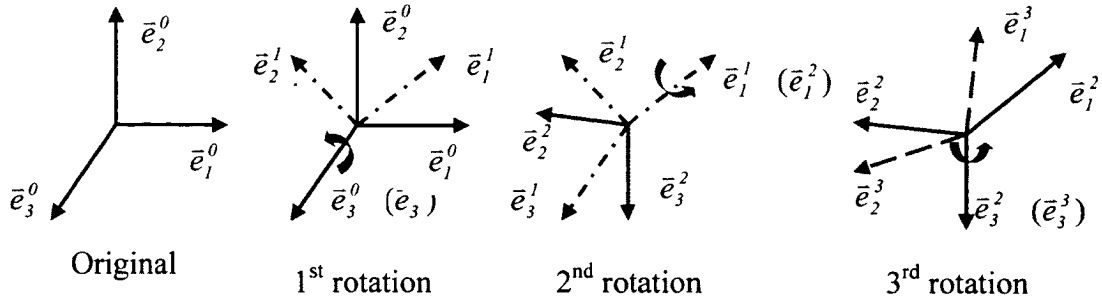
Figure 3.2 Rotations by Euler Angles in Sequence

After three successive rotations, the position vector in the body-fixed coordinate is now projected to the original reference coordinate system as, based upon Eq. 3.12,

$$r = A^1 A^2 A^3 r' = Ar' \tag{3.13}$$

where $A^1 = \begin{bmatrix} \cos\phi & -\sin\phi & 0 \\ \sin\phi & \cos\varphi & 0 \\ 0 & 0 & 1 \end{bmatrix}, A^2 = \begin{bmatrix} 1 & 0 & 0 \\ 0 & \cos\theta & -\sin\theta \\ 0 & \sin\theta & \cos\theta \end{bmatrix}, A^3 = \begin{bmatrix} \cos\psi & -\sin\psi & 0 \\ \sin\psi & \cos\psi & 0 \\ 0 & 0 & 1 \end{bmatrix}.$

The transformation matrix A can be calculated as follows:

$$
\begin{aligned}
A = A^1 A^2 A^3 &= \begin{bmatrix} \cos\phi & -\sin\phi & 0 \\ \sin\phi & \cos\phi & 0 \\ 0 & 0 & 1 \end{bmatrix} \cdot \begin{bmatrix} \cos\psi & -\sin\psi & 0 \\ \cos\theta\sin\psi & \cos\theta\cos\psi & -\sin\theta \\ \sin\theta\sin\psi & \sin\theta\cos\psi & \cos\theta \end{bmatrix} \\
&= \begin{bmatrix} \cos\phi\cos\psi - \sin\phi\cos\theta\sin\psi & -\cos\phi\sin\psi - \sin\phi\cos\theta\cos\psi & \sin\phi\sin\theta \\ \sin\phi\cos\psi + \cos\phi\cos\theta\cos\psi & -\sin\phi\sin\psi + \cos\phi\cos\theta\cos\psi & -\sin\theta\cos\phi \\ \sin\theta\sin\psi & \sin\theta\cos\psi & \cos\theta \end{bmatrix}
\end{aligned} \tag{3.14}
$$

The transformation matrix A can now be evaluated in terms of ϕ, θ, ψ, which are called the Euler angles.

3.2.3 Rodriguez Parameters

The Euler theorem states that a body's rotation is a result of a rotation with respect to a certain axis. Therefore, the new position of a fixed body vector can be traced if the axis of the rotation and the amount of the angular displacement are known. The set of Rodriguez Parameters is one that follows the Euler Theorem.

Let a body be rotated about the unit rotation axis, $c = \begin{pmatrix} c_1 & c_2 & c_3 \end{pmatrix}^T$ with an angular displacement χ. A vector which is fixed on the body is then rotated along with

the body. The vector is initially viewed from the ground or the reference coordinate system as $\boldsymbol{u}' = \begin{pmatrix} u_1' & u_2' & u_3' \end{pmatrix}^T$. After rotation, it is viewed as $\boldsymbol{u} = \begin{pmatrix} u_1 & u_2 & u_3 \end{pmatrix}^T$ from the reference coordinate system. See Fig. 3.3.
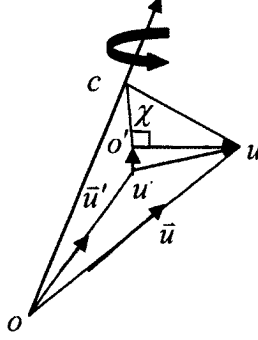
Figure 3.3 Rotation with respect to a Fixed Vector

After the rotation, the relationship between the initial and current vectors is given as:

$$\boldsymbol{u} = \boldsymbol{u}' + \vec{r}_{u'u} = \boldsymbol{u}' + \vec{r}_{u'o'} + \vec{r}_{o'u} \tag{3.15}$$

The vector, $\vec{r}_{o'u}$ is perpendicular to the rotation axis c and the vector $\boldsymbol{u}'$; hence, its unit direction is $\tilde{c}\boldsymbol{u}'/|\tilde{c}\boldsymbol{u}'|$ and its magnitude is $|\vec{r}_{cu}|\sin\chi = |\vec{r}_{cu'}|\sin\chi = |\tilde{c}\boldsymbol{u}'|\sin\chi$, so the vector can be written as:

$$\vec{r}_{o'u} = |\tilde{c}\boldsymbol{u}'|\sin\chi \cdot \tilde{c}\boldsymbol{u}'/|\tilde{c}\boldsymbol{u}'| = \sin\chi\tilde{c}\boldsymbol{u}' \tag{3.16}$$

The vector, $\vec{r}_{u'o'}$ is perpendicular to both the rotation axis c and the vector $\vec{r}_{o'u}$. Hence, its unit direction is $\tilde{c}(\tilde{c}\boldsymbol{u}')/|\tilde{c}\boldsymbol{u}'|$ and its magnitude is $|\vec{r}_{cu'}| - |\vec{r}_{cu'}|\cos\chi = |\tilde{c}\boldsymbol{u}'|(1-\cos\chi)$. As a result, the vector, $\vec{r}_{u'o'}$, can be written as:

$$\vec{r}_{u'o'} = |\tilde{c}\boldsymbol{u}'|(1-\cos\chi) \cdot \tilde{c}(\tilde{c}\boldsymbol{u}')/|\tilde{c}\boldsymbol{u}'| = (1-\cos\chi)\tilde{c}(\tilde{c}\boldsymbol{u}') \tag{3.17}$$

Substituting Eqs. 3.16 and 3.17 into Eq. 3.15, one has:

$$\boldsymbol{u} = \boldsymbol{u}' + (1-\cos\chi)\tilde{c}(\tilde{c}\boldsymbol{u}') + \sin\chi\tilde{c}\boldsymbol{u}' = [I + (1-\cos\chi)\tilde{c}\tilde{c} + \sin\chi\tilde{c}]\boldsymbol{u}' \tag{3.18}$$

The above equation yields a relation

$$\boldsymbol{u} = A\boldsymbol{u}' \tag{3.19}$$

where A is defined as:

$$A = I + (1-\cos\chi)\tilde{c}\tilde{c} + \sin\chi\tilde{c} \tag{3.20}$$

In detail, one has:

$$A = \begin{bmatrix} \cos\chi + (1-\cos\chi)c_1^2 & (1-\cos\chi)c_1c_2 - \sin\chi c_3 & (1-\cos\chi)c_1c_3 + \sin\chi c_2 \\ (1-\cos\chi)c_1c_2 + \sin\chi c_3 & \cos\chi + (1-\cos\chi)c_2^2 & (1-\cos\chi)c_2c_3 - \sin\chi c_1 \\ (1-\cos\chi)c_1c_3 - \sin\chi c_2 & (1-\cos\chi)c_2c_3 + \sin\chi c_1 & \cos\chi + (1-\cos\chi)c_3^2 \end{bmatrix} \quad (3.21)$$

It is not difficult to show that A is an orthogonal matrix. The above equation is called the Rodriguez formula. Let the vector of Rodriguez parameters be defined as:

$$\gamma = c\tan(\chi/2) = \{c_1\tan(\chi/2) \quad c_2\tan(\chi/2) \quad c_3\tan(\chi/2)\}^T = \{\gamma_1 \quad \gamma_2 \quad \gamma_3\}^T$$

$$\sin\chi = 2\sin(\chi/2)\cos(\chi/2) = 2\tan(\chi/2)\cos^2(\chi/2) = \frac{2\tan(\chi/2)}{\sec^2(\chi/2)} = \frac{2\tan(\chi/2)}{1+\tan^2(\chi/2)}.$$

Since $\gamma^T\gamma = c^Tc\tan^2(\chi/2) = \tan^2(\chi/2) = \gamma^2$, $\sin\chi = \frac{2\tan(\chi/2)}{1+\gamma^2}$

$$(1-\cos\chi) = 2\sin^2(\chi/2) = 2\tan^2(\chi/2)\cos^2(\chi/2) = \frac{2\tan^2(\chi/2)}{1+\tan^2(\chi/2)} = \frac{2\tan^2(\chi/2)}{1+\gamma^2}.$$

Eq. 3.20 can be rewritten as:

$$A = I + (1-\cos\chi)\tilde{c}\tilde{c} + \sin\chi\tilde{c} = I + \frac{2\tan^2(\chi/2)}{1+\gamma^2}\tilde{c}\tilde{c} + \frac{2\tan(\chi/2)}{1+\gamma^2}\tilde{c} \quad (3.22)$$

Since $\gamma = c\tan(\chi/2)$, one has $\tilde{\gamma} = \tilde{c}\tan(\chi/2)$. Therefore, the transformation matrix can be simplified as:

$$A = I + \frac{2}{1+\gamma^2}\tilde{\gamma}\tilde{\gamma} + \frac{2}{1+\gamma^2}\tilde{\gamma} \quad (3.23)$$

In detail, one has the transformation matrix in terms of Rodriguez parameters as:

$$A = \frac{1}{1+\gamma^2}\begin{bmatrix} 1+\gamma_1^2-\gamma_2^2-\gamma_3^2 & 2(\gamma_1\gamma_2-\gamma_3) & 2(\gamma_1\gamma_3+\gamma_2) \\ 2(\gamma_1\gamma_2+\gamma_3) & 1+\gamma_2^2-\gamma_1^2-\gamma_3^2 & 2(\gamma_2\gamma_3-\gamma_1) \\ 2(\gamma_1\gamma_3-\gamma_2) & 2(\gamma_2\gamma_3+\gamma_1) & 1+\gamma_3^2-\gamma_1^2-\gamma_2^2 \end{bmatrix} \quad (3.24)$$

3.2.4 Euler Parameters

In the proceeding section, the transformation matrix A is determined by the unit rotation axis, c and the angular displacement χ. The resultant matrix A is given

$$A = I + (1-\cos\chi)\tilde{c}\tilde{c} + \sin\chi\tilde{c} = \cos\chi I + (1-\cos\chi)(cc^T) + \sin\chi\tilde{c}$$
$$= (2\cos^2(\chi/2)-1)I + 2\sin^2(\chi/2)cc^T + 2\sin(\chi/2)\cos(\chi/2)\tilde{c}$$

Let $e_0 \equiv \cos(\chi/2), e = c\sin(\chi/2) \equiv \{e_1 \quad e_2 \quad e_3\}^T$, one has:

$$A = \left(2\cos^2(\chi/2) - 1\right)I + 2\sin(\chi/2)\cos(\chi/2)\tilde{c} + 2\sin^2(\chi/2)cc^T$$
$$= \left(2e_0^2 - 1\right)I + 2e_0\tilde{e} + 2ee^T$$

$$= \begin{bmatrix} 2e_0^2 + 2e_1^2 - 1 & -2e_0e_3 + 2e_1e_2 & 2e_0e_2 + 2e_1e_3 \\ 2e_0e_3 + 2e_1e_2 & 2e_0^2 + 2e_2^2 - 1 & -2e_0e_1 + 2e_2e_3 \\ -2e_0e_2 + 2e_1e_3 & 2e_0e_1 + 2e_2e_3 & 2e_0^2 + 2e_3^2 - 1 \end{bmatrix} \tag{3.25}$$

The above four parameters e_0, e_1, e_2, e_3 are called Euler parameters. They can be written in a vector form:

$$p = \{e_0 \quad e_1 \quad e_2 \quad e_3\}^T \tag{3.26}$$

The four Euler parameters are not independent. It is easy to get the following relationship between them:

$$p^T p = e_0^2 + e_1^2 + e_2^2 + e_3^2 = 1 \tag{3.27}$$

3.2.5 Matrix Exponential Function

According to the Rodriguez formula described in Section 3.2.3, the transformation matrix can be expressed as $A = I + (1 - \cos\chi)\tilde{c}\tilde{c} + \sin\chi\tilde{c}$ in which $\sin\chi$ and $\cos\chi$ can be expanded by Taylor series as:

$$\sin\chi = \chi - \chi^3/3! + \chi^5/5! - \cdots + (-1)^n \chi^{2n+1}/(2n+1)!.$$

$$\cos\chi = 1 - \chi^2/2! + \chi^4/4! - \cdots + (-1)^n \chi^{2n}/2n!.$$

The transformation matrix A then becomes

$$A = I + \left[\chi^2/2! - \chi^4/4! + \cdots - (-1)^n \chi^{2n}/2n!\right]\tilde{c}\tilde{c} + \chi - \chi^3/3! + \chi^5/5! - \cdots + (-1)^n \chi^{2n+1}/(2n+1)!\tilde{c} \tag{3.28}$$

It can be proved that $(\tilde{c})^{2n-1} = (-1)^{n-1}\tilde{c}$ inductively. Hence, one has:

$$A = I + \chi\tilde{c} + \frac{\chi^2}{2!}(\tilde{c})^2 + \frac{\chi^3}{3!}(\tilde{c})^3 + \cdots + \frac{\chi^n}{n!}(\tilde{c})^n = \sum_{k=0}^{\infty} \frac{(\chi\tilde{c})^k}{k!} = exp(\chi\tilde{c}) \tag{3.29}$$

One may consider a finite rotation through angle θ about the axis is a summation of an infinite number of small successive rotations. Assuming that a body is rotated about a unit vector a with an infinitely small angle $\Delta\theta$, one has the first order change of the transformation matrix, ΔA due to such a small rotation is given by:

$$\Delta A = I + (1 - \cos \Delta\theta)\tilde{a}\tilde{a} + \sin \Delta\theta\tilde{a} \approx I + \Delta\theta\tilde{a} = \exp(\Delta\theta\tilde{a}) \tag{3.30}$$

If the vector a is expressed in the body-fixed coordinate system, the new transformation matrix after such a small rotation becomes:

$$A_{n+1} = A_n \cdot \Delta A \tag{3.31a}$$

On the other hand, if the vector a is expressed in the reference coordinate system, the relation becomes:

$$A_{n+1} = \Delta A \cdot A_n \tag{3.31b}$$

Approximating $\Delta\theta$ as θ/N where N is a large number, a rotation of θ about the axis may be represented as:

$$A = \left(I + \frac{A\theta}{N}\right)^N \approx e^{A\theta} \tag{3.32}$$

It can be seen that Euler's theorem essentially states that all rotations may be represented in this form.

3.3 Relationships between Different Expressions of Transformation Matrix

In the preceding section, it was shown that the orthogonal transformation matrix can be defined by different forms: direction cosines, Eq. 3.12, Euler angles, Eq. 3.14, Rodriguez formula, Eq. 3.21, Rodriguez parameters, Eq. 3.24, Euler parameters, Eq. 3.25 and an Exponential matrix, Eq. 3.29. However, these parameters are related to each other through the transformation matrix. The following subsections discuss the relationships between the different expressions.

3.3.1 Euler Angles from Transformation Matrix

Based upon the definition given in Eq. 3.14, the Euler angles can be obtained through the last row and the last column of the transformation matrix as

$$\theta = \cos^{-1}(a_{33}), \quad \phi = \cos^{-1}(-a_{23}/\sin\theta), \quad \psi = \cos^{-1}(a_{32}/\sin\theta).$$

It can be seen that the relation can become singular when $\theta = n\pi$. Thus, the Euler angles may not be uniquely determined from the known transformation matrix.

3.3.2 Rodriguez Formula from Transformation Matrix

Equation 3.21 can find the angle of rotation χ and unit vector $\mathbf{c}$ in the Rodriguez

formula in terms of the transformation matrix. These relations

$\chi = \cos^{-1}((trA - 1)/2)$, where $trA = a_{11} + a_{22} + a_{33}$, is the trace of the transformation

matrix A. and $c_1 = (a_{32} - a_{23})/(2\sin\chi), c_2 = (a_{13} - a_{31})/(2\sin\chi), c_3 = (a_{21} - a_{12})/(2\sin\chi)$

It can also be seen that the relation can become singular, if $\chi = n\pi$.

3.3.3 Rodriguez Parameters from Transformation Matrix

To find the Rodriguez parameters in Eq. 3.24, one has

$$\gamma_1 = -(a_{32} - a_{23})/4trA, \gamma_2 = -(a_{13} - a_{31})/4trA, \gamma_3 = -(a_{21} - a_{12})/4trA.$$

It can be seen that Rodriguez parameters can always be found uniquely from the given

transformation matrix under any circumstance.

3.3.4 Euler Parameters from Transformation Matrix

To find the Euler parameters in Eq. 3.25, one can add the diagonal term together

and apply Eq. 3.27 to find e_0 as:

$$e_0^2 = (trA + 1)/4.$$

Using the off-diagonal term, one find the other three as follows:

$$e_1 = (a_{32} - a_{23})/4e_0, e_2 = (a_{13} - a_{31})/4e_0, e_3 = (a_{21} - a_{12})/4e_0.$$

Note that $e_0 = 0$, for $\chi = n\pi$ in the above equations, cannot be used to calculate the Euler

parameters. However, Euler parameters can be uniquely determined according to the

diagonal term as:

$$e_0 = 0, e_1^2 = (1 + a_{11})/2, e_2^2 = (1 + a_{22})/2, e_3^2 = (1 + a_{33})/2.$$

The sign of e_1, e_2 and e_3 can be determined as either negative or positive at the same

time.

It can be seen that Euler parameters can be uniquely determined in any situation. Hence,

the Euler parameters will be used in this study to avoid singularity.

3.4 The Coordinate Partitioning Method

The derivation of the equation of motion for a flexible multi-body system has been given in Chapter 2 in detail. The resultant equation is a combination of differential and algebraic equations (DAEs). The equations of motion for a flexible multi-body system can be symbolically represented as:

$$\begin{bmatrix} M & C_q^T \\ C_q & 0 \end{bmatrix} \begin{Bmatrix} \ddot{q} \\ \lambda \end{Bmatrix} = \begin{Bmatrix} f \\ C_{qq} \end{Bmatrix} \tag{3.33}$$

where M is the generalized mass matrix, f is the general force vector, λ is the Lagrange multipliers and q is the system generalized coordinates. The components of q are not independent of each other, due to the kinematic constraints, $C(t,q) = 0$. The velocities and the accelerations of the system generalized coordinates should satisfy $C_q \dot{q} + C_t = 0$ and $C_{qq} = -\left(C_q \dot{q} \right)_{,q} \dot{q} - 2C_{qt} \dot{q} - C_{tt}$, respectively. The constraint Jacobian matrix, C_q, is the constraint Jacobian matrix, whose dimension is $m \times n$, where m is the number of total constraints, and n is the number of the system generalized coordinates.

These DAEs cannot be solved directly using the integration scheme suitable for the ordinary differential equation (ODE). The coordinate partitioning method [45, 87] is widely used by dividing the system generalized coordinates q into two parts: independent coordinates q_I, which equals the system degrees of freedom, and the dependent ones, q_d. In other words, the system generalized coordinates q can be written as:

$$q = \begin{Bmatrix} q_d \\ q_I \end{Bmatrix} \tag{3.34}$$

Let the nonlinear kinematic constraints be independent of each other, and their number is m. Thus, the Jacobian matrix, C_q has a full row rank, which can be rearranged in the following form:

$$C_q = \begin{bmatrix} C_{q_d} & \vdots & C_{q_I} \end{bmatrix} \tag{3.35}$$

Selection of q_d is to ensure that $C_{q_d} = \partial C / \partial q_d$ is a $m \times m$ non-singular square matrix. The matrix $C_{q_I} = \partial C / \partial q_I$ is $m \times (n - m)$, rectangular.

The first order time derivative of the constraint equations can be spanned as:

$$0 = C_q \dot{q} + C_t = \begin{bmatrix} C_{q_d} & C_{q_I} \end{bmatrix} \begin{Bmatrix} \dot{q}_d \\ \dot{q}_I \end{Bmatrix} + C_t = C_{q_d} \dot{q}_d + C_{q_I} \dot{q}_I + C_t \qquad (3.36)$$

Then, the velocities of the dependent coordinates can be calculated using the velocities of the independent coordinates as follows:

$$\dot{q}_d = -C_{q_d}^{-1} C_{q_I} \dot{q}_I - C_{q_d}^{-1} C_t \qquad (3.37)$$

Consequently, the entire set of the velocity vector, can be spanned in a matrix form as:

$$\dot{q} = \begin{Bmatrix} \dot{q}_d \\ \dot{q}_I \end{Bmatrix} = \begin{bmatrix} -C_{q_d}^{-1} C_{q_I} \\ I \end{bmatrix} \dot{q}_I + \begin{Bmatrix} -C_{q_d}^{-1} C_t \\ 0 \end{Bmatrix} \equiv D \dot{q}_I + \alpha \qquad (3.38)$$

where

$$D = \begin{bmatrix} -C_{q_d}^{-1} C_{q_I} \\ I \end{bmatrix} \qquad (3.39)$$

and

$$\alpha = \begin{Bmatrix} -C_{q_d}^{-1} C_t \\ 0 \end{Bmatrix} \qquad (3.40)$$

Similarly, one can decompose the acceleration vector based upon the second row of the equation of motion, Eq. 3.33 as follows:

$$\begin{bmatrix} C_{q_d} & C_{q_I} \end{bmatrix} \begin{bmatrix} \ddot{q}_d \\ \ddot{q}_I \end{bmatrix} - C_{qq} = C_{q_d} \ddot{q}_d + C_{q_I} \ddot{q}_I - C_{qq} = 0 \qquad (3.41)$$

Thus, one can obtain the acceleration of the independent coordinates as:

$$\ddot{q}_d = -C_{q_d}^{-1} C_{q_I} \ddot{q}_I + C_{q_d}^{-1} C_{qq} \qquad (3.42)$$

Thus, the system acceleration vector can be written in terms of $\ddot{q}_I$ as:

$$\ddot{q} = \begin{bmatrix} \ddot{q}_d \\ \ddot{q}_I \end{bmatrix} = D \ddot{q}_I + \begin{Bmatrix} C_{,q_d}^{-1} C_{,qq} \\ 0 \end{Bmatrix} \equiv D \ddot{q}_I + \gamma \qquad (3.43)$$

where $\gamma = \begin{Bmatrix} C_{q_d}^{-1} C_{qq} \\ 0 \end{Bmatrix}$.

Consequently, the first row of the equations of motion, Eq. 3.33, for a flexible multi-body system can be rewritten in terms of the independent coordinates, $\ddot{q}_I$, as:

$$M(D \ddot{q}_I + \gamma) + C_q^T \lambda = f \qquad (3.44)$$

Pre-multiplying the above equation by the matrix D^T, one has:

$$D^T M(D\ddot{q}_I + \gamma) + D^T C_q^T \lambda = D^T f \tag{3.45}$$

Using the definitions of matrices D and C_q from Eqs. 3.39 and 3.35, one has:

$$D^T C_q^T = (C_q D)^T = \left(\begin{bmatrix} C_{q_d} & C_{q_I} \end{bmatrix} \begin{bmatrix} -C_{q_d}^{-1} C_{q_I} \\ I \end{bmatrix} \right)^T = \left(-C_{q_d} C_{q_d}^{-1} C_{q_I} + C_{q_I} I \right)^T = 0.$$

Consequently, the constraint forces $C_q^T \lambda$ can be eliminated from Eq. 3.45. This procedure of eliminating the constraint forces is called the embedding technique [33]. Finally, Eq. 3.45 becomes an ordinary differential equation in terms of independent coordinates $\ddot{q}_I$ as:

$$D^T M D \ddot{q}_I = D^T f - D^T M \gamma \tag{3.46}$$

The coordinate partitioning method has converted the DAEs in Eq.3.33 to the second order ODEs in Eq. 3.46 in terms of independent coordinates q_I. Consequently, the commonly used numerical methods for solving the ODE can be used here to solve for q_I and $\dot{q}_I$. The specific steps are given below.

At time step t_n, the values of the independent coordinates q_{I,t_n} and the corresponding velocities vector $\dot{q}_{I,t_n}$ are assumed to be known. The dependent velocities $\dot{q}_{d,t_n}$ and the accelerations $\ddot{q}_{d,t_n}$ can be calculated accordingly based upon Eqs. 3.36 and 3.42. On the other hand, the dependent coordinates q_{d,t_n}, must be solved by using the Newton-Raphson iterative method as the constraint equation $C(t,q) = 0$ most likely nonlinear. Once all of the system coordinates and velocities are known at time step t_n, Eq. 3.46 can be used to solve for the acceleration vector $\ddot{q}_{I,t_{n+1}}$. One has:

$$\ddot{q}_{I,t_{n+1}} = \left(D_{t_n}^T M_{t_n} D_{t_n} \right)^{-1} \left(D_{t_n}^T f_{t_n} - D_{t_n}^T M_{t_n} \gamma_{t_n} \right) \tag{3.47}$$

The acceleration vector for independent coordinates at t_{n+1}, can be integrated to solve for the velocity vector $\dot{q}_{I,t_{n+1}}$ and the position vector $q_{I,t_{n+1}}$. One can then repeat the process to find the dependent coordinates $q_{d,t_{n+1}}$, the dependent velocities $\dot{q}_{d,t_{n+1}}$ and the dependent acceleration $\ddot{q}_{d,t_{n+1}}$ at t_{n+1}.

3.5 The Projection Method [43-44, 88]

The projection method has been used in various disciplines, including fluid dynamics by Chorin [13], which solves the DAEs in two steps. Through LU decomposition, the leading coefficient matrix of Eq. 3.33 can be rewritten as:

$$\begin{bmatrix} M & C_q^T \\ C_q & 0 \end{bmatrix} = \begin{bmatrix} M & 0 \\ C_q & -C_q M^{-1} C_q^T \end{bmatrix} \begin{bmatrix} I & M^{-1} C_q^T \\ 0 & I \end{bmatrix} \tag{3.47}$$

which spans Eq. 3.33 as

$$\begin{bmatrix} M & C_q^T \\ C_q & 0 \end{bmatrix} \begin{Bmatrix} \ddot{q} \\ \lambda \end{Bmatrix} = \begin{bmatrix} M & 0 \\ C_q & -C_q M^{-1} C_q^T \end{bmatrix} \begin{bmatrix} I & M^{-1} C_q^T \\ 0 & I \end{bmatrix} \begin{Bmatrix} \ddot{q} \\ \lambda \end{Bmatrix} = \begin{bmatrix} f \\ C_{qq} \end{bmatrix} \tag{3.48}$$

The above decomposition helps to set up a two-step solution procedure. The procedure introduces two intermediate variables, $\ddot{q}^*$ and λ^*, which are the solutions of the following equation:

$$\begin{bmatrix} M & 0 \\ C_q & -C_q M^{-1} C_q^T \end{bmatrix} \begin{Bmatrix} \ddot{q}^* \\ \lambda^* \end{Bmatrix} = \begin{bmatrix} f \\ C_{qq} \end{bmatrix} \tag{3.49}$$

and

$$\begin{Bmatrix} \ddot{q}^* \\ \lambda^* \end{Bmatrix} = \begin{bmatrix} I & M^{-1} C_q^T \\ 0 & I \end{bmatrix} \begin{Bmatrix} \ddot{q} \\ \lambda \end{Bmatrix} \tag{3.50}$$

The intermediate variables, $\ddot{q}^*$ can be obtained from the first row of Eq. 3.49 as

$$\ddot{q}^* = M^{-1} f \tag{3.51}$$

The second row of Eq. 3.49 gives

$$C_q \ddot{q}^* - C_q M^{-1} C_q^T \lambda^* = C_{qq} \tag{3.52}$$

The combination of Eqs. 3.51 and 3.52 gives the value of λ^* as

$$\lambda^* = (C_q M^{-1} C_q^T)^{-1} (C_q \ddot{q}^* - C_{qq}) = (C_q M^{-1} C_q^T)^{-1} (C_q M^{-1} f - C_{qq}) \tag{3.53}$$

Equation 3.50 defines the relations between intermediate variables, $\ddot{q}^*$ and λ^* and the true ones,

$$\ddot{q}^* = \ddot{q} + M^{-1} C_q^T \lambda \tag{3.54}$$

and

$$\lambda^* = \lambda \tag{3.55}$$

Substituting Eqs. 3.51 and 3.53 into Eq. 3.54, one has $\ddot{q}$ as

$$\ddot{q} = \ddot{q}^* - M^{-1}C_q^T\lambda = M^{-1}\left(Pf + C_q^T(C_qM^{-1}C_q^T)^{-1}C_{qq}\right) \tag{3.56}$$

where the projection matrix, P, is given by

$$P = I - C_q^T(C_qM^{-1}C_q^T)^{-1}C_qM^{-1} \tag{3.57}$$

Notice that the projection matrix derived here satisfies the conditions:

$$PP = P \text{ and } PC_q^T = 0.$$

Eq. 3.56 is a set of ordinary differential equations (ODEs) which can be solved numerically by standard ODE solvers. The set of ODEs derived by the project method are described in terms of the system generalized coordinates. Comparing to the coordinates partitioning method, the projection method obviates the need to divide the system generalized coordinates into dependent and independents coordinates, though it produces a larger size of ODEs.

The ODEs derived by the projection method satisfy the constraints imposed on the acceleration term $\ddot{q}$ automatically, which can be integrated to obtain q and $\dot{q}$. However, these newly obtained displacement and the velocity terms may not satisfy the constraints imposed upon them. This is corrected by introducing a minimization approach.

One can enforce the constraint $C(t,q) = 0$ by minimizing the error:

$$\min_{\Delta q} \quad f(\Delta q) = C^T(t,q+\Delta q) \cdot C(t,q+\Delta q) + \Delta q^T W \Delta q \tag{3.58}$$

where q is the initial value of the system coordinate, Δq is the correction needed to improve the solution to satisfy the displacement constraints and W is a weighting diagonal matrix. In this study, the weighting matrix is set as the identity matrix. It implies that all the system coordinates have the same effect on the constraints. The last term, $\Delta q^T W \Delta q$ is added to ensure that the correction is achieved with a minimal change of q. To further simplify the process, the 1st order approximation of the error term is derived as:

$$
\begin{aligned}
f(\Delta q) &= C^T(t,q+\Delta q) \cdot C(t,q+\Delta q) + \Delta q^T W \Delta q \\
&= \left[C(t,q_0) + C_{,q}\Delta q\right]^T \cdot \left[C(t,q_0) + C_{,q}\Delta q\right] + \Delta q^T W \Delta q \\
&= C(t,q_0)^T \cdot C(t,q_0) + \Delta q^T C_{,q}^T C(t,q_0) + C(t,q_0)^T C_{,q}\Delta q + \Delta q^T C_{,q}^T C_{,q}\Delta q + \Delta q^T W \Delta q
\end{aligned} \tag{3.59}
$$

where $C_q = \left.\dfrac{\partial C}{\partial q}\right|_{q_0}$ is evaluated at q_0.

The necessary condition of the above minimization problem yields:

$$\frac{\partial f}{\partial \Delta q} = 2C_q^T C(t,q_0) + 2\left(W + C_q^T C_q\right)\Delta q = 0 \tag{3.60}$$

which gives a simple relation to find the correction, Δq,

$$\Delta q = \left(W + C_q^T C_q\right)^{-1} C_q^T C(t,q_0) \tag{3.61}$$

One can then update q_{New} as:

$$q_{New} = q + \Delta q \tag{3.62}$$

The above equation can be repeated to update the q until the displacement constraints satisfy $|C(t,q)| \leq \varepsilon$, where ε is a small value, such as 10^{-6}.

The velocity constraints equations $C_q \dot{q} = -C_t$ can also be enforced in a similar way. The velocity correction can be obtained through a minimization process:

$$\min_{\Delta \dot{q}} \quad f(\Delta \dot{q}) = \left[C_q \cdot (\dot{q} + \Delta \dot{q}) + C_t\right]^T \left[C_q \cdot (\dot{q} + \Delta \dot{q}) + C_t\right] + \Delta \dot{q}^T W \Delta \dot{q} \tag{3.63}$$

where $\dot{q}$ is the initial value, $\Delta \dot{q}$ is the correction needed to improve the error, and W is a weighting diagonal matrix. The necessary condition of the above minimization problem yields:

$$\frac{\partial f}{\partial \Delta \dot{q}} = 2C_q^T \cdot C_q \cdot (\dot{q} + \Delta \dot{q}) + 2C_q^T \cdot C_t + 2W\Delta \dot{q} = 0 \tag{3.64}$$

which gives the improvement $\Delta \dot{q}$ as:

$$\Delta \dot{q} = -\left(C_q^T \cdot C_q + W\right)^{-1} \left(C_q^T \cdot C_q \dot{q} + C_q^T \cdot C_t\right) \tag{3.65}$$

Again, the update $\dot{q}_{New}$ is obtained by:

$$\dot{q}_{New} = \dot{q} + \Delta \dot{q} \tag{3.66}$$

The above equation can be repeated until $\dot{q}_{new}$ satisfies the velocity constraints $|C_q \dot{q} + C_t| < \varepsilon$.

The proposed optimization method on the displacement and velocity constraints is demonstrated using slider-crank mechanisms in Chapter 4.

CHAPTER 4

PLANAR SLIDER-CRANK MECHANISM: A MULTI-BODY

EXAMPLE

A simple planar slider-crank mechanism will serve as a multi-body example to demonstrate the formulation and the solution algorithms introduced in previous chapters. Several options exist for solution methods; location to place the body-fixed coordinate system and the sequence of integral evaluation and ODE iteration are studied. Three solution methods are considered: the direct method, the coordinate partitioning method and the projection method. The left end and the center of the connecting rod are considered in this study as two alternative locations to place the origin of the body-fixed coordinate system. Finally, the geometrical integrals are evaluated prior to the ODE iterations or evaluated on-the-fly within the ODE iteration. Various combinations of these options are examined and compared for their numerical accuracy and computational efficiency.

This chapter is divided into 9 sections. The problem parameters of the slider-crank mechanism are introduced in Section 4.1. The equation of motion for a single pendulum, which models the crank, is introduced in Section 4.2. The equation of motion for a free flexible beam, which models the connecting rod, is given in Section 4.3.Constraints that join the single pendulum with the connecting rod to form the slider-crank mechanism are introduced in Section 4.4. The differential algebraic equation that represents the slider-crank mechanism is derived in Section 4.5. The case when the connecting rod is modeled as a rigid link is considered in Section 4.6. Its solution methods and numerical results are reported in Sections 4.7 and 4.8. The case when the connecting rod is modeled as a flexible beam is shown in Section 4.9.

4.1 Slider-crank Mechanism Problem Statement

A slider-crank mechanism is widely used in the industry due to its simplicity. The problem is an extension of a double pendulum with a position constraint imposed at the free end. The elasticity of the connecting rod is considered in the latter part of this study.

A slider-crank mechanism is usually considered to be made of four bodies: the ground, the crank, the connecting rod and the slider. However, in this study, the slider is taken as a massless point. The slider-crank mechanism studied in this chapter is shown in Fig. 4.1. The left end of the rigid crank is pinned to the ground, at Point O and its right end is connected to the flexible connecting rod by a revolute joint at Point A. The right end of the connecting rod is connected to the slider, Point B, which can only move along the x axis. Thus, the y coordinate of Point B is maintained as a constant. The slider-crank mechanism is subjected to a transient force at Point B. This distinguishes the current study from most of the existing studies where the external torque is applied at Point O to maintain a prescribed angular velocity of the crank.
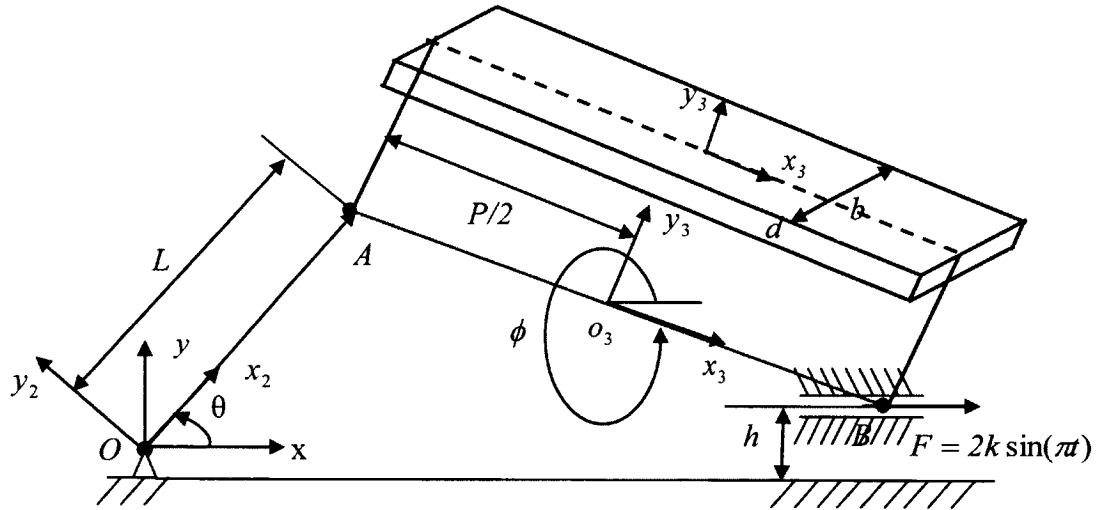
Figure 4.1 The Slider-Crank Mechanism

The slider-crank mechanism studied here is limited to move only in the x-y plane. Hence, the rigid crank and the rigid connecting rod move with three degrees of freedom (DOFs) each: two translations along the x and the y axes respectively and one rotation about the z axis. The pinned joints at Points O and A produce four constraints in total, two each, while Point B yields one constraint. Thus, the slider-mechanism is subjected to five

constraints in total. Therefore, a rigid slider-crank mechanism enjoys only one degree of freedom.

The geometrical and the material properties of the crank and the connecting rod that make the slider-crank mechanism are summarized in Table 4.1.

Table 4.1: The Geometry and Material Properties of the System

Parameters, Units	Crank	Connecting Rod
Length, mm	L=300	P=500
Width b, mm	b=50	
Height d, mm	d=10	
Cross-Section Area $b \times d$, mm^2	A=500	
Height of Slider h, mm	46.5	
Density, Ns^2/mm^4	$\rho = 7.833 \times 10^{-9}$	
Acceleration, mm/s^2	$g = 9.81 \times 10^3$	
Mass, Ns^2/mm	$m_2 = 1.175 \times 10^{-3}$	$m_3 = 1.958 \times 10^{-3}$
Moment Inertia $I_{yy} = db^3/12 mm^4$	$I_{yy} = 4.1667 \times 10^3$	
Moment Inertia $I_{zz} = bd^3/12 mm^4$	$I_{zz} = 1.0417 \times 10^5$	
Young's Modulus, MPa	2.06×10^5	

4.2 Equation of Motion for the Rigid Crank

The global coordinate system (x, y) and the body fixed coordinate system $\left(x_2', y_2'\right)$ of the rigid crank are shown in Fig. 4.2. The rigid crank is a rectangular beam. The origin of the body fixed coordinate is at Point O, which is the center of the left end face of the rigid crank. The crank is pinned to the ground at Point O. The dimension of the crank is $L(length) \times b(width) \times d(thickness)$. Hence, the ranges for the local coordinate are defined as follows:

$$0 \le x_2' \le L, \quad -d/2 \le y_2' \le d/2 \text{ and} -b/2 \le z_2' \le b/2.$$
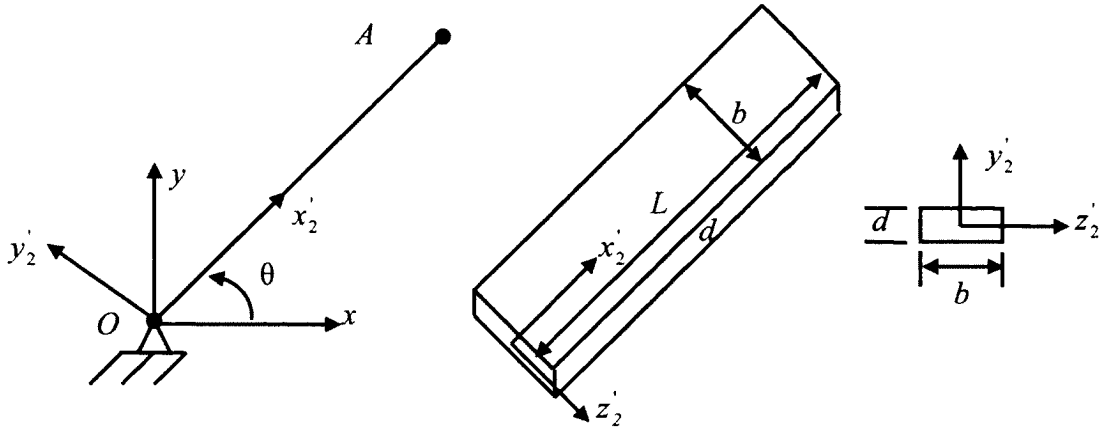
Figure 4.2 Rigid Crank

The general equation of motion for a constrained rigid body has been derived in Chapter 2 and is written as:

$$M^2\ddot{q}^2 - f^2 + C_q^T\lambda = 0 \qquad (4.1)$$

where the mass matrix, $M^2 = \begin{bmatrix} m_2 & -(AI_{\bar{r}})_2 \\ -(AI_{\bar{r}})_2^T & -(I_{\bar{r}\bar{r}})_2 \end{bmatrix} \equiv \begin{bmatrix} M_{RR}^2 & M_{R\theta}^2 \\ M_{\theta R}^2 & M_{\theta\theta}^2 \end{bmatrix}$,

the force vector $f^2 = \left\{ \begin{array}{c} (Vf_b - A\tilde{\omega}'\tilde{\omega}'I_{\bar{r}} + \mathbf{F})^2 \\ (I_{\bar{r}}A^T f_b / \rho + \tilde{\omega}'I_{\bar{r}\bar{r}}\omega' + T'^T)^2 \end{array} \right\} \equiv \left\{ \begin{array}{c} f_R^2 \\ f_\theta^2 \end{array} \right\}$,

the system generalized coordinates $q^2 = \{R_2^x \quad R_2^y \quad R_2^z \quad \Pi_2^x \quad \Pi_2^y \quad \Pi_2^y\}^T$, and the constraint Jacobian matrix

$$C_q^2 = \begin{bmatrix} \dfrac{\partial C_1^2}{\partial R_x^2} & \dfrac{\partial C_1^2}{\partial R_y^2} & \cdots & \dfrac{\partial C_1^2}{\partial \theta_z^2} \\[2mm] \dfrac{\partial C_2^2}{\partial R_x^2} & \dfrac{\partial C_2^2}{\partial R_y^2} & \cdots & \dfrac{\partial C_2^2}{\partial \theta_z^2} \\[2mm] \vdots & \vdots & \vdots & \vdots \\[2mm] \dfrac{\partial C_n^2}{\partial R_x^2} & \dfrac{\partial C_n^2}{\partial R_y^2} & \cdots & \dfrac{\partial C_n^2}{\partial \theta_z^2} \end{bmatrix}.$$

The detailed derivation of each of the terms in Eq. 4.1 in terms of the problem parameters given in Table 4.1 are in order.

Since the crank rotates respect to the z' axis, the transformation matrix A from the body fixed coordinates to the global coordinates is as follows:

$$A = \begin{bmatrix} \cos\theta & -\sin\theta & 0 \\ \sin\theta & \cos\theta & 0 \\ 0 & 0 & 1 \end{bmatrix}.$$

The linear moment $I_{\tilde{r}}$ in the mass matrix, M^2 is calculated as follows:

$$I_{\tilde{r}} =$$

$$\int_\Omega \rho\tilde{r}'dv = \rho\int_\Omega \begin{bmatrix} 0 & 0 & y' \\ 0 & 0 & -x' \\ -y' & x' & 0 \end{bmatrix} dv = \rho \begin{bmatrix} 0 & 0 & \int_\Omega y'dv \\ 0 & 0 & -\int_\Omega x'dv \\ -\int_\Omega y'dv & \int_\Omega x'dv & 0 \end{bmatrix} = \frac{1}{2}m_2 L \begin{bmatrix} 0 & 0 & 0 \\ 0 & 0 & -1 \\ 0 & 1 & 0 \end{bmatrix}.$$

Therefore, the coupling mass term, $M_{R\theta}^2$, is given by

$$M_{R\theta}^2 = -AI_{\tilde{r}} = -\begin{bmatrix} \cos\theta & -\sin\theta & 0 \\ \sin\theta & \cos\theta & 0 \\ 0 & 0 & 1 \end{bmatrix} \cdot \frac{1}{2}m_2 L \begin{bmatrix} 0 & 0 & 0 \\ 0 & 0 & -1 \\ 0 & 1 & 0 \end{bmatrix} = -\frac{1}{2}m_2 L \begin{bmatrix} 0 & 0 & \sin\theta \\ 0 & 0 & -\cos\theta \\ 0 & 1 & 0 \end{bmatrix}.$$

The mass moment $I_{\tilde{r}\tilde{r}}$ is calculated as follows:

$$I_{\tilde{r}\tilde{r}} = \int_\Omega \rho\tilde{r}\tilde{r}'dv = \rho\int_\Omega \begin{bmatrix} -y'^2 & x'y' & 0 \\ x'y' & -x'^2 & 0 \\ 0 & 0 & -x'^2 - y'^2 \end{bmatrix} dv = -\frac{1}{12}m_2 \begin{bmatrix} d^2 & 0 & 0 \\ & 4L^2 & 0 \\ sym. & & 4L^2 + d^2 \end{bmatrix}.$$

Substituting these terms into the mass matrix M^2, one has:

$$M^2 = \begin{bmatrix} m_2 & -AI_{\tilde{r}} \\ sym & -I_{\tilde{r}\tilde{r}} \end{bmatrix} = \frac{1}{12}m_2 \begin{bmatrix} 12 & 0 & 0 & 0 & 0 & -6L\sin\theta \\ & 12 & 0 & 0 & 0 & 6L\cos\theta \\ & & 12 & 0 & -6L & 0 \\ & & & d^2 & 0 & 0 \\ & sym. & & & 4L^2 & 0 \\ & & & & & 4L^2 + d^2 \end{bmatrix} \tag{4.2}$$

As for the generalized force term, one has:

$$f_R^2 = Vf_b - A\tilde{\omega}'\tilde{\omega}'I_{\tilde{r}} + F$$

$$= V_2 \left\{ \begin{matrix} 0 \\ -\rho g \\ 0 \end{matrix} \right\} - \begin{bmatrix} \cos\theta & -\sin\theta & 0 \\ \sin\theta & \cos\theta & 0 \\ 0 & 0 & 1 \end{bmatrix} \begin{bmatrix} 0 & -\dot{\theta} & 0 \\ \dot{\theta} & 0 & 0 \\ 0 & 0 & 0 \end{bmatrix} \begin{bmatrix} 0 & -\dot{\theta} & 0 \\ \dot{\theta} & 0 & 0 \\ 0 & 0 & 0 \end{bmatrix} \left\{ \begin{matrix} \frac{1}{2}m_2 L \\ 0 \\ 0 \end{matrix} \right\} = \frac{1}{2}m_2 \left\{ \begin{matrix} \dot{\theta}^2 L\cos\theta \\ -2g + \dot{\theta}^2 L\sin\theta \\ 0 \end{matrix} \right\}.$$

$$f_\theta^2 = I_{\tilde{r}}A^T f_b / \rho + \tilde{\omega}'I_{\tilde{r}\tilde{r}}\omega' + T'^T$$

$$= \frac{1}{2} m_2 L \begin{bmatrix} 0 & 0 & 0 \\ 0 & 0 & -1 \\ 0 & 1 & 0 \end{bmatrix} \begin{bmatrix} \cos\theta & \sin\theta & 0 \\ -\sin\theta & \cos\theta & 0 \\ 0 & 0 & 1 \end{bmatrix} \left\{ \begin{array}{c} 0 \\ -\rho g \\ 0 \end{array} \right\} / \rho$$

$$+ \frac{1}{12} m_2 \dot{\theta}^2 \begin{bmatrix} 0 & -1 & 0 \\ 1 & 0 & 0 \\ 0 & 0 & 0 \end{bmatrix} \begin{bmatrix} -d^2 & 0 & 0 \\ 0 & -4L^2 & 0 \\ 0 & 0 & -4L^2 - d^2 \end{bmatrix} \left\{ \begin{array}{c} 0 \\ 0 \\ 1 \end{array} \right\} = \frac{1}{2} m_2 L \left\{ \begin{array}{c} 0 \\ 0 \\ -g\cos\theta \end{array} \right\}.$$

Finally, one has the generalized force term as:

$$f^2 = \left\{ \begin{array}{c} f_R^2 \\ f_\theta^2 \end{array} \right\} = \frac{1}{2} m_2 \left\{ \begin{array}{c} \dot{\theta}^2 L \cos\theta \\ -2g + \dot{\theta}^2 L \sin\theta \\ 0 \\ 0 \\ 0 \\ -Lg\cos\theta \end{array} \right\} \tag{4.3}$$

The rigid crank is pinned at its left end and allowed to rotate respect to the z' axis only. Therefore, the rigid crank is limited to one degree of freedom. Hence, the constraints for the planar rigid crank are as follows:

$$C_1 = R_2^x = 0, C_2 = R_2^y = 0, C_3 = R_2^z = 0, C_4 = \Pi_2^x = 0, C_5 = \Pi_2^y = 0.$$

The corresponding constraint Jacobian matrix is then given as follows:

$$C_q = \begin{bmatrix} \dfrac{\partial C_1}{\partial R_x^2} & \dfrac{\partial C_1}{\partial R_y^2} & \cdots & \dfrac{\partial C_1}{\partial \theta_z^2} \\ \dfrac{\partial C_2}{\partial R_x^2} & \dfrac{\partial C_2}{\partial R_y^2} & \cdots & \dfrac{\partial C_2}{\partial \theta_z^2} \\ \vdots & \vdots & \vdots & \vdots \\ \dfrac{\partial C_5}{\partial R_x^2} & \dfrac{\partial C_5}{\partial R_y^2} & \cdots & \dfrac{\partial C_5}{\partial \theta_z^2} \end{bmatrix} = \begin{bmatrix} 1 & 0 & 0 & 0 & 0 & \vdots & 0 \\ 0 & 1 & 0 & 0 & 0 & \vdots & 0 \\ 0 & 0 & 1 & 0 & 0 & \vdots & 0 \\ 0 & 0 & 0 & 1 & 0 & \vdots & 0 \\ 0 & 0 & 0 & 0 & 1 & \vdots & 0 \end{bmatrix} \equiv \begin{bmatrix} C_{qd} & \vdots & C_{ql} \end{bmatrix} \tag{4.4}$$

Using the coordinate partitioning method described in Chapter 3, one has the equation of motion in terms of independent coordinates $\ddot{q}_I$ as:

$$D^T M D \ddot{q}_I = D^T f \tag{4.5}$$

where $D = \begin{bmatrix} -C_{qd}^{-1} C_{ql} \\ I \end{bmatrix} = \begin{bmatrix} 0 & 0 & 0 & 0 & 0 & 1 \end{bmatrix}^T$, $q_I = \theta_z$.

Substituting the calculated M, f and D into Eq. 4.5, one has:

$$D^T MD = \begin{bmatrix} 0 \\ 0 \\ 0 \\ 0 \\ 0 \\ 1 \end{bmatrix}^T \frac{1}{12}m_2 \begin{bmatrix} 12 & 0 & 0 & 0 & 0 & -6L\sin\theta_z \\ & 12 & 0 & 0 & 0 & 6L\cos\theta_z \\ & & 12 & 0 & -6L & 0 \\ & & & d^2 & 0 & 0 \\ & sym. & & & 4L^2 & 0 \\ & & & & & 4L^2+d^2 \end{bmatrix} \begin{bmatrix} 0 \\ 0 \\ 0 \\ 0 \\ 0 \\ 1 \end{bmatrix} \ddot\theta_z = \frac{4L^2+d^2}{12}m_2\ddot\theta_z,$$

and

$$D^T f = \begin{bmatrix} 0 & 0 & 0 & 0 & 0 & 1 \end{bmatrix} \frac{1}{2}m_2 \begin{Bmatrix} \dot\theta_z^2 L\cos\theta_z \\ -2g+\dot\theta_z^2 L\sin\theta_z \\ 0 \\ 0 \\ 0 \\ -Lg\cos\theta_z \end{Bmatrix} = -\frac{1}{2}m_2 gL\cos\theta_z.$$

At last, the governing equation of motion for the rigid crank, pinned to the ground at its left end is as follows:

$$\frac{4L^2+b^2}{12}m_2\ddot\theta_z = -\frac{1}{2}m_2 gL\cos\theta_z \tag{4.6}$$

Alternatively, the rigid crank may be viewed as a single pendulum subjected to its gravity as shown in Fig. 4.3.
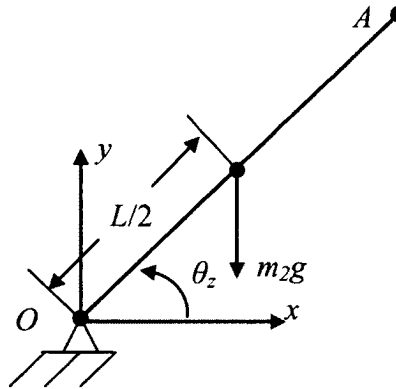
Figure 4.3 Force Diagram of Rigid Crank

The only external force applied on the rigid crank is its own weight. According to the equation of equilibrium, the total moment with respect to Point O is zero. Hence, one has:

$$M_o + J\ddot{\theta}_z = 0 \tag{4.7}$$

where M_o is the moment produced by the weight, $M_o = m_2 gL/2 \cos\theta_z$.

J is the moment inertia of the rigid crank respect to point O:

$$J = \int_\Omega \rho\left(x^2 + y^2\right)dv = \frac{1}{3}\rho bdL^3 + \frac{1}{12}\rho bLd^3 = \frac{1}{12}m_2(4L^2 + d^2).$$

Equation 4.7 yields the equation of motion of the crank as:

$$\frac{1}{2}m_2 gL\cos\theta_z + \frac{1}{12}m_2\left(4L^2 + d^2\right)\ddot{\theta}_z = 0 \tag{4.8}$$

which is identical to that in Eq. 4.6.

4.3 Equation of Motion for the Flexible Connecting Rod

The body fixed coordinate system can be defined in many different ways. It is selected to place the origin of the body-fixed coordinate system at the left end of the crank in the derivation given in Section 4.2. For the flexible connecting rod, the origin of the body fixed coordinate system is placed at its center of gravity. This can simplify the calculation of the linear moment inertia term in the equation of motion. Later, while modeling the rigid connecting rod in Section 4.6, two cases are considered: one places the origin of the body-fixed coordinate system at the left end of the rod, and the other places it at the center. Results of both cases are compared to each other to investigate the effects of the origin location on computational efficiency.
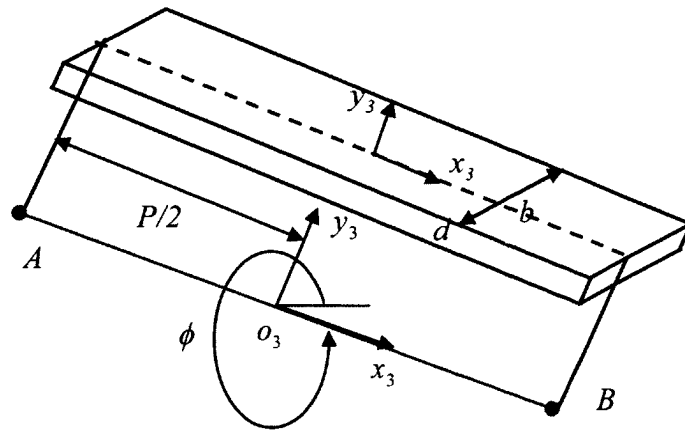
Figure 4.4 Body-fixed Coordinates for the Connecting Rod

The equation of motion for a free flexible body derived in Chapter 2 is employed here for the flexible connecting rod of concern,

$$\left(\mathbf{M}^3\ddot{\mathbf{q}}^3 - \mathbf{f}^3\right)^T \delta\mathbf{q}^3 = 0 \tag{4.9}$$

where

$$M^3 = \begin{bmatrix} M_{RR} & M_{R\theta} & M_{Rq} \\ & M_{\theta\theta} & M_{\theta q} \\ \text{sym.} & & M_{qq} \end{bmatrix} = \begin{bmatrix} m_3 I_3 & -A_3 I_{\tilde{e}} & A_3 I_{N}\psi \\ & -(I_{\tilde{r}_3\tilde{r}_3} + I_{\tilde{r}_3\tilde{e}} + I_{\tilde{e}\tilde{r}_3} + I_{\tilde{e}\tilde{e}}) & (I_{\tilde{r}_3 N} + I_{\tilde{e}N})\psi \\ & \text{sym} & \psi^T I_{N^T N}\psi \end{bmatrix} \tag{4.10}$$

$\ddot{q}^3 = \{\ddot{R}_3 \quad \ddot{\Pi}'_3 \quad \ddot{a}\}^T = \{\ddot{R}^x_3 \quad \ddot{R}^y_3 \quad \ddot{R}^z_3 \quad \ddot{\Pi}'^x_3 \quad \ddot{\Pi}'^y_3 \quad \ddot{\Pi}'^z_3 \quad \ddot{a}\}^T$, where a is the

modal coordinates used to approximate the elastic displacement. The force vector is given by

$$f^3 = \begin{Bmatrix} f_R \\ f_\theta \\ f_q \end{Bmatrix} = \begin{Bmatrix} V_3 f_b - A_3 \tilde{\omega}'_3 \tilde{\omega}'_3 I_e - 2A_3 \tilde{\omega}'_3 I_{\dot{e}} + F \\ I_{\tilde{e}} A^T_3 f_b / \rho + \tilde{\omega}'_3 (I_{\tilde{r}_3\tilde{r}_3} + I_{\tilde{r}_3\tilde{e}} + I_{\tilde{e}\tilde{r}_3} + I_{\tilde{e}\tilde{e}})\omega'_3 + 2(I_{\tilde{e}\tilde{r}_3} + I_{\tilde{e}\tilde{e}})^T \omega'_3 + T' \\ -\psi^T K \psi a + I_{N\psi}{}^T A^T_3 f_b / \rho + (I_{\tilde{r}_3\tilde{\omega}'_3 N\psi} + I_{\tilde{e}\tilde{\omega}'_3 N\psi})^T \omega'_3 - 2I^T_{\tilde{e}N\psi}\omega'_3 + W' \end{Bmatrix} \tag{4.11}$$

Since the only external force in this case is the force along x direction applied at point B, one has:

$$F = \{F_x \quad 0 \quad 0\}^T, \quad T' = \sum_{i=1}^{N}\left(\tilde{r}'_{ei} A^T F_i + T^T_i\right) = (\tilde{r}'^B_3 + \tilde{e}^B)A^T_3 F, \text{ and}$$

$$W' = \sum_{i=1}^{N}\left[(AN)^T F_i\right] = \psi^T_B A^T_3 F.$$

Therefore, the generalized force term for the flexible connecting rod is as follows:

$$f^3 = \begin{Bmatrix} V_3 f_b - A_3 \tilde{\omega}'_3 \tilde{\omega}'_3 I_e - 2A_3 \tilde{\omega}'_3 I_{\dot{e}} + F \\ I_{\tilde{e}} A^T_3 f_b / \rho + \tilde{\omega}'_3 (I_{\tilde{r}_3\tilde{r}_3} + I_{\tilde{r}_3\tilde{e}} + I_{\tilde{e}\tilde{r}_3} + I_{\tilde{e}\tilde{e}})\omega'_3 + 2(I_{\tilde{e}\tilde{r}_3} + I_{\tilde{e}\tilde{e}})^T \omega'_3 + (\tilde{r}'^B_3 + \tilde{e}^B)A^T_3 F \\ -\psi^T K \psi a + I^T_{N\psi} A^T_3 f_b / \rho + (I_{\tilde{r}_3\tilde{\omega}'_3 N\psi} + I_{\tilde{e}\tilde{\omega}'_3 N\psi})^T \omega'_3 - 2I^T_{\tilde{e}N\psi}\omega'_3 + \psi^T_B A^T_3 F \end{Bmatrix} \tag{4.12}$$

It should be Noted that Eqs. 4.10~4.12 define the generalized mass matrix and the force term for a general 3D free flexible body. Since this study is a planar analysis, the degrees of freedom R^z_3, Π'^x_3, and Π'^y_3 can be eliminated from Eqs. 4.10~12.

Consequently, the coefficients in the mass matrix, Eq. 4.10, can be simplified individually as:

$$m_3 I_3 = \begin{bmatrix} m_3 & 0 & 0 \\ 0 & m_3 & 0 \\ 0 & 0 & m_3 \end{bmatrix} \quad M_{RR}^3 = \begin{bmatrix} m_3 & 0 \\ 0 & m_3 \end{bmatrix} = m_3 I_2 .$$

$$-A_3 I_{\tilde{e}} = -\begin{bmatrix} \cos\phi & -\sin\phi & 0 \\ \sin\phi & \cos\phi & 0 \\ 0 & 0 & 1 \end{bmatrix} \begin{bmatrix} 0 & 0 & I_{e_y} \\ 0 & 0 & -I_{e_x} \\ -I_{e_y} & I_{e_x} & 0 \end{bmatrix} = \begin{bmatrix} 0 & 0 & -\cos\phi I_{e_y} -\sin\phi I_{e_x} \\ 0 & 0 & -\sin\phi I_{e_y} +\cos\phi I_{e_x} \\ I_{e_y} & -I_{e_x} & 0 \end{bmatrix} .$$

Similarly, $M_{R\theta}^3$, M_{Rq}^3, $M_{\theta\theta}^3$, and $M_{\theta q}^3$ can be obtained by simplifying the related terms in Eq. 4.10 as:

$$M_{R\theta}^3 = \begin{bmatrix} -\cos\phi I_{e_y} -\sin\phi I_{e_x} \\ -\sin\phi I_{e_y} +\cos\phi I_{e_x} \end{bmatrix} .$$

$$A_3 I_N \psi = \begin{bmatrix} \cos\phi & -\sin\phi & 0 \\ \sin\phi & \cos\phi & 0 \\ 0 & 0 & 1 \end{bmatrix} \begin{bmatrix} I_{N\psi 1}^1 & I_{N\psi 1}^2 & \cdots & I_{N\psi 1}^{Nm} \\ I_{N\psi 2}^1 & I_{N\psi 2}^2 & \cdots & I_{N\psi 2}^{Nm} \\ 0 & 0 & \cdots & 0 \end{bmatrix}$$

$$= \begin{bmatrix} \cos\phi I_{N\psi 1}^1 -\sin\phi I_{N\psi 2}^1 & \cos\phi I_{N\psi 1}^2 -\sin\phi I_{N\psi 2}^2 & \cdots & \cos\phi I_{N\psi 1}^{Nm} -\sin\phi I_{N\psi 2}^{Nm} \\ \sin\phi I_{N\psi 1}^1 +\cos\phi I_{N\psi 2}^1 & \sin\phi I_{N\psi 1}^2 +\cos\phi I_{N\psi 2}^2 & \cdots & \sin\phi I_{N\psi 1}^{Nm} +\cos\phi I_{N\psi 2}^{Nm} \\ 0 & 0 & 0 \end{bmatrix} .$$

$$M_{Rq}^3 = \begin{bmatrix} \cos\phi I_{N\psi 1}^1 -\sin\phi I_{N\psi 2}^1 & \cos\phi I_{N\psi 1}^2 -\sin\phi I_{N\psi 2}^2 & \cdots & \cos\phi I_{N\psi 1}^{Nm} -\sin\phi I_{N\psi 2}^{Nm} \\ \sin\phi I_{N\psi 1}^1 +\cos\phi I_{N\psi 2}^1 & \sin\phi I_{N\psi 1}^2 +\cos\phi I_{N\psi 2}^2 & \cdots & \sin\phi I_{N\psi 1}^{Nm} +\cos\phi I_{N\psi 2}^{Nm} \end{bmatrix}$$

$$-(I_{\tilde{r}_3 \tilde{r}_3} + I_{\tilde{r}_3 \tilde{e}} + I_{\tilde{e}\tilde{r}_3} + I_{\tilde{e}\tilde{e}}) = \begin{bmatrix} I_{11} & I_{12} & I_{13} \\ I_{21} & I_{22} & I_{23} \\ I_{31} & I_{32} & I_{x'^2+y'^2} +2I_{x'e_x+y'e_y} +I_{e_x^2+e_y^2} \end{bmatrix} .$$

$$M_{\theta\theta}^3 = I_{x'^2+y'^2} +2I_{x'e_x+y'e_y} +I_{e_x^2+e_y^2} = I_{(x'+e_x)^2+(y'+e_y)^2} .$$

$$(\tilde{r}_3' + \tilde{e})N\psi = \begin{bmatrix} 0 & -z' & y'+e_y \\ z' & 0 & -x'-e_x \\ -y'-e_y & x'+e_x & 0 \end{bmatrix} \begin{bmatrix} N\psi_1^1 & N\psi_1^2 & \cdots & N\psi_1^{Nm} \\ N\psi_2^1 & N\psi_2^2 & \cdots & N\psi_2^{Nm} \\ 0 & 0 & \cdots & 0 \end{bmatrix}$$

$$= \begin{bmatrix} -z'N\psi_2^1 & \cdots & -z'N\psi_2^{Nm} \\ z'N\psi_1^1 & \cdots & z'N\psi_1^{Nm} \\ (x'+e_x)N\psi_2^1 -(y'+e_y)N\psi_1^1 & \cdots & (x'+e_x)N\psi_2^{Nm} -(y'+e_y)N\psi_1^{Nm} \end{bmatrix}$$

$$(I_{\bar{r}_j N} + I_{\bar{e}N})\psi = \begin{bmatrix} \underline{0} & \cdots & \underline{0} \\ \underline{0} & \cdots & \underline{0} \\ I_{x'e_x N\psi_2^1} - I_{y'e_y N\psi_1^1} & \cdots & I_{x'e_x N\psi_2^{Nm}} - I_{y'e_y N\psi_1^{Nm}} \end{bmatrix}$$

$$M^3_{\theta q} = \begin{bmatrix} I_{x'e_x N\psi_2^1} - I_{y'e_y N\psi_1^1} & \cdots & I_{x'e_x N\psi_2^{Nm}} - I_{y'e_y N\psi_1^{Nm}} \end{bmatrix}.$$

As a result, the generalized mass matrix in a planar problem is as follows:

$$M =$$

$$\begin{bmatrix} m_3 & 0 & -\cos\phi I_{e_y} - \sin\phi I_{e_x} & \cos\phi I^1_{N\psi_1} - \sin\phi I^1_{N\psi_2} & \cdots & \cos\phi I^{Nm}_{N\psi_1} - \sin\phi I^{Nm}_{N\psi_2} \\ 0 & m_3 & -\sin\phi I_{e_y} + \cos\phi I_{e_x} & \sin\phi I^1_{N\psi_1} + \cos\phi I^1_{N\psi_2} & \cdots & \sin\phi I^{Nm}_{N\psi_1} + \cos\phi I^{Nm}_{N\psi_2} \\ & & I_{(x'+e_x)^2+(y'+e_y)^2} & I_{x'e_x N\psi_2^1} - I_{y'e_y N\psi_1^1} & \cdots & I_{x'e_x N\psi_2^{Nm}} - I_{y'e_y N\psi_1^{Nm}} \\ & sym. & & & & \psi^T I_{N^T N}\psi \end{bmatrix} \quad (4.13)$$

Similarly, the detail expressions for the required terms in the generalized force vector are summarized below as:

$$f_R = V_3 f_b - A_3 \tilde{\omega}'_3 \tilde{\omega}'_3 I_e - 2A_3 \tilde{\omega}'_3 I_{\dot{e}} + F$$

$$= V_3 \left\{ \begin{matrix} 0 \\ -\rho g \\ 0 \end{matrix} \right\} - \begin{bmatrix} \cos\phi & -\sin\phi & 0 \\ \sin\phi & \cos\phi & 0 \\ 0 & 0 & 1 \end{bmatrix} \begin{bmatrix} 0 & -1 & 0 \\ 1 & 0 & 0 \\ 0 & 0 & 0 \end{bmatrix} \begin{bmatrix} 0 & -1 & 0 \\ 1 & 0 & 0 \\ 0 & 0 & 0 \end{bmatrix} \dot{\phi}^2 \left\{ \begin{matrix} I_{e_x} \\ I_{e_y} \\ 0 \end{matrix} \right\}$$

$$- 2 \begin{bmatrix} \cos\phi & -\sin\phi & 0 \\ \sin\phi & \cos\phi & 0 \\ 0 & 0 & 1 \end{bmatrix} \begin{bmatrix} 0 & -1 & 0 \\ 1 & 0 & 0 \\ 0 & 0 & 0 \end{bmatrix} \dot{\phi} \left\{ \begin{matrix} I_{\dot{e}_x} \\ I_{\dot{e}_y} \\ 0 \end{matrix} \right\} + \left\{ \begin{matrix} F \\ 0 \\ 0 \end{matrix} \right\}$$

$$= \left\{ \begin{matrix} (\cos\phi I_{e_x} - \sin\phi I_{e_y})\dot{\phi}^2 + 2(\sin\phi I_{\dot{e}_x} + \cos\phi I_{\dot{e}_y})\dot{\phi} + F \\ -m_3 g + (\sin\phi I_{e_x} + \cos\phi I_{e_y})\dot{\phi}^2 - 2(\cos\phi I_{\dot{e}_x} - \sin\phi I_{\dot{e}_y})\dot{\phi} \\ \underline{0} \end{matrix} \right\}.$$

$$f^3_R = \left\{ \begin{matrix} (\cos\phi I_{e_x} - \sin\phi I_{e_y})\dot{\phi}^2 + 2(\sin\phi I_{\dot{e}_x} + \cos\phi I_{\dot{e}_y})\dot{\phi} + F \\ -m_3 g + (\sin\phi I_{e_x} + \cos\phi I_{e_y})\dot{\phi}^2 - 2(\cos\phi I_{\dot{e}_x} - \sin\phi I_{\dot{e}_y})\dot{\phi} \end{matrix} \right\}.$$

$$f^3_\theta = I_{\bar{e}} A^T_3 f_b / \rho + \tilde{\omega}'_3 (I_{\bar{r}_j \bar{r}_j} + I_{\bar{r}_j \bar{e}} + I_{\bar{e}\bar{r}_j} + I_{\bar{e}\bar{e}})\omega'_3 + 2(I_{\bar{e}\bar{r}_j} + I_{\bar{e}\bar{e}})^T \omega'_3 + (\tilde{r}^B_3 + \tilde{e}^B)A^T_3 F.$$

$$\tilde{\omega}'_3 (I_{\bar{r}_j \bar{r}_j} + I_{\bar{r}_j \bar{e}} + I_{\bar{e}\bar{r}_j} + I_{\bar{e}\bar{e}})\omega'_3 = \begin{bmatrix} 0 & -1 & 0 \\ 1 & 0 & 0 \\ 0 & 0 & 0 \end{bmatrix} \begin{bmatrix} I_{11} & I_{12} & 0 \\ I_{12} & I_{22} & 0 \\ 0 & 0 & I_{33} \end{bmatrix} \left\{ \begin{matrix} 0 \\ 0 \\ 1 \end{matrix} \right\} \dot{\phi}^2 = 0.$$

$$\tilde{e}\tilde{r}_3' + \tilde{e}\tilde{e} = \begin{bmatrix} 0 & 0 & \dot{e}_y \\ 0 & 0 & -\dot{e}_x \\ -\dot{e}_y & \dot{e}_x & 0 \end{bmatrix} \begin{bmatrix} 0 & 0 & y'+e_y \\ 0 & 0 & -x'-e_x \\ -y'-e_y & x'+e_x & 0 \end{bmatrix}$$

$$= \begin{bmatrix} -\dot{e}_y(y'+e_y) & \dot{e}_y(x'+e_x) & 0 \\ \dot{e}_x(y'+e_y) & -\dot{e}_x(x'+e_x) & 0 \\ 0 & 0 & -\dot{e}_y(y'+e_y)-\dot{e}_x(x'+e_x) \end{bmatrix}.$$

$$2(I_{\tilde{e}\tilde{r}_3} + I_{\tilde{e}\tilde{e}})^T \omega_3' = 2 \begin{bmatrix} I^{11}_{\tilde{e}\tilde{r}_3\tilde{e}} & I^{12}_{\tilde{e}\tilde{r}_3\tilde{e}} & 0 \\ I^{21}_{\tilde{e}\tilde{r}_3\tilde{e}} & I^{22}_{\tilde{e}\tilde{r}_3\tilde{e}} & 0 \\ 0 & 0 & I^{33}_{\tilde{e}\tilde{r}_3\tilde{e}} \end{bmatrix}^T \begin{Bmatrix} 0 \\ 0 \\ 1 \end{Bmatrix} \dot{\phi} = 2 \begin{Bmatrix} 0 \\ 0 \\ I^{33}_{\tilde{e}\tilde{r}_3\tilde{e}} \end{Bmatrix} \dot{\phi}.$$

$$f_\theta^3 = \begin{bmatrix} 0 & 0 & I_{e_y} \\ 0 & 0 & -I_{e_x} \\ -I_{e_y} & I_{e_x} & 0 \end{bmatrix} \begin{bmatrix} \cos\phi & \sin\phi & 0 \\ -\sin\phi & \cos\phi & 0 \\ 0 & 0 & 1 \end{bmatrix} \begin{Bmatrix} 0 \\ -\rho g \\ 0 \end{Bmatrix} / \rho$$

$$+ 2 \begin{Bmatrix} 0 \\ 0 \\ I^{33}_{\tilde{e}\tilde{r}_3\tilde{e}} \end{Bmatrix} \dot{\phi} + \begin{bmatrix} 0 & 0 & e_B^y \\ 0 & 0 & -r_{3B}'^x - e_B^x \\ -e_B^y & r_{3B}'^x + e_B^x & 0 \end{bmatrix} \begin{bmatrix} \cos\phi & \sin\phi & 0 \\ -\sin\phi & \cos\phi & 0 \\ 0 & 0 & 1 \end{bmatrix} \begin{Bmatrix} F \\ 0 \\ 0 \end{Bmatrix} + 2 \begin{Bmatrix} 0 \\ 0 \\ I^{33}_{\tilde{e}\tilde{r}_3\tilde{e}} \end{Bmatrix} \dot{\phi}$$

$$= \left\{ \begin{array}{c} \overline{} \\ \overline{} \\ (\sin\phi I_{e_y} - \cos\phi I_{e_x})g + 2I^{33}_{\tilde{e}\tilde{r}_3\tilde{e}}\dot{\phi} - F[e_B^y\cos\phi + (r_{3B}'^x + e_B^x)\sin\phi] \end{array} \right\}.$$

$$f_\theta^3 = (\sin\phi I_{e_y} - \cos\phi I_{e_x})g + 2I^{33}_{\tilde{e}\tilde{r}_3\tilde{e}}\dot{\phi} - F[e_B^y\cos\phi + (r_{3B}'^x + e_B^x)\sin\phi]$$

Therefore, the generalized force vector in a planar problem is as follows:

$$f = \left\{ \begin{array}{c} (\cos\phi I_{e_x} - \sin\phi I_{e_y})\dot{\phi}^2 + 2(\sin\phi I_{e_x} + \cos\phi I_{e_y})\dot{\phi} + F \\ -m_3 g + (\sin\phi I_{e_x} + \cos\phi I_{e_y})\dot{\phi}^2 - 2(\cos\phi I_{e_x} - \sin\phi I_{e_y})\dot{\phi} \\ (\sin\phi I_{e_y} - \cos\phi I_{e_x})g + 2I^{33}_{\tilde{e}\tilde{r}_3\tilde{e}}\dot{\phi} - F[e_B^y\cos\phi + (r_{3B}'^x + e_B^x)\sin\phi] \\ -\psi^T K\psi a + \psi^T I_N{}^T A_3^T f_b / \rho + \psi^T (I_{\tilde{r}_3\tilde{\omega}_3 N} + I_{\tilde{e}\tilde{\omega}_3 N})^T \omega_3' - 2\psi^T I_{\tilde{e}N}^T \omega_3' + \psi_B^T A_3^T F \end{array} \right\} \quad (4.14)$$

Finally, the equation of motion for the flexible connecting rod on a 2D plane can be recast as follows:

$$(\mathbf{M}\ddot{q} - f)^T \delta\mathbf{q} = 0 \quad (4.15)$$

where the mass matrix M, and the generalized force term f are defined in Eqs. 4.13 and

4.14 respectively. The vector, $q = \{R_3^x \quad R_3^y \quad \phi \quad a\}^T$ is the system generalized coordinates in a planar problem.

The integrals, such as $I_{\tilde{r}_3 \tilde{\omega}_3' N}$, in the above equations are a function of unknowns, q. These integrals can be calculated in two different ways: one is in the ODE-loop and the other calculated prior to ODE iterations by using modal superposition method. The details of these two methods have been discussed in Chapter 3. Appendix 1 gives the expressions of these integrals pertaining to a rectangular beam.

4.4 Constraints in the Slider-Crank Mechanism

The connecting rod of concern is subjected to two types of constraints: a pin-joint constraint connected to the rigid crank and a prismatic joint constraint connected to the massless slider.

The rigid crank and the flexible connecting rod should have the same position vector at all time at the connecting pin-joint A. It can be mathematically expressed as:

$$C_1 = r_2^A - r_3^A = A_2 r_2'^A - R_3 - A_3 \left(r_3'^A + e^A \right) = 0 \tag{4.16}$$

Differentiating the above equation with respect to time once, one has:

$$\dot{C}_1 = A_2 \tilde{\omega}_2' r_2'^A - \dot{R}_3 - A_3 \tilde{\omega}_3' (r_3'^A + e^A) - A_3 \dot{e}^A$$

$$= -A_2 \tilde{r}_2'^A \omega_2' - \dot{R}_3 + A_3 (\tilde{r}_3'^A + \tilde{e}^A) \omega_3' - A_3 \psi_A \dot{a} = 0.$$

which yields a virtual variation of C_1 as

$$\delta C_1 = -\delta R_3 + A_3 (\tilde{r}_3'^A + \tilde{e}^A) \delta \Pi_3' - A_2 \tilde{r}_2'^A \delta \Pi_2' - A_3 \psi_A \delta a = 0 \tag{4.17}$$

Differentiating Eq. 4.16 twice with respect to time, one has:

$$\ddot{C}_1 = A_2 \tilde{\omega}_2' \tilde{\omega}_2' r_2'^A + A_2 \tilde{\alpha}_2' r_2'^A - \ddot{R}_3 - A_3 \tilde{\omega}_3' \tilde{\omega}_3' (r_3'^A + e^A) - A_3 \tilde{\alpha}_3' (r_3'^A + e^A) - 2A_3 \tilde{\omega}_3' \dot{e}^A - A_3 \ddot{e}^A.$$

In the matrix format, the last two equations can be recast as,

$$C_{1_q} \delta q = \left[-A_2 \tilde{r}_2'^A \quad -I \quad A_3 (\tilde{r}_3'^A + \tilde{e}^A) \quad -A_3 \psi_A \right] \{ \delta \Pi_2' \quad \delta R_3 \quad \delta \Pi_3' \quad \delta a \}^T = 0 \tag{4.18}$$

$$C_{1_q} \ddot{q} = \left[-A_2 \tilde{r}_2'^A \quad -I \quad A_3 (\tilde{r}_3'^A + \tilde{e}^A) \quad -A_3 \psi_A \right] \{ \alpha_2' \quad \ddot{R}_3 \quad \alpha_3' \quad \ddot{a} \}^T$$

$$= -A_2 \tilde{\omega}_2' \tilde{\omega}_2' r_2'^A + A_3 \tilde{\omega}_3' \tilde{\omega}_3' (r_3'^A + e^A) + 2A_3 \tilde{\omega}_3' \dot{e}^A \equiv C_{1_{qq}} \tag{4.19}$$

Next, the slider and the flexible connecting rod are connected by the prismatic joint. The slider can only move along the x direction at the joint. The constraint equation for the prismatic joint can then be put together as

$$C_2 = e_j^T\left(r_3^B - R_B\right) = e_j^T\left[R_3 + A_3\left(r_3'^B + e^B\right)\right] - e_j^T R_B = 0 \qquad (4.20)$$

Differentiating the above equation with respect to time once, one has:

$$\dot{C}_2 = e_j^T\left[\dot{R}_3 + A_3\tilde{\omega}_3'\left(r_3'^B + e^B\right) + A_3\dot{e}^B\right] - e_j^T\dot{R}_B = 0.$$

Since $\mathbf{R}_B = [x_B(t)\quad h\quad 0]^T$, one has $e_j^T\dot{R}_B = [0\quad 1\quad 0][\dot{x}_B(t)\quad 0\quad 0]^T = 0$.

Therefore, the equation for $\dot{C}_2$ can be simplified as

$$\dot{C}_2 = e_j^T\left[\dot{R}_3 + A_3\tilde{\omega}_3'\left(r_3'^B + e^B\right) + A_3\dot{e}^B\right] = 0 \qquad (4.21)$$

Differentiating the above equation with respect to time once again, one has

$$\ddot{C}_2 = e_j^T\left[\ddot{R}_3 + A_3\tilde{\omega}_3'\tilde{\omega}_3'\left(r_3'^B + e^B\right) + A_3\tilde{\alpha}_3'\left(r_3'^B + e^B\right) + 2A_3\tilde{\omega}_3'\dot{e}^B + A_3\ddot{e}^B\right] = 0.$$

In a matrix format, the last two equations can be recast as

$$C_{2_q}\delta q = \begin{bmatrix}0 & e_j^T & -e_j^T A_3\left(\tilde{r}_3'^B + \tilde{e}^B\right) & e_j^T A_3\psi_B\end{bmatrix}\{\delta\Pi_2'\quad \delta R_3\quad \delta\Pi_3'\quad \delta a\}^T = 0 \quad (4.22)$$

$$C_{2_q}\ddot{q} = \begin{bmatrix}0 & e_j^T & -e_j^T A_3\left(\tilde{r}_3'^B + \tilde{e}^B\right) & e_j^T A_3\psi_B\end{bmatrix}\{\alpha_2'\quad \ddot{R}_3\quad \alpha_3'\quad \ddot{a}\}^T$$
$$= -e_j^T A_3\tilde{\omega}_3'\tilde{\omega}_3'\left(r_3'^B + e^B\right) - 2e_j^T A_3\tilde{\omega}_3'\dot{e}^B \equiv C_{2_{qq}} \qquad (4.23)$$

Assembling the above two constraints, Eqs. 4.16 and 4.20, together, one has the constraint matrix for the slider-crank mechanism as follows:

$$C = \left\{\begin{array}{l}A_2 r_2'^A - R_3 - A_3\left(r_3'^A + e^A\right) \\ e_j^T\left[R_3 + A_3\left(r_3'^B + e^B\right)\right] - e_j^T R_B\end{array}\right\} = 0 \qquad (4.24)$$

The first order variations of Eq. 4.24 yields

$$C_q\delta q = \begin{bmatrix}-A_2\tilde{r}_2'^A & -I & A_3\left(\tilde{r}_3'^A + \tilde{e}^A\right) & -A_3\psi_A \\ 0 & e_j^T & -e_j^T A_3\left(\tilde{r}_3'^B + \tilde{e}^B\right) & e_j^T A_3\psi_B\end{bmatrix}\{\delta\Pi_2'\quad \delta R_3\quad \delta\Pi_3'\quad \delta a\}^T = 0 \quad (4.25)$$

and the second order time derivative of C gives

$$C_q\ddot{q} = \begin{bmatrix}-A_2\tilde{r}_2'^A & -I & A_3\left(\tilde{r}_3'^A + \tilde{e}^A\right) & -A_3\psi_A \\ 0 & e_j^T & -e_j^T A_3\left(\tilde{r}_3'^B + \tilde{e}^B\right) & e_j^T A_3\psi_B\end{bmatrix}\{\alpha_2'\quad \ddot{R}_3\quad \alpha_3'\quad \ddot{a}\}^T$$

$$= \begin{bmatrix}-A_2\tilde{\omega}_2'\tilde{\omega}_2'r_2'^A + A_3\tilde{\omega}_3'\tilde{\omega}_3'\left(r_3'^A + e^A\right) + 2A_3\tilde{\omega}_3'\dot{e}^A \\ -e_j^T A_3\tilde{\omega}_3'\tilde{\omega}_3'\left(r_3'^B + e^B\right) - 2e_j^T A_3\tilde{\omega}_3'\dot{e}^B\end{bmatrix} \equiv C_{qq} \qquad (4.26)$$

Eqs 4.24 ~4.26 are the constraints on the displacement, the velocity and the acceleration respectively for a general 3D slider-crank mechanism. However, for a planar analysis, the degrees of freedom $\delta\Pi_2'^x$, $\delta\Pi_2'^y$, δR_3^z, $\delta\Pi_3'^x$ and $\delta\Pi_3'^y$ can be eliminated. The terms in Eq.

4.24 can then be reduced in a 2D application as:

$$A_2 r_2^{\prime A} - R_3 - A_3\left(r_3^{\prime A} + e^A\right) =$$

$$\begin{bmatrix} \cos\theta & -\sin\theta & 0 \\ \sin\theta & \cos\theta & 0 \\ 0 & 0 & 1 \end{bmatrix}\begin{bmatrix} L \\ 0 \\ 0 \end{bmatrix} - \begin{bmatrix} R_3^x \\ R_3^y \\ 0 \end{bmatrix} - \begin{bmatrix} \cos\phi & -\sin\phi & 0 \\ \sin\phi & \cos\phi & 0 \\ 0 & 0 & 1 \end{bmatrix}\begin{bmatrix} r_{3A}^{\prime x} + e_A^x \\ e_A^y \\ 0 \end{bmatrix}$$

$$= \begin{bmatrix} L\cos\theta - R_3^x - \left(r_{3A}^{\prime x} + e_A^x\right)\cos\phi + e_A^y\sin\phi \\ L\sin\theta - R_3^y - \left(r_{3A}^{\prime x} + e_A^x\right)\sin\phi - e_A^y\cos\phi \\ \rule{6cm}{0.4pt} \\ 0 \end{bmatrix} = 0.$$

$$e_j^T\left[R_3 + A_3\left(r_3^{\prime B} + e^B\right)\right] - e_j^T R_B = \begin{Bmatrix} 0 \\ 1 \\ 0 \end{Bmatrix}^T\left(\begin{bmatrix} R_3^x \\ R_3^y \\ 0 \end{bmatrix} + \begin{bmatrix} \cos\phi & -\sin\phi & 0 \\ \sin\phi & \cos\phi & 0 \\ 0 & 0 & 1 \end{bmatrix}\begin{bmatrix} r_{3B}^{\prime x} + e_B^x \\ e_B^y \\ 0 \end{bmatrix} - \begin{Bmatrix} X_B(t) \\ h \\ 0 \end{Bmatrix}\right)$$

$$= R_3^y + \left(r_{3B}^{\prime x} + e_B^x\right)\sin\phi + e_B^y\cos\phi - h = 0.$$

As a result, the displacement constraints in a 2D plane are reduced to:

$$C = \begin{bmatrix} L\cos\theta - R_3^x - \left(r_{3A}^{\prime x} + e_A^x\right)\cos\phi + e_A^y\sin\phi \\ L\sin\theta - R_3^y - \left(r_{3A}^{\prime x} + e_A^x\right)\sin\phi - e_A^y\cos\phi \\ R_3^y + \left(r_{3B}^{\prime x} + e_B^x\right)\sin\phi + e_B^y\cos\phi - h \end{bmatrix} = 0 \qquad (4.27)$$

where the values of $r_{3A}^{\prime x}$ and $r_{3B}^{\prime x}$ are dependent upon the origin of the selected body fixed

coordinates. If the origin of body-fixed coordinate is placed at the center of gravity, one

has $r_{3A}^{\prime x} = -P/2$, $r_{3B}^{\prime x} = P/2$, while at the left end, $r_{3A}^{\prime x} = 0$, $r_{3B}^{\prime x} = P$.

The Jacobian matrix C_q, in Eq. 4.25, can be repeated here as

$$C_q = \begin{bmatrix} -A_2 \tilde{r}_2^{\prime A} & -I & A_3(\tilde{r}_3^{\prime A} + \tilde{e}^A) & -A_3\psi_A \\ 0 & e_j^T & -e_j^T A_3\left(\tilde{r}_3^{\prime B} + \tilde{e}^B\right) & e_j^T A_3\psi_B \end{bmatrix},$$

which can also be simplified for a 2D application as

$$-A_2\tilde{r}_{2A}' = -\begin{bmatrix} \cos\theta & -\sin\theta & 0 \\ \sin\theta & \cos\theta & 0 \\ 0 & 0 & 1 \end{bmatrix}\begin{bmatrix} 0 & 0 & 0 \\ 0 & 0 & -L \\ 0 & L & 0 \end{bmatrix} = \begin{bmatrix} 0 & 0 & -L\sin\theta \\ 0 & 0 & L\cos\theta \\ 0 & -L & 0 \end{bmatrix}.$$

$$A_3(\tilde{r}_{3A}' + \tilde{e}_A) = \begin{bmatrix} \cos\phi & -\sin\phi & 0 \\ \sin\phi & \cos\phi & 0 \\ 0 & 0 & 1 \end{bmatrix}\begin{bmatrix} 0 & 0 & e_A^y \\ 0 & 0 & -r_{3A}^{\prime x} - e_A^x \\ -e_A^y & r_{3A}^{\prime x} + e_A^x & 0 \end{bmatrix}$$

$$= \begin{bmatrix} 0 & 0 & e_A^y \cos\phi + (r_{3A}'^x + e_A^x)\sin\phi \\ 0 & 0 & e_A^y \sin\phi - (r_{3A}'^x + e_A^x)\cos\phi \\ -e_A^y & r_{3A}'^x + e_A^x & 0 \end{bmatrix}.$$

$$-A_3\psi_A = -\begin{bmatrix} \cos\phi & -\sin\phi & 0 \\ \sin\phi & \cos\phi & 0 \\ 0 & 0 & 1 \end{bmatrix}\begin{bmatrix} \Psi_{1A}^I & \cdots & \Psi_{1A}^{Nm} \\ \Psi_{2A}^I & \cdots & \Psi_{2A}^{Nm} \\ 0 & 0 & 0 \end{bmatrix}$$

$$= \begin{bmatrix} -\Psi_{1A}^I\cos\phi + \Psi_{2A}^I\sin\phi & \cdots & -\Psi_{1A}^{Nm}\cos\phi + \Psi_{2A}^{Nm}\sin\phi \\ -\Psi_{1A}^I\sin\phi - \Psi_{2A}^I\cos\phi & \cdots & -\Psi_{1A}^{Nm}\sin\phi - \Psi_{2A}^{Nm}\cos\phi \\ 0 & 0 & 0 \end{bmatrix}.$$

$$-\mathbf{e}_j^T A_3\tilde{r}_{3B}' = -\begin{Bmatrix} 0 \\ 1 \\ 0 \end{Bmatrix}^T\begin{bmatrix} \cos\phi & -\sin\phi & 0 \\ \sin\phi & \cos\phi & 0 \\ 0 & 0 & 1 \end{bmatrix}\begin{bmatrix} 0 & 0 & e_B^y \\ 0 & 0 & -r_{3B}'^x - e_B^x \\ -e_B^y & r_{3B}'^x + e_B^x & 0 \end{bmatrix}$$

$$= -\begin{Bmatrix} \sin\phi \\ \cos\phi \\ 0 \end{Bmatrix}^T\begin{bmatrix} 0 & 0 & e_B^y \\ 0 & 0 & -r_{3B}'^x - e_B^x \\ -e_B^y & r_{3B}'^x + e_B^x & 0 \end{bmatrix} = \begin{Bmatrix} 0 & 0 & -e_B^y\sin\phi + (r_{3B}'^x + e_B^x)\cos\phi \end{Bmatrix}.$$

$$\mathbf{e}_j^T A_3\psi_B = \begin{Bmatrix} 0 \\ 1 \\ 0 \end{Bmatrix}^T\begin{bmatrix} \cos\phi & -\sin\phi & 0 \\ \sin\phi & \cos\phi & 0 \\ 0 & 0 & 1 \end{bmatrix}\begin{bmatrix} \Psi_{1B}^I & \cdots & \Psi_{1B}^{Nm} \\ \Psi_{2B}^I & \cdots & \Psi_{2B}^{Nm} \\ 0 & 0 & 0 \end{bmatrix}$$

$$= \begin{Bmatrix} 0 \\ 1 \\ 0 \end{Bmatrix}^T\begin{bmatrix} \Psi_{1B}^I\cos\phi - \Psi_{2B}^I\sin\phi & \cdots & \Psi_{2B}^{Nm}\cos\phi - \Psi_{2B}^{Nm}\sin\phi \\ \Psi_{1B}^I\sin\phi + \Psi_{2B}^I\cos\phi & \cdots & \Psi_{1B}^{Nm}\sin\phi + \Psi_{2B}^{Nm}\cos\phi \\ 0 & 0 & 0 \end{bmatrix}$$

$$= \begin{Bmatrix} \Psi_{1B}^I\sin\phi + \Psi_{2B}^I\cos\phi & \cdots & \Psi_{1B}^{Nm}\sin\phi + \Psi_{2B}^{Nm}\cos\phi \end{Bmatrix}.$$

Finally, the Jacobian matrix C_q is obtained for the 2D slider-crank mechanism as:

$$C_q = \begin{bmatrix} -L\sin\theta & -1 & 0 & e_A^y\cos\phi+(r_{3A}'^x+e_A^x)\sin\phi & -\Psi_{1A}^I\cos\phi+\Psi_{2A}^I\sin\phi & \cdots & -\Psi_{1A}^{Nm}\cos\phi+\Psi_{2A}^{Nm}\sin\phi \\ L\cos\theta & 0 & -1 & e_A^y\sin\phi-(r_{3A}'^x+e_A^x)\cos\phi & -\Psi_{1A}^I\sin\phi-\Psi_{2A}^I\cos\phi & \cdots & -\Psi_{1A}^{Nm}\sin\phi-\Psi_{2A}^{Nm}\cos\phi \\ 0 & 0 & 1 & -e_B^y\sin\phi+(r_{3B}'^x+e_B^x)\cos\phi & \Psi_{1B}^I\sin\phi+\Psi_{2B}^I\cos\phi & \cdots & \Psi_{1B}^{Nm}\sin\phi+\Psi_{2B}^{Nm}\cos\phi \end{bmatrix} \quad (4.28)$$

The C_{qq} term given in Eq. 4.26 is repeated here

$$C_{qq} = \begin{bmatrix} -A_2\tilde{\omega}_2'\tilde{\omega}_2'r_2'^A + A_3\tilde{\omega}_3'\tilde{\omega}_3'(r_3'^A + e^A) + 2A_3\tilde{\omega}_3'\dot{e}^A \\ -e_j^T A_3\tilde{\omega}_3'\tilde{\omega}_3'(r_3'^B + e^B) - 2e_j^T A_3\tilde{\omega}_3'\dot{e}^B \end{bmatrix},$$

which can be explicitly spelled out for the given connecting rod as follows:

$$-A_2\tilde{\omega}_2'\tilde{\omega}_2'r_2'^A = -\begin{bmatrix} \cos\theta & -\sin\theta & 0 \\ \sin\theta & \cos\theta & 0 \\ 0 & 0 & 1 \end{bmatrix}\begin{bmatrix} 0 & -1 & 0 \\ 1 & 0 & 0 \\ 0 & 0 & 0 \end{bmatrix}\begin{bmatrix} 0 & -1 & 0 \\ 1 & 0 & 0 \\ 0 & 0 & 0 \end{bmatrix}\dot{\theta}^2\begin{Bmatrix} L \\ 0 \\ 0 \end{Bmatrix} = \begin{Bmatrix} L\cos\theta \\ L\sin\theta \\ 0 \end{Bmatrix}\dot{\theta}^2.$$

$$A_3\tilde{\omega}_3'\tilde{\omega}_3'(r_3'^A + e^A) = \begin{bmatrix} \cos\phi & -\sin\phi & 0 \\ \sin\phi & \cos\phi & 0 \\ 0 & 0 & 1 \end{bmatrix}\begin{bmatrix} 0 & -1 & 0 \\ 1 & 0 & 0 \\ 0 & 0 & 0 \end{bmatrix}\begin{bmatrix} 0 & -1 & 0 \\ 1 & 0 & 0 \\ 0 & 0 & 0 \end{bmatrix}\dot{\phi}^2\begin{Bmatrix} r_{3A}'^x + e_A^x \\ e_A^y \\ 0 \end{Bmatrix}$$

$$= \begin{Bmatrix} e_A^y\sin\phi - (r_{3A}'^x + e_A^x)\cos\phi \\ -e_A^y\cos\phi - (r_{3A}'^x + e_A^x)\sin\phi \\ 0 \end{Bmatrix}\dot{\phi}^2.$$

$$2A_3\tilde{\omega}_3'\dot{e}^A = 2\begin{bmatrix} \cos\phi & -\sin\phi & 0 \\ \sin\phi & \cos\phi & 0 \\ 0 & 0 & 1 \end{bmatrix}\begin{bmatrix} 0 & -1 & 0 \\ 1 & 0 & 0 \\ 0 & 0 & 0 \end{bmatrix}\dot{\phi}\begin{Bmatrix} \dot{e}_A^x \\ \dot{e}_A^y \\ 0 \end{Bmatrix} = 2\begin{Bmatrix} -\dot{e}_A^x\sin\phi - \dot{e}_A^y\cos\phi \\ \dot{e}_A^x\cos\phi - \dot{e}_A^y\sin\phi \\ 0 \end{Bmatrix}\dot{\phi}.$$

$$-e_j^T A_3\tilde{\omega}_3'\tilde{\omega}_3'(r_3'^B + e^B) = -\begin{Bmatrix} 0 \\ 1 \\ 0 \end{Bmatrix}^T\begin{bmatrix} \cos\phi & -\sin\phi & 0 \\ \sin\phi & \cos\phi & 0 \\ 0 & 0 & 1 \end{bmatrix}\begin{bmatrix} 0 & -1 & 0 \\ 1 & 0 & 0 \\ 0 & 0 & 0 \end{bmatrix}\begin{bmatrix} 0 & -1 & 0 \\ 1 & 0 & 0 \\ 0 & 0 & 0 \end{bmatrix}\dot{\phi}^2\begin{Bmatrix} r_{3B}'^x + e_B^x \\ e_B^y \\ 0 \end{Bmatrix}$$

$$= [(r_{3B}'^x + e_B^x)\sin\phi + e_B^y\cos\phi]\dot{\phi}^2.$$

$$-2e_j^T A_3\tilde{\omega}_3'\dot{e}^B = -2\begin{Bmatrix} 0 \\ 1 \\ 0 \end{Bmatrix}^T\begin{bmatrix} \cos\phi & -\sin\phi & 0 \\ \sin\phi & \cos\phi & 0 \\ 0 & 0 & 1 \end{bmatrix}\begin{bmatrix} 0 & -1 & 0 \\ 1 & 0 & 0 \\ 0 & 0 & 0 \end{bmatrix}\dot{\phi}\begin{Bmatrix} \dot{e}_B^x \\ \dot{e}_B^y \\ 0 \end{Bmatrix} = 2\dot{\phi}(\dot{e}_B^y\sin\phi - \dot{e}_B^x\cos\phi).$$

Finally, C_{qq} for the 2D slider-crank mechanism is given by

$$C_{qq} = \begin{Bmatrix} L\cos\theta\dot{\theta}^2 + [e_A^y\sin\phi - (r_{3A}'^x + e_A^x)\cos\phi]\dot{\phi}^2 - 2(\dot{e}_A^x\sin\phi + \dot{e}_A^y\cos\phi)\dot{\phi} \\ L\sin\theta\dot{\theta}^2 - [e_A^y\cos\phi + (r_{3A}'^x + e_A^x)\sin\phi]\dot{\phi}^2 + 2(\dot{e}_A^x\cos\phi - \dot{e}_A^y\sin\phi)\dot{\phi} \\ [(r_{3B}'^x + e_B^x)\sin\phi + e_B^y\cos\phi]\dot{\phi}^2 + 2(\dot{e}_B^y\sin\phi - \dot{e}_B^x\cos\phi)\dot{\phi} \end{Bmatrix} \quad (4.29)$$

The constraint equations derived here, along with the equations of motion for the crank and the connecting rod, are used in Section 4.5 to form the equation of motion for the slider-crank mechanism.

4.5 Equation of Motion for the Planar Slider-Crank Mechanism with a Flexible Connecting Rod

Collecting the equations of motion for the rigid crank, Eq. 4.6, the flexible connecting rod, Eq.4.15, and system constraints, Eqs. 4.27 ~ 4.29, together, one forms the equation of motion for a planar slider-crank mechanism as:

$$\begin{bmatrix} M & C_q^T \\ C_q & 0 \end{bmatrix} \begin{Bmatrix} \ddot{q} \\ \lambda \end{Bmatrix} = \begin{Bmatrix} f \\ C_{qq} \end{Bmatrix} \tag{4.30}$$

where

$$M =$$

$$\begin{bmatrix} m_2 \dfrac{4L^2 + d^2}{12} & 0 & 0 & 0 & 0 & 0 \\ & m_3 & 0 & -\cos\phi I_{e_y} - \sin\phi I_{e_x} & \cos\phi I_{N\psi1}^l - \sin\phi I_{N\psi2}^l & \cdots & \cos\phi I_{N\psi1}^{Nm} - \sin\phi I_{N\psi2}^{Nm} \\ & & m_3 & -\sin\phi I_{e_y} + \cos\phi I_{e_x} & \sin\phi I_{N\psi1}^l + \cos\phi I_{N\psi2}^l & \cdots & \sin\phi I_{N\psi1}^{Nm} + \cos\phi I_{N\psi2}^{Nm} \\ & & & I_{(x'+e_x)^2+(y'+e_y)^2} & I_{x'e_x N\psi_2^l} - I_{y'e_y N\psi_1^l} & \cdots & I_{x'e_x N\psi_2^{Nm}} - I_{y'e_y N\psi_1^{Nm}} \\ & \text{sym.} & & & & & \psi^T I_{N^T N} \psi \end{bmatrix} \tag{4.31}$$

$$\ddot{q} = \begin{Bmatrix} \ddot{\theta} & \ddot{R}_3^x & \ddot{R}_3^y & \ddot{\phi} & \ddot{a} \end{Bmatrix}^T \tag{4.32}$$

$$f = \begin{Bmatrix} -m_2 gL/2\cos\theta \\ \left(\cos\phi I_{e_y} - \sin\phi I_{e_y}\right)\dot{\phi}^2 + 2\left(\sin\phi I_{e_x} + \cos\phi I_{e_y}\right)\dot{\phi} + F \\ -m_3 g + \left(\sin\phi I_{e_x} + \cos\phi I_{e_y}\right)\dot{\phi}^2 - 2\left(\cos\phi I_{e_x} - \sin\phi I_{e_y}\right)\dot{\phi} \\ \left(\sin\phi I_{e_y} - \cos\phi I_{e_x}\right)g + 2I_{e\bar{r}_3e}^{33}\dot{\phi} - F\left[e_y^B\cos\phi + \left(x'^B + e_x^B\right)\sin\phi\right] \\ -\psi^T K\psi a + \psi^T I_N{}^T A_3^T f_b / \rho + \psi^T (I_{\bar{r}_3\omega_3' N} + I_{\bar{e}\omega_3' N})^T \omega_3' - 2\psi^T I_{\bar{e}N}^T \omega_3' + \psi_B^T A_3^T F \end{Bmatrix} \tag{4.33}$$

$$C = \begin{bmatrix} L\cos\theta - R_3^x - \left(r_{3A}'^x + e_A^x\right)\cos\phi + e_A^y\sin\phi \\ L\sin\theta - R_3^y - \left(r_{3A}'^x + e_A^x\right)\sin\phi - e_A^y\cos\phi \\ R_3^y + \left(r_{3B}'^x + e_A^x\right)\sin\phi + e_B^y\cos\phi - h \end{bmatrix} = 0 \tag{4.34}$$

$$C_q = \begin{bmatrix} -L\sin\theta & -1 & 0 & e_A^y\cos\phi + (r_{3A}'^x + e_A^x)\sin\phi & -\Psi_{A1}^l\cos\phi + \Psi_{A2}^l\sin\phi & \cdots & -\Psi_{A1}^{Nm}\cos\phi + \Psi_{A2}^{Nm}\sin\phi \\ L\cos\theta & 0 & -1 & e_A^y\sin\phi - (r_{3A}'^x + e_A^x)\cos\phi & -\Psi_{A1}^l\sin\phi - \Psi_{A2}^l\cos\phi & \cdots & -\Psi_{A1}^{Nm}\sin\phi - \Psi_{A2}^{Nm}\cos\phi \\ 0 & 0 & 1 & -e_B^y\sin\phi + (r_{3B}'^x + e_B^x)\cos\phi & \Psi_{B1}^l\sin\phi + \Psi_{B2}^l\cos\phi & \cdots & \Psi_{B1}^{Nm}\sin\phi + \Psi_{B2}^{Nm}\cos\phi \end{bmatrix} \tag{4.35}$$

and

$$C_{qq} = \begin{Bmatrix} L\cos\theta\dot{\theta}^2 + \left[e_A^y\sin\phi - (r_{3A}'^x + e_A^x)\cos\phi\right]\dot{\phi}^2 - \left(\dot{e}_A^x\sin\phi + \dot{e}_A^y\cos\phi\right)\dot{\phi} \\ L\sin\theta\dot{\theta}^2 - \left[e_A^y\cos\phi + (r_{3A}'^x + e_A^x)\sin\phi\right]\dot{\phi}^2 + \left(\dot{e}_A^x\cos\phi - \dot{e}_A^y\sin\phi\right)\dot{\phi} \\ \left[(r_{3B}'^x + e_B^x)\sin\phi + e_B^y\cos\phi\right]\dot{\phi}^2 + 2\left(\dot{e}_B^y\sin\phi - \dot{e}_B^x\cos\phi\right)\dot{\phi} \end{Bmatrix} \tag{4.36}$$

For the benefit of the coordinates partitioning method, the generalized system coordinates are rearranged in the order of dependent and independent coordinates as

$$\ddot{q} = \left\{ \ddot{R}_3^x \quad \ddot{R}_3^y \quad \ddot{\phi} \quad \ddot{\theta} \quad \ddot{a} \right\}^T$$ (4.37)

Accordingly, the constrained equation of motion is then given by

$$\begin{bmatrix} M & C_q^T \\ C_q & 0 \end{bmatrix} \begin{Bmatrix} \ddot{q} \\ \lambda \end{Bmatrix} = \begin{Bmatrix} f \\ C_{qq} \end{Bmatrix}$$ (4.38)

However, one has

$$M =$$

$$\begin{bmatrix} m_3 & 0 & -\cos\phi I_{e_y} - \sin\phi I_{e_x} & 0 & \cos\phi I_{N\psi 1}^1 - \sin\phi I_{N\psi 2}^1 & \cdots & \cos\phi I_{N\psi 1}^{Nm} - \sin\phi I_{N\psi 2}^{Nm} \\ & m_3 & \sin\phi I_{e_y} + \cos\phi I_{e_x} & 0 & \sin\phi I_{N\psi 1}^1 + \cos\phi I_{N\psi 2}^1 & \cdots & \sin\phi I_{N\psi 1}^{Nm} + \cos\phi I_{N\psi 2}^{Nm} \\ & & I_{(x'+e_x)^2 + (y'+e_y)^2} & 0 & I_{x'e_x N\psi 2}^1 - I_{y'e_y N\psi 1}^1 & \cdots & I_{x'e_x N\psi 2}^{Nm} - I_{y'e_y N\psi 1}^{Nm} \\ & & & m_2\dfrac{4L^2+d^2}{12} & 0 & 0 & 0 \\ & \text{sym.} & & & & & \psi^T I_{N^T N}\psi \end{bmatrix}$$ (4.39)

$$f = \left\{ \begin{array}{c} \left(\cos\phi I_{e_x} - \sin\phi I_{e_y}\right)\dot{\phi}^2 + 2\left(\sin\phi I_{\dot{e}_x} + \cos\phi I_{\dot{e}_y}\right)\dot{\phi} + F \\ -m_3 g + \left(\sin\phi I_{e_x} + \cos\phi I_{e_y}\right)\dot{\phi}^2 - 2\left(\cos\phi I_{\dot{e}_x} - \sin\phi I_{\dot{e}_y}\right)\dot{\phi} \\ \left(\sin\phi I_{e_y} - \cos\phi I_{e_x}\right)g + 2I_{\dot{e}r_3\dot{e}}^{33}\dot{\phi} - F\left[e_B^y \cos\phi + \left(r_{3B}^{\prime x} + e_B^x\right)\sin\phi\right] \\ -m_2 gL/2\cos\theta \\ -\psi^T K\psi a + \psi^T I_N^T A_3^T f_b/\rho + \psi^T (I_{\dot{r}_j\tilde{\omega}_j N} + I_{\tilde{e}\tilde{\omega}_j N})^T \omega_3' - 2\psi^T I_{\tilde{e}N}^T \omega_3' + \psi_B^T A_3^T F \end{array} \right\}$$ (4.40)

The constraint equation, Eq.4.34, is rewritten as follows:

$$C = \begin{bmatrix} L\cos\theta - R_3^x - \left(r_{3A}^{\prime x} + e_A^x\right)\cos\phi + e_A^y \sin\phi \\ L\sin\theta - R_3^y - \left(r_{3A}^{\prime x} + e_A^x\right)\sin\phi - e_A^y \cos\phi \\ R_3^y + \left(r_{3B}^{\prime x} + e_B^x\right)\sin\phi + e_B^y \cos\phi - h \end{bmatrix} = 0.$$

Adding the second row to the third row of the above equation to remove the unknown R_3^y, one has:

$$L\sin\theta + \left(r_{3B}^{\prime x} - r_{3A}^{\prime x} + e_B^x - e_A^x\right)\sin\phi - \left(e_B^y - e_A^y\right)\cos\phi - h = 0$$ (4.41)

Since $r_{3B}^{\prime x} - r_{3A}^{\prime x} = P$, where P is the length of the connecting rod, regardless where the origin of the connecting rod is placed, Eq. 4.41 becomes:

$$L\sin\theta + \left(P + e_B^x - e_A^x\right)\sin\phi - \left(e_B^y - e_A^y\right)\cos\phi - h = 0.$$

Dividing by $\sqrt{\left(P + e_B^x - e_A^x\right)^2 + \left(e_B^y - e_A^y\right)^2}$ on the both sides of the above equation and

using the trigonometric formula, one has:

$$\sin(\phi + \alpha) = (h - L\sin\theta)\Big/ \sqrt{(P + e_B^x - e_A^x)^2 + (e_B^y - e_A^y)^2} \qquad (4.42)$$

where $\alpha = \arctan[(e_B^y - e_A^y)/(P + e_B^x - e_A^x)]$.

Solving Eq. 4.42, one has

$$\phi = \arcsin\left((h - L\sin\theta)\Big/ \sqrt{(P + e_B^x - e_A^x)^2 + (e_B^y - e_A^y)^2}\right) - \alpha \qquad (4.43)$$

Once ϕ is obtained, R_3^x and R_3^y can be solved easily based upon the constraint equation,

Eq. 4.34 as $R_3^x = L\cos\theta - (r_{3A}'^x + e_A^x)\cos\phi + e_A^y \sin\phi$ and

$R_3^y = L\sin\theta - (r_{3A}'^x + e_A^x)\sin\phi - e_A^y \cos\phi$.

Select R_3^x, R_3^y as dependent variables and ϕ, a as independent variables, the matrix given

by Eq. 4.35 can be divided as

$$C_q = \begin{bmatrix} C_{qd} & \vdots & C_{ql} \end{bmatrix} \qquad (4.44)$$

where

$$C_{qd} = \begin{bmatrix} -1 & 0 & e_A^y \cos\phi + (r_{3A}'^x + e_A^x)\sin\phi \\ 0 & -1 & e_A^y \sin\phi - (r_{3A}'^x + e_A^x)\cos\phi \\ 0 & 1 & -e_B^y \sin\phi + (r_{3B}'^x + e_B^x)\cos\phi \end{bmatrix} \qquad (4.45)$$

and

$$C_{ql} = \begin{bmatrix} -L\sin\theta & -\Psi_{1A}^1 \cos\phi + \Psi_{2A}^1 \sin\phi & \cdots & -\Psi_{1A}^{Nm} \cos\phi + \Psi_{2A}^{Nm} \sin\phi \\ L\cos\theta & -\Psi_{1A}^1 \sin\phi - \Psi_{2A}^1 \cos\phi & \cdots & -\Psi_{1A}^{Nm} \sin\phi - \Psi_{2A}^{Nm} \cos\phi \\ 0 & \Psi_{1B}^1 \sin\phi + \Psi_{2B}^1 \cos\phi & \cdots & \Psi_{1B}^{Nm} \sin\phi + \Psi_{2B}^{Nm} \cos\phi \end{bmatrix} \qquad (4.46)$$

According to Eqs. 3.37 and 3.42 in Chapter 3, one has the dependent velocity term and

the dependent acceleration term as follows:

$$\{\dot{R}_3^x \quad \dot{R}_3^y \quad \dot{\phi}\}^T = -C_{qd}^{-1} C_{ql} \begin{Bmatrix} \dot{\theta} \\ \dot{a} \end{Bmatrix} \qquad (4.47)$$

$$\{\ddot{R}_3^x \quad \ddot{R}_3^y \quad \ddot{\phi}\}^T = -C_{qd}^{-1} C_{ql} \begin{Bmatrix} \ddot{\theta} \\ \ddot{a} \end{Bmatrix} + C_{qd}^{-1} C_{qq} \qquad (4.48)$$

where C_{qq} is defined in Eq. 4.36.

4.6 Equation of Motion for the Planar Slider-Crank Mechanism with a Rigid Connecting Rod

Two sets of equations of motion for the rigid slider-crank mechanism are derived in this section. In the first case, the origin of the body-fixed coordinate system of the connecting rod is placed at its center. In the other, it is placed at its left end. The equation of motion derived in the preceding section for the slider-crank mechanism with a flexible connecting rod can be directly used here since the rigid slider-crank mechanism is its special case.

4.6.1 Origin at the Center of Gravity

Eliminating the terms related to the elastic displacement and the mode shape in Eq. 4.38, one has the equation of motion for the rigid slider-crank mechanism:

$$\begin{bmatrix} M & C_q^T \\ C_q & 0 \end{bmatrix} \begin{Bmatrix} \ddot{q} \\ \lambda \end{Bmatrix} = \begin{Bmatrix} f \\ C_{qq} \end{Bmatrix} \tag{4.49}$$

If the origin of the body-fixed coordinate system is located at the center of the connecting rod, $r_{3A}'^x = -P/2$ and $r_{3B}'^x = P/2$. Substituting these values into Eqs. 4.39, 4.40 and 4.34 and eliminating the flexible term, one has

$$M = \begin{bmatrix} m_3 & 0 & 0 & 0 \\ & m_3 & 0 & 0 \\ & & I_{x'^2+y'^2} & 0 \\ sym. & & & m_2\dfrac{4L^2+d^2}{12} \end{bmatrix} = \begin{bmatrix} m_3 & 0 & 0 & 0 \\ & m_3 & 0 & 0 \\ & & m_3\dfrac{P^2+d^2}{12} & 0 \\ & & & m_2\dfrac{4L^2+d^2}{12} \end{bmatrix} \tag{4.50}$$

$$f = \begin{Bmatrix} \left(\cos\phi I_{x'} - \sin\phi I_{y'}\right)\dot{\phi}^2 + F \\ -m_3 g + \left(\sin\phi I_{x'} + \cos\phi I_{y'}\right)\dot{\phi}^2 \\ \left(\sin\phi I_{y'} - \cos\phi I_{x'}\right)g - Fr_{3B}'^x\sin\phi \\ -m_2 gL/2\cos\theta \end{Bmatrix} = \begin{Bmatrix} F \\ -m_3 g \\ -Fr_{3B}'^x\sin\phi \\ -m_2 gL/2\cos\theta \end{Bmatrix} = \begin{Bmatrix} F \\ -m_3 g \\ -FP/2\sin\phi \\ -m_2 gL/2\cos\theta \end{Bmatrix} \tag{4.51}$$

$$C = \begin{bmatrix} L\cos\theta - R_3^x - r_{3A}'^x\cos\phi \\ L\sin\theta - R_3^y - r_{3A}'^x\sin\phi \\ R_3^y + r_{3B}'^x\sin\phi - h \end{bmatrix} = \begin{bmatrix} L\cos\theta - R_3^x + P/2\cos\phi \\ L\sin\theta - R_3^y + P/2\sin\phi \\ R_3^y + P/2\sin\phi - h \end{bmatrix} = 0 \tag{4.52}$$

Adding the second row to the third row in the above constraints equation, one has

$$L\sin\theta + P\sin\phi - h = 0 \tag{4.53}$$

From the above equation, one can obtain the value of $\sin\phi$ when θ is obtained from the ODE solution. However, it is difficult to determine the sign of $\cos\phi$.

Assuming that the crank rotates counter-clockwise for a complete cycle from 0 to 2π, one can determine the 8 key configurations of the slider-crank mechanism. These key configurations are shown in Fig. 4.5, where Points O, A and B mark the pinned end of the crank, the pinned joint between the crank and the connecting rod and the massless slider, respectively. The angle ϕ is measured counter-clockwise from the positive global x axis to the positive local x axis. The latter is pointing from point A to B.
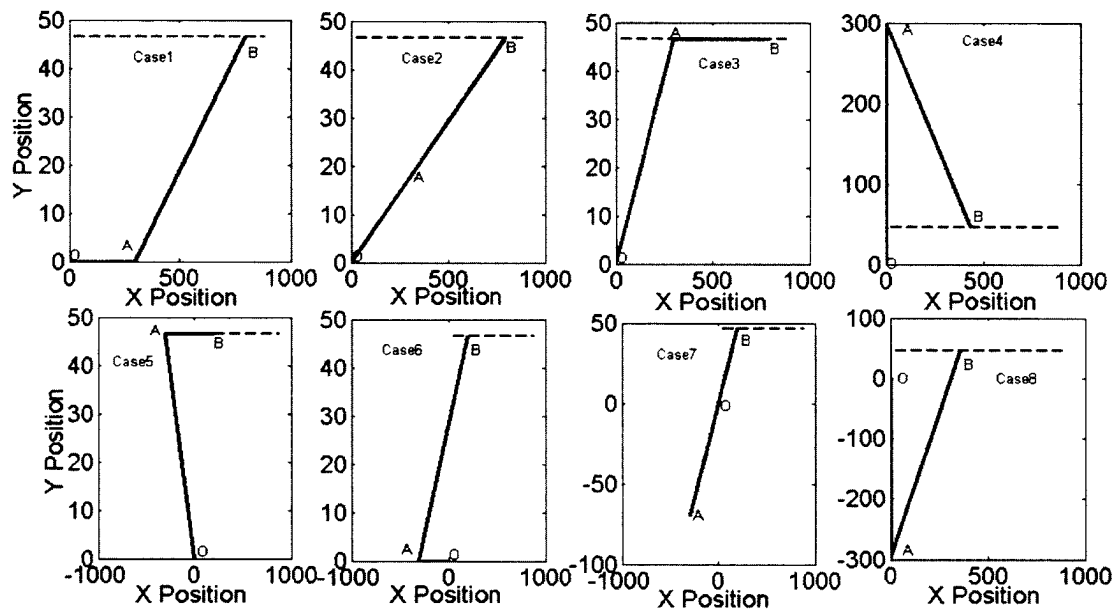
Figure 4.5 Possible Configurations of the Crank-Slider Mechanism in a Full Cycle

The details of the figures are discussed as follows.

1).The rigid crank OA is aligned with the $+x$ *axis*

Case 1 is the initial position in which $\sin\phi = 0.093$ or $\phi \approx 0.093$ radians. The force starts to pull the slider to the right which causes the crank to rotate with respect to point O counter-clockwise. As a result, the rotation angle, θ, of the rank will increase gradually, while the rotation angle, ϕ, will decrease.

2).Points O, A, and B are in a line

Case 2 is the position when the rigid crank and the connecting rod are in a line, in

which $\sin\phi = 0.0581$ or $\phi \approx 0.0581$ radians. In this case, Point B of the connecting rod reaches the maximal distance measured from Point O. From Case 1 to 2; it can be seen that Point B moves further from Point O, and the value of ϕ decreases. It means that $\cos\phi$ is always positive between Cases 1 and 2.

3). The connecting rod AB parallels the $+x$ axis

The value of ϕ in this case decreases to zero. That is $\cos\phi = 1$ and $\tan\phi = 0$. From Case 2 to 3, the value of ϕ is gradually reduced to zero. However, after this, Point A will move vertically higher than Point B. In this case, the value of ϕ will further be reduced from 0 or 2π.

4). The rigid crank OA is aligned with the $+y$ axis

The value of ϕ at Case 4 is 5.751 or -0.5317 radians. From Case 3 to Case 4, Point B moves closer to Point O. Though the value of ϕ decreases, it still falls between $3\pi/2$ and 2π. Thus, $\cos\phi$ is always positive between Cases 3 and 4.

5). The connecting rod AB parallels the x axis

In Case 5, ϕ becomes 2π. The value of ϕ is increased from Case 4 to Case 5 to reach 2π. However, it falls between $3\pi/2$ and 2π. After Case 5, Point A will move lower than Point B. Thus, ϕ increases up from zero to become positive.

6). The rigid crank OA is aligned with the $-x$ axis

It can be noted that the value of ϕ is increased from 0 radians in Case 5 to 0.093 radians in Case 6.

7). Points A, O and B are in a line

In Case 7, Point B of the connecting rod reaches the shortest distance to Point O. The value of ϕ is increased from 0.093 radians in Case 6 to 0.235 radians in Case 7.

8). The rigid crank OA is aligned with the $-y$ axis

The value of ϕ is increased from 0.235 in Case 7 to 0.766 radians in Case 8. Finally, the crank will complete a cycle moving from Case 8 to Case 1, during which the value of ϕ is reduced from 0.766 radians to 0.093 radians.

Based upon the dimensions of the mechanism given in this study, it can be observed that, for the crank to complete a cycle counter-clockwise, the value of ϕ falls in

$-\pi/2 < \phi < \pi/2$; i.e., in the first and the fourth quadrant. Hence, the value of ϕ can be found by $\phi = \arcsin[(h - L\sin\theta)/P]$. Furthermore, one can compute the location of the origin of the body-fixed coordinate based upon the constraint equations:

$R_j^x = L\cos\theta + P/2\cos\phi$ and $R_j^y = L\sin\theta + P/2\sin\phi$.

The general formula for Jacobian matrices, C_q, C_{qd} and C_{ql} given in Eqs. 4.35, 4.45 and 4.46 can be found for the given mechanism as

$$C_q = \begin{bmatrix} -1 & 0 & r_{3A}^{'x}\sin\phi & -L\sin\theta \\ 0 & -1 & -r_{3A}^{'x}\cos\phi & L\cos\theta \\ 0 & 1 & r_{3B}^{'x}\cos\phi & 0 \end{bmatrix} = \begin{bmatrix} -1 & 0 & -P/2\sin\phi & -L\sin\theta \\ 0 & -1 & P/2\cos\phi & L\cos\theta \\ 0 & 1 & P/2\cos\phi & 0 \end{bmatrix} \quad (4.54)$$

$$C_{qd} = \begin{bmatrix} -1 & 0 & r_{3A}^{'x}\sin\phi \\ 0 & -1 & -r_{3A}^{'x}\cos\phi \\ 0 & 1 & r_{3B}^{'x}\cos\phi \end{bmatrix} = \begin{bmatrix} -1 & 0 & -P/2\sin\phi \\ 0 & -1 & P/2\cos\phi \\ 0 & 1 & P/2\cos\phi \end{bmatrix} \quad (4.55a)$$

and

$$C_{ql} = \begin{bmatrix} -L\sin\theta \\ L\cos\theta \\ 0 \end{bmatrix} \quad (4.55b)$$

The inverse of C_{qd} can be explicitly found as follows:

$$C_{q_d}^{-1} = \frac{1}{P\cos\phi}\begin{bmatrix} -P\cos\phi & -P/2\sin\phi & -P/2\sin\phi \\ 0 & -P/2\cos\phi & P\cos\phi \\ 0 & 1 & 1 \end{bmatrix} = \begin{bmatrix} -1 & -1/2\tan\phi & -1/2\tan\phi \\ 0 & -1/2 & 1 \\ 0 & 1/P\cos\phi & 1/P\cos\phi \end{bmatrix}.$$

Since $\cos\phi$ never becomes zero, C_{qd} is always invertible during the motion for the mechanism of concern. One may assure the non-singularity of C_{qd} by examining the constraint, Eq. 4.53 which yields $\sin\phi = (h - L\sin\theta)/P = \pm 1$ when $\cos\phi$ becomes zero. Assuming that $\sin\phi = 1$, one obtains $\sin\theta = (h - P)/L = (46.5 - 500)/300$, which is less than -1. Thus, it is unattainable.

In the case when $\sin\phi = -1$, one has $\sin\theta = (h + P)/L = (46.5 + 500)/300$, which is greater than 1. Again, it is unattainable.

It can be concluded that $\cos\phi$ cannot be zero for the slider-crank given in this study. It is also concluded that the matrix C_{qd} is non-singular and, thus, invertible. Therefore, the dependent coordinates (R_j^x, R_j^y, ϕ) can be expressed in terms of the

independent coordinate θ. The dependent velocity terms can be expressed based upon Eq. 3.37 in Chapter 3 as:

$$\{\dot{R}_3^x \quad \dot{R}_3^y \quad \dot{\phi}\}^T = -C_{q_d}^{-1}C_{q_i}\dot{\theta} =$$

$$-\begin{bmatrix} -1 & -1/2\tan\phi & -1/2\tan\phi \\ 0 & -1/2 & 1 \\ 0 & 1/P\cos\phi & 1/P\cos\phi \end{bmatrix}\begin{bmatrix} -L\sin\theta \\ L\cos\theta \\ 0 \end{bmatrix}\dot{\theta} = \begin{Bmatrix} -L\sin\theta + L/2\tan\phi\cos\theta \\ L/2\cos\theta \\ -L\cos\theta/(P\cos\phi) \end{Bmatrix}\dot{\theta} \quad (4.56)$$

Based upon Eq. 3.42 in Chapter 3, the dependent acceleration terms can be expressed as:

$$\{\ddot{R}_3^x \quad \ddot{R}_3^y \quad \ddot{\phi}\}^T = -C_{q_d}^{-1}C_{q_i}\ddot{\theta} + C_{q_d}^{-1}C_{qq}$$

$$= \begin{Bmatrix} -L\sin\theta + L/2\tan\phi\cos\theta \\ L/2\cos\theta \\ -L\cos\theta/(P\cos\phi)1 \end{Bmatrix}\ddot{\theta} + \begin{bmatrix} -1 & -1/2\tan\phi & -1/2\tan\phi \\ 0 & -1/2 & 1 \\ 0 & 1/P\cos\phi & 1/P\cos\phi \end{bmatrix}\begin{Bmatrix} L\cos\theta\dot{\theta}^2 + P/2\cos\phi\dot{\phi}^2 \\ L\sin\theta\dot{\theta}^2 + P/2\sin\phi\dot{\phi}^2 \\ P/2\sin\phi\dot{\phi}^2 \end{Bmatrix}$$

$$= \begin{Bmatrix} -L\sin\theta + L/2\tan\phi\cos\theta \\ L/2\cos\theta \\ -L\cos\theta/(P\cos\phi) \end{Bmatrix}\ddot{\theta} + \begin{Bmatrix} [-L\cos\theta\dot{\theta}^2 - P/2\cos\phi\dot{\phi}^2 \\ -1/2\tan\phi(L\sin\theta\dot{\theta}^2 + P\sin\phi\dot{\phi}^2)] \\ -L/2\sin\theta\dot{\theta}^2 \\ (L\sin\theta\dot{\theta}^2 + P\sin\phi\dot{\phi}^2)/(p\cos\phi) \end{Bmatrix} \quad (4.57)$$

where C_{qq} is given by

$$C_{qq} = \begin{Bmatrix} L\cos\theta\dot{\theta}^2 - r_{3A}'^x\cos\phi\dot{\phi}^2 \\ L\sin\theta\dot{\theta}^2 - r_{3A}'^x\sin\phi\dot{\phi}^2 \\ r_{3B}'^x\sin\phi\dot{\phi}^2 \end{Bmatrix} = \begin{Bmatrix} L\cos\theta\dot{\theta}^2 + P/2\cos\phi\dot{\phi}^2 \\ L\sin\theta\dot{\theta}^2 + P/2\sin\phi\dot{\phi}^2 \\ P/2\sin\phi\dot{\phi}^2 \end{Bmatrix} \quad (4.58)$$

4.6.2 Origin at the Left End

If the origin of the body-fixed coordinate system is placed at the left end of the rigid connecting rod, $r_{3A}'^x = 0$ and $r_{3B}'^x = P$. The body-fixed coordinate system $x_3' - y_3'$ is assumed to make an angle ϕ with the global coordinate system, $x - y$, as shown in Fig. 4.6.
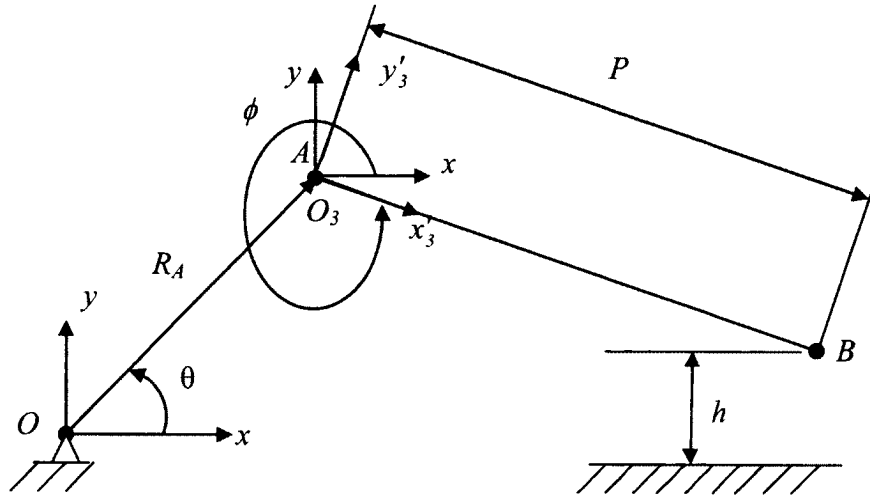
Figure 4.6 The Origin of the Body-fixed Coordinates is at Left End Point A

When the origin of the body fixed coordinate system is not at the center of gravity, the linear moment is no longer zero. In this case, the linear moment is calculated as follows:

$$I_{r'} = \int_\Omega \rho r' dv = \rho \int_\Omega \begin{Bmatrix} x' \\ y' \\ 0 \end{Bmatrix} dv = \frac{1}{2} m_3 P \begin{Bmatrix} 1 \\ 0 \\ 0 \end{Bmatrix}, \text{ and } I_{\tilde{r}} = \frac{1}{2} m_3 P \begin{bmatrix} 0 & 0 & 0 \\ 0 & 0 & -1 \\ 0 & 1 & 0 \end{bmatrix}.$$

The equation of motion for the rigid slider-crank mechanism is as follows:

$$\begin{bmatrix} M & C_q^T \\ C_q & 0 \end{bmatrix} \begin{Bmatrix} \ddot{q} \\ \lambda \end{Bmatrix} = \begin{Bmatrix} f \\ C_{qq} \end{Bmatrix} \tag{4.59}$$

Since the linear moment cannot be eliminated, the mass matrix is no longer a diagonal matrix. The terms in Eq. 4.59 can be simplified with $r'^x_{3A} = 0$ and $r'^x_{3B} = P$ as

$$M = \begin{bmatrix} m_3 I_3 & -A_3 I_{\tilde{r}} & 0 \\ & I_{\tilde{r}_3 \tilde{r}_3} & 0 \\ sym. & m_2 \dfrac{4L^2 + d^2}{12} \end{bmatrix}.$$

$$-A_3 I_{\tilde{r}} = -\frac{1}{2} m_3 P \begin{bmatrix} \cos\phi & -\sin\phi & 0 \\ \sin\phi & \cos\phi & 0 \\ 0 & 0 & 1 \end{bmatrix} \begin{bmatrix} 0 & 0 & 0 \\ 0 & 0 & -1 \\ 0 & 1 & 0 \end{bmatrix} = -\frac{1}{2} m_3 P \begin{bmatrix} 0 & 0 & \sin\phi \\ 0 & 0 & -\cos\phi \\ 0 & 1 & 0 \end{bmatrix}.$$

Therefore, one has,

$$M = \begin{bmatrix} m_3 & 0 & -m_3 P/2\sin\phi & 0 \\ & m_3 & m_3 P/2\cos\phi & 0 \\ & & m_3\dfrac{4P^2+d^2}{12} & 0 \\ \text{sym.} & & & m_2\dfrac{4L^2+d^2}{12} \end{bmatrix} \tag{4.60}$$

As for the generalized force term, one has

$$f = \begin{Bmatrix} \left(\cos\phi I_{x'}-\sin\phi I_{y'}\right)\dot\phi^2 + F \\ -m_3 g + \left(\sin\phi I_{x'}+\cos\phi I_{y'}\right)\dot\phi^2 \\ \left(\sin\phi I_{y'}-\cos\phi I_{x'}\right)g - Fr_{3B}'^x\sin\phi \\ -m_2 gL/2\cos\theta \end{Bmatrix} = \begin{Bmatrix} m_3 P/2\cos\phi\dot\phi^2 + F \\ -m_3 g + m_3 P/2\sin\phi\dot\phi^2 \\ -m_3 gP/2\cos\phi - FP\sin\phi \\ -m_2 gL/2\cos\theta \end{Bmatrix} \tag{4.61}$$

Similarly, the constraints C, the Jacobian matrix C_q, C_{qd}, C_{ql} and C_{qq} can be found as

$$C = \begin{bmatrix} L\cos\theta - R_3^x - r_{3A}'^x\cos\phi \\ L\sin\theta - R_3^y - r_{3A}'^x\sin\phi \\ R_3^y + r_{3B}'^x\sin\phi - h \end{bmatrix} = \begin{bmatrix} L\cos\theta - R_3^x \\ L\sin\theta - R_3^y \\ R_3^y + P\sin\phi - h \end{bmatrix} = 0 \tag{4.62}$$

$$C_q = \begin{bmatrix} -1 & 0 & r_{3A}'^x\sin\phi & -L\sin\theta \\ 0 & -1 & -r_{3A}'^x\cos\phi & L\cos\theta \\ 0 & 1 & r_{3B}'^x\cos\phi & 0 \end{bmatrix} = \begin{bmatrix} -1 & 0 & 0 & -L\sin\theta \\ 0 & -1 & 0 & L\cos\theta \\ 0 & 1 & P\cos\phi & 0 \end{bmatrix} \tag{4.63}$$

$$C_{qd} = \begin{bmatrix} -1 & 0 & r_{3A}'^x\sin\phi \\ 0 & -1 & -r_{3A}'^x\cos\phi \\ 0 & 1 & r_{3B}'^x\cos\phi \end{bmatrix} = \begin{bmatrix} -1 & 0 & 0 \\ 0 & -1 & 0 \\ 0 & 1 & P\cos\phi \end{bmatrix} \tag{4.64a}$$

$$C_{ql} = \begin{bmatrix} -L\sin\theta \\ L\cos\theta \\ 0 \end{bmatrix} \tag{4.64b}$$

and

$$C_{qq} = \begin{Bmatrix} L\cos\theta\dot\theta^2 - r_{3A}'^x\cos\phi\dot\phi^2 \\ L\sin\theta\dot\theta^2 - r_{3A}'^x\sin\phi\dot\phi^2 \\ r_{3B}'^x\sin\phi\dot\phi^2 \end{Bmatrix} = \begin{Bmatrix} L\cos\theta\dot\theta^2 \\ L\sin\theta\dot\theta^2 \\ P\sin\phi\dot\phi^2 \end{Bmatrix} \tag{4.65}$$

Based upon Eq. 4.64a, one has

$$C_{qd}^{-1} = \frac{1}{P\cos\phi}\begin{bmatrix} -P\cos\phi & 0 & 0 \\ 0 & -P\cos\phi & 0 \\ 0 & 1 & 1 \end{bmatrix} = \begin{bmatrix} -1 & 0 & 0 \\ 0 & -1 & 0 \\ 0 & 1/P\cos\phi & 1/P\cos\phi \end{bmatrix}.$$

Again, based upon the discussion in Section 4.6.1, C_{qd} is not singular and invertible during the motion of the mechanism. Consequently, the velocity of the dependent coordinates can be written in terms of the velocities of the independent coordinates as:

$$\{\dot{R}_3^x \quad \dot{R}_3^y \quad \dot{\phi}\}^T = -C_{q_d}^{-1}C_{q_i}\dot{\theta} =$$

$$-\begin{bmatrix} -1 & 0 & 0 \\ 0 & -1 & 0 \\ 0 & 1/P\cos\phi & 1/P\cos\phi \end{bmatrix}\begin{bmatrix} -L\sin\theta \\ L\cos\theta \\ 0 \end{bmatrix}\dot{\theta} = \begin{Bmatrix} -L\sin\theta \\ L\cos\theta \\ -L\cos\theta/(P\cos\phi) \end{Bmatrix}\dot{\theta} \qquad (4.66)$$

Similarly, the accelerations of the dependent coordinates can be obtained in terms of $\ddot{\theta}$ as

$$\{\ddot{R}_3^x \quad \ddot{R}_3^y \quad \ddot{\phi}\}^T = -C_{q_d}^{-1}C_{q_i}\ddot{\theta} + C_{q_d}^{-1}C_{qq}$$

$$= \begin{Bmatrix} -L\sin\theta \\ L\cos\theta \\ -L\cos\theta/(P\cos\phi) \end{Bmatrix}\ddot{\theta} + \begin{bmatrix} -1 & 0 & 0 \\ 0 & -1 & 0 \\ 0 & 1/P\cos\phi & 1/P\cos\phi \end{bmatrix}\begin{Bmatrix} L\cos\theta\dot{\theta}^2 \\ L\sin\theta\dot{\theta}^2 \\ P\sin\phi\dot{\phi}^2 \end{Bmatrix}$$

$$= \begin{Bmatrix} -L\sin\theta \\ L\cos\theta \\ -L\cos\theta/(P\cos\phi) \end{Bmatrix}\ddot{\theta} + \begin{Bmatrix} -L\cos\theta\dot{\theta}^2 \\ -L\sin\theta\dot{\theta}^2 \\ (L\sin\theta\dot{\theta}^2 + P\sin\phi\dot{\phi}^2)/(P\cos\phi) \end{Bmatrix} \qquad (4.67)$$

By comparing the equation of motion derived in Sub-sections 4.6.1 and 4.6.2, it can be seen that the mass matrix in Eq. 4.49 is diagonal but not in Eq. 4.59, and the force matrix in Eq. 4.49 is simpler than that in Eq. 4.59. The formulation simplicity is the advantage of the case which places the origin of the body-fixed coordinate system at the center of gravity.

4.7 Direct Method for the Rigid Slider-Crank Mechanism

The direct method described here is the one that derives the equation of motion explicitly in terms of the independent coordinates for the slider-crank mechanism of concern. The constraint conditions are used in the derivation of the equation of motion to substitute the dependent coordinates by the independent ones directly without relying on the Lagrange multipliers. In this study, the direct method is used as the benchmark to verify the numerical results obtained by the coordinate partitioning method and the projection method. Again, the derivation discussed here allows the origin of the body-fixed coordinate system of the connecting rod to be placed at its center or at its left end.

4.7.1 Origin at the Center of Gravity

The constraint equations that define the relationship between the dependent coordinates and the independent ones have been derived and given by Eq. 4. 52 for the case when the origin is placed at the center of the gravity as:

$$C = \begin{bmatrix} L\cos\theta - R_3^x + P/2\cos\phi \\ L\sin\theta - R_3^y + P/2\sin\phi \\ R_3^y + P/2\sin\phi - h \end{bmatrix} = 0 \, .$$

Similarly, according to Eq. 4.56, the dependent velocities are related to the independent ones are given by

$$\begin{Bmatrix} \dot{R}_3^x \\ \dot{R}_3^y \\ \dot{\phi} \end{Bmatrix} = \begin{Bmatrix} -L\sin\theta + L/2\tan\phi\cos\theta \\ L/2\cos\theta \\ -L\cos\theta/(P\cos\phi) \end{Bmatrix} \dot{\theta} \, .$$

Hence, one has the virtual displacement as

$$\delta q = \begin{Bmatrix} \delta R_3^x \\ \delta R_3^y \\ \delta\phi \\ \delta\theta \end{Bmatrix} = \begin{Bmatrix} -L\sin\theta + L/2\tan\phi\cos\theta \\ L/2\cos\theta \\ -L\cos\theta/(P\cos\phi) \\ 1 \end{Bmatrix} \delta\theta \equiv \beta\delta\theta \tag{4.68}$$

wher $\beta^T = \begin{pmatrix} -L\sin\theta + (L/2)\tan\phi\cos\theta & -L\sin\theta + (L/2)\tan\phi\cos\theta & -L\cos\theta/(P\cos\phi) & 1 \end{pmatrix}$

in which $\sin\phi = (h - L\sin\theta)/P$ and $\cos\phi = \sqrt{1 - \sin^2\phi}$. The independent accelerations, according to Eq. 4.57, can be written in terms of the independent ones as:

$$\begin{Bmatrix} \ddot{R}_3^x & \ddot{R}_3^y & \ddot{\phi} \end{Bmatrix}^T =$$

$$\begin{Bmatrix} -L\sin\theta + L/2\tan\phi\cos\theta \\ L/2\cos\theta \\ -L\cos\theta/(P\cos\phi)1 \end{Bmatrix} \ddot{\theta} + \begin{Bmatrix} -L\cos\theta\dot{\theta}^2 - P/2\cos\phi\dot{\phi}^2 - 1/2\tan\phi(L\sin\theta\dot{\theta}^2 + P\sin\phi\dot{\phi}^2) \\ -L/2\sin\theta\dot{\theta}^2 \\ (L\sin\theta\dot{\theta}^2 + P\sin\phi\dot{\phi}^2)/(p\cos\phi) \end{Bmatrix} .$$

Hence, the dependent and independent accelerations can be combined as:

$$\ddot{q} = \begin{Bmatrix} \ddot{R}_3^x \\ \ddot{R}_3^y \\ \ddot{\phi} \\ \ddot{\theta} \end{Bmatrix} = \begin{Bmatrix} -L\sin\theta + L/2\tan\phi\cos\theta \\ L/2\cos\theta \\ -L\cos\theta/(P\cos\phi) \\ 1 \end{Bmatrix} \ddot{\theta} + \begin{Bmatrix} -L\cos\theta\dot{\theta}^2 - P/2\cos\phi\dot{\phi}^2 - 1/2\tan\phi(L\sin\theta\dot{\theta}^2 + P\sin\phi\dot{\phi}^2) \\ -L/2\sin\theta\dot{\theta}^2 \\ (L\sin\theta\dot{\theta}^2 + P\sin\phi\dot{\phi}^2)/(p\cos\phi) \\ 0 \end{Bmatrix} \tag{4.69}$$

$$\equiv \beta\ddot{\theta} + \eta$$

$$\text{where } \eta = \begin{cases} -L\cos\theta\dot\theta^2 - P/2\cos\phi\dot\phi^2 - 1/2\tan\phi(L\sin\theta\dot\theta^2 + P\sin\phi\dot\phi^2) \\ -L/2\sin\theta\dot\theta^2 \\ (L\sin\theta\dot\theta^2 + P\sin\phi\dot\phi^2)/(p\cos\phi) \\ 0 \end{cases}.$$

Substituting Eqs. 4.68 and 4.69 into the equation of virtual work, Eq. 4.9, one has

$$(M\ddot{q} - f)^T \delta q = [M(\beta\ddot\theta + \eta) - f]^T \beta\delta\theta = 0 \tag{4.70}$$

Note that θ is an independent variable, which is free from constraints. Hence, one has:

$$[M(\beta\ddot\theta + \eta) - f]^T \beta = 0 \tag{4.71}$$

or

$$(\beta^T M\beta)\ddot\theta + \eta^T M\beta = f^T \beta \tag{4.72}$$

As a result, one has

$$\ddot\theta = (\beta^T M\beta)^{-1}(f^T\beta - \eta^T M\beta) \tag{4.73}$$

where M, f, β and η are defined by Eqs. 4.50, 4.51, 4.68 and 4.69, respectively.

4.7.2 Origin at the Left End

In this case, the constraint equation is given by Eq. 4.62 as,

$$C = \begin{bmatrix} L\cos\theta - R_3^x \\ L\sin\theta - R_3^y \\ R_3^y + P\sin\phi - h \end{bmatrix} = 0.$$

The dependent velocity terms can be written in terms of the independent one as, according to Eq. 4.66,

$$\begin{Bmatrix} \dot R_3^x \\ \dot R_3^y \\ \dot\phi \end{Bmatrix} = \begin{Bmatrix} -L\sin\theta \\ L\cos\theta \\ -L\cos\theta/(P\cos\phi) \end{Bmatrix}\dot\theta.$$

Hence, one has

$$\delta q = \begin{Bmatrix} \delta R_3^x \\ \delta R_3^y \\ \delta\phi \\ \delta\theta \end{Bmatrix} = \begin{Bmatrix} -L\sin\theta \\ L\cos\theta \\ -L\cos\theta/(P\cos\phi) \\ 1 \end{Bmatrix}\delta\theta \equiv \beta\delta\theta \tag{4.74}$$

where $\boldsymbol{\beta}^T = \{-L\sin\theta \quad L\cos\theta \quad -L\cos\theta/(P\cos\phi) \quad 1\}$ in which $\sin\phi = (h - L\sin\theta)/P$

and $\cos\phi = \sqrt{1 - \sin^2\phi}$. Similarly, the dependent acceleration terms can be written in

terms of the independent acceleration based upon Eq. 4.67 as:

$$
\begin{Bmatrix} \ddot{R}_3^x \\ \ddot{R}_3^y \\ \ddot{\phi} \end{Bmatrix} = \begin{Bmatrix} -L\sin\theta \\ L\cos\theta \\ -L\cos\theta/(P\cos\phi) \end{Bmatrix} \ddot{\theta} + \begin{Bmatrix} -L\cos\theta\dot{\theta}^2 \\ -L\sin\theta\dot{\theta}^2 \\ (L\sin\theta\dot{\theta}^2 + P\sin\phi\dot{\phi}^2)/(P\cos\phi) \end{Bmatrix}.
$$

Hence, the above equation can be extended to represent the entire system coordinates as

$$
\ddot{q} = \begin{Bmatrix} \ddot{R}_3^x \\ \ddot{R}_3^y \\ \ddot{\phi} \\ \ddot{\theta} \end{Bmatrix} = \begin{Bmatrix} -L\sin\theta \\ L\cos\theta \\ -L\cos\theta/(P\cos\phi) \\ 1 \end{Bmatrix} \ddot{\theta} + \begin{Bmatrix} -L\cos\theta\dot{\theta}^2 \\ -L\sin\theta\dot{\theta}^2 \\ (L\sin\theta\dot{\theta}^2 + P\sin\phi\dot{\phi}^2)/(P\cos\phi) \\ 0 \end{Bmatrix} \equiv \boldsymbol{\beta}\ddot{\theta} + \boldsymbol{\eta} \quad (4.75)
$$

where $\boldsymbol{\eta} = \begin{Bmatrix} -L\cos\theta\dot{\theta}^2 \\ -L\sin\theta\dot{\theta}^2 \\ (L\sin\theta\dot{\theta}^2 + P\sin\phi\dot{\phi}^2)/(P\cos\phi) \\ 0 \end{Bmatrix}.$

Finally, one arrives at a single equation to represent the equation of motion for the

rigid slider-crank, in which the origin of the connecting rod is placed at the left end as:

$$
\ddot{\theta} = (\boldsymbol{\beta}^T M \boldsymbol{\beta})^{-1}(f^T \boldsymbol{\beta} - \boldsymbol{\eta}^T M \boldsymbol{\beta}) \tag{4.76}
$$

where $M, f, \boldsymbol{\beta}$ and $\boldsymbol{\eta}$ are defined in Eqs. 4.60, 4.61, 4.74 and 4.75, respectively.

4.8 Numerical Results for the Rigid Slider-Crank Mechanism

The numerical results obtained from the equation of motions derived by different

methods are summarized in this section. These methods include the coordinate

partitioning method and the projection method and the direct method. The details of the

coordinate partitioning method and the projection method are discussed in Chapter 3,

while the direct method is discussed in Section 4.7. Each method produces two equations

of motion based upon whether the location of the origin of the body fixed coordinate

system is at the center or at the left end of the connecting rod. Therefore, six sets of

results are presented in this section. These results are compared with each other based

upon computational accuracy and efficiency.

4.8.1 Computational Accuracy

Two cases are considered here: one with a harmonic force $F = 200\sin(\pi t)$ and the other with $F = 2000\sin(\pi t)$. Since the force takes two seconds to complete a cycle, the analysis is run for three seconds so as to catch the key features of the response. The time interval of analysis to report the result is set to be 0.025 seconds. In the direct and the coordinate partitioning methods, the angular displacement of the crank, θ, is the only unknown, whose initial value and initial velocity are set to be:

$\theta(0) = \arcsin(h/L) = 0.1556$ and $\dot{\theta}(0) = 0$, respectively. On the other hand, the projection method is made of four generalized coordinates: the angular displacement of the crank, θ, the angular displacement of the connecting rod, ϕ, and the position of the connecting rod, R_j^x and R_j^y at the origin of its coordinate system. The corresponding initial values are set to be $\phi(0) = \dot{\phi}(0) = \dot{R}_j^x(0) = \dot{R}_j^y(0) = 0$. In the case when the origin is placed at the center of gravity, the initial position of the connecting rod are given by

$R_j^x(0) = L\cos\theta + P/2\cos\phi = 546.37$ and $R_j^y(0) = L\sin\theta + P/2\sin\phi = 46.5$.

In the case when the origin is placed at the left end of the connecting rod, one has:

$R_j^x(0) = L\cos(\theta) = 296.3743$ and $R_j^y(0) = L\sin(\theta) = 46.5$.

Only the results of the angular displacement and the velocity of the crank and the connecting rod are reported here. This is because the other parameters, such as the position of CG of the connecting rod, can be computed based upon these four values.

The results obtained based upon the direct method, the coordinate partitioning method and the projection method are summarized in Figs. 4.7 and 4.8.

Figs 4.7 and 4.8 indicate that these three methods yield almost identical results. Thus, it can be concluded that the projection method has been validated, which can be a useful alternative when it is difficult to determine the independent coordinates based upon the constraint equations. The results also indicate that the location selection for the origin of the local coordinate system bears no effect on accuracy. However, the origin of the local coordinate system has effect on the computational efficiency. It will be introduced in Sub-section 4.8.2.
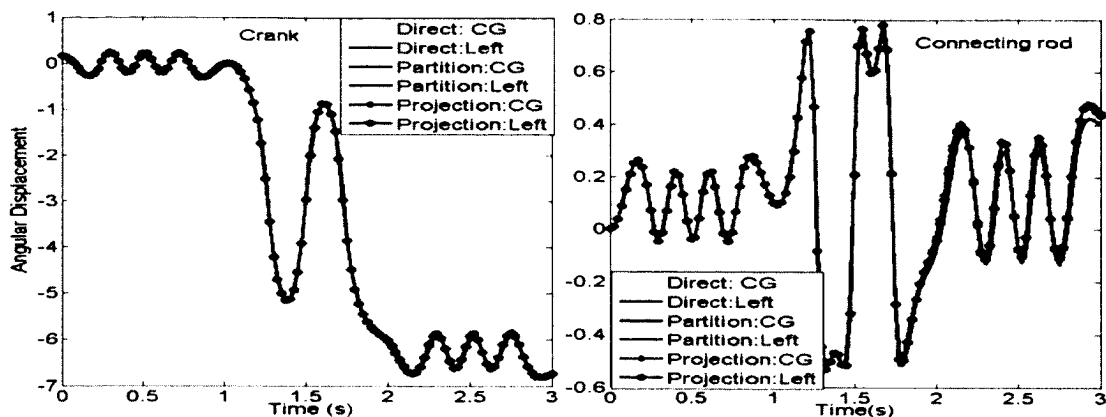
Figure 4.7 Angular Displacements of the Crank and the Rod under 200N Force
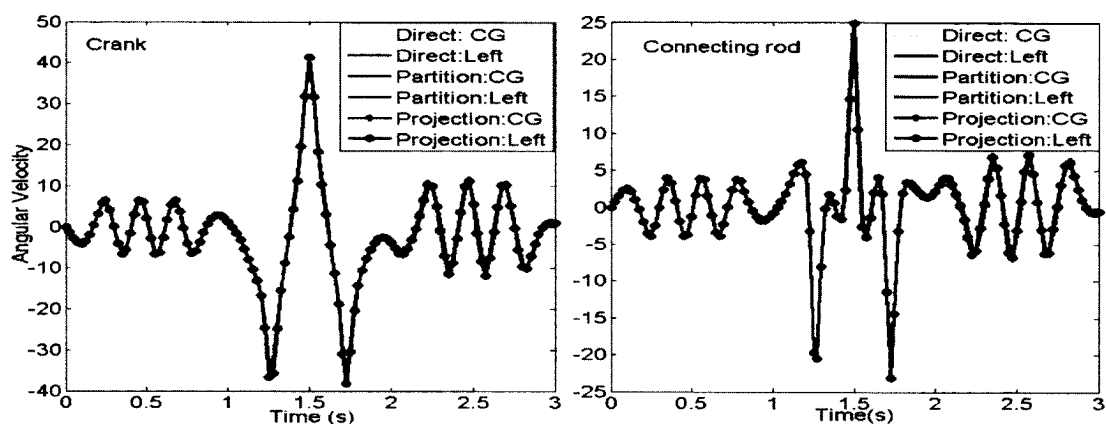
Figure 4.8 Angular Velocities of the Crank and the Rod under 200N Force

Next, Figs. 4.9 and 4.10 show the results pertaining to a larger force, 2000N.
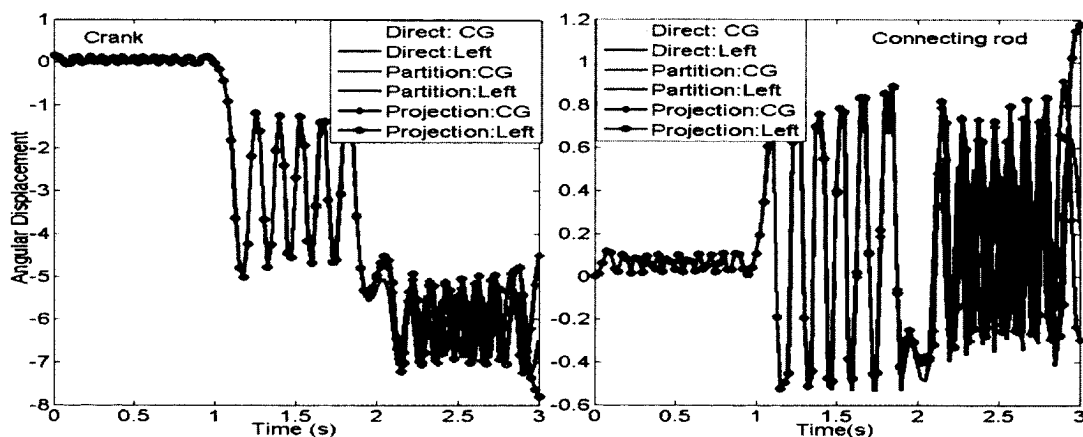
Figure 4.9 Angular Displacements of the Crank and the Rod under 2000N Force
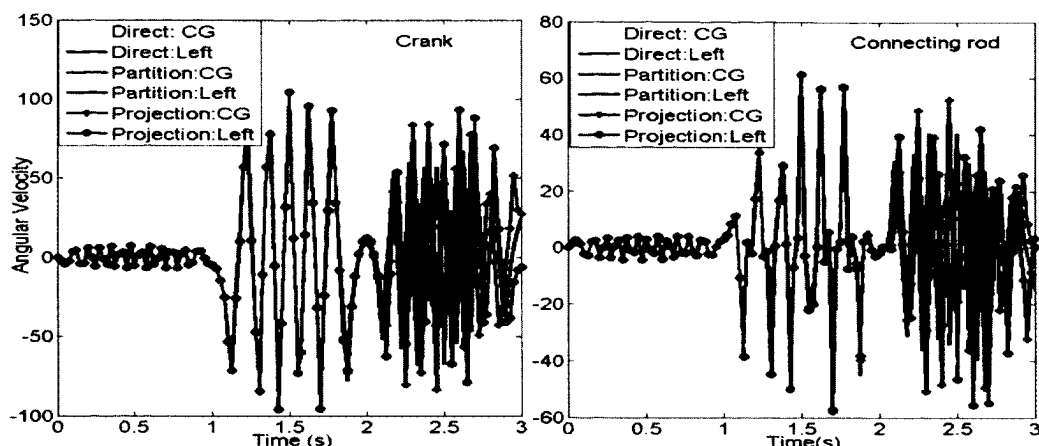
Figure 4.10 Angular Velocities of the Crank and the Rod under 2000N Force

Figs 4.9 and 4.10 indicate that the direct and the coordinate partitioning methods yield identical results for the force of 2000N and the projection method exhibits deviation, particularly after 2 seconds. One reason for this deviation could be the fact that the projection method doesn't provide an automatic mechanism to enforce the displacement and the velocity constraints. An optimization method has been proposed in Chapter 3 to aid the projection method to impose the displacement and the velocity constraint. The proposed optimization method is then incorporated in the solution algorithm of the projection method at every time step called by ODE. However, the displacement and the velocity constrains in the projection method can be imposed externally through the optimization method after solving the ODE at each time interval. The optimization method has been discussed in detail in Chapter 3.

Figs 4.11~4.14 show the results obtained by the project methods with and without the constraints correction. The results reported here are only for the case when the origin is placed at the center of the connecting rod. The results are improved, though they still deviate from those of the direct method. Nevertheless, the optimization method proposed in Chapter 3 is valid for constraint correction.
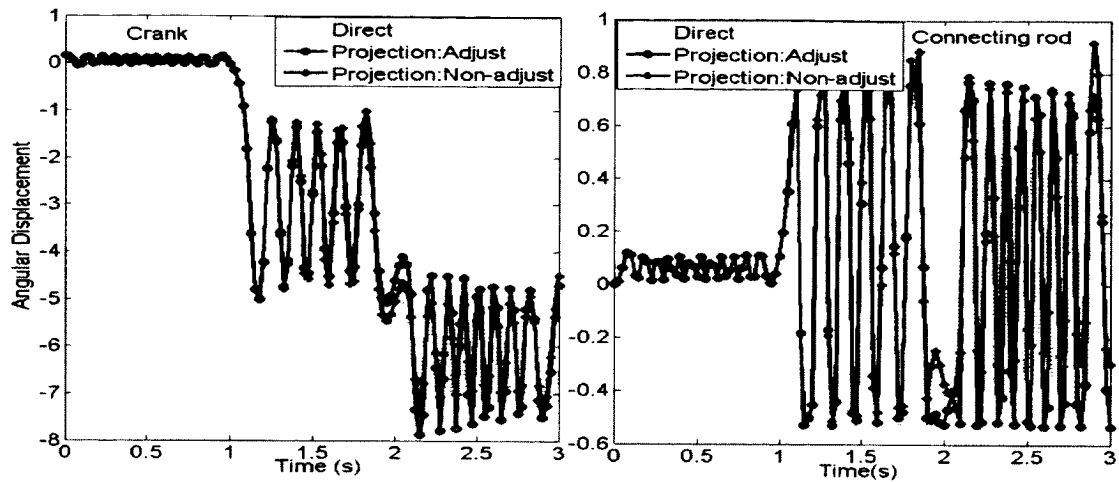
Figure 4.11 Angular Displacement Comparisons for the Crank and the Rod
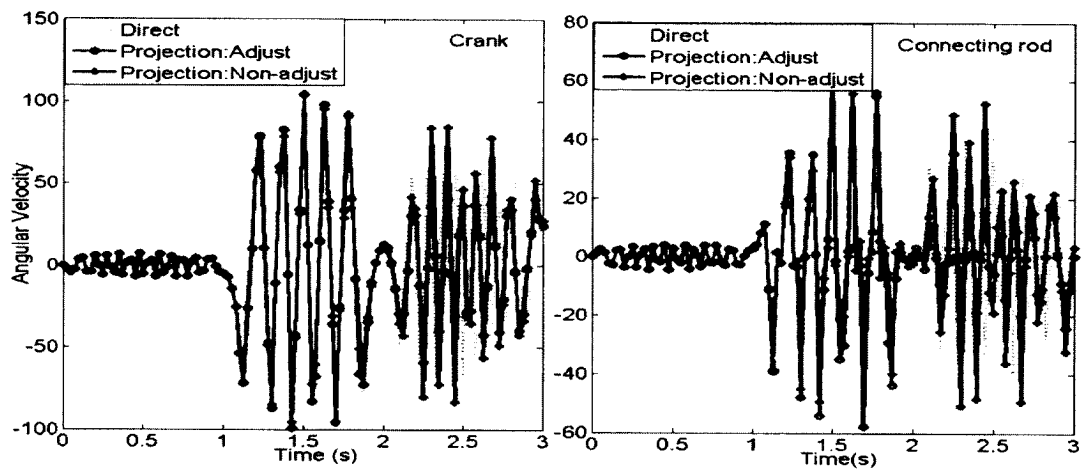
Figure 4.12 Angular Velocity Comparisons for the Crank and the Rod
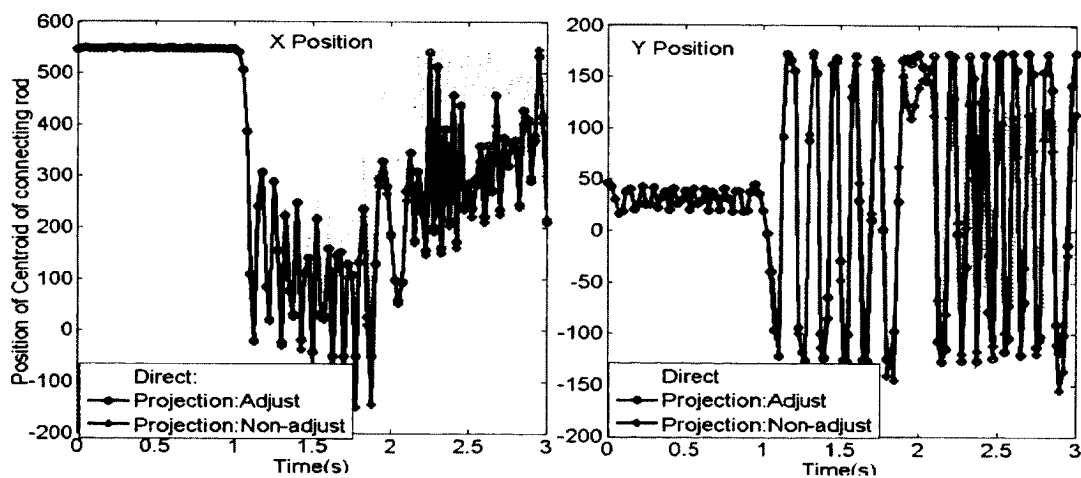
Figure 4.13 Position Comparisons at CG of the Rod under 2000N Force
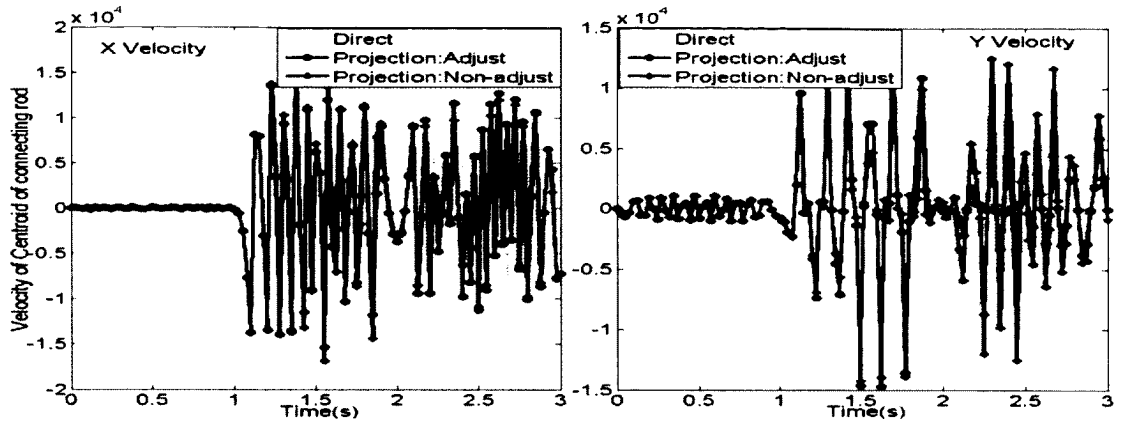
Figure 4.14 Velocity Comparisons at CG of the Rod under 2000N Force

The values of the displacement and the velocity constraints at Joint *A* and Joint *B* with correction are compared with those without correction and shown in Figs. 4.15~4.20. It can be seen that the displacement and the velocity constraints are satisfied after constraint correction by the proposed optimization procedure.
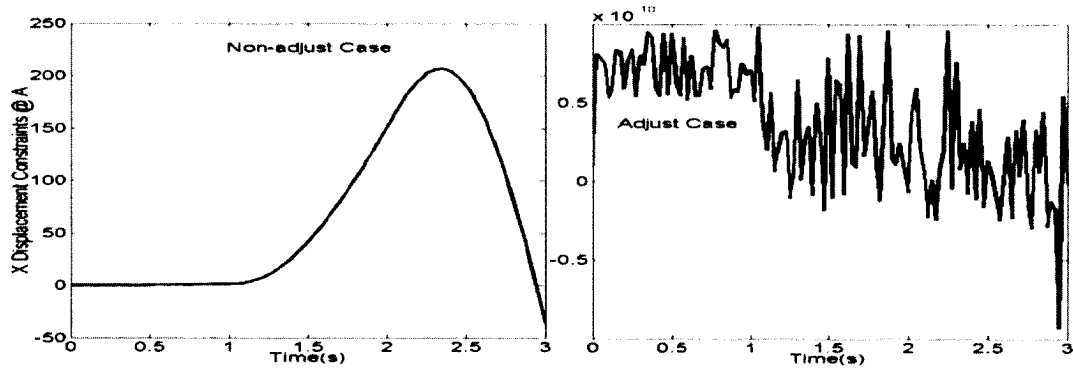
Figure 4.15 Displacement Constraints along *x* at Point *A*
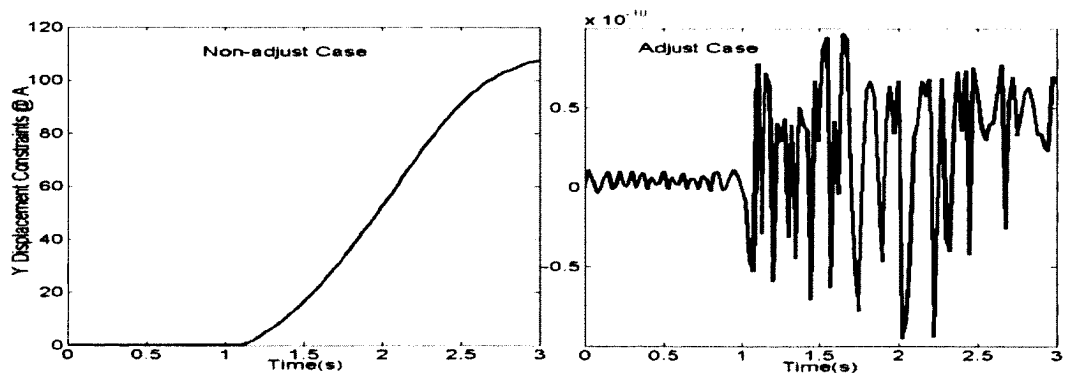
Figure 4.16 Displacement Constraints along *y* at Point *A*
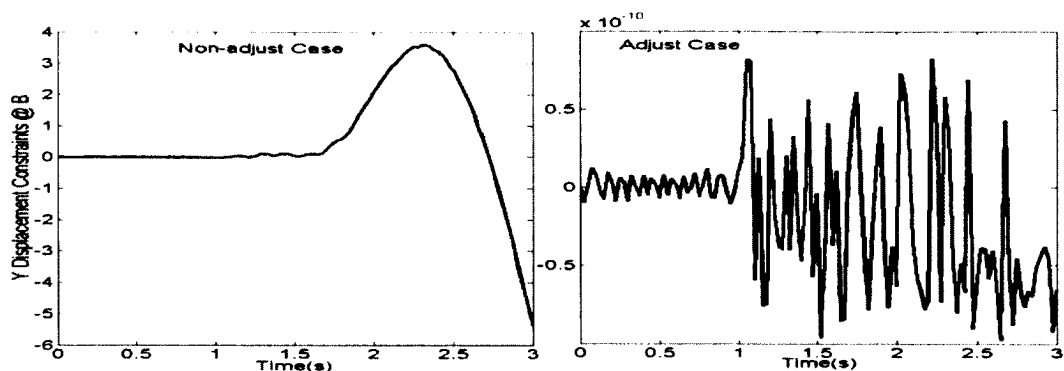
Figure 4.17 Displacement Constraints along *y* at Point *B*
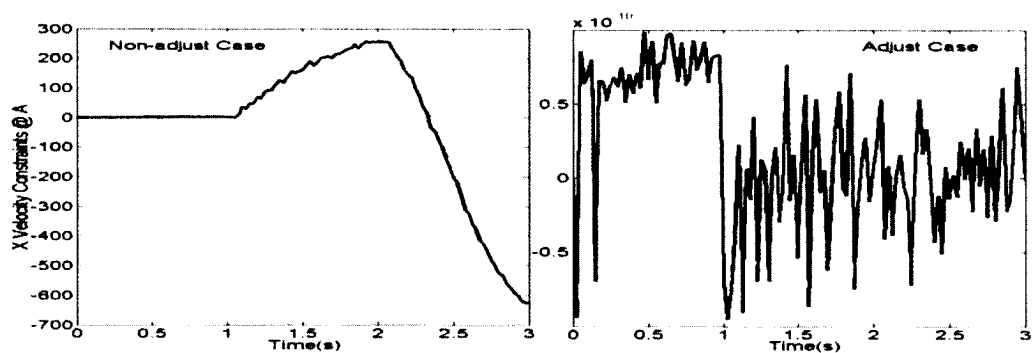
Figure 4.18 Velocity Constraints along *x* at Point *A*
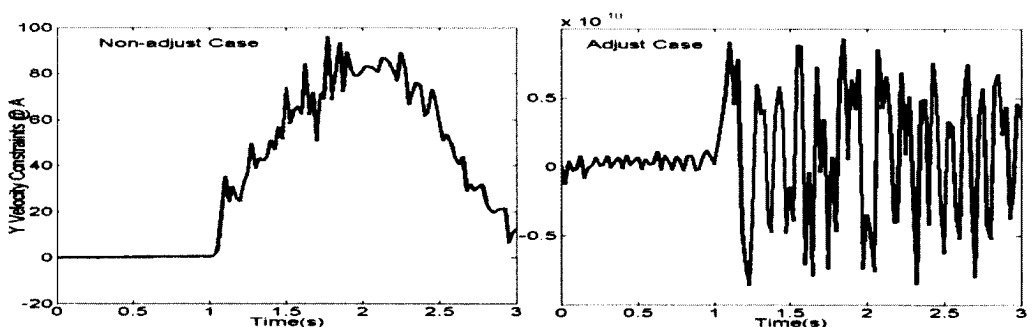
Figure 4.19 Velocity Constraints along *y* at Point *A*
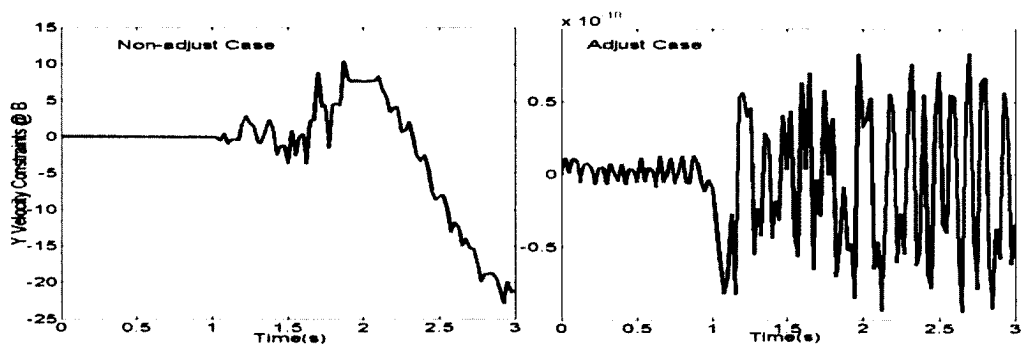
Figure 4.20 Velocity Constraints along *y* at Point *B*

4.8.2 Computational Efficiency

The Matlab built-in function *ode23s* is used to solve the required ODE, which can handle a stiff equation. The run time duration is set for 3 seconds, and the time interval for reporting the results is 0.025 seconds. The absolute and relative tolerances are the default values 10^{-6}. The code is run on a PC. The average value of three different runs is taken as the CPU time because each run gives a different time. Detailed results are summarized in Table 4.2.

Table 4.2 Time Consumption of Different Methods for the Rigid Body

Method	Direct Method		Coord. Partition		Projection Method			
Origin	CG	Left	CG	Left	CG	Adjust	Left	Adjust
1st run	1.051s	1.086s	1.196s	1.241s	2.562s	0.205s	2.645s	0.212s
2nd run	1.019s	1.054s	1.183s	1.237s	2.461s	0.180s	2.524s	0.218s
3rd run	1.012s	1.046s	1.170s	1.212s	2.496s	0.191s	2.527s	0.198s
Average	1.027s	1.062s	1.183s	1.230s	2.506s	0.192s	2.565s	0.209s

Table 4.2 reveals that, as expected, the direct method is faster than the coordinate partitioning method and the projection method. The coordinate partitioning method requires additional time to solve the nonlinear constraints on displacements and velocities, while the projection method has to solve a larger set of equations. Table 4.2 also reveals that placing the origin of the body-fixed coordinate at the center of the body is preferable to placing it at the left end.

4.9 Numerical Results for the Flexible Slider-Crank Mechanism

The system generalized coordinates for the slider-crank mechanism with a flexible connecting rod include the modal coordinate *a* . The latter is used to approximate the elastic displacement, which complicates problem formulation and solution algorithm. When the connecting rod is taken as flexible, the generalized mass matrix and the force term are no longer time invariants. The applied force considered here has a magnitude of 2000N.

4.9.1 Results Comparison between Rigid and Flexible Systems

In the flexible dynamics analysis, three cases are studied. In the first case, the problem is solved by the coordinate partitioning method, in which the integrals are calculated within the ODE iterations. In the second case, the problem is still solved by the coordinate partitioning method; however, the integrals are calculated prior to the ODE iterations. In the third case, the projection method is used in which the integrals are calculated prior to the ODE iterations. In all these three cases, the origin of the body-fixed coordinate system of the flexible connecting rod is placed at its center. The flexible connecting rod is discretized into 12 beam elements. Nine eigen-vectors are selected for analysis. Their frequencies are below 20,000 Hz. The mode shapes of the selected 9 modes are depicted in Fig. 4.21. All except mode 7 are bending modes.
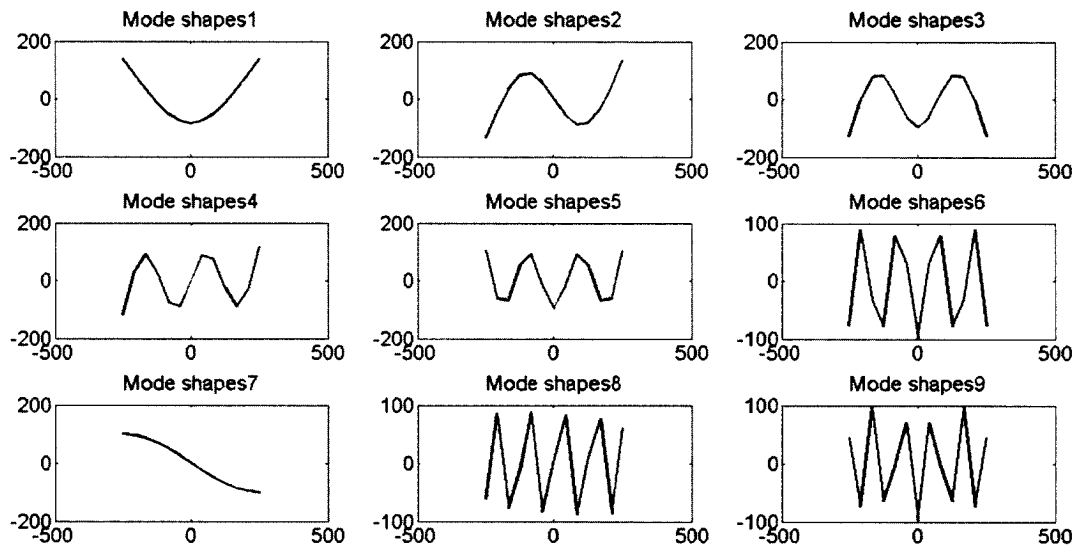
Figure 4.21 Mode Shapes of the Flexible Connecting Rod

The initial conditions used for the flexible dynamic analysis are set to be the same as those of the rigid analysis. The initial value for the modal coordinate a and its first order derivation $\dot{a}$ are both set to be zeros.

The rigid results obtained by the direct method are set as the benchmark for comparison. The comparisons between the results of the rigid body and the flexible body dynamic analysis are reported in Figs. 4.22~4.25.
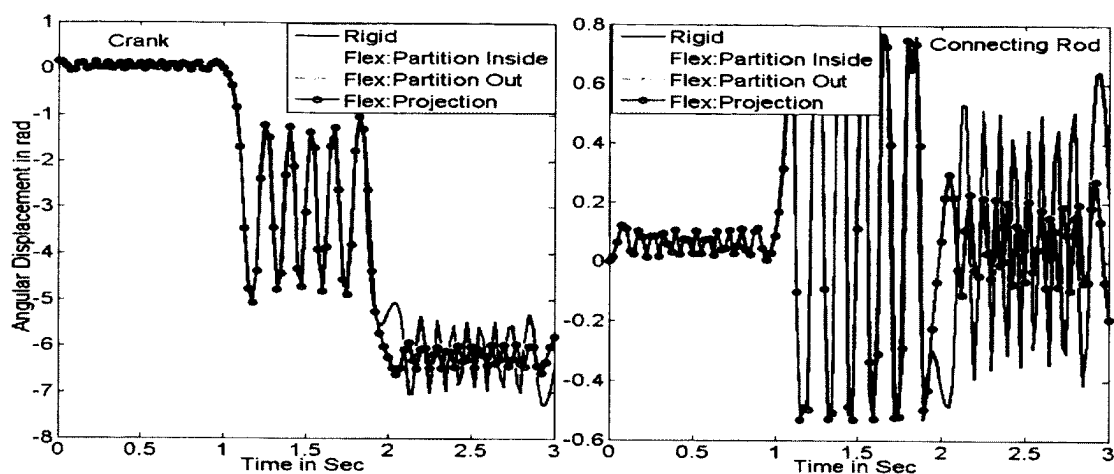
Figure 4.22 Angular Displacements of the Crank and the Connecting Rod
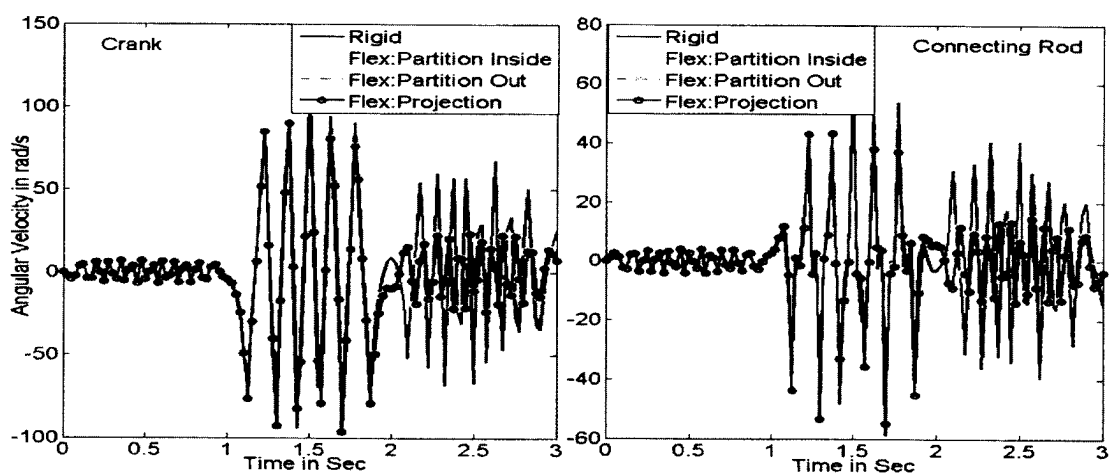
Figure 4.23 Angular Velocities of the Crank and the Connecting Rod
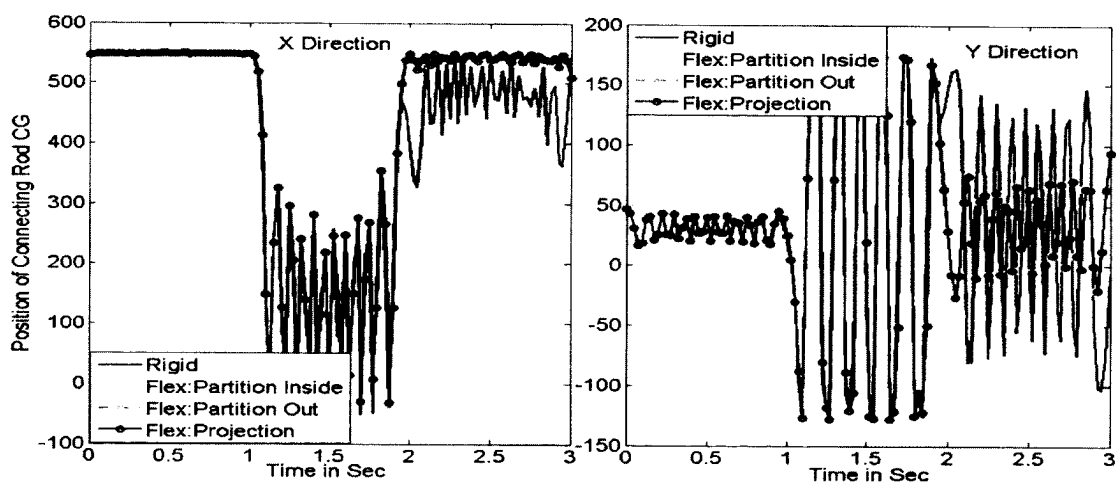
Figure 4.24 Positions of Center of the Connecting Rod
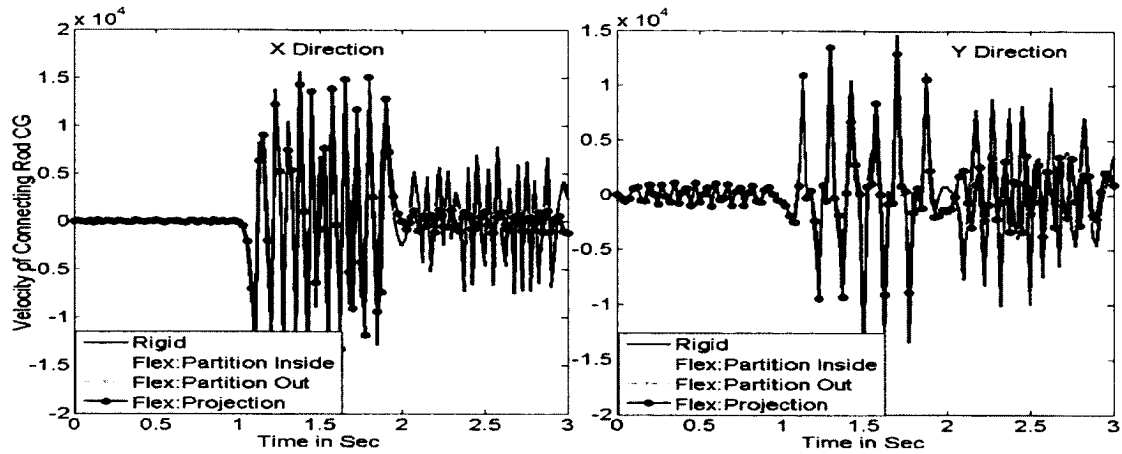
Figure 4.25 Velocities at CG of Connecting Rod

It can be observed from Figs. 4.22 and 4.23 that the angular displacements and the velocities of the rigid model match well those of the flexible model in the first second of analysis time period. Afterwards, the angular displacement of the rigid model reached a much higher value than the flexible model. The angular velocity of the rigid model is running faster and larger than that of the flexible model. Similar trends can be observed in Figs. 4.24 and 4.25 for the displacement and the velocity at the center of the flexible connecting rod. This is to be expected since some of the kinetic energy is consumed by the strain energy of the flexible connecting rod due to elastic deformation. The snap shots of configurations of the rigid and the flexible models at seven different time instants during motion are shown in Figs. 4.26 and 4.27, respectively. Two large jumps are observed from 1.0 to 1.5s and 1.5 to 2.0s for both the rigid and the flexible models.
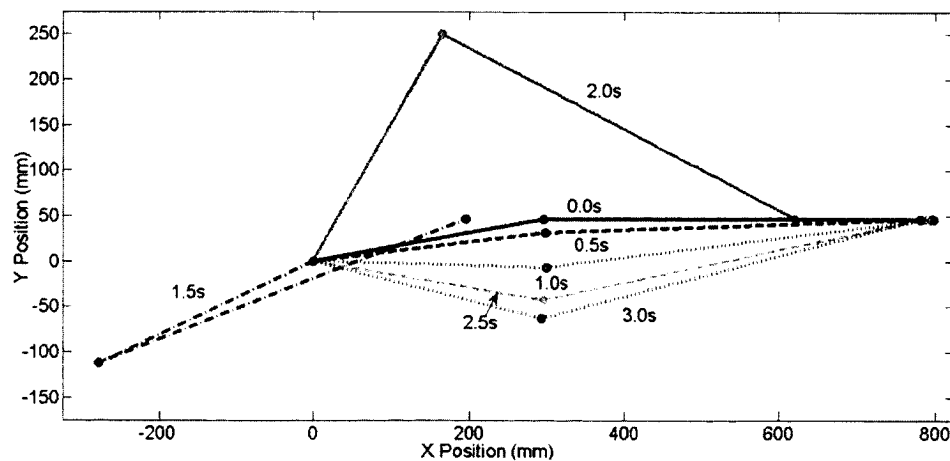
Figure 4.26 Configurations of the Rigid System at Different Times
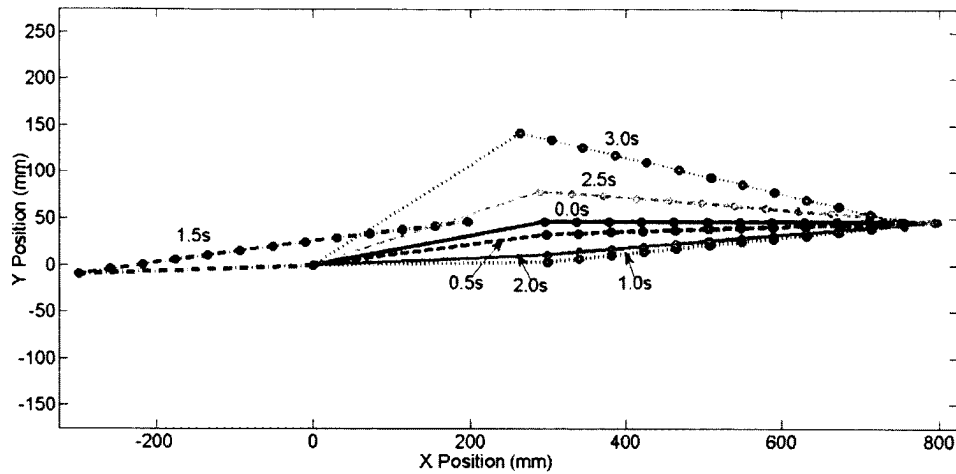
Figure 4.27 Configurations of the Flexible System at Different Times

The elastic deformations are expressed in terms of linear combination of the mode shapes based upon the mode superposition technique. The modal coordinates can be used to measure the contributions of each mode shapes toward the total elastic deformation. The time histories of the modal coordinates are shown in Fig. 4.28. It can be observed that the dominant mode is the first mode, which is the first bending mode of the beam indicated in Fig. 4.21.
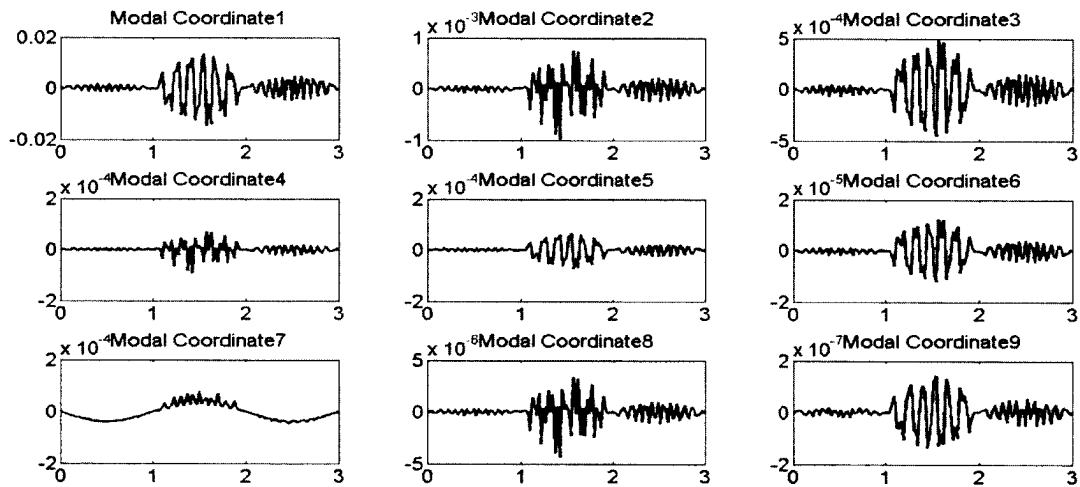
Figure 4.28 Time Histories of Modal Coordinates

For the projection method, the displacement and velocity constraints histories after constraint correction are shown in Figs. 4.29~4.31. The constraints are satisfied well through the optimization.
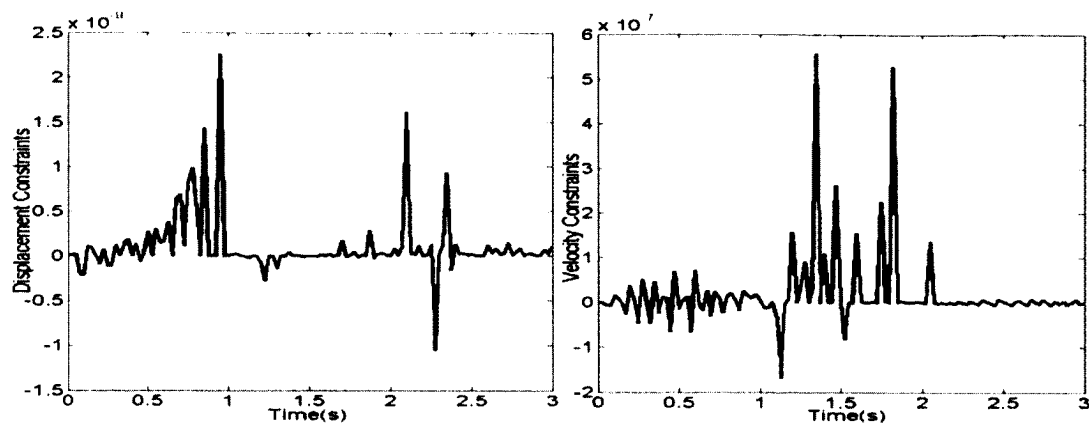
Figure 4.29 Displacement/ Velocity Constraints along x at Point A
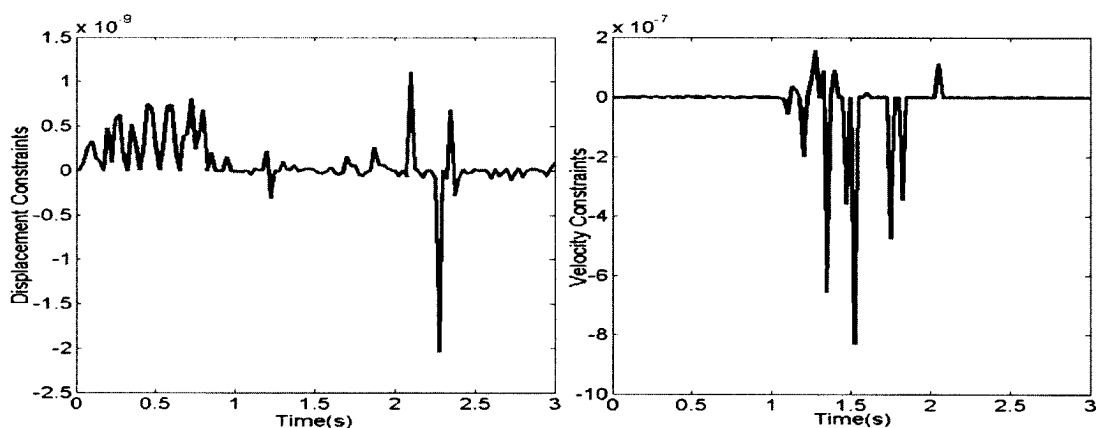
Figure 4.30 Displacement/ Velocity Constraints along y at Point A
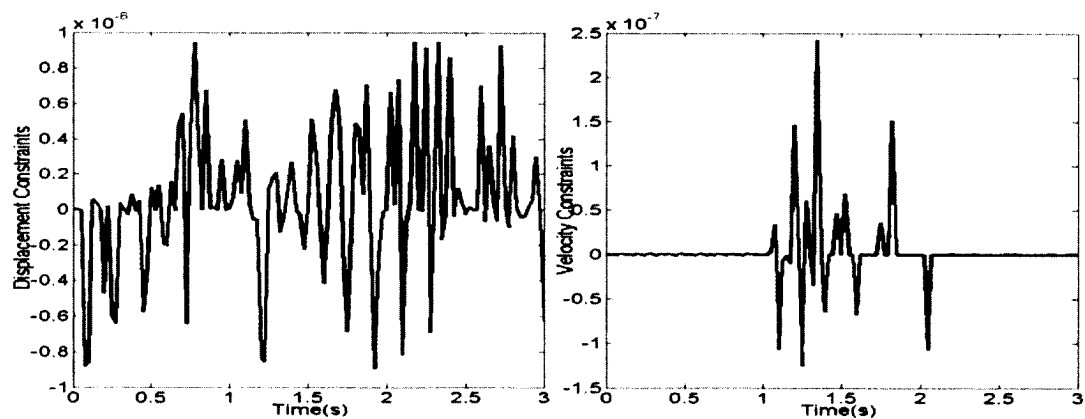
Figure 4.31 Displacement/ Velocity Constraints along y at Point B

4.9.2 Computational Time Comparison for Different Methods

Similarly as in analysis of the rigid slider-crank mechanism, the CPU time is also obtained to check the efficiencies of the methods used for the flexible one. The average value of three different runs is taken as the CPU time for each method, which is shown in Table 4.3.

Table 4.3 Time Consumption for the Flexible Dynamic Analysis

0-3s	Rigid		Flexible			
dt=.025	Coord.	Projection	Coord. Partition		Projection	
@CG	Partition		In-Loop	Prior	Prior	Correction
1st	1.196s	2.562s	3369.27s	1504.51s	2385.96s	0.38s
2nd	1.183s	2.461s	3364.17s	1507.19s	2332.96s	0.35s
3rd	1.390s	2.496s	3361.21s	1510.26s	2343.87s	0.32s
Avg	1.256s	2.506s	**3364.89s**	1507.32s	2354.26s	0.35s
Time saving %			55.20	30.03	----	

It can be observed from Table 4.3 that the flexible dynamic analysis consumes much more CPU time than the rigid one. This is because the elastic deformation greatly increases the complexity of the system equation. The off-diagonal terms in the generalized mass matrix are no longer zero for the flexible model regardless where the origin of the body fixed coordinate is placed. Furthermore, the elastic deformations complicate the integrals in the system equation and increase the number of the independent variables. All of these complexities increase the demand for computational time.

It should be noted that calculating the geometrical integrals prior to the ODE iterations can greatly improve the computational efficiency for both the coordinate partitioning method and the projection method.

Although the projection method takes more computational time compared with the coordinate partitioning method, it has a distinct advantage as it does not require identifying the dependent and the independent coordinates. The identification process can encounter singularity which can be overcome though with additional solution complexity.

CHAPTER 5

PRESSURE DISTRIBUTION RECONSTRUCTION FOR THE

CRAFT UNDER IMPACT

Planing craft is widely used in military, sport and recreational purposes due to its fast speed and convenience. However, when operated at high speeds under a complex environment, the hull surface may experience dynamic instability due to high magnitude, repetitive pressure impact. This hydrodynamic impact between the hull and waves has an adverse effect on the overall performance of the craft including ride quality, personnel comfort, habitability and safety, equipment reliability, etc. Hence, understanding wave-induced hydrodynamic pressure is essential to design a craft that can achieve proper seakeeping and habitability characteristics.

One of the major challenges that designers face in the early craft design process is the determination of the hydrodynamic pressure loads. Nowadays, designers typically rely on classification societies or semi-empirical design methods to calculate design loads on the hull surface by using the acceleration information from the model or full-scale test. These empirical methods are straightforward and easy; however, they sacrifice accuracy.

The main topics in this chapter are presented in the following order: First, a filtering process is introduced in Section 5.1 to eliminate the high-frequency noise present in the raw pressure data collected from the pressure transducers. The filtering process is made of FFT, low-pass Butterworth filter and the demeaning method. Subsequently, in Section 5.2, the maximum pressure peak is sought among the filtered data so as to investigate when and how the impact event occurred. As a result, the starting point of an impact wave and its velocity along each transverse section on boat hull can be determined. Next, in Section 5.3, the linear momentary pressure reconstruction algorithm is employed to map the pressure distribution on the wet surface on the boat hull as a function of a 2D coordinate (x, S), where x is along the longitudinal direction of the boat hull and S is along the transverse direction. Finally, in Section 5.4, the pressure distribution is mapped from a 2D surface, (x, S) to the 3D finite element model of the boat hull in terms of coordinates in (x, y, z).

5.1 Test Data Processing

Noise can always be found in raw test data. It may come from the device itself, from human operations, or even from the nearby environment. Noise in the test data can obscure the key features, such as peaks of the test data and lead to the incorrect conclusions. Hence, it is very important to process the raw test data to eliminate the noise as much as possible before analyzing it.

In this study, the hull-water impact pressure data was acquired through the full-scale tests of a craft conducted in irregular waves. 42 pressure transducers in total, noted as PT, are placed over the hull surface to collect the pressure distribution information. The time histories of the impact pressure test data are plotted in Fig. 5.1 at different transverse hull sections which are arranged along the longitudinal (fore-aft) direction.
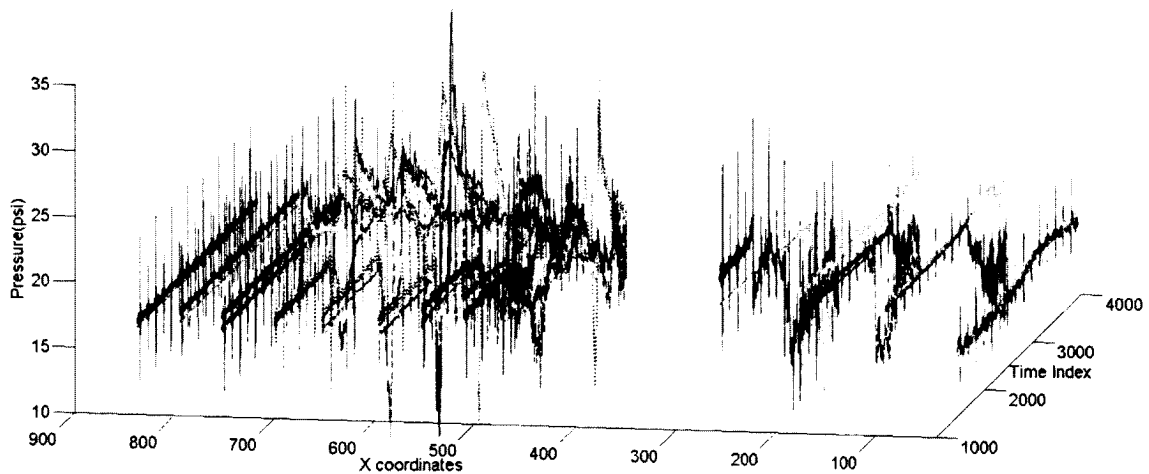
Figure 5.1 The Raw Test Impact Pressure Data for a Craft

It can be seen from Fig. 5.1 that the raw test data of impact pressure is not smooth at all. It is full of suddenly sharp spikes and disturbances. Hence, the raw test data cannot be used as it is to find the peaks and trends. Such spikes and disturbances can be observed more clearly in Figs. 5.2 and 5.3, each of which displays the time histories of a pair of pressure transducers. Note that the time interval Δt between a pair of consecutive indices is $5 \times 10^{-5} s$.
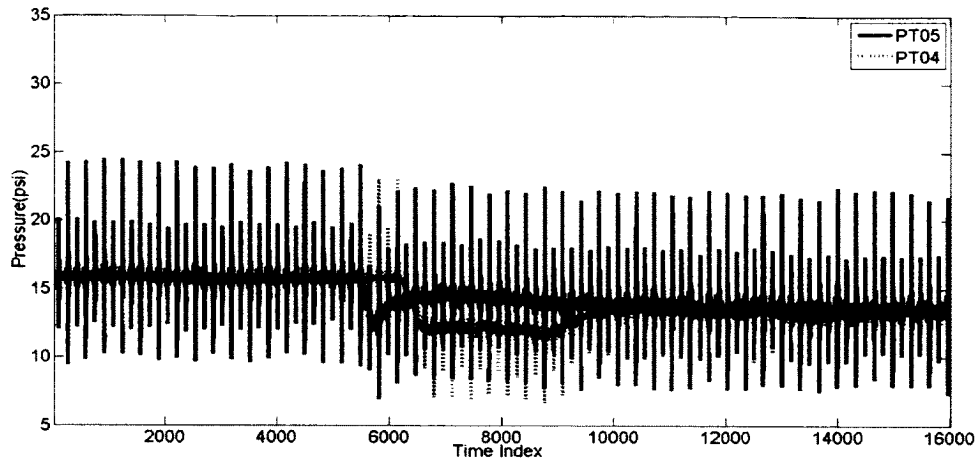
Figure 5.2 The Raw Pressure Data at PT04/05
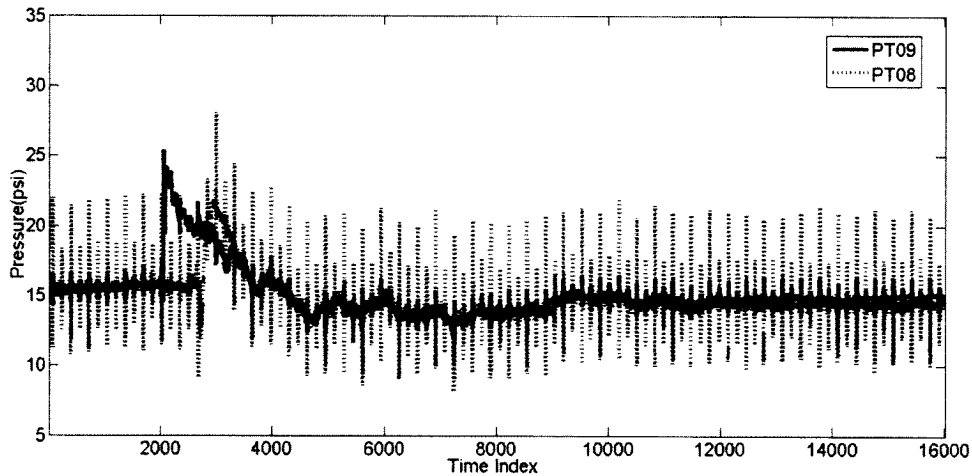
Figure 5.3 The Raw Pressure Data at PT08/09

The fluctuations of small pressure peaks can be observed in Figs. 5.2 and 5.3. Such disturbances call for the data filtering. Many sudden rising up and down in pressures collected at PT 04/05 can be observed in Fig. 5.2. However, the pressure collected at PT 08/09 rise up sharply at Time Index 2000 and then gradually drops to a normal level in Fig. 5.3. This implies that the craft encounters a slamming wave impact. The filtering of the raw test data is discussed in detail in the following section.

The data filtering process consists of two steps. In the first step, the Fast Fourier Transform (FFT) is used to represent the raw data in the frequency domain. As a result, the resultant Power Spectra Density (PSD), i.e., the energy distribution, of the pressure

data can be clearly measured and plotted. The information of PSD helps determine the cutoff frequency of the low pass Butterworth filter used as the second step for data filtering. The selection of the cutoff frequency is critical in determining the goodness of the filtering data. The cutoff frequency is selected in such a way that the remaining data will see no disturbance and the trend of the original data is preserved.

The impact pressure test data collected at the pressure transducers, PT05 and 08, are used to demonstrate the data filtering process. It is shown in the frequency domain in Figs. 5.4 and 5.5 after the FFT process. The associated raw pressure data in the time domain are shown in these figures as well.
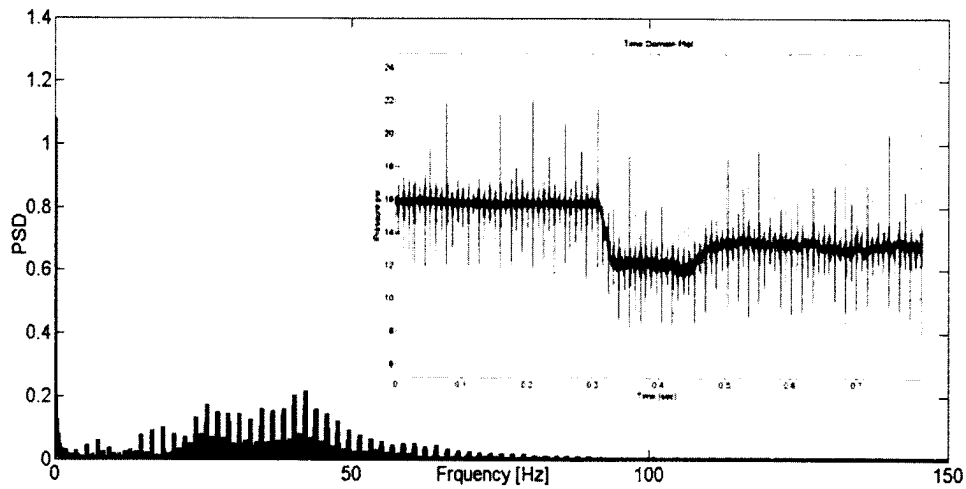
Figure 5.4 Frequency Spectra for PT05
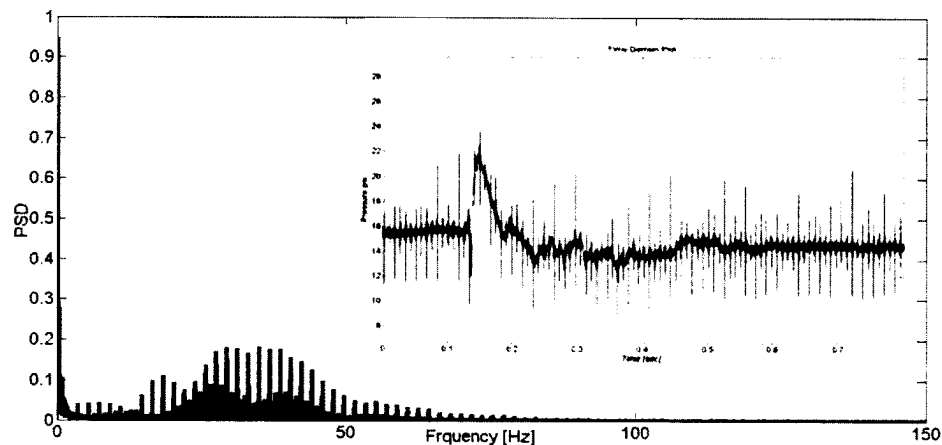
Figure 5.5 Frequency Spectra for PT08

The frequency spectra in Figs. 5.4 and 5.5 reveal that the PSD is mainly distributed in low frequencies, especially at 0 Hz. The PSD is close to zero when frequency is higher than 100Hz. The raw data is then processed with the cutoff frequency of 100 Hz. The filtered results are shown in Figs. 5.6 and 5.7, along with those obtained with other two cutoff frequencies, 20 and 50 Hz. The 100 Hz is shown to be the best among these three cutoff frequencies. It removes sufficiently high frequency oscillations while preserving the content of peak rigid body responses.
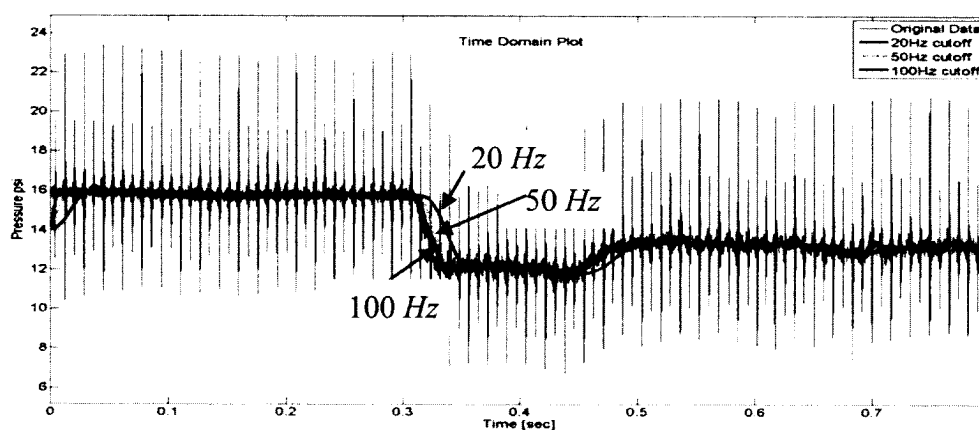
Figure 5.6 Different Cutoff Frequencies for Pressure Data PT05
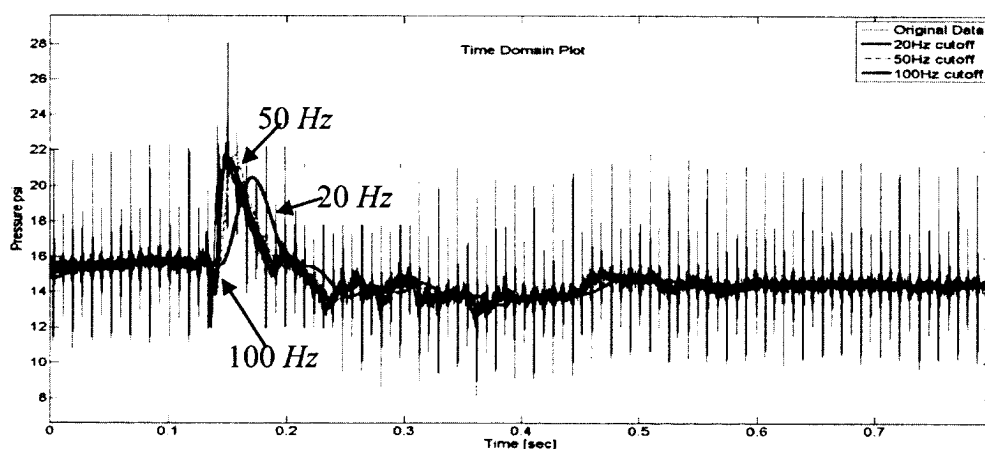
Figure 5.7 Different Cutoff Frequencies for Pressure Data PT08

Though the filtered data matches well the raw pressure data as shown in Figs. 5.6 and 5.7, some discrepancies between them were found at the beginning of the pressure profile. This can be observed in the zoomed-in figures in Figs. 5.8 and 5.9. A process called demeaning is then applied to deal with this issue. The raw pressure data is first deducted by its mean in the demeaning process. The processes of FFT and the low pass filter are then applied to the demeaned data. The mean is added back to the filtered data to complete the process. The filtered data with/without demeaning are compared in Fig.5.8 for the pressure data at PT05 and in Fig.5.9 for PT08. These two figures demonstrate the importance of the demeaning method in processing the pressure data.
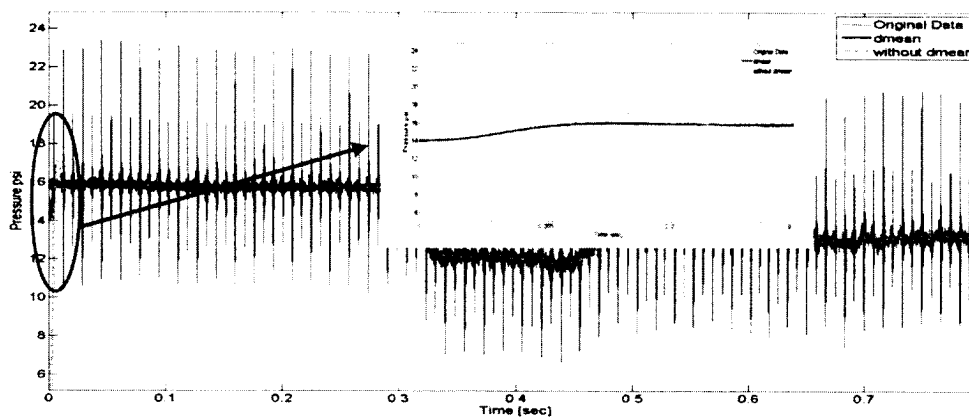
Figure 5.8 The Filtered Data Comparisons with/without Demeaning for PT05
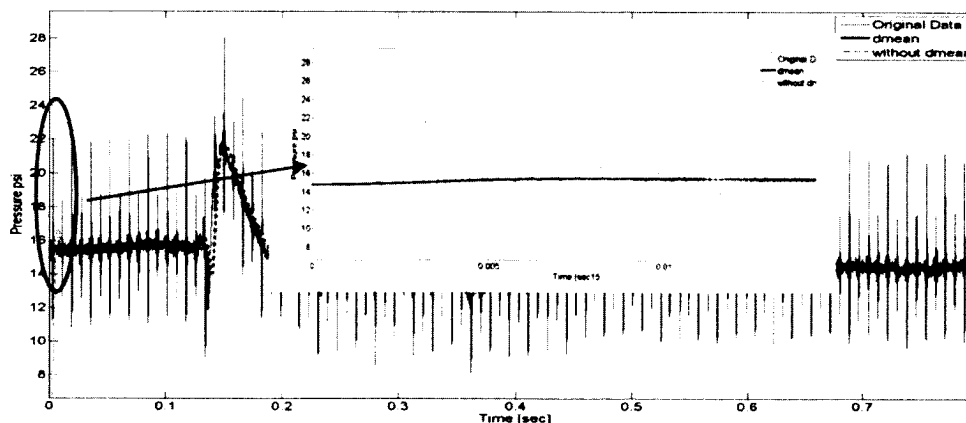
Figure 5.9 The Filtered Data Comparisons with/without Demeaning for PT08

In short, the steps of the pressure data processing procedure used in this research are summarized below:

1. *Demeaning*: Subtracting the mean of the raw test data, and then adding back the original mean to the filtered data.

2. *FFT*: Showing the frequency spectra of the demeaned data.

3. *Cutoff frequency*: Selecting the cutoff frequency based upon FFT results.

4. *Low-pass filter*: Applying the Butterworth low-pass filter with the selected cutoff frequency based upon PSD data.

5. *Filtering evaluation*: Comparing the filtered data with the raw test data to make a judgment whether accepting the filtered data.

The resulting pressure data at PT04/05 and PT08/09 are shown in Figs. 5.10 and 5.11, respectively. Compared with those in Figs. 5.2 and 5.3, the filtered data is smoother and without any high frequency peaks. The slamming impact is clearly displayed in Fig 5.11. The time histories of the pressure profiles collected at all the pressure transducers in about 0.8 seconds, after filtering, are shown in Fig. 5.12. A slamming impact pressure is observed near the second quarter length of the boat from the bow.
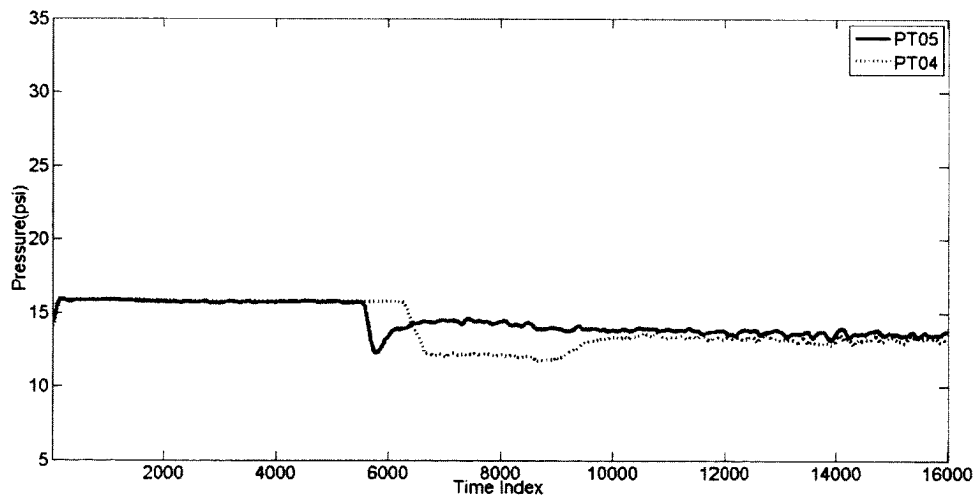
Figure 5.10 The Filtered Pressure Data for PT 04/05
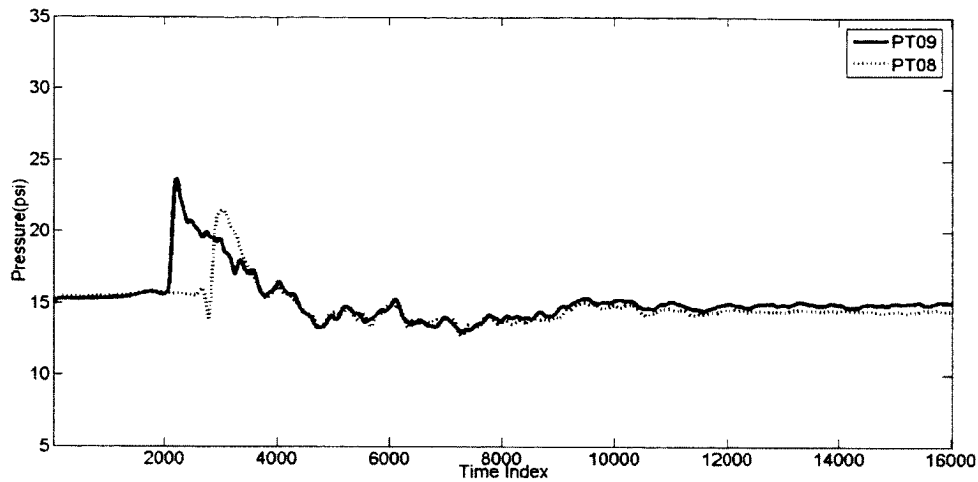
Figure 5.11 The Filtered Pressure Data for PT 08/09
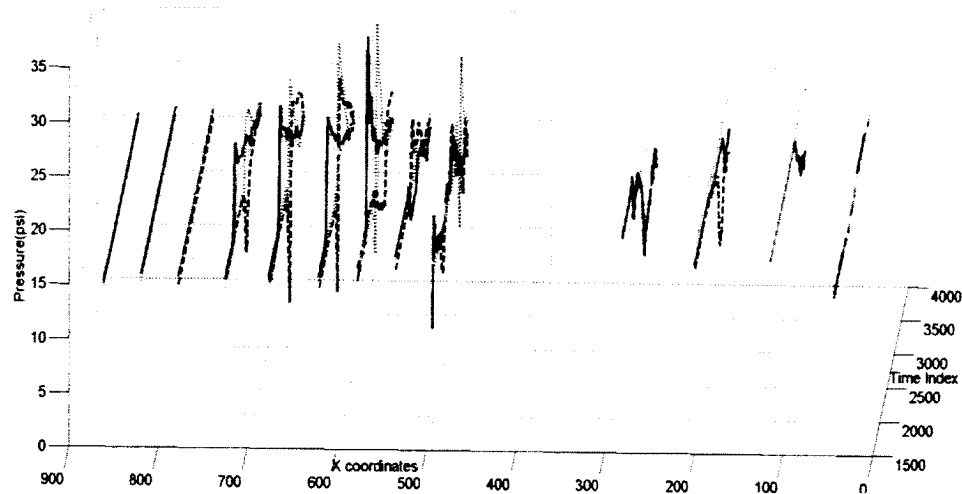
Figure 5.12 The Filtered Pressure Data at All Pressure Transducers

5.2 Linear Pressure Reconstruction

The number of the pressure transducers used in the full-scale test is often quite limited. Therefore, the pressure data collected usually does not provide enough information for the traditional curve-fitting method to produce a pressure distribution with acceptable accuracy. Instead, the method proposed by Rosen [92, 93] is used in this section to construct the pressure distribution. Subsection 5.2.1 introduces the layout of the pressure transducers from which the pressure data is collected. Sub-section 5.2.2 provides details of Rosen's method.

5.2.1 The Layout of the Pressure Transducers

The full-scale test for a craft was conducted in irregular waves to collect the time histories of the hydrodynamic pressure at 42 different locations distributed over the hull surface. The layout of the pressure transducers [64, 65, 91] is shown in Fig. 5.13. Based upon the pressure characteristic along the hull surface, these 42 pressure transducers can be classified into 3 groups. The first group includes 8 transducers, PT00 to 07 which are in the bow zone. The second group includes 24 transducers, PT08 to31 which cover most of the impact area, called the impact zone. The final group includes 10 transducers, PT32 to41, which are in the stern zone
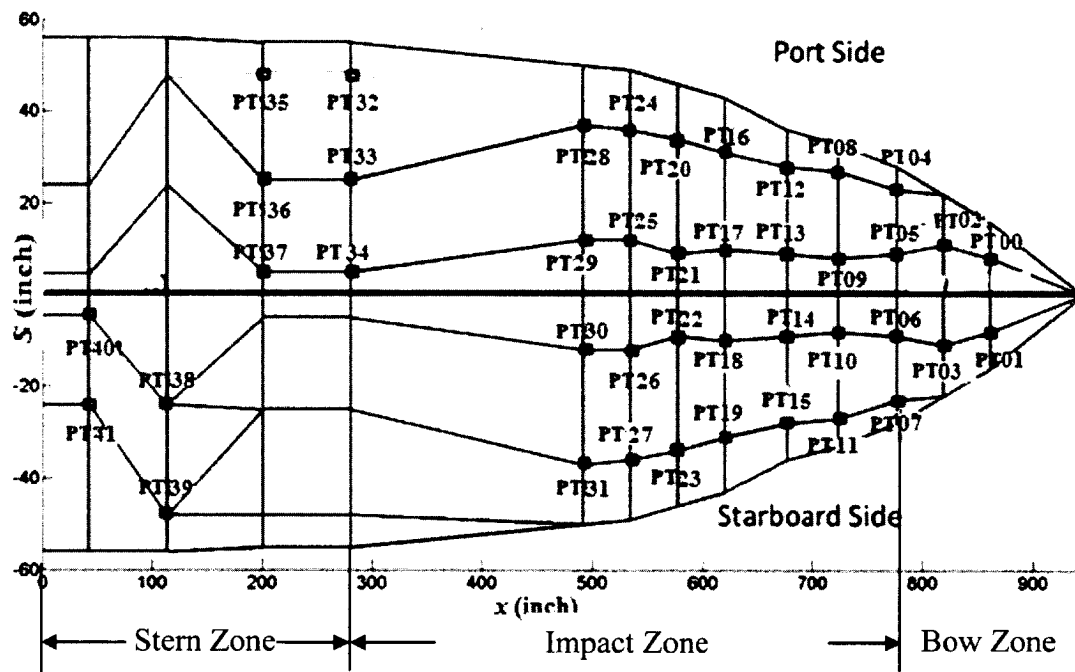
Figure 5.13 Layout of the Pressure Transducers

The impact pressures collected at the transducers placed at the port and the starboard sides in the bow zone are shown in Figs. 5.14 and 5.15. The pressure histories collected at the transducers in this period of time indicate no sign of impact as they remain fairly constant close to the air pressure. This is because the hull surface located at the bow zone exposed to the air. Nevertheless, it can be observed that the pressures on the starboard side are relatively higher than those on the port side. This non-symmetric pressure distribution implies that the physical phenomena of the oblique wave coming

from the starboard side to the port side.
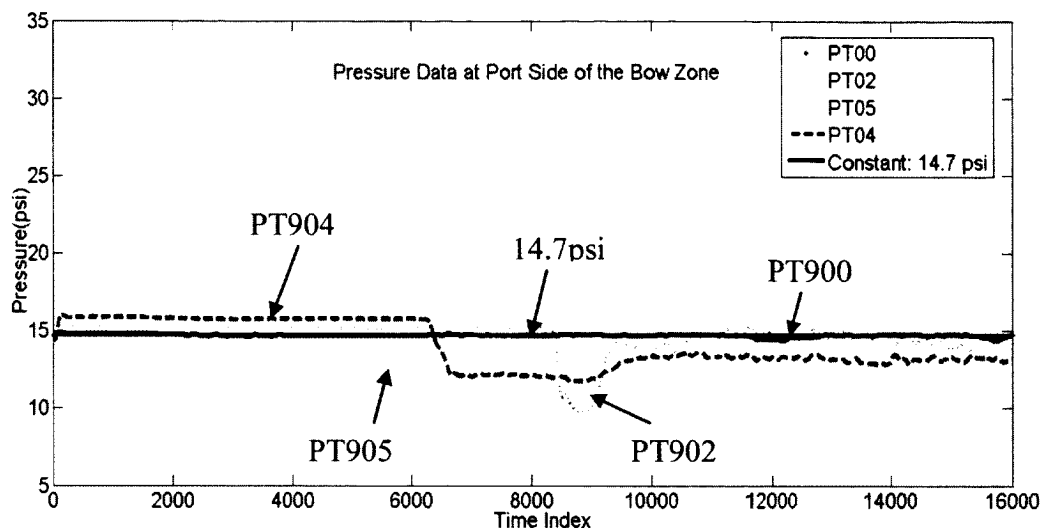
Figure 5.14 Filtered Pressure Data at the Port Side of the Bow Zone
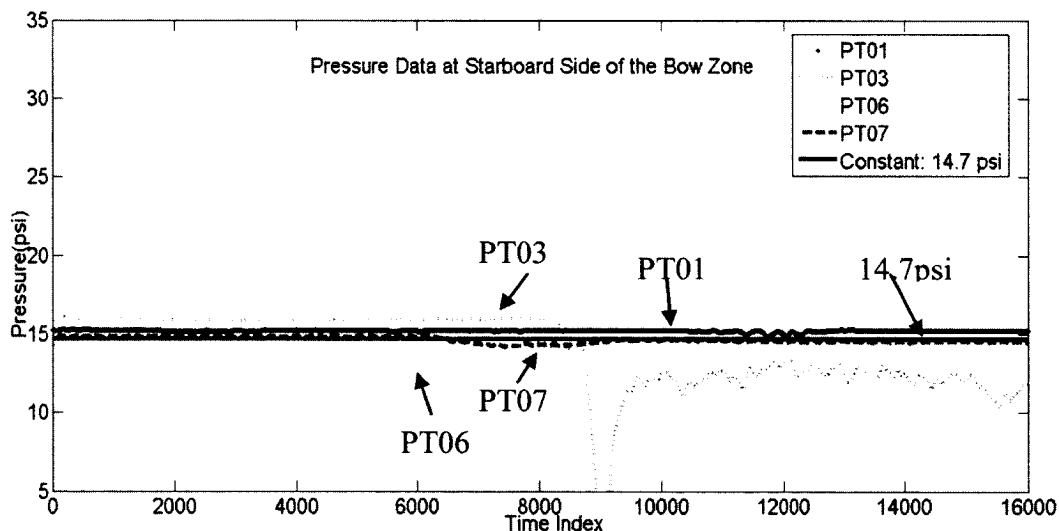
Figure 5.15 Filtered Pressure Data at the Starboard Side of the Bow Zone

The pressure histories of transducers placed in the impact zone of the port side and of the starboard side are plotted in Figs. 5.16, and 5.17, respectively, for the period of time indices from 1,500 to 4,000 and for duration of 0.125 seconds. The pressure histories of the pair of the transducers placed on the same transverse section in the impact zone are plotted in the same figure.
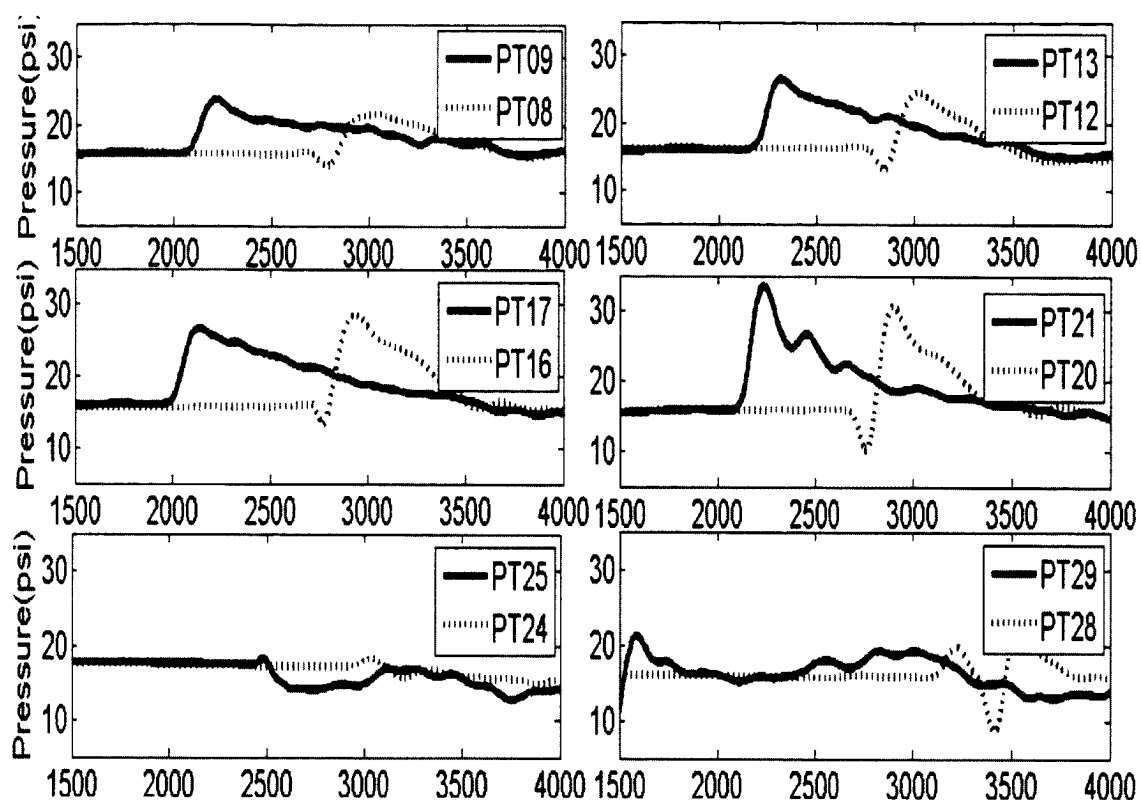
Figure 5.16 Filtered Pressure Data at the Port Side of the Impact Zone
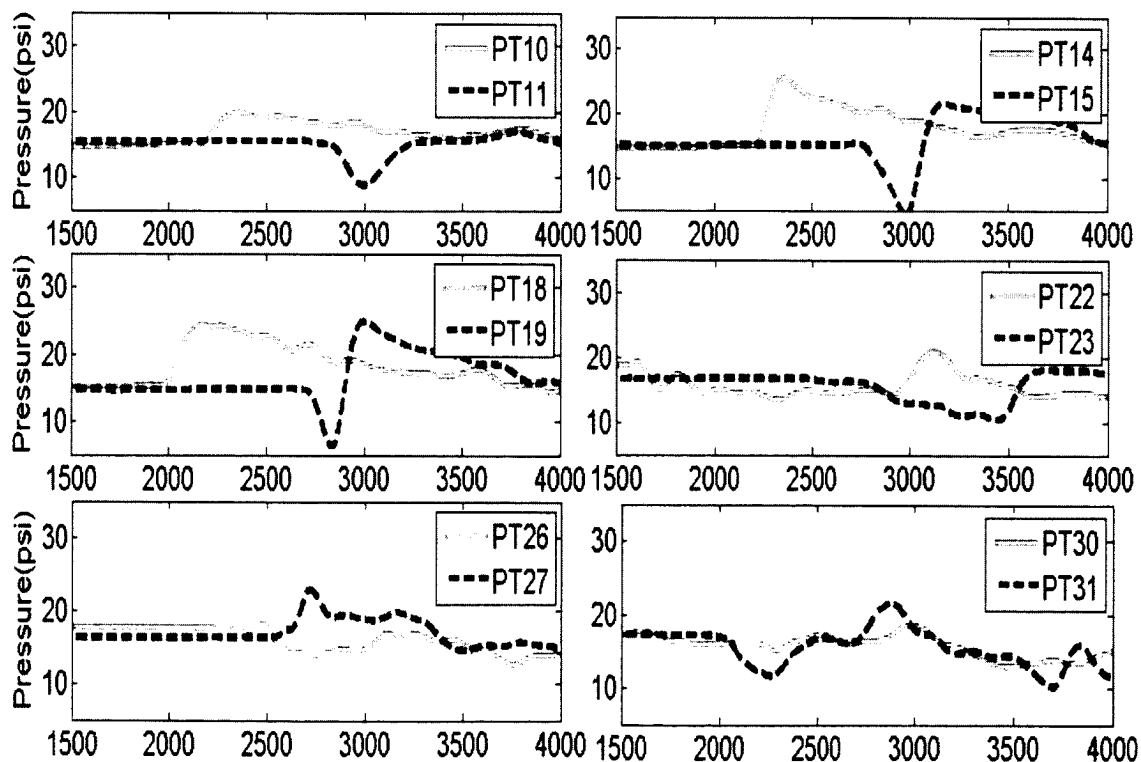
Figure 5.17 Filtered Pressure Data at the Starboard Side of the Impact Zone

Each transducer observed a pressure peak during the impact period of concern. Furthermore, the pressure peak at the transducer closer to the keel appeared earlier than that at the transducer closer to the chine. The rise and the fall of the pressure histories shown in the figures clearly indicate that a wave impacts the boat hull surface. In addition, the peak sequence implies that the wave propagates from the keel to the chine.

The pressures histories collected at the transducers placed in the stern zone are shown in Fig. 5.18. It can be observed that the hydrodynamic pressure is close to uniform, particularly at the beginning of the impact duration of concern. Most of the time, the stern is immersed in the water. Hence, it is assumed in this study that the pressure is symmetric with respect to the keel in the stern zone.
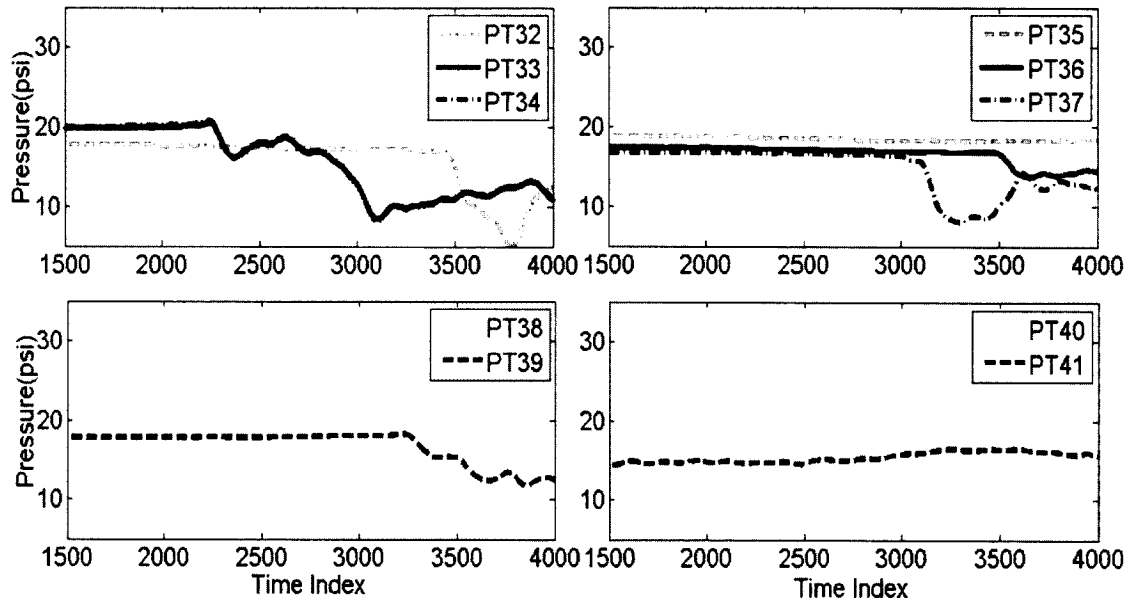
Figure 5.18 Filtered Pressure Data at the Stern Zone

5.2.2 Scheme of the Pressure Reconstruction

Hydrodynamic pressures captured by two pressure transducers, PT_1 and PT_2 placed at location S_1 and S_2 along the same transverse section on the craft hull surface are schematically illustrated in Fig.5.19. Rosen assumed in his pressure construction procedure that the water particles move at a constant speed from the keel to the chine along the same transverse section. The impact wave speed is perceived as the same as the

water particle speed traveling from the keel to the chine along a transverse section.
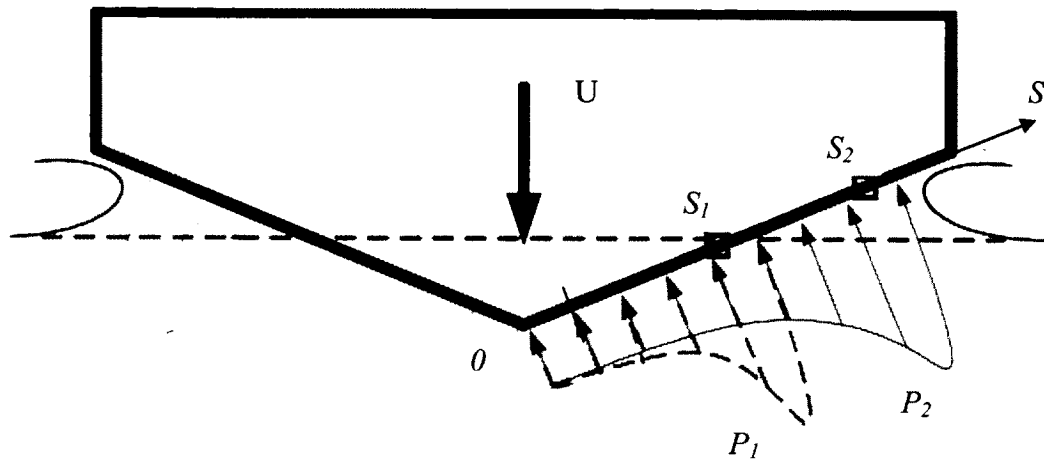
Figure 5.19 Wave Traveling along a Transverse Section

In this study, the beginning of a wave profile at the location of a pressure transducer is considered as the time of a minimum pressure right before the maximal pressure peak. The wave impact starting time can be conveniently identified in the pressure history of a transducer. For instance, the starting times for impact waves at the pressure transducers PT09 and 08 are identified in Fig. 5.20 as T_{s1} and T_{s2}, respectively.
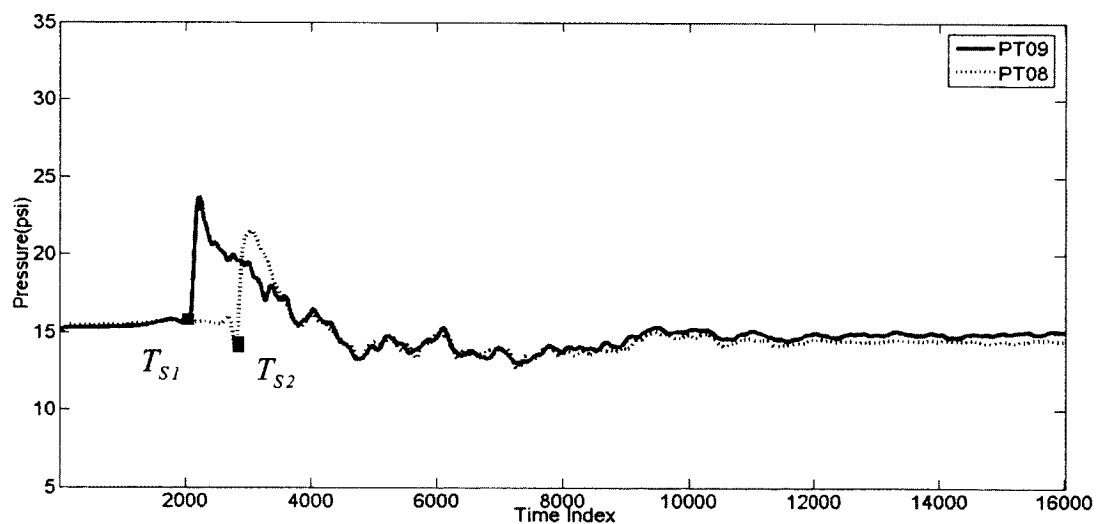
Figure 5.20 The Starting Times at PT09/08

Thus, the pulse velocity along the transverse section, which is assumed to be constant, can be determined through the following equation:

$$V = (S_2 - S_1)/(T_{s2} - T_{s1}) \qquad (5.1)$$

where S_1 and S_2 are the locations of the transducers along the same transverse section. Note that $S_2 > S_1$ and $T_{s2} > T_{s1}$ in this case. All fluid particles in this particular wave impact will travel with the speed V along the same transverse section. This assumption helps to find the pressure, $P(S, T)$, at any time and at any location along the transverse direction where the corresponding pair of transducers has been placed.

5.2.3 Pressure Reconstruction along S Direction

Fig. 5.21 shows the pressure distribution, $P(S, T)$, in the traveling distance S along the transverse direction and the time space T. The fluid particle that arives at S at time T is the one that starts the journey at the time, $\overline{T_1}$ at the location of the Tranducer, S_1 and arrived at the location of the second Transducer, S_2 at $\overline{T_2}$. The pressure $P(S,T)$ is then obtained by linear interpolation of the pressure data, $P_1(S_1, \overline{T_1})$ and $P_2(S_2, \overline{T_2})$. Note that the latter can be read from the pressure data histories recorded at the transducers.
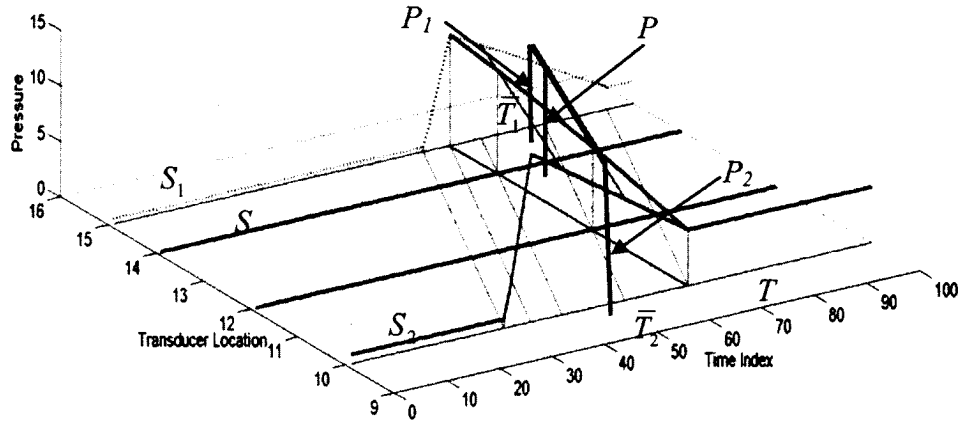
Figure 5.21 Pressure Reconstruction Scheme along a Transverse Direction

The concept discussed above can be conveniently extended to the full-scale

testing data collected in the impact zone. Fig. 5.22 shows a S-T diagram of a typical transverse section presented in Fig. 5.13. Two of the transducers are placed on the port side and two on the starboard side. The goal here is to compute the pressures $P(S_A, T)$, $P(S_B, T)$ and $P(S_C, T)$ at points S_A, S_B, and S_C which are physically aligned in the same transverse direction with the locations, S_1 and S_2. The inclined lines passing through S_A, S_B and S_C in Fig. 5.22 indicate the trajectories of the fluid particles. These inclined lines share the same slope in the (S, T) plane, as the slope represents the traveling speed of the fluid particles which is defined by Eq. 5.1. Note that T_{s1} and T_{s2} denote the starting times of the impact wave recorded by the pressure transducers at S_1 and S_2. They can be found based upon the pressure histories collected at the transducers at S_1 and S_2.

The inclined line can be used to find the pressure at any point in the (S, T) plane. For example, the inclined line passes the point (S_A, T) represents the trajectory of the fluid particle that passes the pressure transducer S_1 at time $\overline{T}_{A1}$ and the pressure transducer S_2 at time $\overline{T}_{A2}$. The similarity between triangles helps to find the values of times, $\overline{T}_{Ai}$, $i = 1,2$ as

$$\overline{T}_{i,A} = T + \frac{(S_i - S_A)}{(S_2 - S_1)}(T_{s2} - T_{s1}), \quad i = 1,2 \tag{5.2}$$

The pressure at point (S_A, T) can then be obtained through linear interpolation based upon the pressures recorded at the transducer S_1 at time $\overline{T}_{A1}$ and the transducer S_2 at time $\overline{T}_{A2}$ at the pressure transducers; i.e.,

$$P(S_A, T) = P(S_1, \overline{T}_{1,A}) + \frac{S_A - S_1}{S_2 - S_1}[P(S_2, \overline{T}_{2,A}) - P(S_1, \overline{T}_{1,A})] \tag{5.3}$$

The assumption employed here is that the pressure is distributed linearly along each inclined line. A minor modification is needed if either of $\overline{T}_{1,A}$ or $\overline{T}_{2,A}$ goes beyond the targeted range of time period.
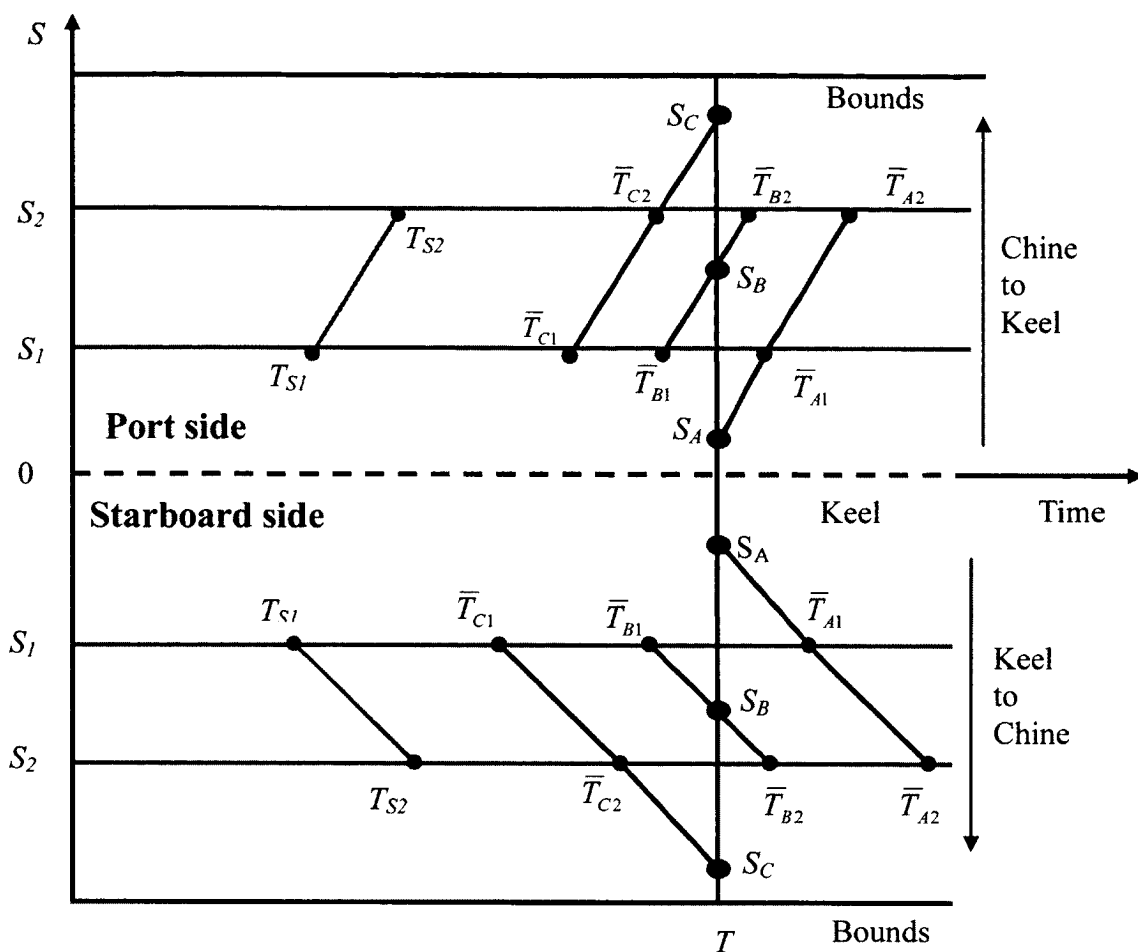
Figure 5.22 The Scheme to Find T_1 and T_2

The starting time index and wave velocities of an impact wave along a given transverse section in the impact zone are summarized in Table 5.1.

Table 5.1 The Starting Time Index and Wave Velocities at the Impact Zone

	Side	PT #	Coord. x	Coord. S	Starting Index	Vel. (in/s)
Impact Zone	Port	PT11	724 in	8	2068	493.51
		PT10		27	2838	
	Starboard	PT12		-8	2185	388.15
		PT13		-27	3164	

Table 5.1 The Starting Time Index and Wave Velocities in the Impact Zone (Cont.)

	Side	PT #	Coord. x	Coord. S	Starting Index	Vel. (in/s)
	Port	PT15	676 in	9	2198	522.70
		PT14		28	2925	
	Starboard	PT16		-9	2236	409.48
		PT17		-28	3164	
	Port	PT19	620 in	10	2042	516.61
		PT18		31	2855	
	Starboard	PT20		-10	2022	428.20
		PT21		-31	2893	
	Port	PT41	577 in	9	2144	753.01
		PT40		34	2808	
	Starboard	PT42		-9	3037	868.06
		PT43		-34	3613	
	Port	PT45	535 in	12	2444	546.88
		PT44		36	2956	
	Starboard	PT46		-12	2444	1458.33
		PT47		-36	2636	
	Port	PT49	493 in	12	2743	1207.73
		PT48		37	3157	
	Starboard	PT50		-12	2499	1298.70
		PT51		-37	2834	

The pressure distribution along the transverse section in the impact zone at x=724 inches is shown in Fig. 5.23. The pressure data is reported at 30 locations along the transverse section at time 0.94 seconds, including those of the transducers. The more points that are introduced, the better the result will be.
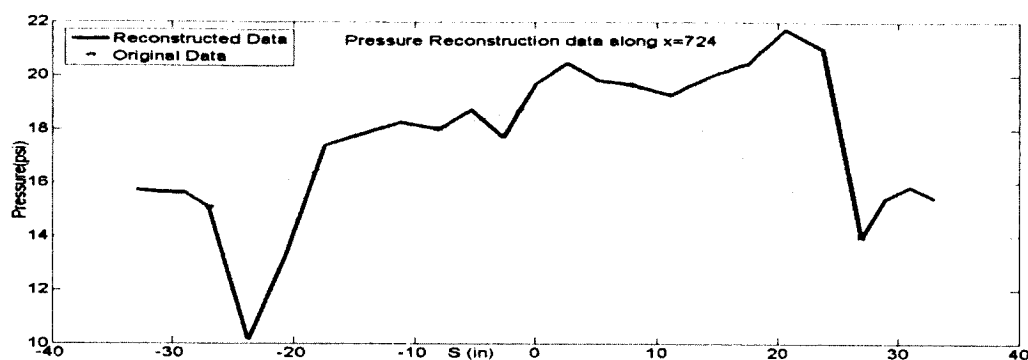
Figure 5.23 Pressure Reconstruction along *x*=724 inches at the Impact Zone

On the other hand, the pressure at time *T* at any point along a transverse section in the bow and the stern zones will be computed by linearly interpolating the pressure data collected at the transducers at the same time, *T*. This is because there is no wave impact found in these two zones. The pressure distributions along a transverse section in the bow zone and the stern zone are reported in Figs. 2.24 and 2.25, respectively. The pressures around the stern zone are symmetric with respect to the keel.
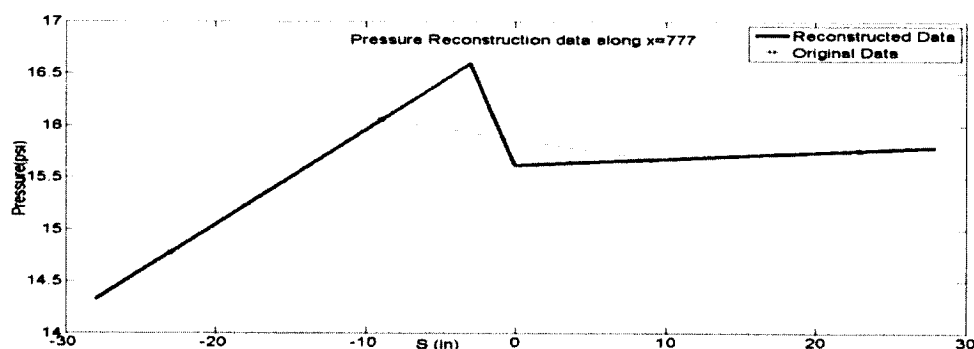
Figure 5.24 Pressure Reconstruction along *x*=777 inch at the Bow Zone
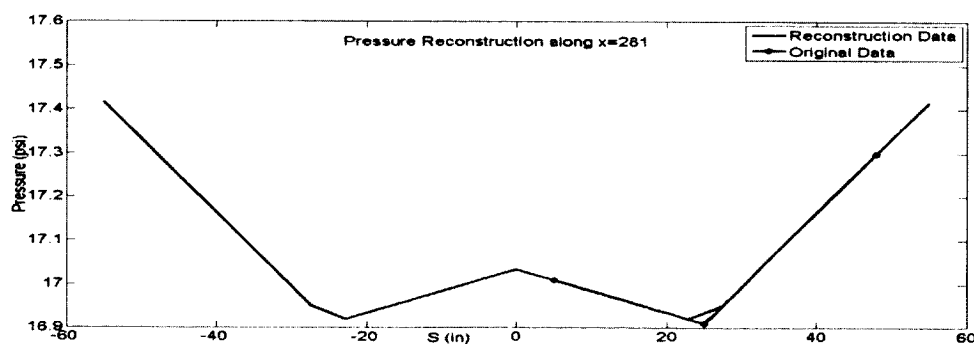
Figure 5.25 Pressure Reconstruction along *x*=281 inch at the Stern zone

5.2.4 Pressure Reconstruction on (S, x) Plane

Once the pressure history along each transverse section S is obtained based upon the scheme discussed in Section 5.2.3, it can be extended to the entire (S, x) space on the bottom surface of the boat. The pressure at (S, x) can be obtained by linearly interpolating the pressures at the points (S, x_1) and (S, x_2) on the transverse sections as shown in Fig. 5.26.
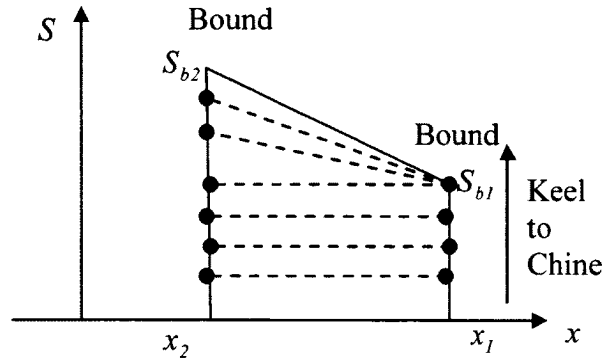
Figure 5.26 Pressure Reconstruction Scheme between Two Adjacent Sections

If $S_{b1} < S \le S_{b2}$, the maximal S value, S_{max} along the line connecting two points (S_{b2}, x_2) and (S_{b1}, x_1) is determined as:

$$S_{max} = S_{b1} + \frac{x_1 - x}{x_1 - x_2}[S_{b2} - S_{b1}]$$ (5.4)

If $S > S_{max}$, the associated point is out of range. The pressure at (S, x) is set to be zero. If $S \le S_{max}$, Point S'_{b2} is the intersection between the transverse section on x_2 and an extension line that passing through (S_{b1}, x_1) and (S, x), and the intersection point with transverse section x_2 as:

$$S'_{b2} = S_{b1} + \frac{x_1 - x_2}{x_1 - x}[S - S_{b1}]$$ (5.5)

Hence, the pressure at the point (S, x) can be determined linearly based upon the pressure data found at (S_{b1}, x_1) and (S'_{b2}, x_2).

The pressure distribution along each transverse section S is referred to as the line

distribution, while the complete pressure distribution on the plane (S, x) is referred to as a 2D distribution.

The pressure distribution at 0.94 seconds on the bottom of the craft is shown in Fig. 5.27. Its associated pressure contour plot is displayed in Fig. 5.28.
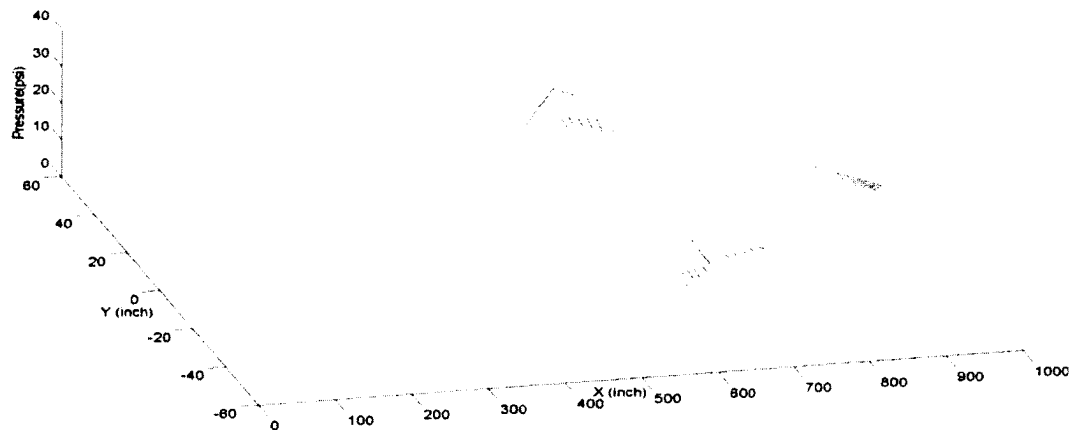
Figure 5.27 2D Pressure Distribution on the Craft at t=0.94s
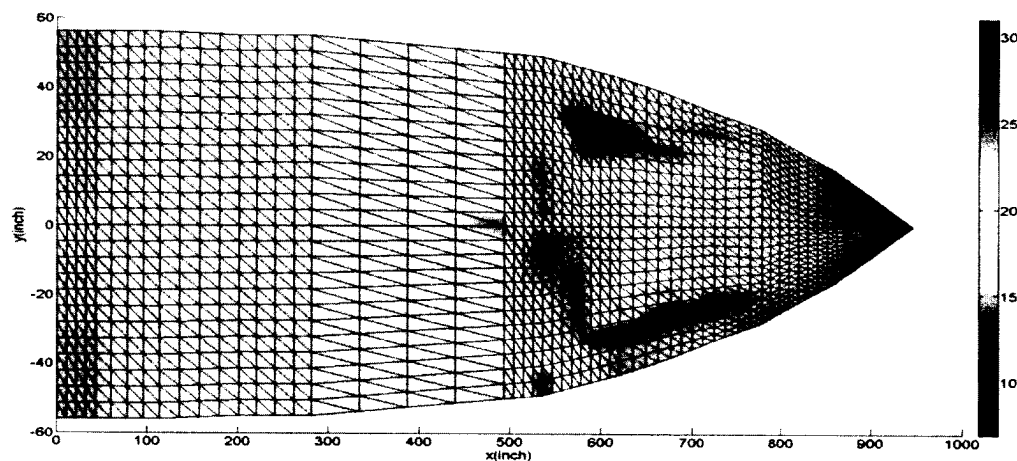
Figure 5.28 2D Pressure Contour at t=0.94s

It can be seen clearly that the maximum pressure occurs at the impact zone. The pressure at the port side is higher than the pressure at the starboard side. The impact wave starts from the port side and moves to the starboard side. The values of the pressure at the bow and stern zones are much less than the ones at the impact zone. The pressure distribution obtained here is similar to that presented in Allen [58].

5.3 Pressure Distribution Mapped onto 3D Finite Element Model

The previous sections discussed the procedure to construct a pressure distribution on the 2D plane in (S,x) based upon the pressure data read from the pressure transducers. This pressure distribution needs to be mapped to the surface of the 3D finite element model of the craft for dynamic analysis.

A wire-frame model of an artificial craft is created to demonstrate the pressure mapping process. The craft hull and the shapes of sample transverse sections are shown in Fig. 5.29.
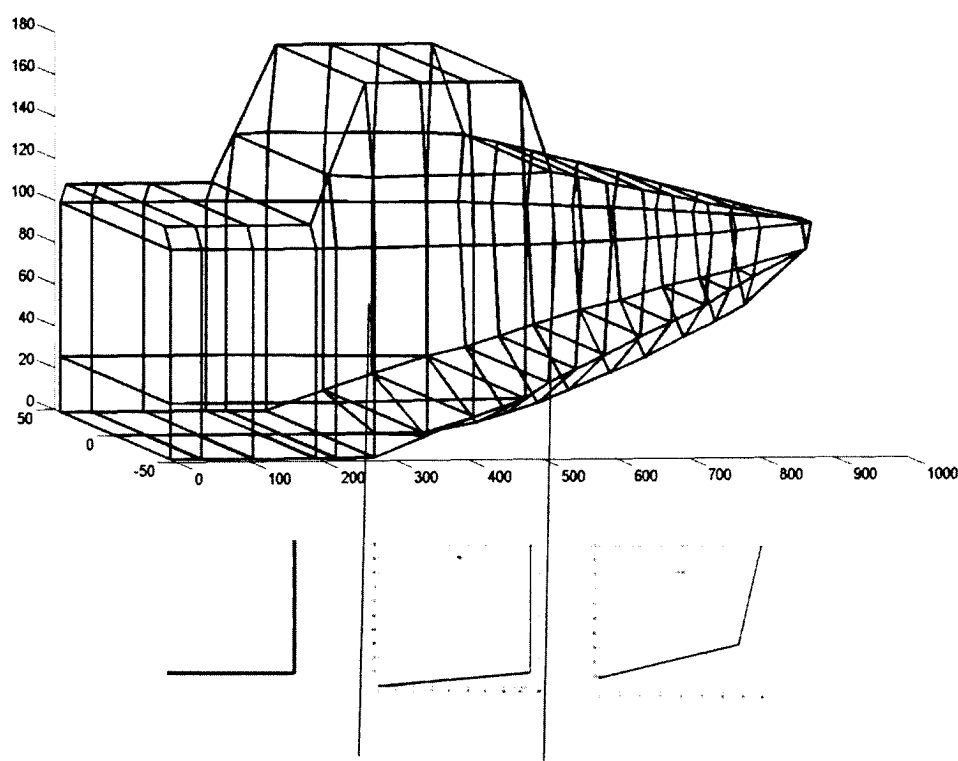
Figure 5.29 Hull Profile and Shapes of Sample Transverse Sections of the Craft

In the stern zone, the bottom line of the transverse section is set to be horizontal, though the sideline is vertical. The bottom surface of the transverse section in the impact zone is no longer flat, though the sideline also remains vertical. In the bow zone, both the bottom and the sideline are no longer straight. The details of the transverse section profiles in the stern and the impact zones are shown in Figs. 5.30 and 5.31.
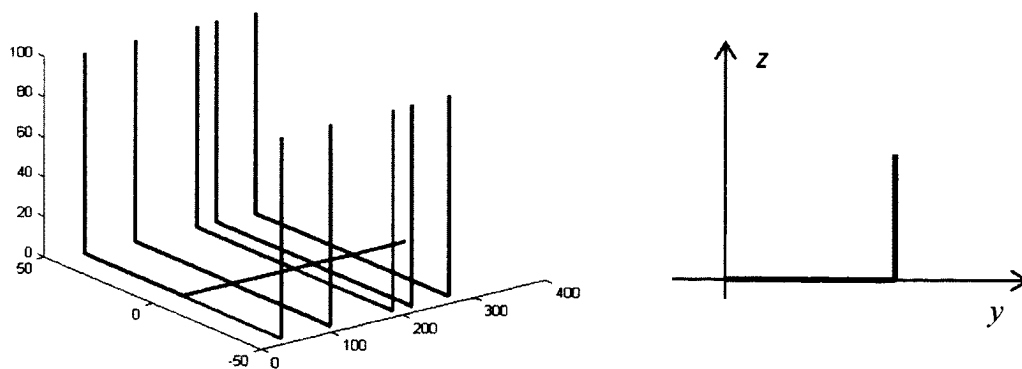
Figure 5.30 Transverse Section Shape at the Stern Zone
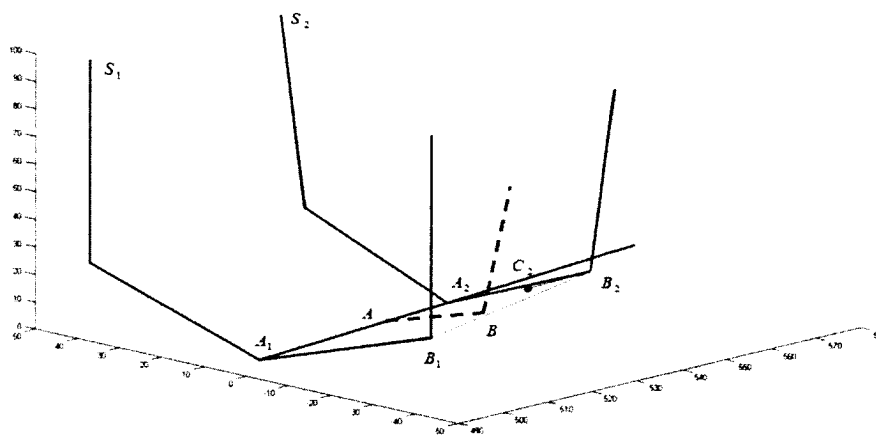
Figure 5.31 Transverse Section Shape at the Impact Zone

Given any nodal coordinate in (x, y, z) on the wetted surface in the finite element model, simple geometric relation can be used to find the corresponding arc length, S measured from the keel. The pressure values at each node on the wetted surface are thus obtained and are ready to be used for a transient analysis in Chapter 6. As an example, the pressure contour plot at $t=0.94$ seconds on the surface of the 3D finite element model is shown in Fig. 5.32. The pressure contour plot on the bottom of the 3D finite element boat model is shown in Fig. 5.33 (a). In comparison, the same pressure contour plotted on the (S, x) plane is in Fig. 5.33(b).
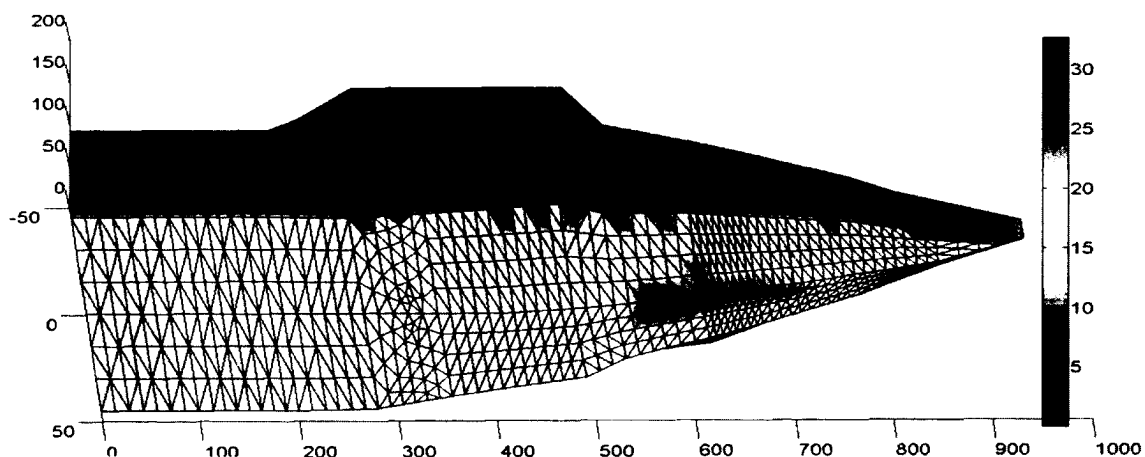
Figure 5.32 Pressure Contour Plot for the 3D Finite Element Model
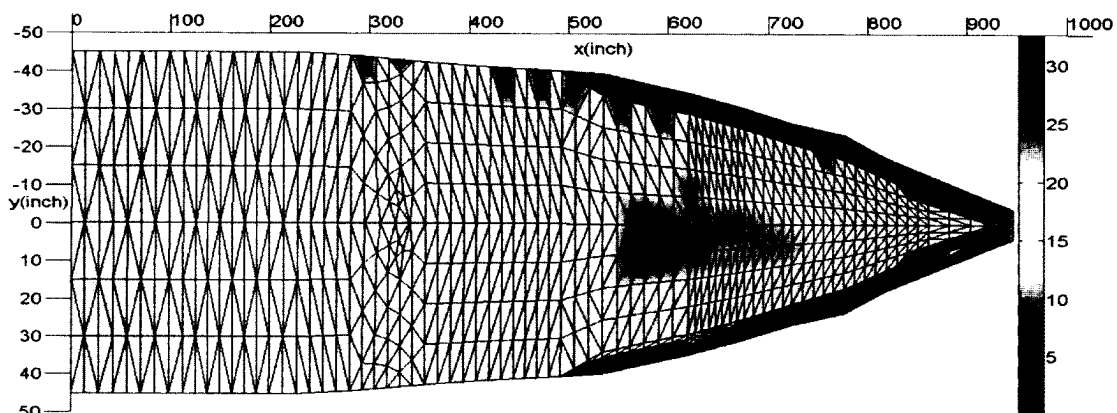
a. Pressure Contour on the Bottom of the 3D Finite Element Boat Model
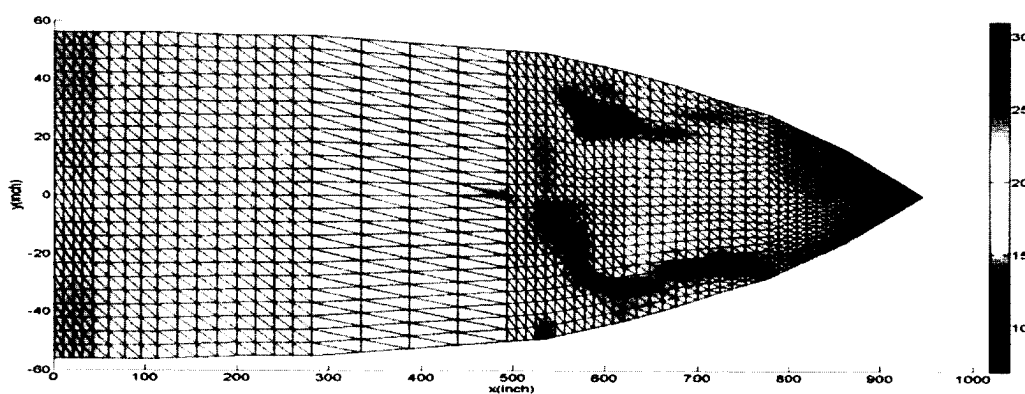
b. Pressure Contour on the (S, x) Plane

Figure 5.33 Comparison of Pressure Contour Plots on the 3D Model and the 2D Plane at

$t=0.94$ seconds

CHAPTER 6

DYNAMIC ANALYSIS OF A FLEXIBLE CRAFT IN WAVES

A boat model under the dynamic pressure load that was constructed in Chapter 5 is analyzed in this chapter. The analysis is done by employing the equations and procedures derived in Chapters 2 and 3 for flexible body dynamics. In the current chapter, methods to analyze a 3D flexible structure under large angle rotation are also investigated.

For a complex structure, the elastic deformation is usually described using the finite element method. Hence, the finite element model of the craft is built first in section 6.1. Modal analysis is then conducted in MSC/ Nastran to obtain the mode shapes, mode frequencies, and the modal element stress. The time history nodal force is calculated from the pressure information at the nodes in the finite element model based upon the same work done by these two loads in section 6.3. The local coordinate of each element is built to make sure that the local z axis is along the thickness of the triangular element. Subsequently, the nodal force is converted to the body-fixed coordinates of the finite element model as the externally applied force. The numerical methods on dynamics of the 3D flexible multi-body system are introduced in section 6.4. The first one is Newmark's method, in which the transformation matrix is calculated using the exponential matrix. The second one is the mixed order technique with additional Euler parameters. The main idea of the mixed order technique is to introduce the additional Euler parameters to the governing equation of motion without eliminating the angular velocity. The transformation matrix is described using the Euler parameters. The integrals in the equation of motion are calculated as constants for the triangular element in section 6.5. The rigid dynamic analysis of the craft is performed to predict the motion of the craft in section 6.6. The flexible dynamic analysis of the craft is performed to determine the stress distribution of the craft in section 6.7. The element stress is calculated based upon the modal element stress using the least mean square error technique in section 6.8.

6.1 Finite Element Model of the Craft

Generally, the finite element model can be generated two ways. In the first, it is constructed based upon the geometry information of the structure from bottom to up. The second involves the meshing of the geometry model generated from CAD software directly. In order to describe the location and motion of any arbitrary point on the craft, one must determine the coordinate system first. It has been shown in Chapter 2 that the linear inertia vanishes if the origin of the body-fixed coordinate is located at the center of gravity (CG). However, in this study, the origin is located at the center of the rear end because the location of CG cannot be obtained easily at first due to the complex structure of the craft. The ox axis is positive from the stern towards the bow of the craft. The oy axis is positive from the starboard side towards the portside of the craft. The oz axis is positive upwards and goes through the centre of the trailing edge. The xoz plane is symmetric about the central plane of the craft. The half geometry model of a simple 3D craft used in this study is shown in Fig. 6.1. The bottom of the boat is carefully laid out so that it covers the transverse sections shown in Fig. 5.28. The interior partitions are added to stiffen the boat structure. The body-fixed coordinate system and its origin are also marked in the figure.
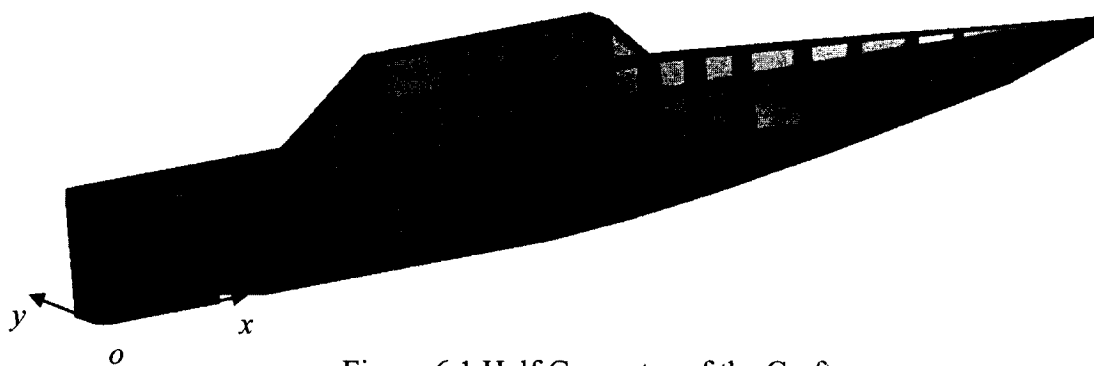
Figure 6.1 Half Geometry of the Craft

Only the half finite element model needs to be generated; the entire finite element model can be easily obtained by mirroring the half model with respect to the xoz plane. In summary, the entire structure is discretized into 4,653 nodes and 10,660 triangular shell elements. The edge length of any triangular element is limited to be within 1 inch. The finite element model, which is shown in Fig. 6.2, is classified as three different parts by

setting different properties numbers: interior, upper, and bottom parts. The bottom part is the potential wet surface where the impact may occur. The thickness of the upper and bottom parts is 0.6 inch; however, it is 1.0 inch for the interior part. Hence, the total weight of the aluminum boat is equal to 47,746.00lbs. In order to see the interior structures, the wire-frame mesh model is shown in Fig. 6.3.
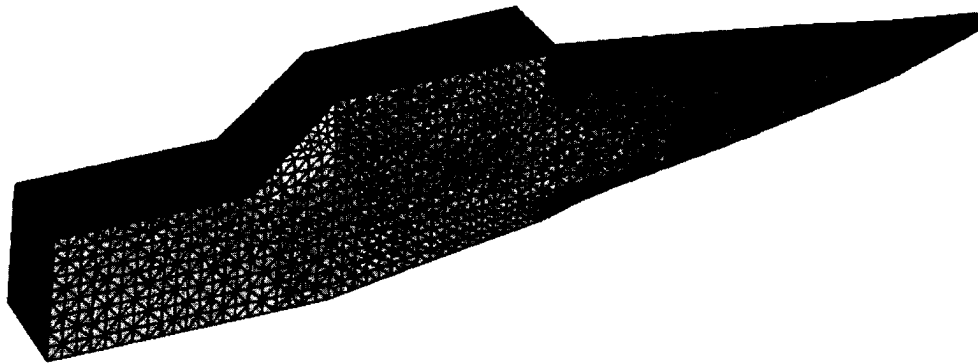
Figure 6.2 Finite Element Model for the Craft
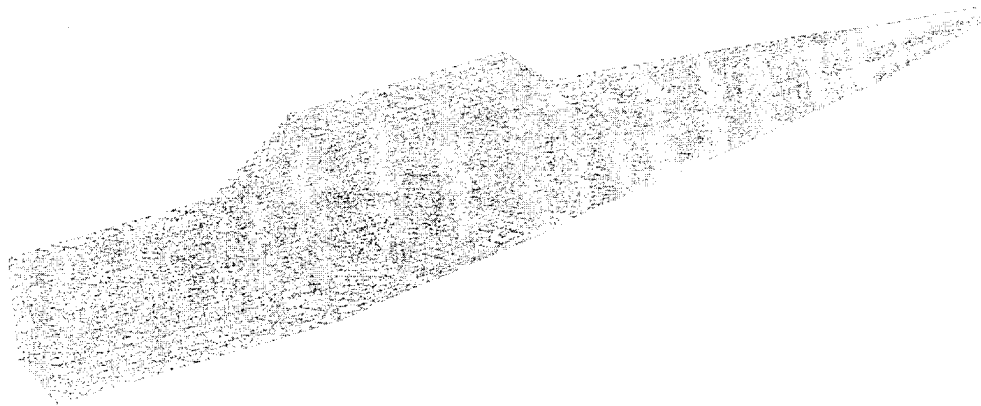
Figure 6.3 Wire Frame of the Finite Element Model

The modal analysis is then performed using the commercial software, MSC/ Nastran. No constraints are imposed for modal analysis on the finite element craft model. In this study, the first 60 elastic mode shapes of the craft are extracted. Eleven of them are displayed in Fig. 6.4. Note that the first two are the global bending modes and the rest are dominated by local vibration modes. The collection of the mode shapes forms the modal matrix Ψ each column of which corresponds to a single mode shape.
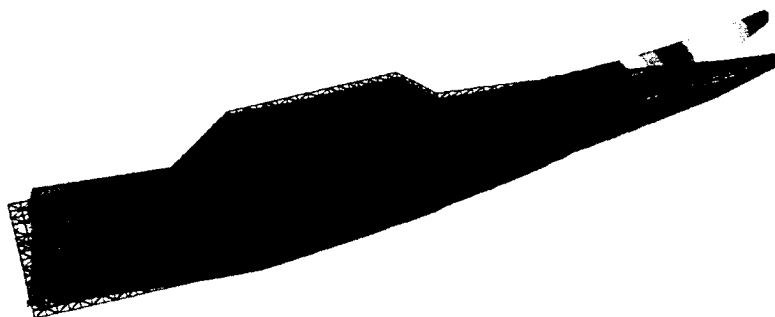
(a) 7th Mode at 23.05Hz
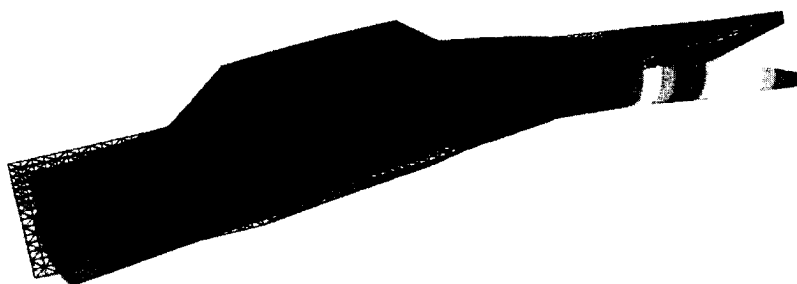
(b) 8th Mode at 23.79Hz
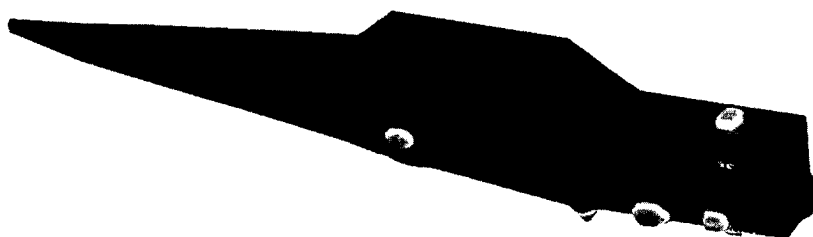
(c) 25th Mode at 44.92Hz
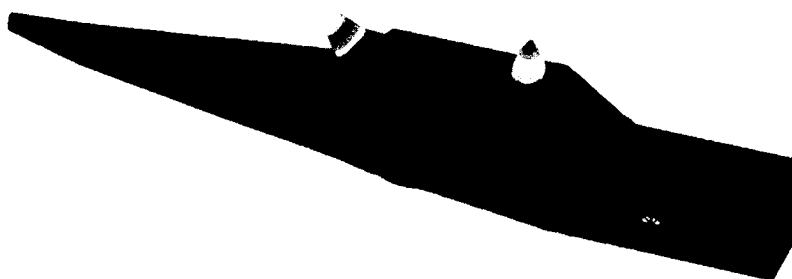
(d) 26th Mode at 45.11Hz
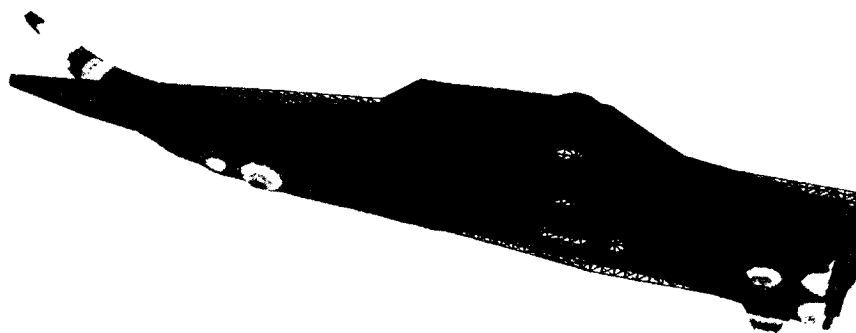
(e) 31th Mode at47.51Hz
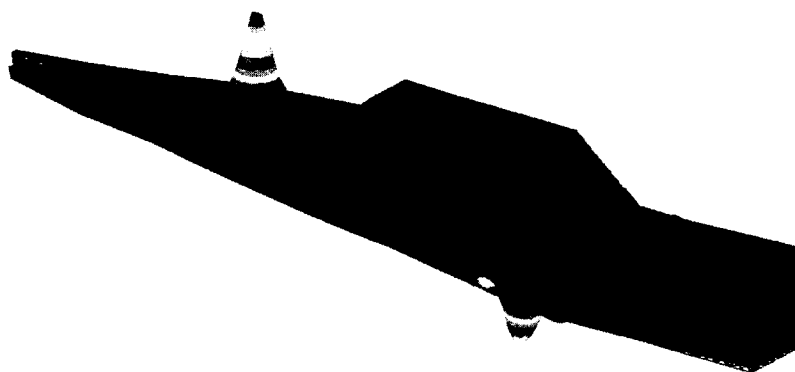
(f) 40th Mode at 54.39Hz
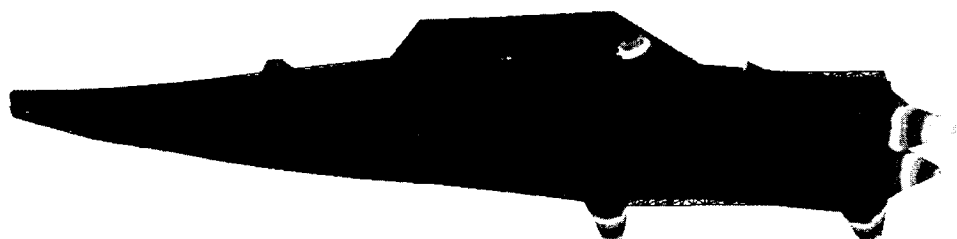
(g) 53th Mode at 59.15Hz

(h) 57th Mode at 61.43Hz

(i) 58th Mode at 62.41Hz
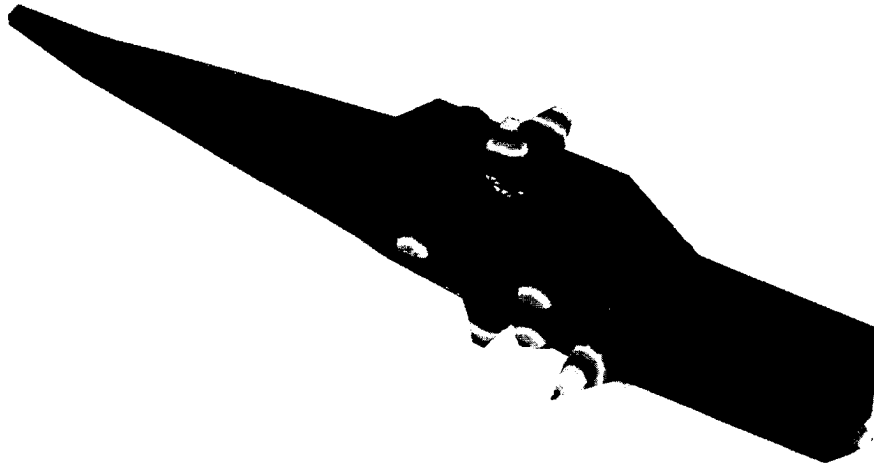
(j) 60th Mode at 62.90Hz

Figure 6.4 Mode Shapes and the Corresponding Frequencies

In the finite element method, the nodal elastic displacement can be expressed in terms of a linear combination of the mode shapes using the mode superposition method. The coefficients of each mode shape are called the modal coordinates, which implies the contribution of each mode shape to the final elastic displacement. The more mode shapes are used, the more accurate the nodal elastic displacement that will be obtained. However, accuracy is achieved at the cost of efficiency. Generally, the mode truncation method is used to extract the mode shapes because it is unreasonable to get all the mode shapes. The main idea of the mode truncation method is that the desired modes are those at the low frequencies because they can be the most dominant modes at which the structure will vibrate; the higher frequency modes have a negligible effect on the vibration.

6.2 Properties of a Triangular Element

The finite element craft model is made of iso-parametric constant strain triangular (CST) elements. Computing the mass moment of inertia and the surface pressure for a given triangular element is the concern of this section. All of these quantities are needed to form the equation of motion for the craft. In Section 6.2.1 the element coordinate system as well as the orientation of the element are set up. Once the orientation of the triangular element is known, the inertial integrals required for the mass matrix of a triangular element can then be computed. This process is introduced in Section 6.2.2. It is followed by Section 6.2.3 which presents a procedure to convert the pressure distribution on a given triangular element into nodal forces.

6.2.1 Orientation of a Triangular Element

A typical triangular element is shown in Fig. 6.5. The element is connected with node 1, 2 and 3 which are placed in the body-fixed coordinate system (x, y, z) with the coordinate (x_i, y_i, z_i), i=1, 2 and 3.
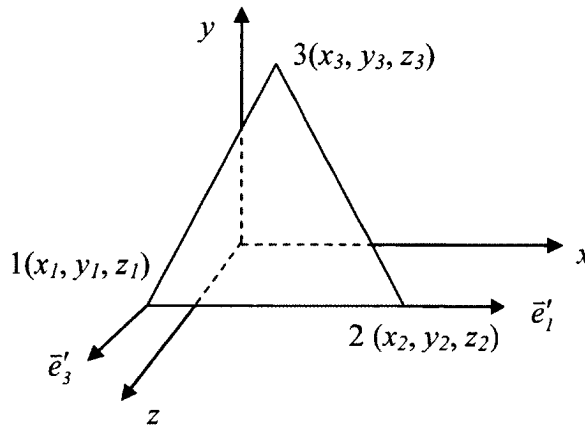
Figure 6.5 Element Coordinate

The element coordinate system, $x'-y'-z'$ [85], is defined such that x' follows the edge connecting node 1 to 2 and z' is normal to the face of the triangle. Set the position vector of a node be $\vec{r}_i$, i=1,2 and 3. The unit vector $\vec{e}_1'$ along the x' axis can be determined as:

$$\vec{e}_1^{'T} = \left(\vec{r}_2^T - \vec{r}_1^T\right)\!/\!\left\|\vec{r}_2 - \vec{r}_1\right\| \tag{6.1a}$$

In a vector, it can be expressed as

$$e_I'^T = \begin{pmatrix} e_{I,x}' & e_{I,y}' & e_{I,z}' \end{pmatrix} = \frac{(x_2 - x_I, \quad y_2 - y_I, \quad z_2 - z_I)}{\sqrt{(x_2 - x_I)^2 + (y_2 - y_I)^2 + (z_2 - z_I)^2}} \qquad (6.1b)$$

The z' axis is the direction of $\vec{e}_3'$, which is obtained as the vector product of $\vec{e}_1'$ and the

vector connecting node 1 to 3, i.e., $\vec{r}_3 - \vec{r}_1$. The detail is given in the following equation,

$$\vec{e}_3' = \vec{e}_I \times (\vec{r}_3 - \vec{r}_I)/\left\| \vec{e}_I \times (\vec{r}_3 - \vec{r}_I) \right\| \qquad (6.2a)$$

where the vector product $\vec{e}_1' \times (\vec{r}_3 - \vec{r}_1)$ can be put into a matrix form as

$$e_3' = \begin{Bmatrix} e_{3,x}' \\ e_{3,y}' \\ e_{3,z}' \end{Bmatrix} = \begin{bmatrix} 0 & -e_{I,z} & e_{I,y} \\ e_{I,z} & 0 & -e_{I,x} \\ -e_{I,y} & e_{I,x} & 0 \end{bmatrix} \begin{Bmatrix} x_3 - x_I \\ y_3 - y_I \\ z_3 - z_I \end{Bmatrix} \qquad (6.2b)$$

Finally, based upon the right hand rule, one can obtain the unit vector $\vec{e}_2'$ along the y' axis

as the cross-product of unit vectors $\vec{e}_3'$ and $\vec{e}_I'$

$$\vec{e}_2' = \vec{e}_3' \times \vec{e}' = \widetilde{e}_3' \vec{e}_I' \qquad (6.3a)$$

It can be put in a vector form as

$$e_2' = \begin{Bmatrix} e_{2,x}' \\ e_{2,y}' \\ e_{2,z}' \end{Bmatrix} = \begin{bmatrix} 0 & -e_{3,z}' & e_{3,y}' \\ e_{3,z}' & 0 & -e_{3,x}' \\ -e_{3,y}' & e_{3,x}' & 0 \end{bmatrix} \begin{Bmatrix} e_{I,x}' \\ e_{I,y}' \\ e_{I,z}' \end{Bmatrix} \qquad (6.3a)$$

Consequently, one has the transformation matrix A as

$$A = \begin{bmatrix} \vec{e}_I' & \vec{e}_2' & \vec{e}_3' \end{bmatrix} \qquad (6.4)$$

The transformation matrix helps to map the vector or the matrix derived based upon the

element coordinate system to the body fixed-coordinate system as

$$f_e = A f_e' \qquad (6.5a)$$

$$I_e = A I_e' A^T \qquad (6.5b)$$

where f_e' and I_e' are in the element coordinate system, while f_e and I_e are in the body-

fixed coordinate system of the craft. The summations of f_e and I_e over the total number

of the elements will give the total force vector f and the mass moment of inertia I of the

craft defined with respect to the body-fixed coordinate system of the craft.

6.2.2 Inertia Integrals for a Triangular Element

For the CST triangular element, the shape functions cannot only be used to approximate the elastic displacement but also the position vector, the pressure distribution and the stress distribution. The elastic deformation at any arbitrary point within the CST element in a 3D space can be defined as follows:

$$
e = \begin{pmatrix} u \\ v \\ w \end{pmatrix} = \begin{cases} \xi u_1 + \eta u_2 + \zeta u_3 \\ \xi v_1 + \eta v_2 + \zeta v_3 \\ \xi w_1 + \eta w_2 + \zeta w_3 \end{cases} = \begin{bmatrix} \xi & 0 & 0 & \eta & 0 & 0 & \zeta & 0 & 0 \\ 0 & \xi & 0 & 0 & \eta & 0 & 0 & \zeta & 0 \\ 0 & 0 & \xi & 0 & 0 & \eta & 0 & 0 & \zeta \end{bmatrix} \begin{bmatrix} u_1 \\ v_1 \\ w_1 \\ u_2 \\ v_2 \\ w_2 \\ u_3 \\ v_3 \\ w_3 \end{bmatrix} \equiv N q_e \quad (6.6)
$$

where (u_1, v_1, w_1), (u_2, v_2, w_2) and (u_3, v_3, w_3) are the elastic displacement components at the vertices of the triangle element of concern in 3D space.

$$
N = \begin{bmatrix} \xi & 0 & 0 & \eta & 0 & 0 & \zeta & 0 & 0 \\ 0 & \xi & 0 & 0 & \eta & 0 & 0 & \zeta & 0 \\ 0 & 0 & \xi & 0 & 0 & \eta & 0 & 0 & \zeta \end{bmatrix} \equiv \begin{bmatrix} \xi I_3 & \eta I_3 & \zeta I_3 \end{bmatrix}
$$ is the shape function matrix, in

which I_3 is a 3×3 identity matrix, ξ, η and ζ are area coordinates. The definitions of the area coordinates are given in Fig. 6.6. q_e is the nodal elastic displacement.

$$\xi = \frac{A_1}{A}$$

$$\eta = \frac{A_2}{A}$$

$$\zeta = \frac{A_3}{A}$$

$$\xi + \eta + \zeta = 1$$

A_1, A_2, A_3, A
Calculated using
Heron Formula
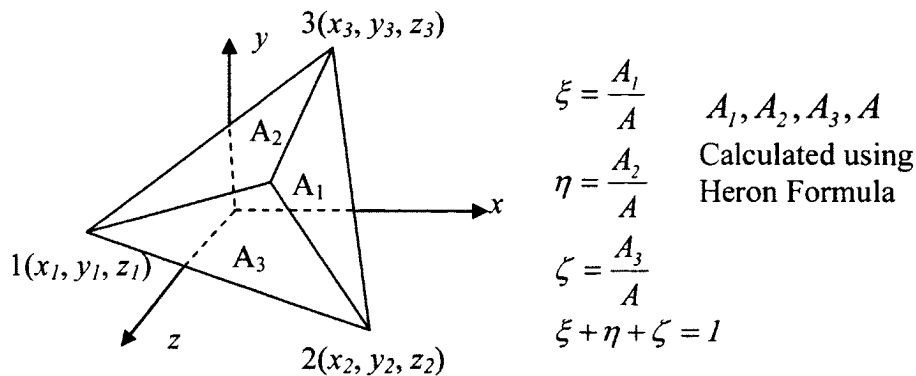
Figure 6.6 Area Coordinate

The area coordinates, ξ, η and ζ defined over a triangular element to provide a convenient means to compute area integrals which are often required for the flexible body dynamic analysis. The general formula for a function of area coordinates is given below

$$\int_{A_i} \xi^a \eta^b \zeta^c dA = \frac{a!b!c!}{(a+b+c+2)!} 2A \tag{6.7}$$

where A is the area of the triangular element in 3D space. It can be calculated using Heron's formula. In detail, one has

$$\int_{A_i} \xi dA = \int_{A_i} \eta dA = \int_{A_i} \zeta dA = \frac{A}{3} \tag{6.8a}$$

$$\int_{A_i} \xi\eta dA = \int_{A_i} \xi\zeta dA = \int_{A_i} \eta\zeta dA = \frac{A}{12} \tag{6.8b}$$

$$\int_{A_i} \xi^2 dA = \int_{A_i} \eta^2 dA = \int_{A_i} \zeta^2 dA = \frac{A}{6} \tag{6.8c}$$

Generally, the nodal elastic displacement q_e at the vertex is approximated in terms of the linear combinations of the mode shapes. It is defined as follows:

$$q_e = \sum_{k=1}^{Nm} \psi_{k,e} a_k \tag{6.9}$$

where N_m is the number of mode shapes selected for modal superposition. In this study, N_m is set to be 16. $\psi_{k,e}$ is the kth mode shape evaluated at the corresponding element. a_k is the amplitude of the mode shape, which is often called the modal coordinate.

The mode shape associated with the particular element has 9 components, three for each node of a triangular element, as

$$\psi_{k,e} = \begin{bmatrix} \psi_{k,e}^1 \\ \psi_{k,e}^2 \\ \vdots \\ \psi_{k,e}^9 \end{bmatrix}.$$

Consequently, the elastic displacement vector in each triangular element, described in Eq. 6.6, is approximated linearly in terms of the nodal displacements as

$$e = Nq_e = \sum_{k=1}^{Nm} (N\psi_{k,e}) a_k \tag{6.10}$$

It should be noted that there is some inconsistency in displacement interpolation between eigenvalue analysis and modal analysis. The interpolation functions used for eigenvalue analysis in this study are linear as defined above. However, the interpolation functions used for modal analysis are high order polynomials used for shell elements.

Here the integration of elastic displacement is taken as an example to show how to calculate the integrals as the constants in the equation of motion.

The definition of integral of elastic displacement is as follows:

$$I_e = \int_V \rho e \, dv \tag{6.11}$$

For any arbitrary element, according to Eq. 6.10, one has the elastic displacement

$$e^i = N q_e^i = N \psi_i a = \sum_{k=1}^{Nm} a_k \cdot N \psi_{k,e}.$$

In detail, one has

$$e^i = \sum_{k=1}^{Nm} a_k \cdot \begin{bmatrix} \xi I_3 & \eta I_3 & \zeta I_3 \end{bmatrix} \begin{bmatrix} \psi_{k,e}^1 \\ \psi_{k,e}^2 \\ \vdots \\ \psi_{k,e}^9 \end{bmatrix} = \sum_{k=1}^{Nm} a_k \cdot \begin{bmatrix} \xi \psi_{k,e}^1 + \eta \psi_{k,e}^4 + \zeta \psi_{k,e}^7 \\ \xi \psi_{k,e}^2 + \eta \psi_{k,e}^5 + \zeta \psi_{k,e}^8 \\ \xi \psi_{k,e}^3 + \eta \psi_{k,e}^6 + \zeta \psi_{k,e}^9 \end{bmatrix} \equiv \sum_{k=1}^{Nm} a_k \cdot \begin{bmatrix} \psi_u \\ \psi_v \\ \psi_w \end{bmatrix}.$$

With the help of results in Eq. 6.8, one has

$$\int_{\Omega_i} \rho e^i dv = \sum_{k=1}^{Nm} a_k \cdot \frac{\rho A_i t_i}{3} \begin{bmatrix} \psi_{k,e}^1 + \psi_{k,e}^4 + \psi_{k,e}^7 \\ \psi_{k,e}^2 + \psi_{k,e}^5 + \psi_{k,e}^8 \\ \psi_{k,e}^3 + \psi_{k,e}^6 + \psi_{k,e}^9 \end{bmatrix} \equiv \sum_{k=1}^{Nm} a_k \cdot I_{N\psi}^{ik} \tag{6.12}$$

where A_i is the area of the triangle element, t_i is the thickness of the triangle element along the local z direction of the element coordinate.

Summing up along the entire domain:

$$I_e = \int_V \rho e dv = \sum_{i=1}^{NE} \sum_{k=1}^{Nm} a_k \int_{\Omega_i} \rho N \psi_{k,e} dv = \sum_{k=1}^{Nm} a_k \sum_{i=1}^{NE} \int_{\Omega_i} \rho e^i dv = \sum_{k=1}^{Nm} a_k I_{N\psi} \tag{6.13}$$

where NE is the number of total elements, $k=1,2, \ldots, Nm$. $I_{N\psi}$ is a $3 \times Nm$ matrix, It should be noted that $I_{N\psi}$ is a constant matrix, so one can calculate it beforehand to reduce the computational expense.

The integrations of the rest of the terms in the mass moment of inertia for the triangular element are documented in detail in Appendix 3.

6.2.3 Pressure Load to Equivalent Nodal Force

The surface pressure obtained in Chapter 5 is reported as a vector of point pressures, each of which is applied at a node of the finite element craft model. This point pressures are now converted into point loads including their magnitudes and directions. It is assumed that the pressure is linearly distributed over and normal to the surface of the triangular element. Thus, the pressure distribution over a typical element can be expressed in terms of area coordinates as

$$p = \left(\xi p_1 + \eta p_2 + \zeta p_3 \right) \tag{6.14}$$

where p_1, p_2 and p_3 are the nodal pressures applied at the vertices of triangular element. The magnitude of the total force applied to the element can be conveniently obtained through area integration as

$$f_e = \int_{\Omega_e} \left(\xi p_1 + \eta p_2 + \zeta p_3 \right) dA = \frac{A_e}{3} \left(p_1 + p_2 + p_3 \right) \tag{6.15}$$

where A_e is the area of the element. The specific nodal forces, on the other hand, are derived in such a way that the work done by these nodal forces is the same as that of the distributed pressure over the element of concern. Let the magnitudes of the nodal forces at the vertices be assigned as f_1', f_2' and f_3' and the corresponding displacements that are normal to the element surface be w_1', w_2' and w_3' These displacements point at the direction of $\bar{e}_3'$ of the element coordinate system. The vertical displacement distribution over the element is again assumed to be linear. Therefore:

$$w' = \xi w_1' + \eta w_2' + \zeta w_3' \tag{6.16}$$

The equivalence between the work done by the pressure and that by the nodal force yields the following equation

$$\int_{\Omega_e} pw'dA = \int_{\Omega_e} \left(\xi p_1 + \eta p_2 + \zeta p_3 \right)\left(\xi w_1' + \eta w_2' + \zeta w_3' \right)dA$$

$$= \frac{A_e}{12}\left(2p_1 + p_2 + p_3 \right)w_1' + \frac{A_e}{12}\left(p_1 + 2p_2 + p_3 \right)w_2' + \frac{A_e}{12}\left(p_1 + p_2 + 2p_3 \right)w_3' \tag{6.17}$$

$$= f_1'w_1' + f_2'w_2' + f_3'w_3'$$

It can be calculated from Eq. 6.17 that magnitude of the equivalent nodal forces is

$$f_1' = \frac{A_e}{12}\left(2p_1 + p_2 + p_3 \right) \tag{6.18a}$$

$$f_2' = \frac{A_e}{12}\left(p_1 + 2p_2 + p_3\right) \tag{6.18b}$$

$$f_3' = \frac{A_e}{12}\left(p_1 + p_2 + 2p_3\right) \tag{6.18c}$$

As for the direction of the nodal forces, they are opposite to the $\vec{e}_3'$, which is normal to the surface of the triangular element. Therefore, the nodal force vector can be derived as

$$\vec{f}_i' = -f_i'\vec{e}_3' \tag{6.19a}$$

for $i=1$, 2 and 3. The corresponding vector form is given by

$$f_i' = \begin{Bmatrix} f_{i,x}' \\ f_{i,y}' \\ f_{i,z}' \end{Bmatrix} = -f_i' \begin{Bmatrix} e_{3,x}' \\ e_{3,y}' \\ e_{3,z}' \end{Bmatrix} \tag{6.19b}$$

These nodal forces can be transformed into the body-fixed coordinate system, with the aid of Eq. 6.5a, and summed up node-by-node to obtain the total force and moment applied at any point on the craft. The results of such an effort are summarized and presented in Figs. 6.7-6.9 in terms of the body-fixed coordinate system, x, y, z axis. These figures reveal that the pressure induced force along the z direction and the moment with respect to the y axis are the dominant resultant force and moment.

The force along the z axis of the local coordinate system and the sum of the total node pressures are shown in Fig. 6.10. It can be observed that both the force and the pressure profiles share the same trend.
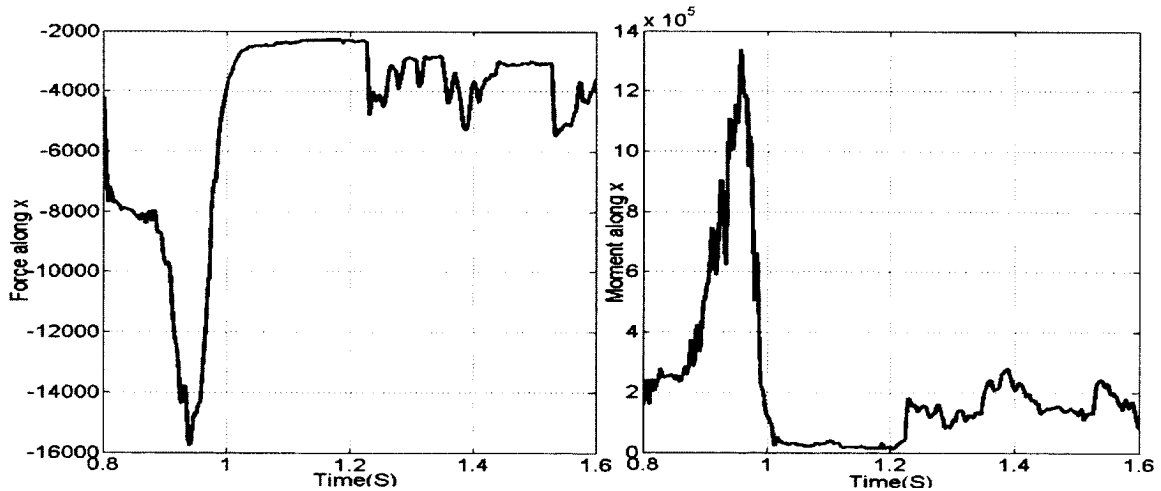
Figure 6.7 Force and Moment along the x axis of Body-fixed Coordinate
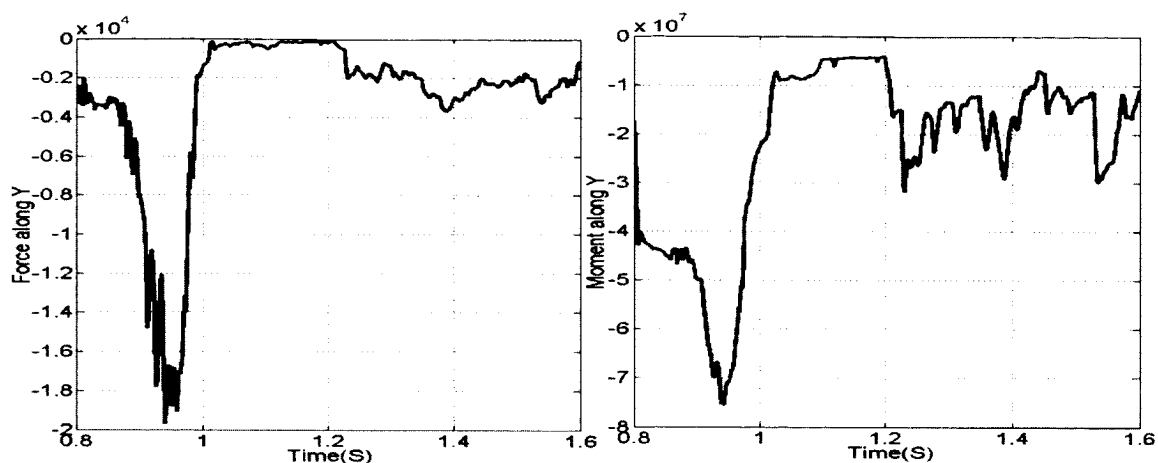
Figure 6.8 Force and Moment along the y axis of Body-fixed Coordinate
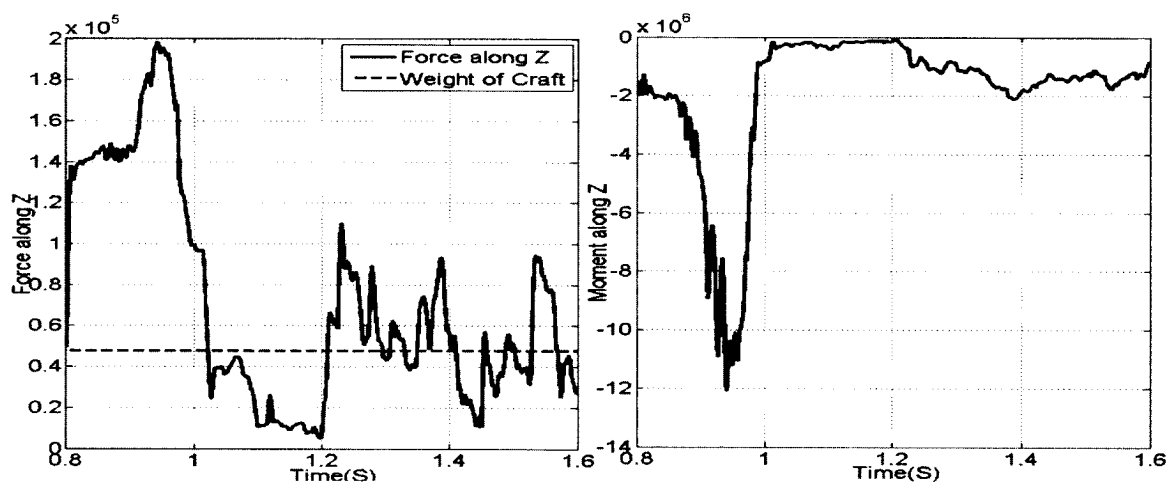
Figure 6.9 Force and Moment along z axis of Body-fixed Coordinate
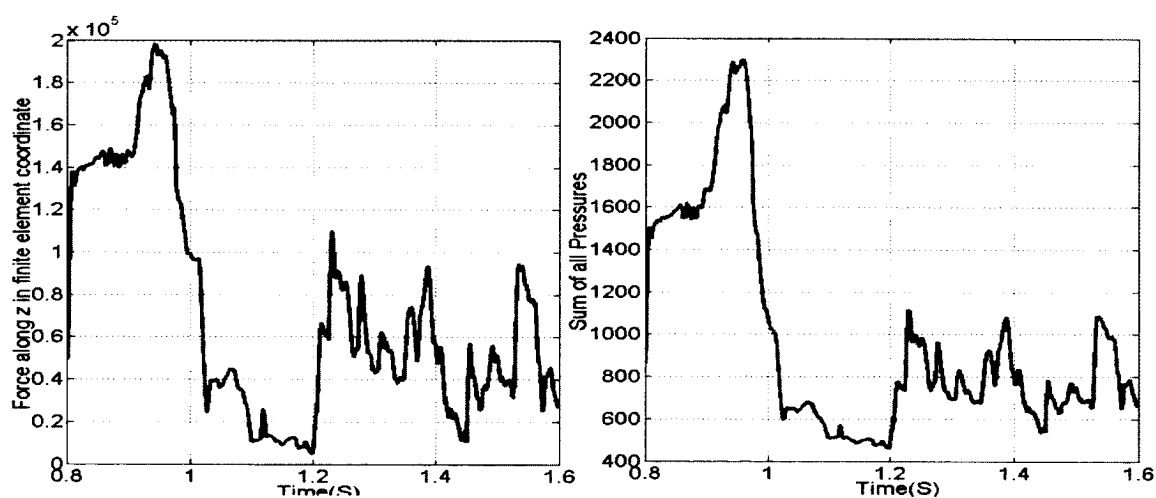
Figure 6.10 Force along the z axis and Pressure in Body-fixed Coordinate

The force contours along x, y, and z axis at $t=0.94$s are shown in Figs. 6.11~13. It can also be observed that the force along z axis is dominant, and the maximum force is located at the stern zone.
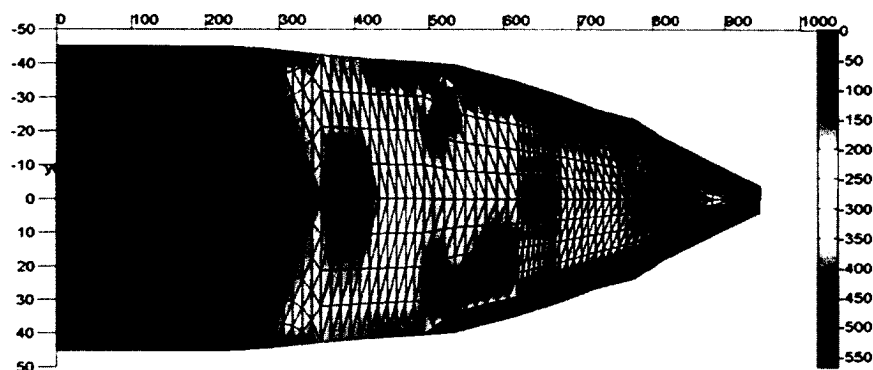
Figure 6.11 Force Contour along the x axis at $t=0.94$s
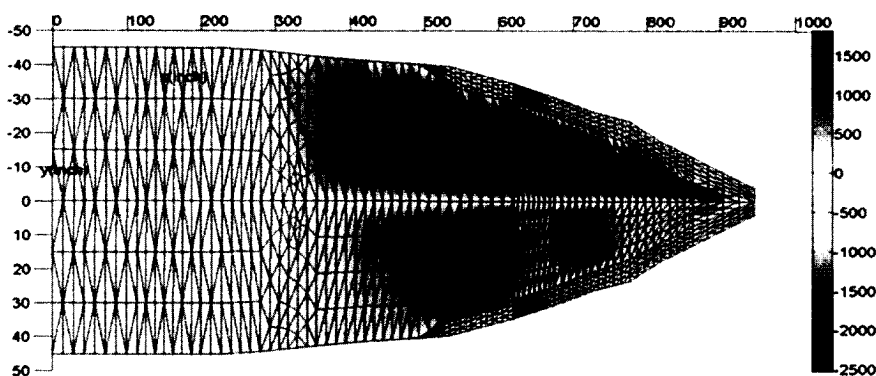
Figure 6.12 Force Contour along the y axis at $t=0.94$s
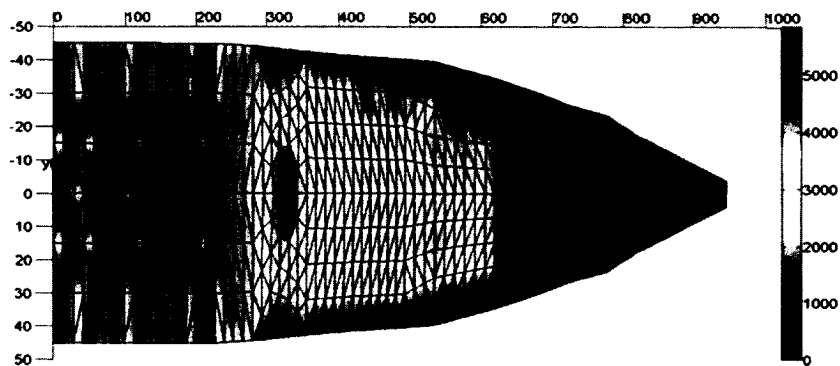
Figure 6.13 Force Contour along the z axis at $t=0.94$s

6.3 Numerical Solution for a 3D Flexible Multi-body System

The derivation of the governing equation of motion for a single flexible system expressed in terms of the modal coordinates has been presented in detail in Chapter 2. It is in the form of a second order ODE as follows:

$$M\ddot{q} = f \tag{6.20}$$

where the unknowns are $\ddot{q}^T = \begin{pmatrix} \ddot{R} & \dot{\omega}' & \ddot{a} \end{pmatrix}$ and the mass moment of inertia and the force vector are given as

$$M = \begin{bmatrix} M_{RR} & M_{R\theta}(a,A) & M_{Ra}(A) \\ M_{\theta R}(a,A) & M_{\theta\theta}(a) & M_{\theta a}(a,A) \\ M_{aR}(A) & M_{a\theta}(a) & M_{aa} \end{bmatrix}$$

$$= \begin{bmatrix} mI_3 & -A(I_{\tilde{r}} + I_{\tilde{e}}) & AI_{N\Psi} \\ -A(I_{\tilde{r}} + I_{\tilde{e}}) & -(I_{\tilde{r}\tilde{r}} + I_{\tilde{r}\tilde{e}} + I_{\tilde{e}\tilde{r}} + I_{\tilde{e}\tilde{e}}) & I_{\tilde{r}N\Psi} + I_{\tilde{e}N\Psi} \\ AI_{N\Psi} & I_{\tilde{r}N\Psi} + I_{\tilde{e}N\Psi} & I_{\Psi^T N^T N\Psi} \end{bmatrix}, \quad \ddot{q} = \begin{Bmatrix} \ddot{R} \\ \dot{\omega}' \\ \ddot{a} \end{Bmatrix} \text{ and }$$

$$f = \begin{Bmatrix} g_R(a,\dot{a},\omega',A) \\ g_\theta(a,\dot{a},\omega',A) \\ g_a(a,\dot{a},\omega',A) \end{Bmatrix}$$

$$= \begin{Bmatrix} Vf_b - A\tilde{\omega}'\tilde{\omega}'(I_{\tilde{r}} + I_{\tilde{e}}) - 2A\tilde{\omega}'I_{\tilde{e}} + F \\ (I_{\tilde{r}} + I_{\tilde{e}})A^T f_b / \rho + \tilde{\omega}'(I_{\tilde{r}\tilde{r}} + I_{\tilde{r}\tilde{e}} + I_{\tilde{e}\tilde{r}} + I_{\tilde{e}\tilde{e}})\omega' + 2(I_{\tilde{e}\tilde{r}} + I_{\tilde{e}\tilde{e}})^T \omega' + T' \\ -\Psi^T K\Psi a + (AI_N \Psi)^T f_b / \rho + (I_{\tilde{r}\tilde{\omega}'N}\Psi + I_{\tilde{e}\tilde{\omega}'N}\Psi)^T \omega' - 2\Psi^T I_{\tilde{e}N}^T \omega' + \Psi^T W' \end{Bmatrix}$$

The rigid body equation is a special case of the above, where $\ddot{q}^T = \begin{pmatrix} \ddot{R} & \dot{\omega}' \end{pmatrix}$, M and f are simplified as $M = \begin{bmatrix} m & -AI_{\tilde{r}} \\ -AI_{\tilde{r}} & -I_{\tilde{r}\tilde{r}} \end{bmatrix}$ and

$$f = \begin{Bmatrix} Vf_b - A\tilde{\omega}'\tilde{\omega}'I_{\tilde{r}} + F \\ I_{\tilde{r}}A^T f_b / \rho + \tilde{\omega}'I_{\tilde{r}\tilde{r}}\omega' + T' \end{Bmatrix} = \begin{Bmatrix} Vf_b - A\tilde{\omega}'\tilde{\omega}'I_{\tilde{r}} + AF' \\ I_{\tilde{r}}A^T f_b / \rho + \tilde{\omega}'I_{\tilde{r}\tilde{r}}\omega' + T' \end{Bmatrix}$$

where F', T' are the time histories of the force and moment induced by the surface pressure in term of the body-fixed coordinate system. The detailed derivations of F' and T' can be found in Section 6.2.3.

One of the difficulties in solving Eq. 6.20 is to update the transformation matrix A, which is a function of the angular displacements. The set of the angular displacements is not a vector and cannot be obtained by directly integrating the angular velocities. Two alternatives are proposed here to overcome such a difficulty: the matrix exponential

method and the Euler parameter method. Both methods are free of singularity in forming A from angular displacements and vice versa. The transformation matrix can be expressed as a matrix exponential of the rotation axis, Ψ as

$$A = \exp\left(\widetilde{\Psi}\right) \tag{6.21}$$

Set the unit vector of Ψ as u. The rotation angle, χ, is then the magnitude of Ψ. Thus, one has

$$\Psi = \chi u$$

where $u = \Psi / \|\Psi\|$. Notice that the time derivative of Eq. 6.21 yields

$$\dot{A} = A\widetilde{\dot{\Psi}}$$

It provides a simple relation to compute the angular velocity

$$\omega' = \dot{\Psi}$$

The transformation matrix can also expressed in terms of the four Euler parameters, $p = \begin{pmatrix} e_0 & e_1 & e_2 & e_3 \end{pmatrix}^T$ as

$$A = E(p)G^T(p) \tag{6.22}$$

where $E = \begin{bmatrix} -e, & -e_0 + \tilde{e} \end{bmatrix}$ and $G = \begin{bmatrix} -e, & -e_0 - \tilde{e} \end{bmatrix}$ in which $e_0 = \cos \chi / 2$ and

$e^T = \begin{pmatrix} e_1 & e_2 & e_3 \end{pmatrix} = u \sin \chi / 2$.

The four parameters in p are not independent and have to satisfy the following conditions,

$$p^T p = 1 \tag{6.23}$$

and their time derivatives

$$p^T \dot{p} = 0 \tag{6.24}$$

The angular velocity in terms of the body-fixed coordinate system is given as:

$$\omega' = 2G\dot{p} \tag{6.25}$$

Either Eq. 6.21 or Eq. 6.22 can be used to solve the dynamic equations, Eq. 6.20. It should be noted that use of the Euler parameters, Eq. 6.22, for dynamic analysis will create new constraints on p and $\dot{p}$, but use of exponential matrix will not. These two numerical approaches will be discussed separately in the following two sub-sections for solving dynamic equations of a body undergoing large rotation.

6.3.1 Matrix Exponential-based Newmark Method

Newmark's method was developed by Nathan M. Newmark [95] in 1959. It is an explicit, unconditional stable method widely used to solve the ODEs in structure dynamics. The Newmark method [40, 96] approximated the velocity and displacement as

$$\dot{u}_n = \dot{u}_{n-1} + (1 - \gamma)\Delta t \ddot{u}_{n-1} + \gamma\Delta t \ddot{u}_n \tag{6.26}$$

$$u_n = u_{n-1} + \Delta t \dot{u}_{n-1} + (1/2 - \beta)\Delta t^2 \ddot{u}_{n-1} + \beta\Delta t^2 \ddot{u}_{n-1} \tag{6.27}$$

where Δt is the time step, γ and β are free parameters. The latter two are limited by $0 \le \gamma, \beta \le 1$. However, they are typically set as $\gamma = 1/2$ and $\beta = 1/4$ to achieve the averaged constant acceleration formulation. It also leads to maximum accuracy and unconditional stability. Hence, Eqs. 6.26 and 6.27 become:

$$\dot{u}_n = \dot{u}_{n-1} + 1/2\,\Delta t(\ddot{u}_{n-1} + \ddot{u}_n) \tag{6.28}$$

$$u_n = u_{n-1} + \Delta t \dot{u}_{n-1} + 1/4\,\Delta t^2(\ddot{u}_{n-1} + \ddot{u}_{n-1}) \tag{6.29}$$

The Newmark method can be conveniently used to solve Eq. 6.20, particularly in the case when the exponential matrix is used to define the transformation matrix and the angular velocity. The update of the transformation matrix in a time-marching scheme is done explicitly as:

$$\Delta\Psi = \Delta t\omega'_{n-1} + 1/2\,\Delta t^2 \dot{\omega}'_{n-1} \tag{6.30}$$

$$A_n = A_{n-1}\exp(\Delta\widetilde{\Psi}) \tag{6.31}$$

while the updates of the angular velocity and the velocity are done implicitly as:

$$\omega'_n = \omega'_{n-1} + 1/2\,\Delta t(\dot{\omega}'_{n-1} + \dot{\omega}'_n) \tag{6.32}$$

$$V_n = V_{n-1} + 1/2\,\Delta t(\ddot{R}_{n-1} + \ddot{R}_n) \tag{6.33}$$

The modal coordinate and the translational displacement can be expressed as:

$$a_n = a_{n-1} + \Delta t\dot{a}_{n-1} + 1/2(\Delta t)^2(\ddot{a}_{n-1} + \ddot{a}_n) \tag{6.34}$$

$$R_n = R_{n-1} + \Delta t\dot{R}_{n-1} + 1/2(\Delta t)^2(\ddot{R}_{n-1} + \ddot{R}_n) \tag{6.35}$$

The above relations can be substituted into Eqs. 6.20 to form a set of nonlinear equations in terms of the unknowns $\dot{\omega}'_n$, $\ddot{a}_n$ and $\ddot{R}_n$. Once solved, Eqs. 6.31~6.35 can be used to update A_n, ω'_n, V_n a_n and R_n.

6.3.2 Euler Parameters-based Method

The angular acceleration and the angular velocity are vectors, though the angular displacement is not. Therefore, the angular velocity can be obtained by directly integrating the angular acceleration, while the angular displacement cannot be obtained by integrating the angular velocity. The latter is the difficulty of dynamic analysis of a body undergoing large rotation.

In this study, a new relation between the time derivative of the Euler parameters, $\dot{p}$ and the angular velocity is derived. The velocity constraint $p^T \dot{p} = 0$ is satisfied automatically in this new relation without introducing additional constraint as far as the concern of rotation. Thus, the procedure to solve the equation of motion follows.

The relation between the angular velocity and the Euler parameters is given by [87]

$$\dot{p} = 1/2\, G^T \omega' \tag{6.36}$$

Its solution, $\dot{p}$, has to satisfy the condition, $p^T \dot{p} = 0$. The proof is as follows:

Substituting Eq. 6.36 in the velocity constraint term,

$$p^T \dot{p} = p^T\, 1/2\, G^T \omega' = 1/2\, p^T G^T \omega' \tag{6.37}$$

Based upon the definition p and G, one has:

$$p^T G^T = \begin{pmatrix} e_0 & e_1 & e_2 & e_3 \end{pmatrix} \begin{bmatrix} -e_1 & -e_2 & -e_3 \\ e_0 & -e_3 & e_2 \\ e_3 & e_0 & -e_1 \\ -e_2 & e_1 & e_0 \end{bmatrix} = \begin{pmatrix} 0 & 0 & 0 \end{pmatrix} \tag{6.38}$$

Substituting Eq. 6.38 into Eq. 6.37:

$$p^T \dot{p} = 0.$$

The equation of motion of concern, Eq. 6.20, is a second order ODE. It can be reformulated as a set of first order ODEs by introducing $\dot{q}$ as unknown. That is, setting $\dot{v} = \ddot{q}$ or more specifically $\dot{v}^T = \begin{pmatrix} \dot{v}_R & \dot{v}_\omega & \dot{v}_a \end{pmatrix} = \begin{pmatrix} \ddot{R} & \dot{\omega}' & \ddot{a} \end{pmatrix}$ or $\dot{R} = v_R$, $\dot{a} = v_a$ and

$v_\omega = \omega'$. The values of v_R and v_a can be integrated to obtain the relative displacement fields, R and a. However, the value of v_ω can't be directly integrated to obtain the angular displacement, as the angular displacement is not a vector. Instead, the relation $v_\omega = \omega'$ is replaced by Eq. 6.36 to solve for p and then the transformation matrix $A(p)$.

The result of this process is a set of the first order ODE's in terms of v, or more precisely $\dot{R}$, $\dot{a}$ and ω', and R, a and p. Thus, Eq.6.20 becomes a set of first order ODE's,

$$\begin{Bmatrix} \dot{v} \\ \dot{R} \\ \dot{p} \\ \dot{a} \end{Bmatrix} = \begin{Bmatrix} M^{-1}f \\ v_R \\ 1/2\,G^T\omega' - p\left(p^T G^T \omega'\right)/\left(2p^T p\right) \\ v_a \end{Bmatrix} \qquad (6.39)$$

The above equation can be solved by employing the first order ODE solver, such as *ode23s* in Matlab. However, in the function call, the solution p needs to be updated in order to satisfy the condition $p^T p = 1$. This can be done through an iteration process set up to improve the value of p by minimizing the error deviated from the condition $p^T p = 1$,

$$\begin{array}{c} \min \\ \Delta p \end{array} \qquad \Delta p^T \Delta p \qquad (6.40)$$
$$subject\ to: \quad p^T p + 2p^T \Delta p - 1 = 0$$

The necessary condition of the above minimization problem yields

$$\Delta p = -\lambda p \qquad (6.41)$$

where the Lagrange multiplier λ can be determined by the constraint as

$$0 = p^T p + 2p^T \Delta p - 1 = p^T p - 2\lambda p^T p - 1 \qquad (6.42)$$

Solving the above equation, one has

$$\lambda = \left(p^T p - 1\right)/\left(2p^T p\right) \qquad (6.43)$$

Substituting Eq. 6. 43 into Eq. 6.41, one has:

$$\Delta p = -\left(p^T p - 1\right)/\left(2p^T p\right)\cdot p \qquad (6.44)$$

In other words, the value of p obtained after integration has to be adjusted by Eq. 6.54, until the error, $\left| p^T p - 1 \right|$ is small. The p update algorithm can then be set up as:

1. Start the correction procedure with p_0 which is the result of Eq.6.39.

2. At iteration i, the change in p, Δp, is given by Eq. 6.44.

3. The updated solution is given by $p_{i+1} = p_i + \Delta p_i$.

4. The process is continued until $\left(p_{i+1}^T p_{i+1} - 1\right) \le \varepsilon$.

6.4 Results of Rigid Body Dynamic Analysis of the Craft

The rigid analysis results of the numerical methods discussed in Section 6.3 will be summarized in this section. These methods include the matrix exponential based Newmark's method and Euler parameters based method. Newmark's method is taken as a benchmark to verify the proposed Euler parameters based method. For each method, the location of the origin of the body-fixed coordinate is set to be coincided with the origin of the global coordinate system. It is located at the center of the tail end. Two time intervals, $\Delta t = 5 \times 10^{-5}$, and $\Delta t = 2.5 \times 10^{-3}$ are selected to request the result report for each method in rigid dynamic analysis. Therefore, there are total four different numerical results. These four numerical results are compared with each other on the basis of computational accuracy and efficiency.

The boat rests upright initially. The starting and the ending time of the simulation are set to be 0.8 and 1.6 seconds, respectively, based upon the test data. The sample frequency of the test data is 20,000Hz, i.e., the test data is recorded at every 5×10^{-5} second. The external forces and moment applied on the craft has been shown in Section 6.2.2. The boat moves forward along x direction with 30 knots (607.61 inch/s) speed. Therefore, $\dot{R} = \{607.61 \quad 0 \quad 0\}^T$. The angular velocity is initially set to be zero, i.e., $\omega' = 0$. The initial value of Euler parameters is $p = \{1 \quad 0 \quad 0 \quad 0\}^T$.

The translational position, velocity and their acceleration of the origin of local coordinate obtained from four different cases are shown in Figs. 6.14~6.16.
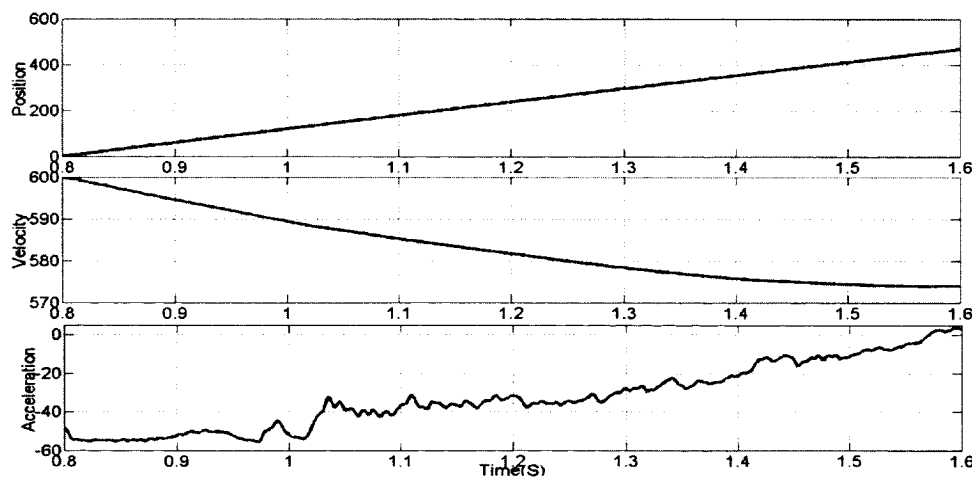
Figure 6.14 Position, Velocity and Acceleration of the Origin along the x axis
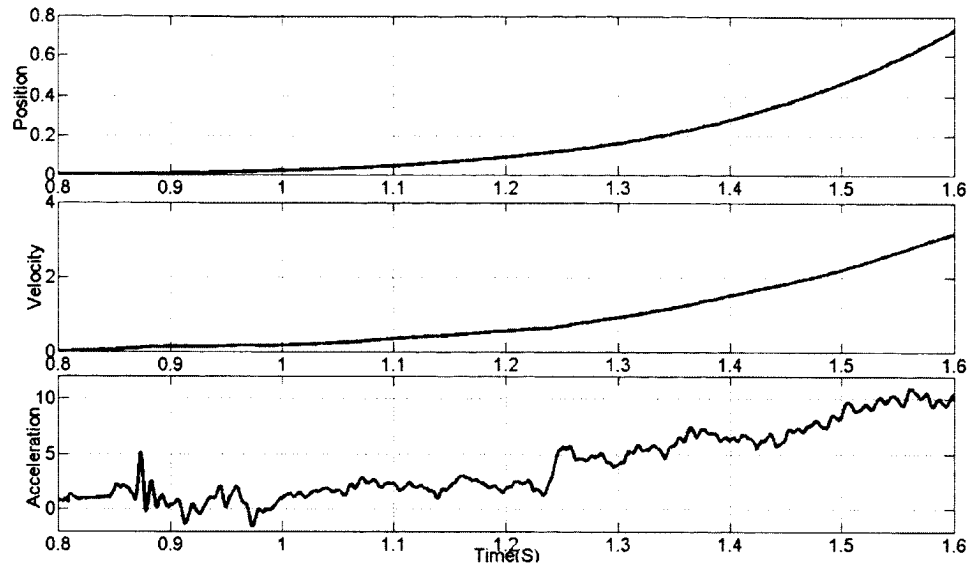
Figure 6.15 Position, Velocity and Acceleration of the Origin along the y axis
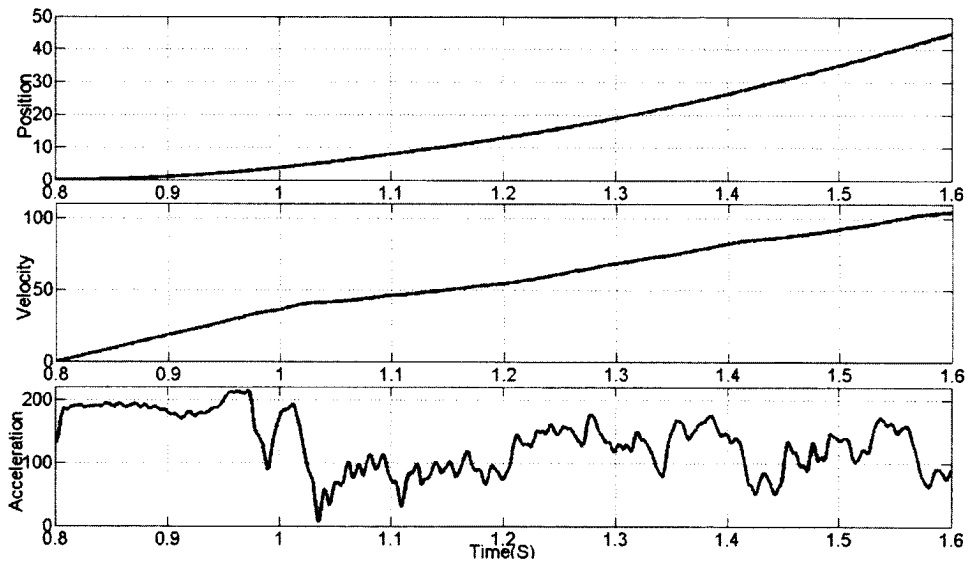
—— Euler Method: $\Delta t = 5 \times 10^{-5}$　　 − − Euler Method: $\Delta t = 2.5 \times 10^{-3}$

······ Newmark Method: $\Delta t = 5 \times 10^{-5}$ − · − Newmark Method: $\Delta t = 2.5 \times 10^{-3}$

Figure 6.16 Position, Velocity and Acceleration of the Origin along the z axis

It can be observed from Figs. 6.14~16 that the position along x direction is almost linear because the initial velocity is very big and the opposite acceleration increased to zero gradually. The displacement along y is very small because the small acceleration along y direction. The position along z increased quarterly.

The angular velocity and angular acceleration of the origin of local coordinate obtained from four different cases are shown in Figs. 6.17~6.19.

—— Euler Method: $\Delta t = 5 \times 10^{-5}$ - - Euler Method: $\Delta t = 2.5 \times 10^{-3}$

······ Newmark Method: $\Delta t = 5 \times 10^{-5}$ - · - Newmark Method: $\Delta t = 2.5 \times 10^{-3}$
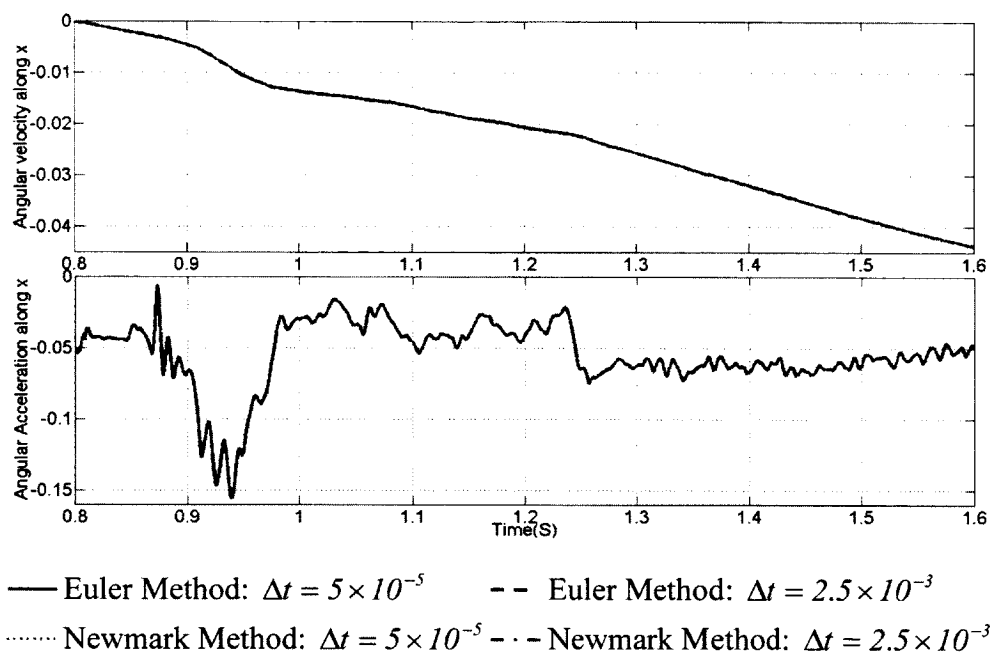
Figure 6.17 Angular Velocity and Acceleration of the Origin along x

—— Euler Method: $\Delta t = 5 \times 10^{-5}$ - - Euler Method: $\Delta t = 2.5 \times 10^{-3}$

······ Newmark Method: $\Delta t = 5 \times 10^{-5}$ - · - Newmark Method: $\Delta t = 2.5 \times 10^{-3}$
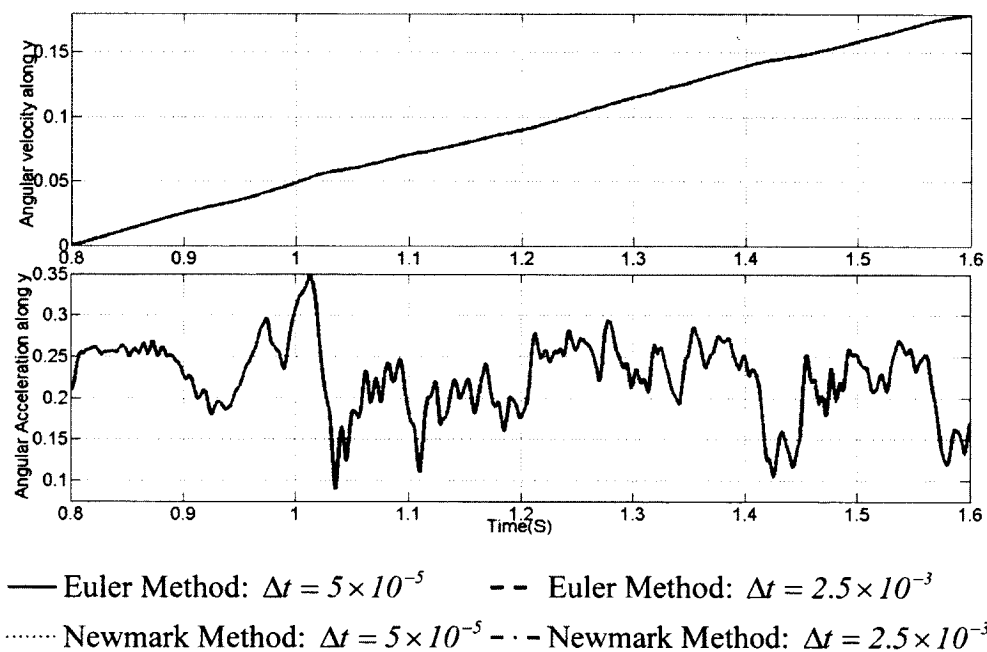
Figure 6.18 Angular Velocity and Acceleration of the Origin along y

—— Euler Method: $\Delta t = 5 \times 10^{-5}$ — — Euler Method: $\Delta t = 2.5 \times 10^{-3}$

········ Newmark Method: $\Delta t = 5 \times 10^{-5}$ - · - Newmark Method: $\Delta t = 2.5 \times 10^{-3}$
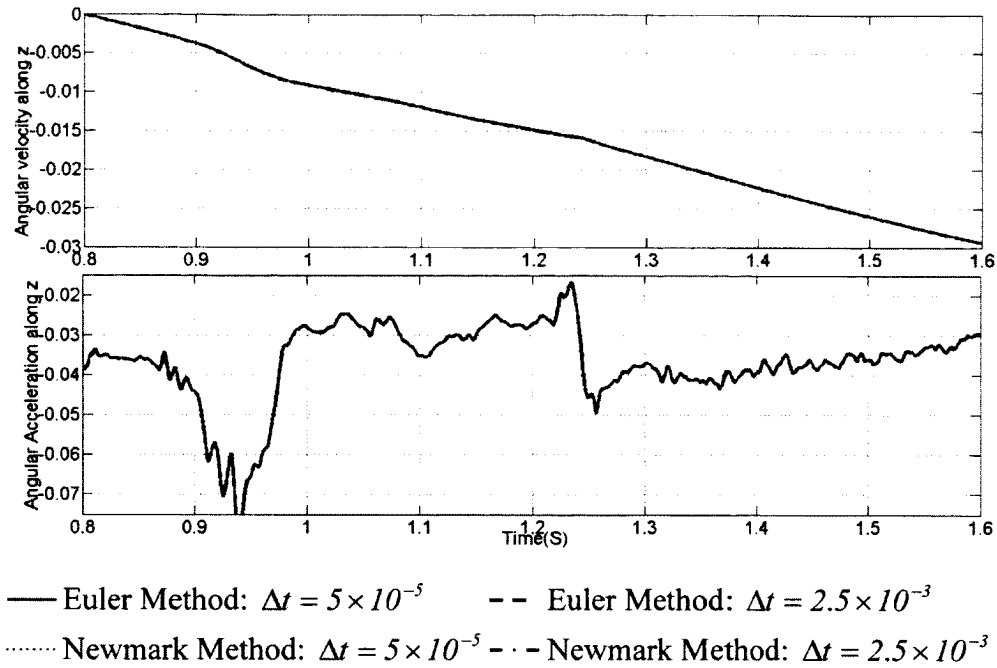
Figure 6.19 Angular Velocity and Acceleration of the Origin along z

It can be observed from Figs. 6.17~6.19 that the rotation motion of the craft is very small compared to the translate motion. The roll along the x axis is negative, which means the parts in positive y go down, while the parts in negative y go up. The pitch along the y axis is positive, which means the parts before the center of gravity go up and the parts after center of gravity go down. This can also be seen from the positive z of origin of the local coordinate. The yaw along the z axis is negative, which means that the craft moves obliquely to the right. This can also be seen from the positive y position of origin in Fig. 6.15. From the quantities of roll, pitch and yaw, it can be seen that the pitch is the dominant rotational motion.

From the above three figures, it can be seen that the amplitude of the angular acceleration along the y axis is the largest. In order to check the differences of these four cases clearly, the zoomed figures for the angular acceleration along y axis is shown in Fig. 6.20. It can be found that these four cases are identical with each other from the zoomed figure.

— Euler Method: $\Delta t = 5 \times 10^{-5}$ – – Euler Method: $\Delta t = 2.5 \times 10^{-3}$

······· Newmark Method: $\Delta t = 5 \times 10^{-5}$ – · – Newmark Method: $\Delta t = 2.5 \times 10^{-3}$
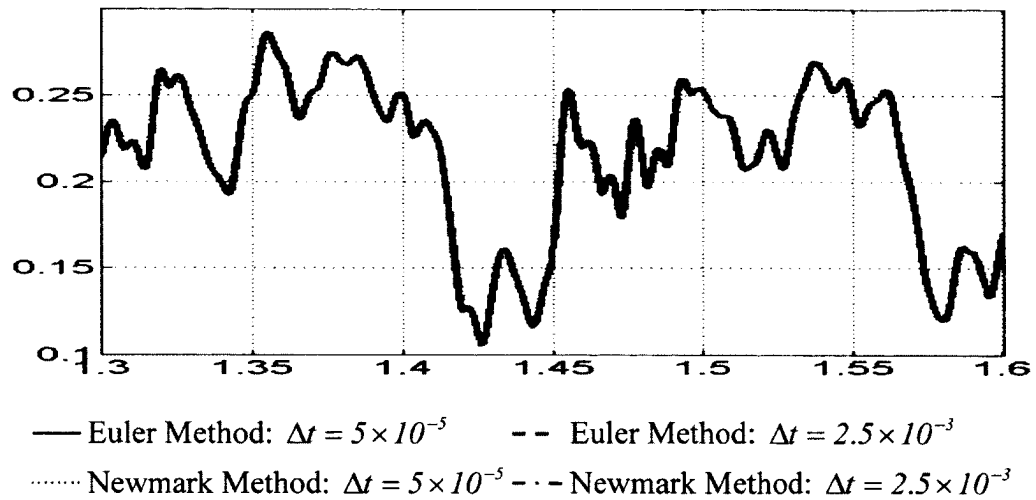
Figure 6.20 Zoomed Angular Acceleration of the Origin along y

The time history position of the maximum vertical force node (85.6, 0, 0) is also shown in Fig. 6.21. The time history position of the node where the maximum force along z is located resembles the motion of the origin of the local coordinate system because these two nodes are both in the same side of the center of gravity. The difference is the magnitude of displacement along x, y and z, which is caused by the effect of the rotational motion.

— Euler Method: $\Delta t = 5 \times 10^{-5}$ – – Euler Method: $\Delta t = 2.5 \times 10^{-3}$

······· Newmark Method: $\Delta t = 5 \times 10^{-5}$ – · – Newmark Method: $\Delta t = 2.5 \times 10^{-3}$
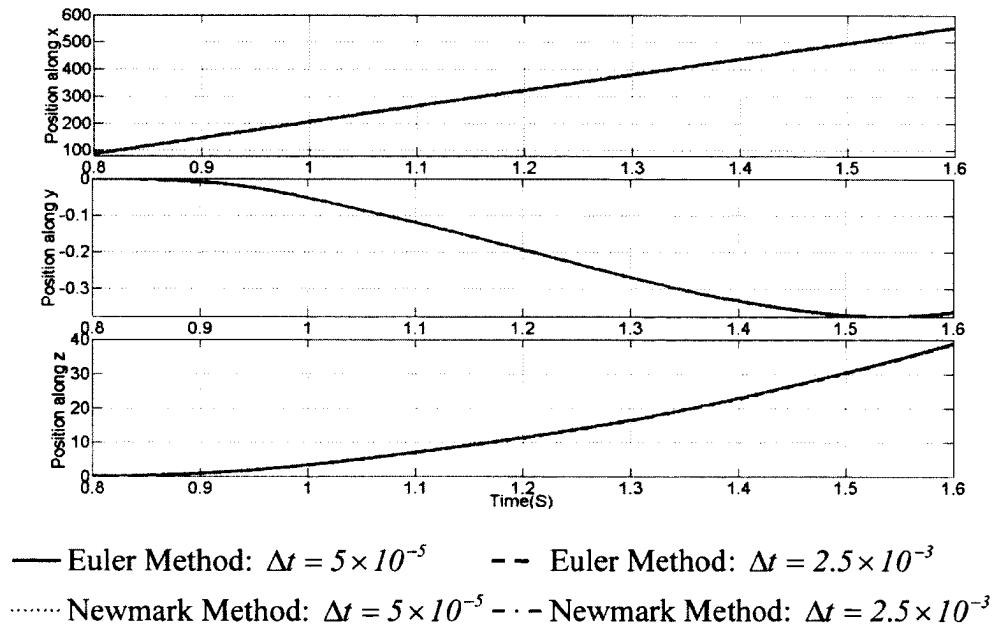
Figure 6.21 Position of the Maximum Force Point

From the translational and rotational results at the origin of the local coordinate system and the maximum force point, it can be seen that the Euler parameter based method and the Newmark method have identical results no matter what the time interval is. This proves that both the Euler parameter based method and the Newmark method are correct.

Although the motion of the craft can be identified from the analysis of the time history of the position of the origin, it can be observed directly and clearly from the animate motion of the craft. The snap shots of configurations of the rigid craft at four different time instants during motion are generated and shown in Fig. 6.22. The same conclusion can be drawn regarding the motion of the craft as in the results analysis in Figs. 6.14~6.19. From (a) to (b), the craft moves forward and obliquely to the right. From (b) to (c), the front part at the bow zone goes down, while the rear end in the stern zone goes up. From (c) to (d), the front part of craft still goes down.

(a) time=0.81505s (b) time=1.1285s (c) time=1.2564s (d) time=1.1285s
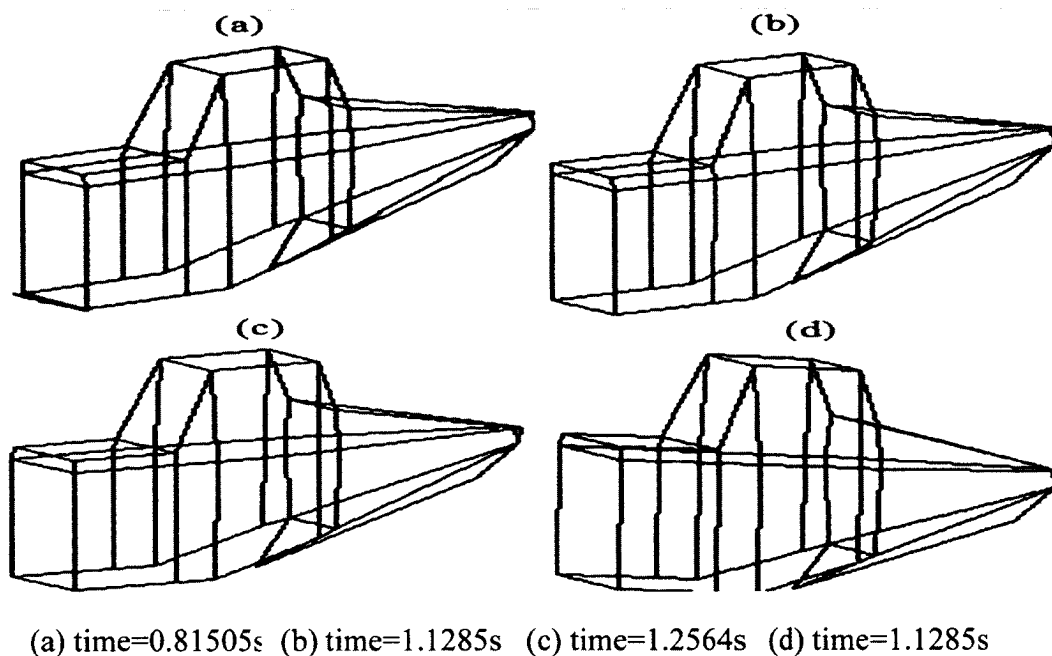
Figure 6.22 Configurations of the Rigid Craft at Different Time

6.5 Results of Flexible Dynamic Analysis of the Craft

The first order equation of motion (Eq. 6.39) for the flexible craft obtained by introducing the Euler parameters can be repeated:

$$
\dot{q} = \left\{ \begin{array}{c} \dot{V} \\ \dot{\omega}' \\ \dot{v} \\ \dot{R} \\ \dot{a} \\ \dot{p} \end{array} \right\} = \left\{ \begin{array}{c} \overline{M}^{-1}\bar{f} \\ \\ V \\ v \\ \frac{1}{2}G^{T}\omega' \end{array} \right\}
$$

where V and R are the velocity and displacement of translation motion of origin of body-fixed coordinate described in the global coordinate, ω' is the angular velocity described in the body-fixed coordinate, a and v are the modal coordinate and its velocity term, $p = \{e_0 \quad e_1 \quad e_2 \quad e_3\}^T \equiv \{e_0 \quad e\}^T$ is Euler parameters, and $G = [-e \quad e_0 - \tilde{e}]$.

$$
\overline{M} = \begin{bmatrix} m\mathbf{I}_3 & -A(I_{\tilde{r}} + I_{\tilde{e}}) & AI_{N\Psi} \\ & -(I_{\tilde{r}\tilde{r}} + I_{\tilde{r}\tilde{e}} + I_{\tilde{e}\tilde{r}} + I_{\tilde{e}\tilde{e}}) & I_{\tilde{r}N\Psi} + I_{\tilde{e}N\Psi} \\ sym. & & I_{\Psi^T N^T N\Psi} \end{bmatrix}.
$$

$$
\bar{f} = \left\{ \begin{array}{c} Vf_b - A\tilde{\omega}'\tilde{\omega}'(I_{r'} + I_e) - 2A\tilde{\omega}'I_{\tilde{e}} + \mathbf{F} \\ (I_{\tilde{r}} + I_{\tilde{e}})A^T f_b / \rho + \tilde{\omega}'(I_{\tilde{r}\tilde{r}} + I_{\tilde{r}\tilde{e}} + I_{\tilde{e}\tilde{r}} + I_{\tilde{e}\tilde{e}})\omega' + 2(I_{\tilde{e}\tilde{r}} + I_{\tilde{e}\tilde{e}})^T \omega' + T' \\ -\Psi^T K\Psi a + (AI_N \Psi)^T f_b / \rho + (I_{\tilde{r}\tilde{\omega}'N}\Psi + I_{\tilde{e}\tilde{\omega}'N}\Psi)^T \omega' - 2\Psi^T I_{\tilde{e}N}^T \omega' + \Psi^T W' \end{array} \right\}.
$$

Compared to the rigid craft, the mass matrix and generalized force term are no more constants regarding the flexible craft. The coefficients in the equation of motion are time-dependent variables due to the elastic deformation. Using the method introduced in subsection 6.2.2, these time-variants need to be calculated only once beforehand.

In the flexible dynamics analysis, four cases are studied. In the first two cases, the problem is solved using the matrix exponential based Newmark method. The time interval for the first case is $\Delta t = 5 \times 10^{-5}$, while $\Delta t = 2.5 \times 10^{-3}$ for the second case. In the last two cases, the Euler parameters based method is used. The time interval for the third and fourth cases are $\Delta t = 5 \times 10^{-5}$ and $\Delta t = 2.5 \times 10^{-3}$, respectively. The initial value of the modal coordinate a and its first order derivation $\dot{a}$ are both zeros, and other initial values are the same as in the rigid craft analysis.

6.5 .1 Results Comparison between Different Methods

The rigid results are set as a benchmark for the flexible dynamic analysis. The results for position and acceleration of the translation motion, angular velocity and acceleration of rotation motion at the origin of local coordinate are identical between the rigid and flexible cases. Here, only the comparison results of the position of the maximum force node between rigid body and flexible body are shown.

The position of maximum force node for the matrix exponential based Newmark Method at two different time intervals is shown in Fig. 6.23.

— Rigid: Newmark Method, $\Delta t = 5 \times 10^{-5}$

········ Flex: Newmark Method: $\Delta t = 2.5 \times 10^{-3}$

– · – Flex: Newmark Method, $\Delta t = 5 \times 10^{-5}$
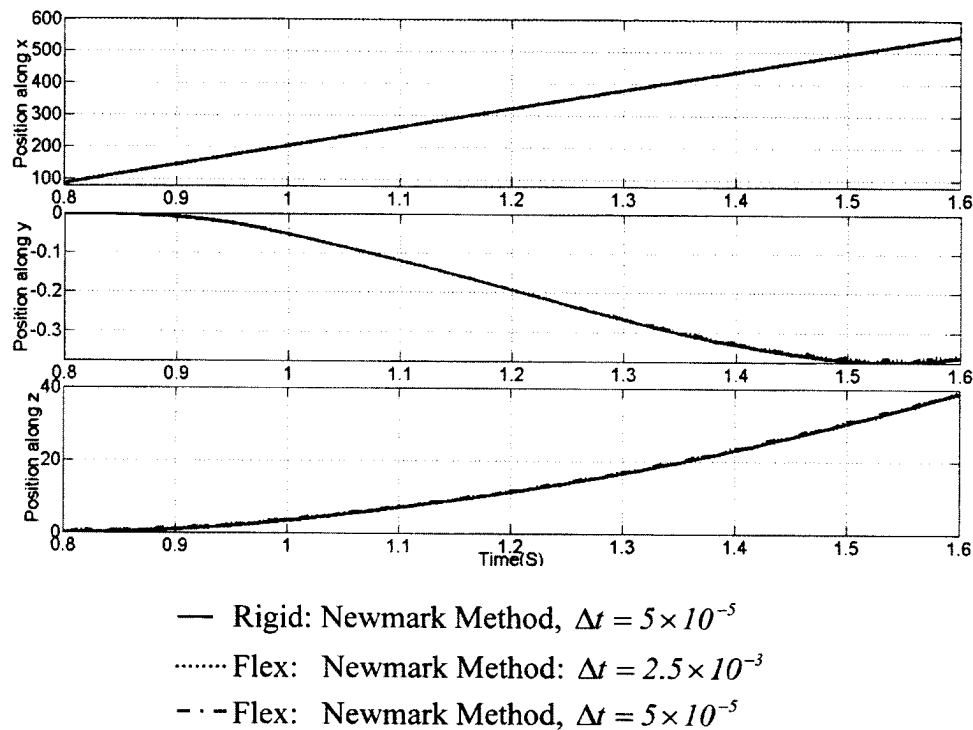
Figure 6.23 Position of the Maximum Force Point for Newmark Method

The differences cannot be found in the whole time domain. However, the differences can be observed in the zoomed figures along y and z. They are shown in Figs. 6.24 and 6.25. It implies that the results of the matrix exponential based upon Newmark Method are dependent on the time step size.
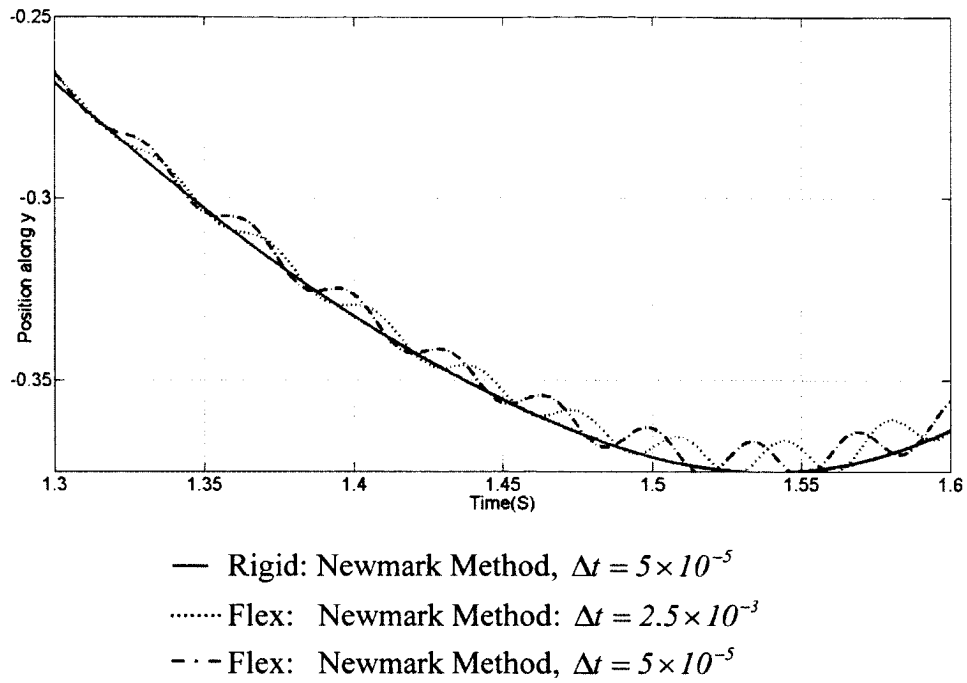
Figure 6.24 Zoomed Position of the Maximum Force Point along y for Newmark Method
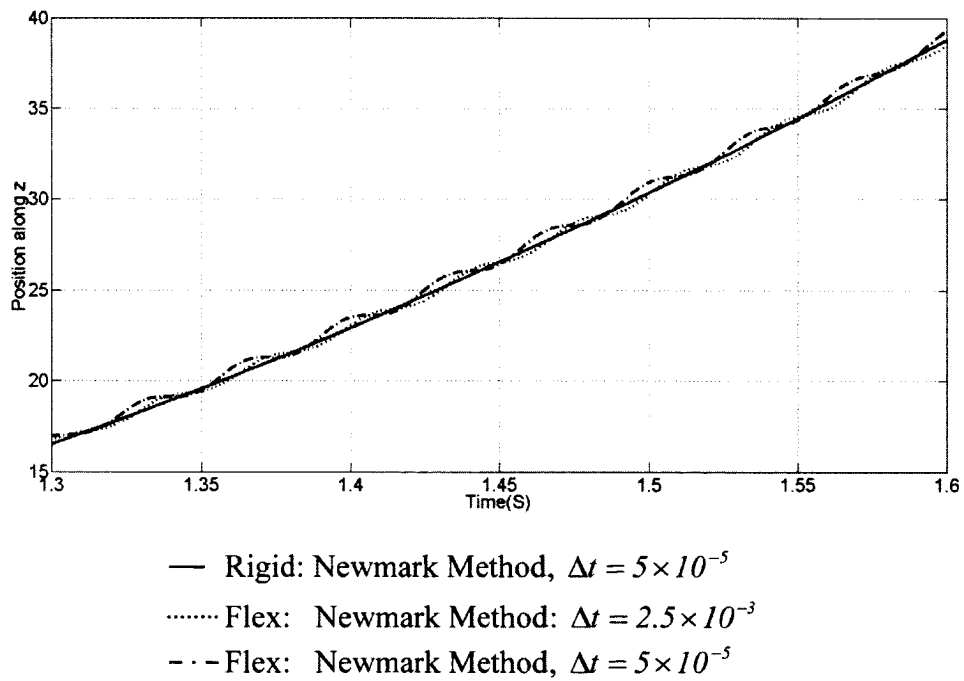
Figure 6.25 Zoomed Position of the Maximum Force Point along z for Newmark Method

The flexible results for the Euler parameters based method with different time intervals are identical. It can be seen from Figs. 6.26 and 6.27 for the zoomed position figures along y and z. The identical results show that the Euler parameter based method is not sensitive to the time step size.
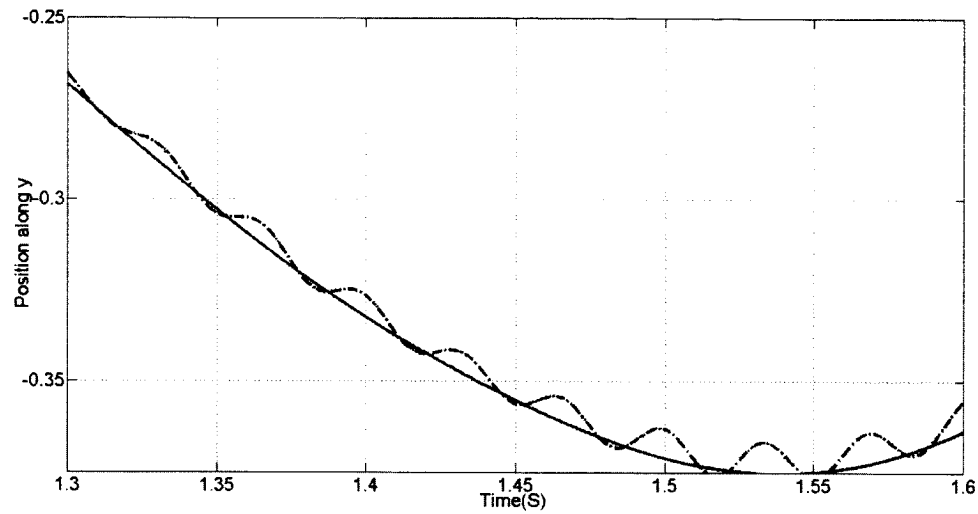
Figure 6.26 Zoomed Position of the Maximum Force Point along y for Euler Method
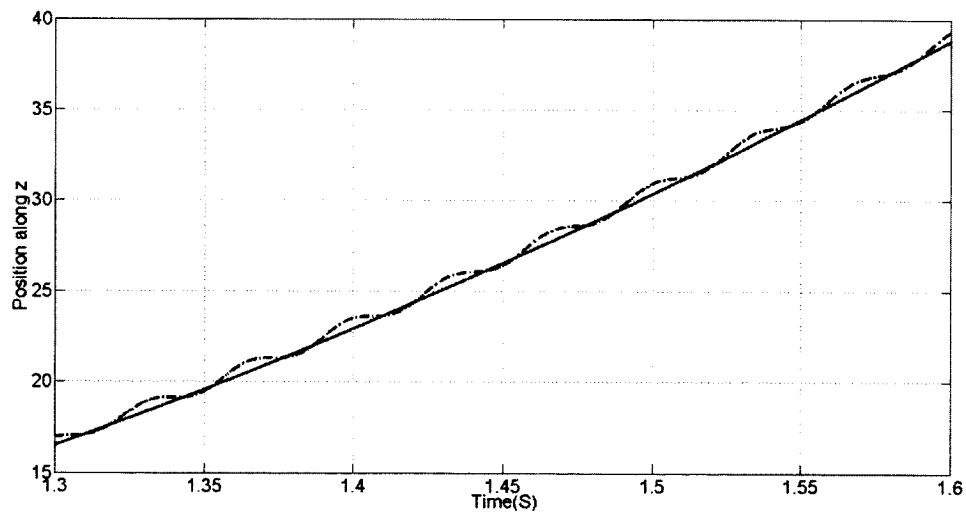
— Rigid: Euler Method, $\Delta t = 5 \times 10^{-5}$

········ Flex: Euler Method: $\Delta t = 2.5 \times 10^{-3}$

– · – Flex: Euler Method, $\Delta t = 5 \times 10^{-5}$

Figure 6.27 Zoomed Position of the Maximum Force Point along z for Euler Method

The flexible results for the Euler parameters based method with time intervals

$\Delta t = 2.5 \times 10^{-3}$ are compared with the matrix exponential based Newmark method with

time intervals $\Delta t = 5 \times 10^{-5}$. The compared results at the origin and maximum force node

are shown in Figs. 6.28 ~6.34.
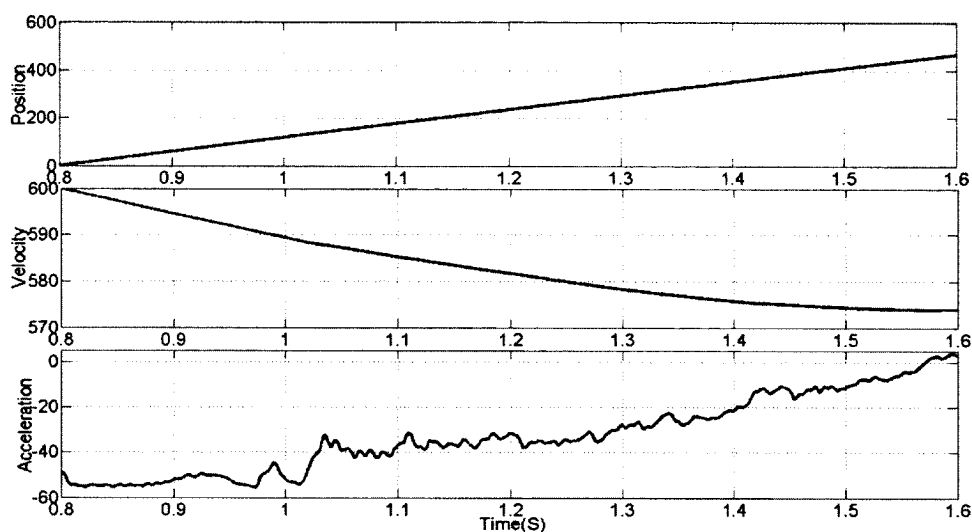
Figure 6.28 Position, Velocity and Acceleration Comparisons of the Origin along the x
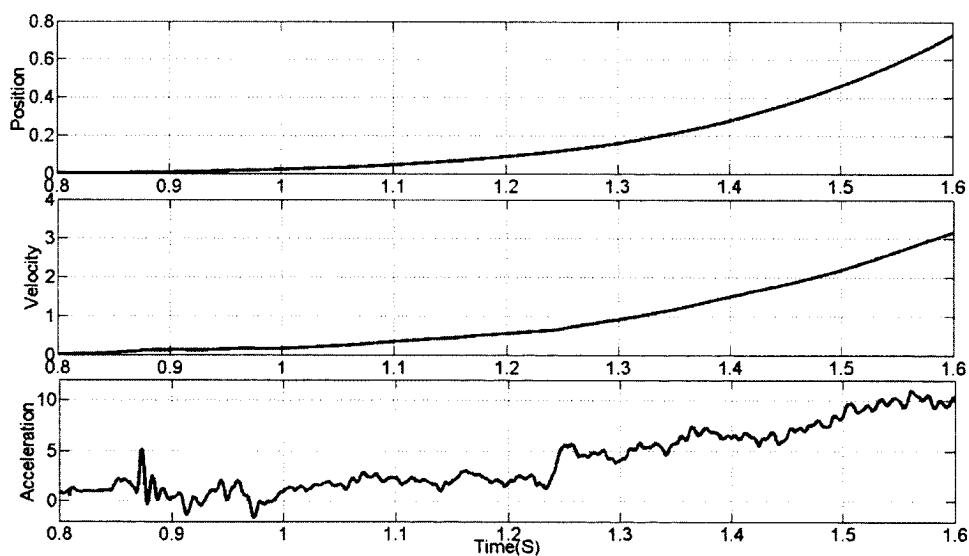
Figure 6.29 Position, Velocity and Acceleration Comparisons of the Origin along the y
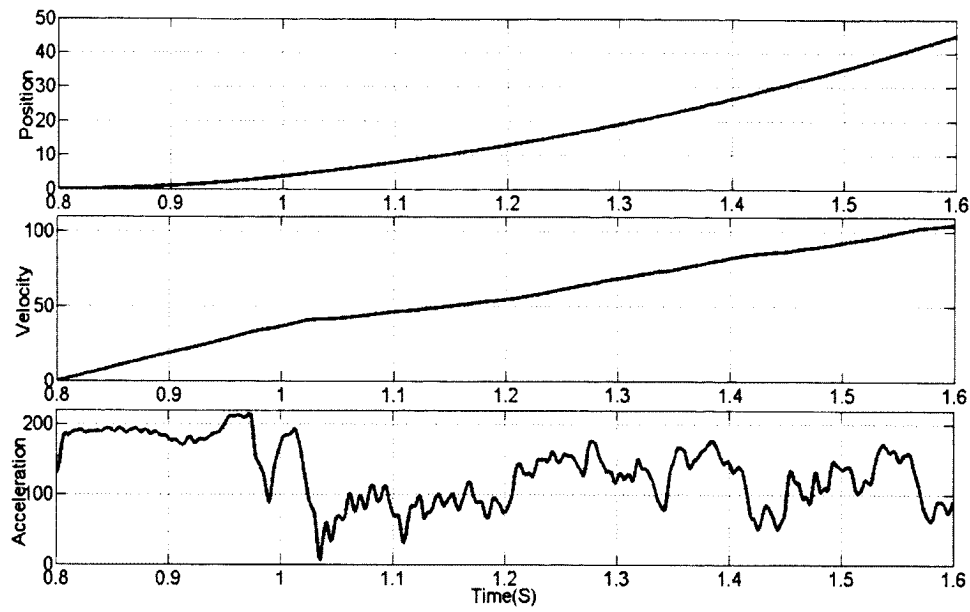
Figure 6.30 Position, Velocity and Acceleration Comparisons of the Origin along the z
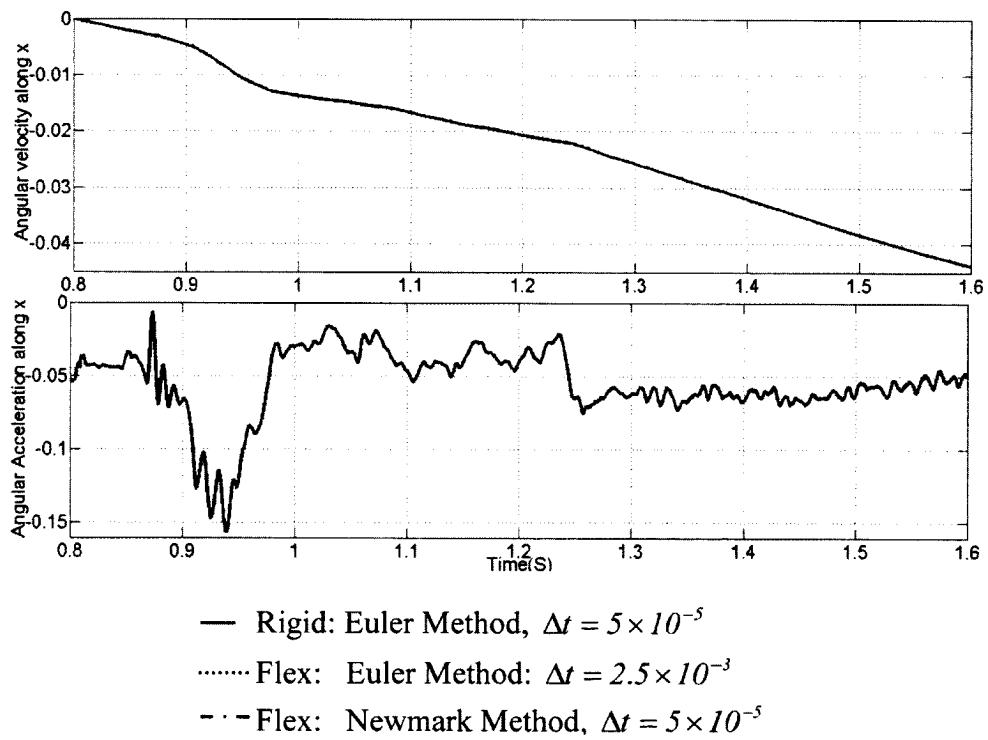
Figure 6.31 Angular Velocity and Acceleration Comparisons of the Origin along x

— Rigid: Euler Method, $\Delta t = 5 \times 10^{-5}$

········ Flex: Euler Method: $\Delta t = 2.5 \times 10^{-3}$

– · – Flex: Newmark Method, $\Delta t = 5 \times 10^{-5}$
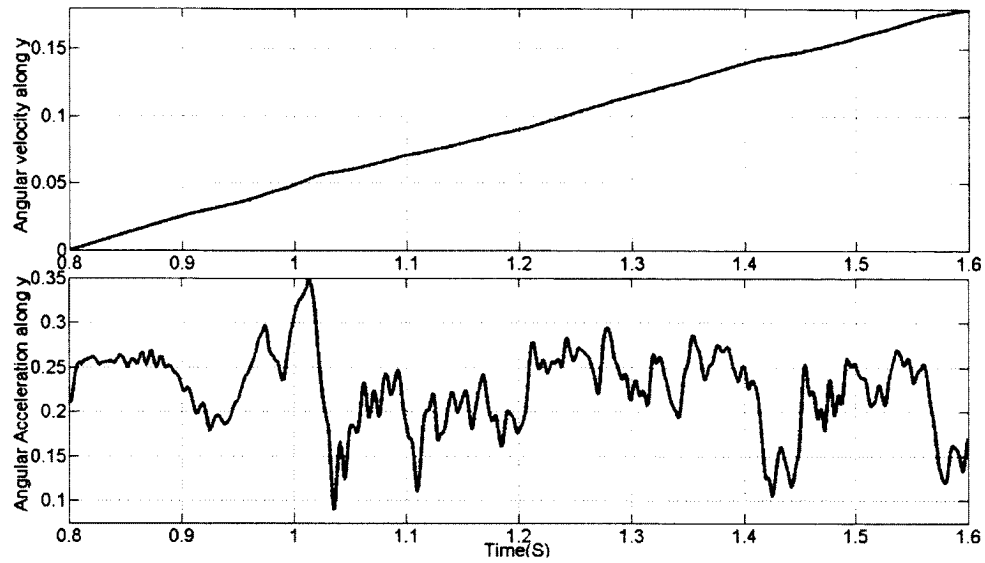
Figure 6.32 Angular Velocity and Acceleration Comparisons of the Origin along y
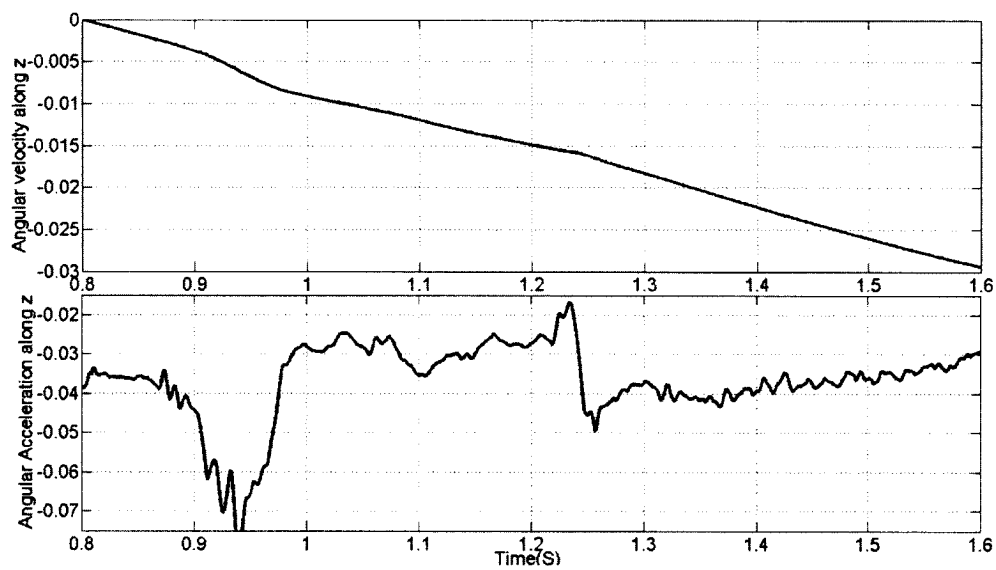
— Rigid: Euler Method, $\Delta t = 5 \times 10^{-5}$

······· Flex: Euler Method: $\Delta t = 2.5 \times 10^{-3}$

– · – Flex: Newmark Method, $\Delta t = 5 \times 10^{-5}$

Figure 6.33 Angular Velocity and Acceleration Comparisons of the Origin along z
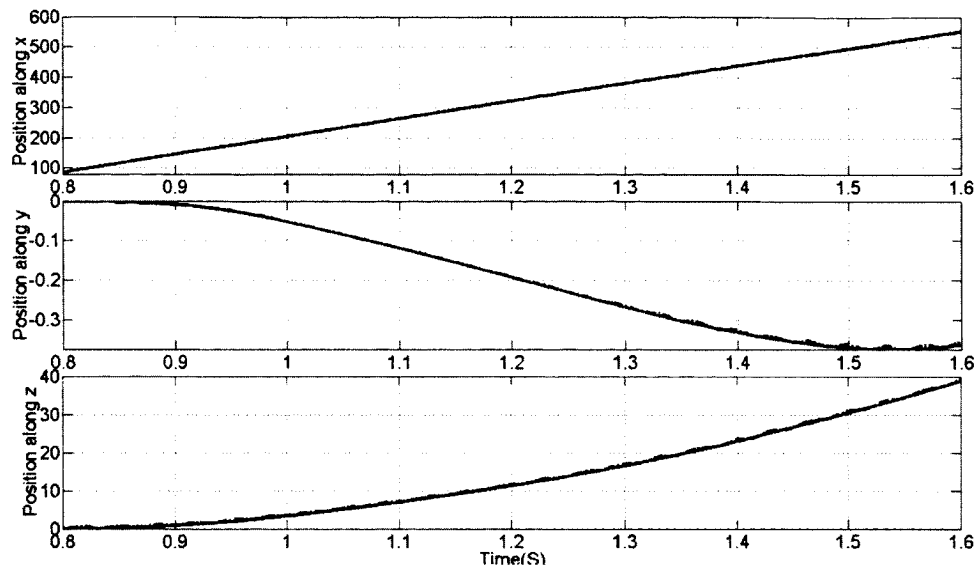
Figure 6.34 Position of the Maximum Force Point for Euler Method

The zoomed position figures along y and z are shown in Figs. 6.35 and 6.36. The identical results between the Euler parameter based method with large time step and the matrix exponential based Newmark method with small time step show that the Euler parameter based method is not sensitive to the time step size.

—— Rigid: Euler Method, $\Delta t = 5 \times 10^{-5}$

········· Flex: Euler Method: $\Delta t = 2.5 \times 10^{-3}$

– · – Flex: Newmark Method, $\Delta t = 5 \times 10^{-5}$
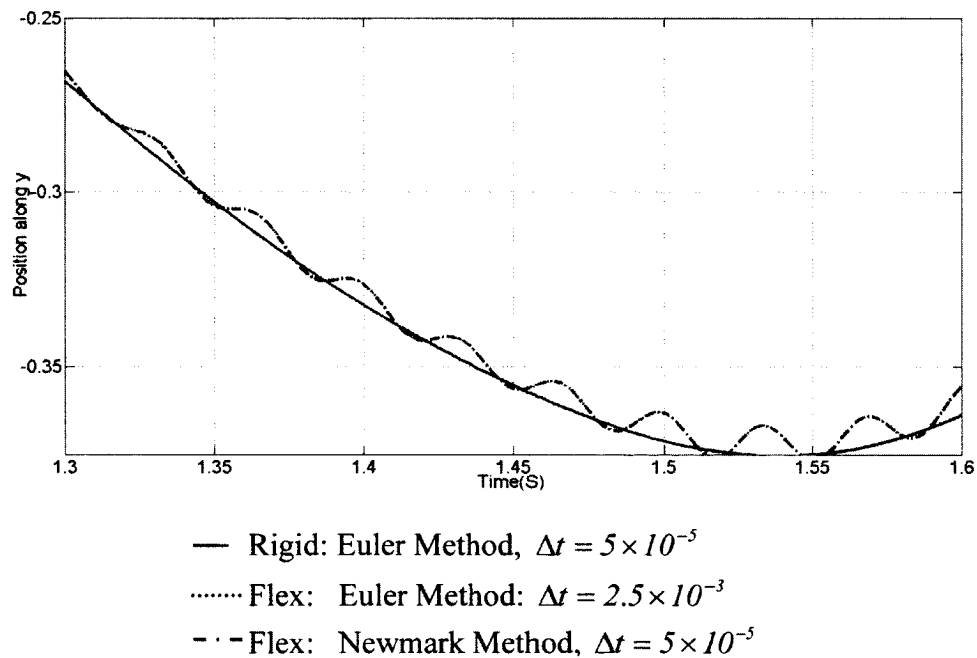
Figure 6.35 Zoomed Position of the Maximum Force Point along y for Euler Method

— Rigid: Euler Method, $\Delta t = 5 \times 10^{-5}$

······· Flex: Euler Method: $\Delta t = 2.5 \times 10^{-3}$

– · – Flex: Newmark Method, $\Delta t = 5 \times 10^{-5}$
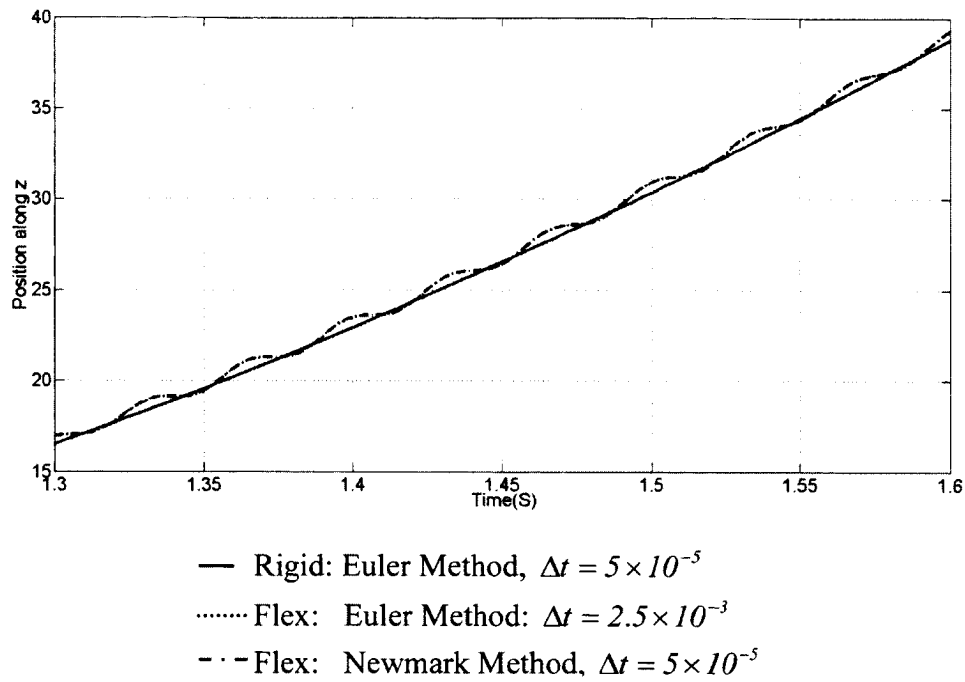
Figure 6.36 Zoomed Position of the Maximum Force Point along z for Euler Method

The time history of the modal coordinate is shown in Fig. 6.37. It can be seen that the second mode in Fig. 6.3 (b) is the dominant mode.
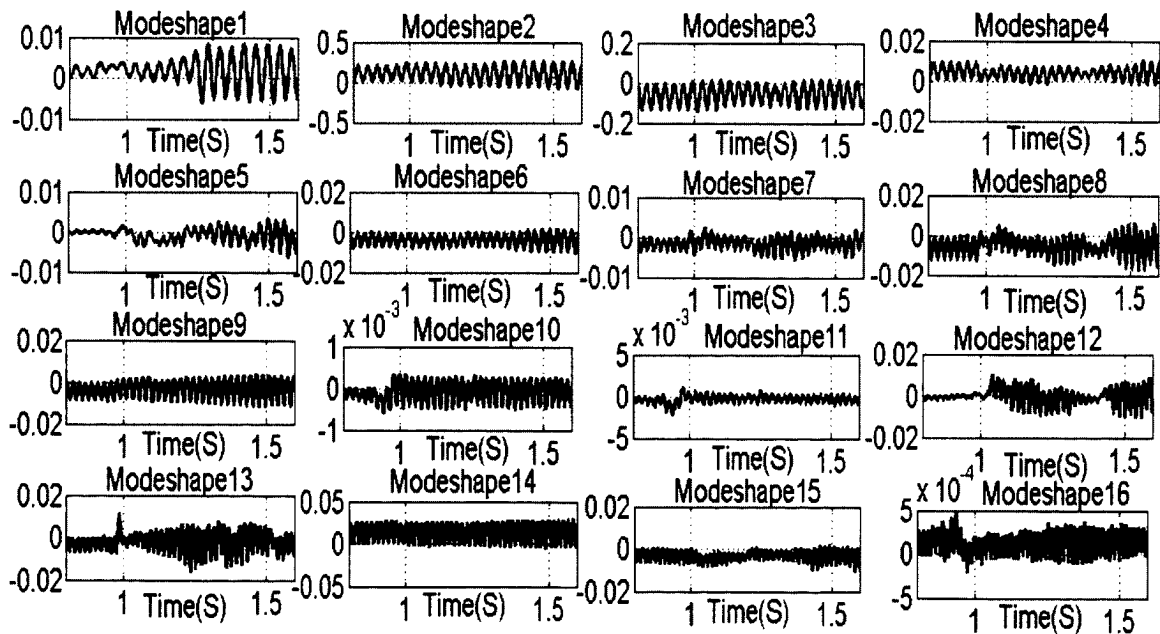
Figure 6.37 Time History of the Modal Coordinate

The deformation of the craft at different times is shown in Fig. 6.38. It can be seen that the elastic deformation along z is dominant as the maximum force is along z. The deformation along y is bent towards the left side.
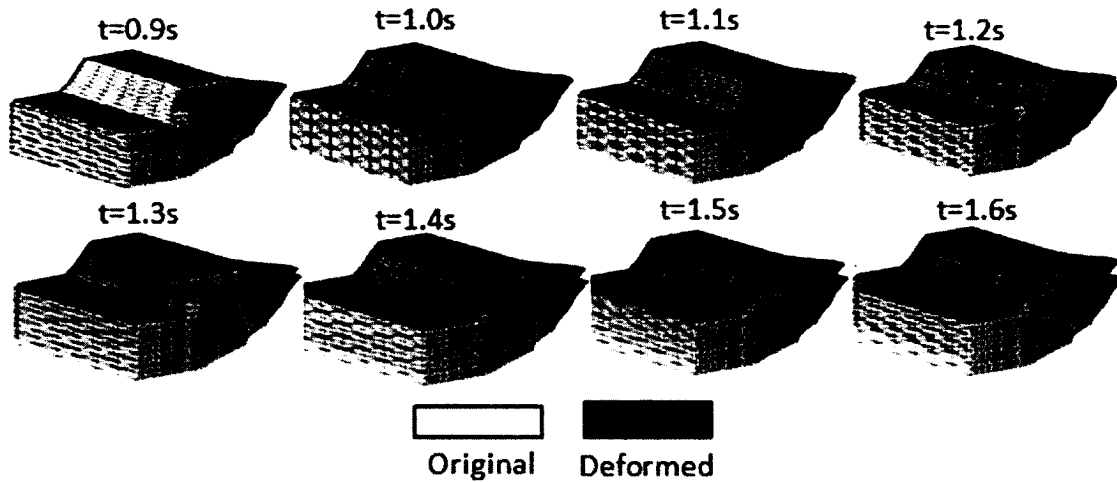
Figure 6.38 Deformations of the Craft at Different Time

6.5.2 Computational Time Comparison for Different Methods

The CPU time is obtained to check the efficiency of the methods used for the rigid craft and the flexible one. The average value of three different runs is taken as the CPU time for each method, which is shown in Table 6.1.

Table 6.1 Time Comparison for the Rigid and Flexible Craft Dynamics

System	Rigid				Flexible			
Method	Euler		Newmark		Euler		Newmark	
Δt	$2.5e^{-3}$	$5e^{-5}$	$2.5e^{-3}$	$5e^{-5}$	$2.5e^{-3}$	$5e^{-5}$	$2.5e^{-3}$	$5e^{-5}$
1st	6.37s	71.40s	8.92s	269.06s	674.79s	86,036s	71.19s	22,488s
2nd	6.32s	70.42s	9.13s	288.74s	685.76s		70.69s	
3rd	6.26s	71.85s	8.27s	272.79s	694.67s		70.65s	
Average	6.32	71.22s	8.77s	276.86s	685.07s		70.86s	

Although the Euler parameters based method consumes significantly more time than the matrix exponential based Newmark method for the flexible dynamics, higher accuracy can be obtained even with a large time step.

6.6 Results of Dynamic Stresses

Once the time history of the elastic displacement is obtained, one can then proceed to compute the dynamic stresses. This can be done using the mode shapes output from the eigenvalue analysis, Ψ, and the modal coordinates a from the solution of the ODE solver. The Von Mises stresses are the quantities to be reported. NASTRAN reports the stresses, $\sigma_{x,i}$, $\sigma_{y,i}$, the shear stress, $\tau_{xy,i}$, and the Von Mises stress, $\sigma_{v,i}$ at the lower and upper surface of each element for the ith mode shape. The modal superposition can be applied here to find the total stresses, σ_x, σ_y and τ_{xy} as the results of dynamic results

$$\sigma_x = \sum_{i=1}^{Nm} a_i \sigma_{x,i} \tag{6.45a}$$

$$\sigma_y = \sum_{i=1}^{Nm} a_i \sigma_{y,i} \tag{6.45b}$$

$$\tau_{xy} = \sum_{i=1}^{Nm} a_i \tau_{xy,i} \tag{6.45c}$$

where a_i, modal coordinate, can be obtained from the solutions of ODEs.

Once the normal stresses, σ_x, σ_y and the shear stress, τ_{xy} are known at the center of each triangular element, one can then use the following equation to find the von Mises stress at the element center [97],

$$\sigma_{v,c} = \sqrt{\sigma_x^2 + \sigma_y^2 - \sigma_x \sigma_y + 3\tau_{xy}^2} \tag{6.46}$$

The von Mises stresses at the centers of all elements can be collected and used to find the von Mises stresses at all nodes. The latter can be used to find the stress distribution over the entire finite element model. The process [85] starts with an assumption that the von Mises stress is distributed linearly over the triangular element. Thus, one has

$$\sigma_v = \left(\xi \sigma_{v,1} + \eta \sigma_{v,2} + \zeta \sigma_{v,3} \right) \equiv n^T \sigma_v \tag{6.47}$$

where $n^T = \begin{bmatrix} \xi & \eta & \zeta \end{bmatrix}$ is the shape function vector, $\sigma_v = \begin{bmatrix} \sigma_{v,1} & \sigma_{v,2} & \sigma_{v,3} \end{bmatrix}^T$ is the nodal Von Mises stress at the vertex of the triangular element is unknown.

The values of the nodal Von Mises stresses, σ_v, can be found by minimizing the error between the constant and the linear stress distribution oven each triangular element. The minimization problem is defined as:

$$\min_{\sigma_v} \quad f(\sigma_v) = \sum_{i=1}^{NE} \frac{1}{2} \int_{\Omega_e} \left(\sigma_{v,c}^{'} - \sigma_v\right)^2 dA \tag{6.48}$$

where NE is the number of elements. With the aid of the interpolation given in Eq. 6.53, the integration in Eq. 6.48 can be carried out to obtain

$$\frac{1}{2} \int_{\Omega_e} \left(\sigma_{v,c}^{'} - \sigma_v\right)^2 dA = \frac{1}{2} \sigma_v^T W_e \sigma_v + \sigma_v^T s_e \tag{6.49}$$

where the vector, $s_e^T = \dfrac{A_e}{3}\begin{pmatrix} 1 & 1 & 1 \end{pmatrix}$ and the square matrix W_e are given by

$$W_e = \int_{\Omega_e} n^T n \, dA = \frac{A_e}{12}\begin{bmatrix} 2 & 1 & 1 \\ 1 & 2 & 1 \\ 1 & 1 & 2 \end{bmatrix}.$$ The summation over the elements gives the total error.

Therefore, the necessary condition of the above minimization problem Eq. 6.49 yields:

$$\frac{\partial f}{\partial \sigma} = W\sigma - R = 0 \tag{6.50}$$

The von Mises stress σ at all vertex nodes in the finite element model can be obtained by solving the above equations as:

$$\sigma = W^{-1} R \tag{6.51}$$

Through the above process, the stress history for the maximum stress point, which is the same as the maximum force point, is shown in Fig. 6.39.
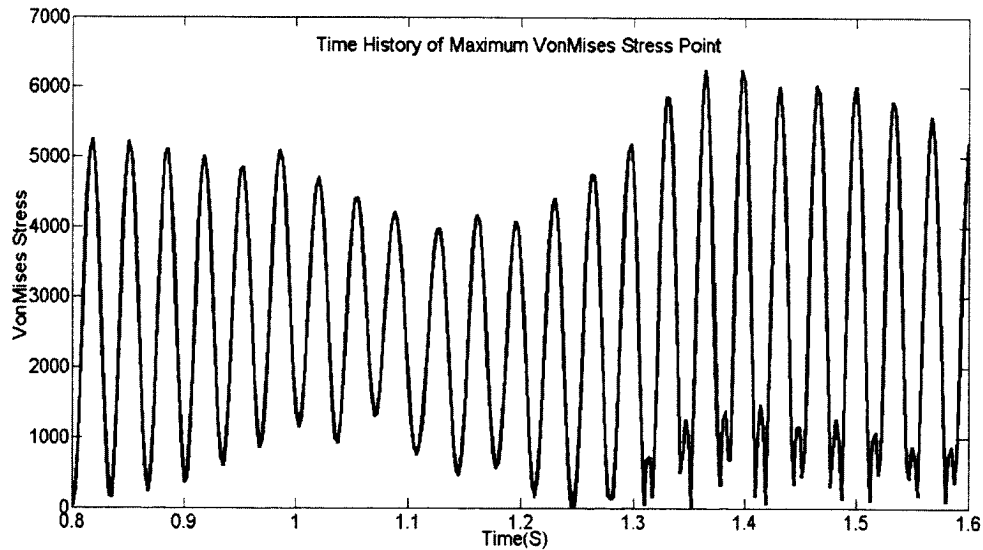
Figure 6.39 Time History of von Mises Stress at Maximum Stress Point

The contour stress distribution along the craft at two time instants is shown here. The first one is maximum pressure time instant, $t=0.94$s; the other is time instant, $t=1.3975$s when the maximum contour stress occurred. It should be noted that the contour stress is calculated from the von Mises stress at each node.

The contour stress of the craft and internal structure are shown in Figs. 6.40 and 6.41. It can be seen that the stress concentrated on the rear end.
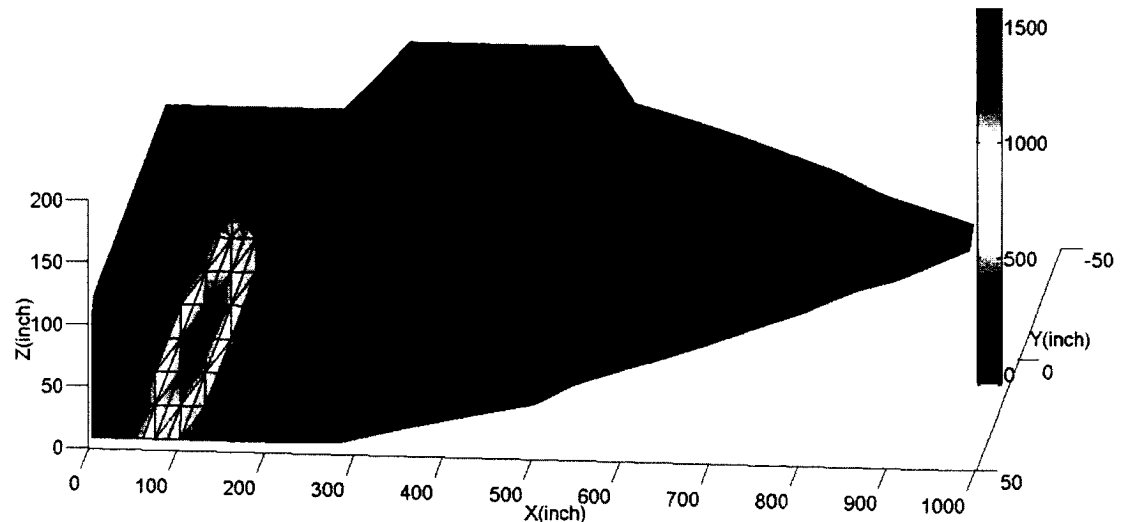
Figure 6.40 Stress Contour at $t=0.94$s
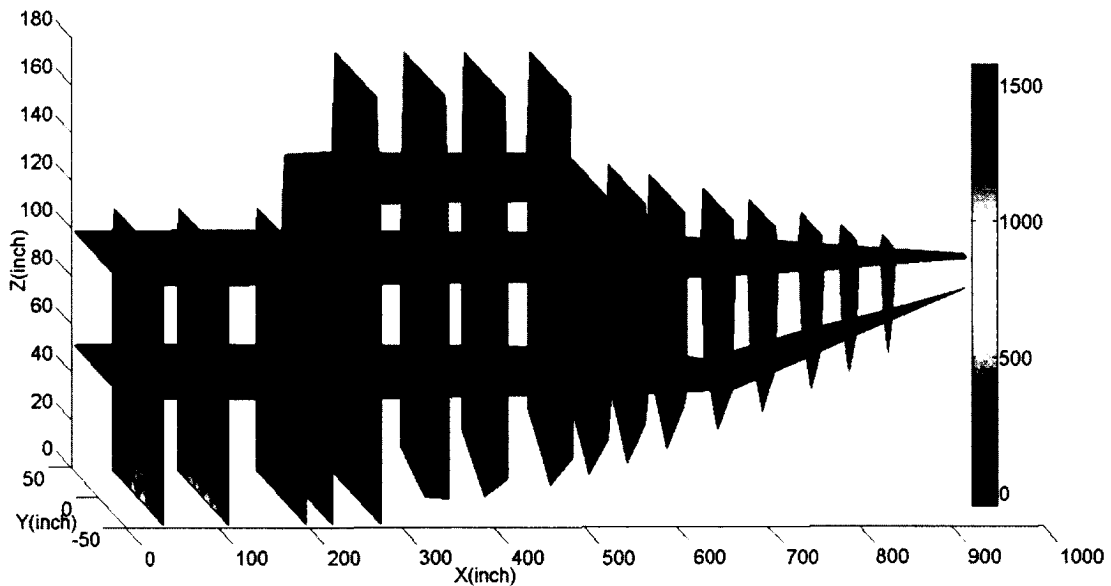
Figure 6.41 Stress Contour of Internal Structure at $t=0.94$s

The maximum contour stress of the craft is shown in Fig. 6.42. The area is also the maximum force location. The contour stress distribution for the internal structure is shown in Fig. 6.43.
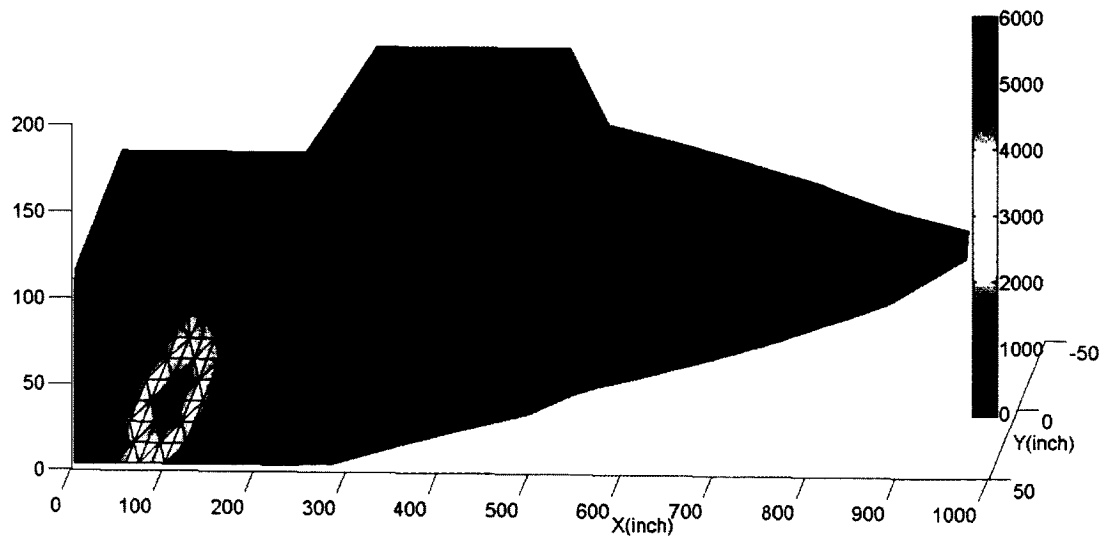
Figure 6.42 Maximum Stress Contour at t=1.3975s
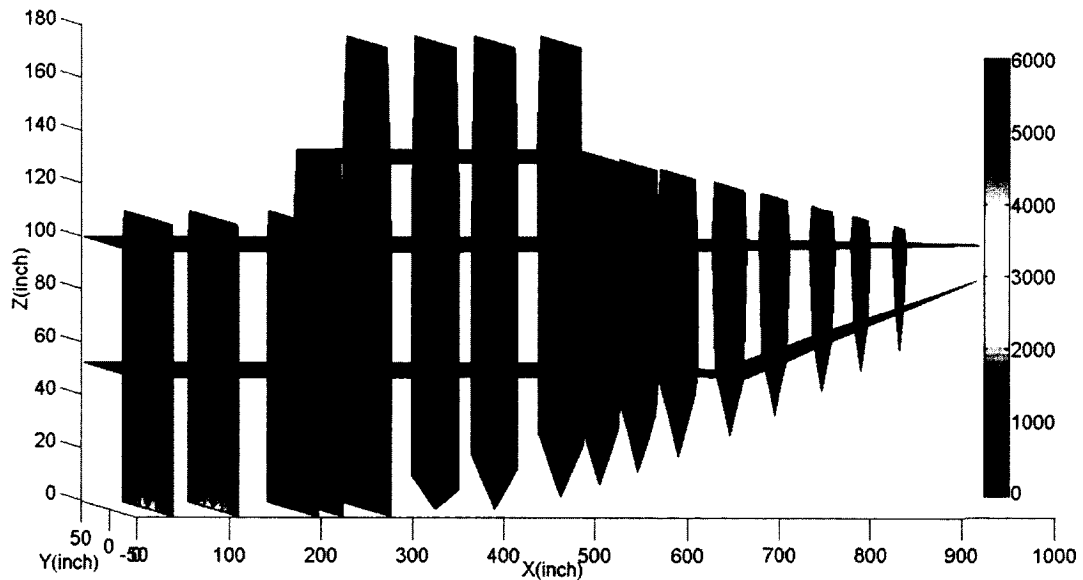
Figure 6.43 Stress Contour of Internal Structure at t=1.3975s

CHAPTER 7

CONCLUSION AND FUTURE WORK

7.1 Summary

This dissertation focuses on the computational dynamics of the flexible multi-body systems and particularly on the accuracy and efficiency issues.

A planar slider-crank mechanism with a flexible connecting rod is taken as a vehicle to show how to calculate the inertia integrals as time-invariant beforehand and solve the governing equation of motion using the proposed projection method with displacement and velocity constraints correction.

The integrals that represent the dynamic coupling between the rigid motion and elastic deformation are calculated as constants in advance by expressing in the explicit format of the modal coordinate. The advantages of this approach are as follows:

1. Reduction in the computational time because the integrals are only needed to be calculated beforehand regardless of the number of times the ODE solver is called.

2. Reduction of the data storage space requirements while avoiding the large dimension matrix multiplication because the integration is done within each element separately rather than in the whole concerned domain.

3. Fewer terms need to be calculated because the time derivation integration terms do not need to be calculated.

4. The equation of motion is no longer related to the finite element code. The commercial finite element code only served as the pre-processor to provide the nodes and elements information and the mode shapes.

The coordinate partitioning method is a widely used numerical method to solve DAEs due to its straightforward characteristic. However, the projection method with constraints correction is proposed to solve the DAEs, in which all the generalized system coordinates are included in the DAEs. The linear approximation of the displacement constraints violation is proposed to find the displacement correction Δq explicitly. Otherwise, it is needed to solve the nonlinear equations to find the displacement correction. Although the number of system variables is increased, the projection method has its own advantages compared to the coordinate partitioning method:

1. It does not need to identify independent and dependent coordinates for the projection method. One reason is that it is very difficult to select independent coordinates in practice. The other reason is that a singularity may occur when the dependent coordinates are calculated in terms of the independent coordinates.

2. The equation of motion does not need to be rearranged in the order of dependent and independent coordinates for the projection method. However, this must be done for the coordinate partitioning method.

3. The time for constraints correction is very small compared to the time consumed by the ODE solver based upon the proposed numerical method.

A 3D flexible craft under the reconstructed pressure load is utilized as an example to show how to perform the dynamic analysis using the additional Euler parameters method. The raw test data for the pressure between the hull surface and the water is processed to eliminate the high frequency noise based upon the FFT and low-pass filter. The linear hydrodynamic pressure distribution reconstruction algorithm is carried out based upon the filtered pressure data. Then the pressure load for 3D finite element model is obtained by converting the 3D coordinates to 2D based upon the assumption that the hull surface is of the V type. Finally, the equivalent nodal external force is calculated from the pressure information at the nodes in the finite element model based upon the same work done by these two loads.

The final first order ODEs for a 3D flexible multi-body are expressed in terms of the angular velocity and of the additional Euler parameters at the same time. The angular velocity is not eliminated from the ODEs. Otherwise, the angular acceleration needs to be expressed as the second order derivation of the Euler parameter, which will cause difficulties. In other words, Euler parameters and angular velocity both are the system generalized coordinates shown in the governing equation of motion. The advantages of the additional Euler parameter methods are as follows:

1. The format of E.O.M. remains unchanged when introducing Euler parameters.

2. Only constraints on 1st order time derivation of Euler parameters are needed.

3. Angular displacement calculations are unnecessary because the time integration of angular velocity is not a vector for 3D problems.

4. No 2nd order derivation of Euler parameters is required.

5. The additional Euler parameter method is not sensitive to the time step compared to the Newmark Method.

The dynamic stress distribution is directly calculated in terms of the modal coordinates obtained from the ODE solver. It obviates the need to run the dynamic analysis in commercial software to obtain the dynamic stress under the displacement loads at each node. Hence, it will save a lot of time in finding the dynamic stress distribution along the structure.

7.2 Future Work

Two demonstration examples in this dissertation are purely beam elements for a 2D slider-crank mechanism and the space triangular elements for the craft. Future work could be extended to suit the mixed element types, such as the quadratic element and the tetrahedral/hexahedral solid element, for the general mechanical system.

The description of the elastic deformation plays a very important role in predicting the flexible multi-body system. It should be noted that in this study the elastic deformation is calculated based upon the mode shapes using the mode superposition technique. Hence, the selection of the mode shapes is very important to capture the elastic deformation accurately. There are two factors that can influence the mode shapes. The first one is the number and how to select the mode shapes. The second one is the components that constitute the mode shape. For the mode number and selection of mode shapes, the mode shapes at the concerned frequency are all extracted and used as modal coordinates in this study. However, some of these mode shapes have a very small contribution to the elastic deformation. Therefore, it is necessary to find a method for selecting the mode shapes. For the components of the mode shape, only the translational DOFs of the triangular elements nodes are used to approximate the elastic deformation. In a future investigation, the rotational DOFs could be incorporated to represent the nodal rotational contributions to the elastic deformation.

The flexible dynamic analysis of the craft in irregular waves is carried out in detail in the current research. Nevertheless, it is based upon a simple finite element model of the craft, which cannot represent the actual craft very well, particularly regarding details of the substructures. Hence, a more detailed finite element model is needed.

REFERENCE:

1. Neubauer, A. H., Cohen, R. and Hall, A.S., "An Analytical Study of the Dynamics of an Elastic Linkage", *Journal of Industrial Engineering, ASME*, Vol. 88, pp. 311-317, 1966.

2. Viscomi, B. V. and Ayre, R. E., "Nonlinear Dynamic Response of Elastic Slider-Crank Mechanism", *Journal of Industrial Engineering, ASME*, Vol. 93, pp. 251-262, 1971.

3. Winfrey, R. C., "Elastic Link Mechanism Dynamics", *Journal of Engineering for Industry*, Vol. 93, Issue 1, pp. 268-272, 1971.

4. Winfrey, R. C., "Dynamic Analysis of Elastic Link Mechanisms by Reduction of Coordinates", *Journal of Engineering for Industry*, Vol. 94, pp. 577-582, 1972.

5. Chu, S. C. and Pan, K. C., "Dynamic Response of a High-Speed Slider-Crank Mechanism With an Elastic Connecting Rod", *Journal of Industrial Engineering, ASME*, Vol.97, Issue 2, pp. 542-550, 1975.

6. De Veubeke, B. F., "The Dynamics of Flexible Bodies", *International Journal of Engineering Science*, Vol. 14, Issue 10, pp. 895-913, 1976.

7. Schiehlen, W., "Multibody System Dynamics: Roots and Perspectives", *Multibody System Dynamics 1*, pp. 149-188, 1997.

8. Shabana, A. A., "Flexible Multibody Dynamics: Review of Past and Recent Developments", *Multibody System Dynamics 1*, pp. 189-222, 1997.

9. Wasfy, T. M. and Noor, A. K., "Computational Strategies for Flexible Multibody Systems", *Applied Mechanics Reviews.*, Vol. 56, pp. 553-613, 2003.

10. Likins, P. W., "Modal Method for the Analysis of Free Rotations of Spacecraft", *American Institute of Aeronautics and Astronautics Journal*, Vol. 5, pp. 1304-1308, 1967.

11. Miline, R. D., "Some Remarks on the Dynamics of Deformable Bodies", *American Institute of Aeronautics and Astronautics Journal*, Vol. 6, pp. 556-558, 1968.

12. Canavin, J. R. and Likins, P. W., "Floating Reference Frames for Flexible Spacecraft", *Journal of Spacecraft and Rockets*, Vol. 14, pp. 724-732, 1977.

13. Rankin, C. C. and Brogan, F. A., "An Element Independent Co-rotational Procedure for the Treatment of Large Rotations", *Journal of Pressure Vessel Technology, ASME*,

Vol. 108, pp. 165-174, 1986.

14. Hsiao, K. M. and Jang, J. Y, "Dynamic Analysis of Planar Flexible Mechanisms by Co-rotational Formulation", *Computer Methods in Applied Mechanics and Engineering*, Vol. 87, pp. 1-14, 1991.

15. Belytschko, T. and Hseih, J., "Non-linear Transient Finite Element Analysis with Convected Coordinates", *International Journal for Numererical Methods in Engineering*, Vol. 7, pp. 255-271, 1973.

16. Shabana, A. A., "Finite Element Incremental Approach and Exact Rigid Body Inertia", *Journal of Mechanical Design, ASME*, Vol. 118, pp. 171-178, 1996.

17. Bauchau, O. A. and Rodriguez, J., "Formulation of Modal-Based Elements in Nonlinear, Flexible Multibody Dynamics", *Journal of Multiscale Computational Engineering*, Vol. 1, No. 2&3, pp. 161-180, 2003.

18. Cavanin, J.R. and Likins, P.W., "Floating reference frames for flexible spacecraft", *Journal of Spacecraft and Rockets,* Vol. 14, No. 12, pp. 724-732, 1977.

19. Drab, C. B., Haslinger, J. R., Pfau, R. U. and Offner, G., "Comparison of the Classical Formulation with the Reference Conditions Formulation for Dynamic Flexible Multibody Systems", *Journal of Computational and Nonlinear Dynamics*, Vol. 2, pp. 337-342, 2007.

20. Shabana, A. A., "Substructure Synthesis Methods for Dynamic Analysis of Multi-body Systems", *Computers and Structures*, Vol. 20, pp. 737-744, 1985.

21. Cardona, A. and Geradin, M., "A Superelement Formulation for Mechanism Analysis", *Computer Methods in Applied Mechanics and Engineering*, Vol. 100, Issue 1, pp. 1-29, 1992.

22. Agrawal, O. P. and Shabana, A. A., "Application of Deformable-body Mean axis to Flexible Multibody System Dynamics", *Computer Methods in Applied Mechanics and Engineering*, Vol. 56, pp. 217-245, 1986.

23. Cardona, A., "Superelements Modelling in Flexible Multibody Dynamics", *Multibody System Dynamics*, Vol. 4, pp. 245-266, 2000.

24. Agrawal, O. P. and Shabana, A. A., "Dynamic Analysis of Multibody Systems Using Component Modes", *Computers and Structures*, Vol. 2, pp. 1303-1312, 1985.

25. Ambrosio, J. A. C., and Goncalves, J. P. C., "Complex Flexible Multibody Systems with Application to Vehicle Dynamics", *Advances in Computational Multibody Dynamics, IDMEC/IST,* Lisbon, Portugal, Sept. 20-23, pp. 241-258, 1999.

26. Kim, S. S. and Haug, E. J., "Selection of Deformation Modes for Flexible Multibody Dynamics", *Mechanics of Structures and Machines*, Vol. 18, Issue 4, pp. 565-586, 1990.

27. Friberg, O., "A Method for Selecting Deformation Modes in Flexible Multibody Dynamics", *International Journal for Numerical Methods in Engineering*, Vol. 32, Issue 8, pp. 1637–1655, 1991.

28. Wu, H. T. and Mani, N. K., "Selection of Modal Basis for Flexible Bodies of Mechanical Systems", *Mechanism and Machine Theory*, Vol. 30, Issue 3, pp. 471-489, 1995.

29. Yoo, W. S. and Haug, E. J., "Dynamics of Articulated Structures. Part I. Theory", *Journal of Structural Mechanics*, Vol. 14, Issue 1, pp. 105-126, 1986.

30. Yoo, W. S. and Haug, E. J., "Dynamics of Articulated Structures. Part II. Computer Implementation and Applications", *Journal of Structural Mechanics*, Vol. 14, Issue 2, pp. 177-189, 1986.

31. Pan, W. and Haug, E. J., "Flexible Multibody Dynamic Simulation Using Optimal Lumped Inertia Matrices", *Computer Methods in Applied Mechanics and Engineering*, Vol. 173, Issue 1–2, pp. 189-200, 1999.

32. Pan, W., Mao, S., Haug, E. J. and Solis, D., "Efficient Modal Approach for Flexible Multibody Dynamic Simulation", *Mechanics Based Design of Structures and Machines*, Vol. 31, Issue 1, pp. 1-23, 2003.

33. Shabana, A. A., *Dynamics of Multibody Systems (3rd edition)*, Cambridge, New York: Cambridge Unversity Press, 2005.

34. Bayo, E. and Avello, A., "Singularity-free Augmented Lagrangian Algorithms for Constrained Multibody Dynamics", *Nonlinear Dynamics*, Vol. 5, No. 2, pp. 209-231, 1994.

35. Book, W. J., "Recursive Lagrangian Dynamics of Flexible Manipulator Arms", *International Journal of robotic Research*, Vol. 3, pp. 87-101, 1984.

36. Kim, S.S. and Haug, E.J., "A Recursive Formulation for Constrained Mechanical

System Dynamics: Part I: Open Loop Systems", *Mechanics of Structures and Machines*, Vol. 15, Issue 3, pp. 359-382, 1987.

37. Kim, S. S. and Haug, E. J., "A Recursive Formulation for Constrained Mechanical System Dynamics: Part II: Closed Loop Systems", *Mechanics of Structures and Machines*, Vol. 15, Issue 4, pp. 481-506, 1987.

38. Changizi, K. and Shabana, A. A., "A Recursive Formulation for the Dynamic Analysis of Open Loop Deformable Multibody Systems", *Journal of Applied Mechanics, ASME*, Vol. 55, pp. 687-693, 1988.

39. Blajer, W., Schiehlen, W. and Schirm, W., "A Projective Criterion to the Coordinate Partitioningng Method for Multibody Dynamics", *Archieve of Applied Mechanics*, Vol. 64, pp. 86-98, 1994.

40. Fisette, P. and Vaneghem, B., "Numerical Integration of Multibody System Dynamic Equations Using the Coordinate Partitioning Method in an Implicit Newmark Scheme", *Computer Methods in Applied Mechanics and Engineering*, Vol. 135, pp. 85-105, 1996.

41. Yoo, W. S. and Kim, O. J., "A Hybrid Coordinate Partitioning Method in Flexible Mechanical System", NATO-ARW on Computational Aspects of Nonlinear Structure System W/ Large Rigid Body Motion, Pultusk, Poland, July2-7, 2000.

42. Yoo, W. S., Kim, S. H. and Kim, O. J., "A Hybrid Scheme Using LU Decomposition and Projection Matrix for Dynamic Analysis of Constrained Multibody Systems", *International Journal of Automotive Technology*, Vol. 2, No. 3, pp. 117-122, 2001.

43. Chorin, A.J., "A Numerical Method for Solving Incompressible Viscous Flow Problems", *Journal of Computational Physics*, Vol. 2, Issue 1, pp. 12-26, 1967.

44. Guermond, J. L., Minev, P. and Shen, J., "An Overview of Projection Methods for Incompressible Flows", *Computer Methods in Applied Mechanics and Engineering*, Vol. 195, pp. 6011-6045, 2006.

45. Wahage, R. A. and Haug, E. J., "Generalized Coordinate Partitioning for Dimension Reduction in Analysis of Constrained Dynamic Systems", *Journal of Mechanical Design, ASME*, Vol. 104, pp. 247-255, 1982.

46. ABS, *Guide for Building and Classing High Speed Craft*, 1997.

47. DNV, *Design Principles, Design Loads, Rules for Classification of High Speed and*

Light Craft, Part 3, Chapter 1, 1996.

48. Lloyd's Register of Shipping, *Rules and Regulations for the Classification of Special Service Craft,* 1998.

49. Heller, S. R. and Jasper, N. H., "On the Structural Design of Planing Craft", RINA, Quarterly Transactions, July, 1960.

50. Savitsky, D., "Hydrodynamic Design of Planing Hulls", *Journal of Marine Technology,* Vol. 1, Issue 1, pp.71–95, 1964.

51. Savitsky, D. and Brown, P. W., "Procedures for Hydrodynamic Evaluation of Planing Hulls in Smooth and Rough Water", *Marine Technology,* Vol. 13, No. 4, pp. 381-400, 1976.

52. Fridsma, G., *A Systematic Study of the Rough-Water Performance of Planing Boats,* Davidson Laboratory, Stevens Institute, Report 1275, 1969.

53. Fridsma, G., *A Systematic Study of the Rough-Water Performance of Planing Boats in Irregular Waves, Part II,* Davidson Laboratory, Stevens Institute, Report SIT-DL-71-1495, 1971.

54. Savitsky, D. and Koebel, J. G., *Seakeeping of Hard Chine Planing Hulls,* Technical research bulletin R-42, SNAME, 1993.

55. Savitsky, D., DeLorme, M. F. and Raju, D., "Inclusion of Whisker Spray Drag in Performance Prediction Method for High-speed Planing Hulls", *Journal of Marine Technology,* Vol. 44, No.1, pp. 35–56, 2007.

56. Spencer, J. S., "Structural Design of Aluminium Crewboats", *Marine Technology,* Vol. 12, No. 3, pp. 267-274, 1975.

57. Henrickson, W. A. and Spencer, J. S., "A Synthesis of Aluminium Crewboat Structural Design", *Marine Technology,* Vol. 19, No.1, pp. 52-72, 1982.

58. Allen, R. G. and Jones, J. R., "A Simplified Method for Determining Structural Design Limit Pressures on High Performance Marine Vehicles", AIAA/SNAME Advanced Marine Vehicle Conference, April, 1978.

59. Grimsley, J. S., *A Comparison of Prediction Methods for Impact Pressures of High-speed Light Craft,* B.S. thesis, Webb Institute of Naval Architecture, Glen Cove, New York, 1998.

60. Koelbel, J. G., "Structural Design for High Speed Craft- Part One", *Professional Boatbuilder*, No. 67, pp. 31-47, 2000.

61. Koelbel, J. G., "Structural Design for High Speed Craft- Part Two", *Professional Boatbuilder*, No. 68, pp. 32-43, 2001.

62. ABS, *Guidance Notes On 'Dynamic Load Approach' And Direct Analysis For High Speed Craft*, American Bureau of Shipping, Houston, Texas, 2003.

63. Rosen A., *Loads and Responses for Planing Craft in Waves*, PhD thesis, Aeronautical and Vehicle Engineering, Division of Naval System, Stockholm, Sweden, 2004.

64. Chiu, F. C., Tiao, W. C. and Guo, J., "Experimental Study on the Nonlinear Pressure Acting on a High Speed Vessel in Irregular Wave", *Journal of Marine Science and Technology*, Vol. 12, pp. 203–217, 2007.

65. Chiu, F. C., Tiao, W. C. and Guo, J., "Experimental Study on the Nonlinear Pressure Acting on a High Speed Vessel in Irregular Wave", *Journal of Marine Science and Technology*, Vol. 14, pp. 228–239, 2009.

66. Lai, C. H and Troesch, A. W., "A Vortex Lattice Method for High-speed Planing", *International Journal for Numerical Methods in Fluids*, Vol. 22, No. 6, pp. 495-513, 1996.

67. Savander, B. R., Scorpio, S. M. and Taylor, R. K., "Steady Hydrodynamic of Planing Surface", *Journal of Ship Research*, Vol. 46, No. 4, pp. 248–279, 2002.

68. Zhao, R. and Faltinsen, O. M., "Water Entry of Two-Dimensional Bodies", *Journal of Fluid Mechanics*, Vol. 246, pp. 593-612, 1993.

69. Zhao, R., Faltinsen, O. M. and Haslum, H. A., "A Simplified Nonlinear Analysis of a High-speed Planing Craft in Calm Water", Proceedings of the Fourth International Conference on Fast Sea Transportation, Australia, 1997.

70. Xie, N., Vassalos, D. and Jasionowski, A., "A study of Hydrodynamics of Three Dimensional Planing Surface", *Journal of Ocean Engineering*, Vol. 32, pp. 1539–1555, 2005.

71. Wang, X., Day, H. and Alexander, A., "Numerical Instability in Linearized Planing Problems", *International Journal of Numerical Methods Engineering*, Vol. 70, pp. 840–875, 2007.

72. Doctors, L. J., "Representation of Three Dimensional Planing Surfaces by Finite Elements", Proceedings of the 1st Conference on Numerical Ship Hydrodynamics, pp. 517-537, 1994.

73. Cheng, X. and Wellicome, J. F., "Study of Planing Hydrodynamics Using Strips of Transversely Variable Pressure", *Journal of Ship Research*, Vol. 38, No. 2, pp. 30-41, 1994.

74. Ghassemi, H. and Ghiasi, M., "A Combined Method for the Hydrodynamic Characteristics of Planing Crafts", *Ocean Engineering*, Vol. 35, pp. 310–322, 2008.

75. Ghassemi, H. and Su, Y. M., "Determining the Hydrodynamic Forces on a Planing Hull in Steady Motion", *Journal of Marine Science and Application*, Vol. 7, pp. 147-156, 2008.

76. Ghassemi, H. and Kohansal, A. R., "Hydrodynamic Analysis of Non-Planing and Planing Hulls By BEM", *Mechanical Engineering*, Vol. 17, No.1, pp. 41-52, 2010.

77. Kohansal, A. R. and Ghassemi, H., "A numerical Modeling of Hydrodynamic Characteristics of Various Planing Hull Forms", *Ocean Engineering*, Vol. 37, pp. 498-510, 2010.

78. Kohansal, A. R., Ghassemi, H. and Ghaisi, M., "Hydrodynamic Characteristics of High Speed Planning Hulls, Including Trim Effects", *Turkish Journal of Engineering and Environmental Science*, Vol. 34, pp. 155-170, 2010.

79. Sun H. and Faltinsen, O. M., Numerical Study of Planing Vessels in Waves, 9th International Conference on Hydrodynamics, Oct. 11-15, 2010, Shanghai, Chian.

80. Faltinsen, O. M. and Sun, H., "Dynamic Behavior of Semi-displacement and Planning Vessels in Calm Water and Waves", IX HSMV Naples, May 25-27, 2011.

81. Sun, H. and Faltinsen, O. M., "Dynamic Motion of Planning Vessels in Head Seas", *Journal of Marine Science and Technology*, Vol. 16, pp. 168–180, 2011.

82. Stenius, I., Finite *Element Modelling of Hydroelasticity in Hull-water Impacts*, PhD Thesis, Aeronautical and Vehicle Engineering, Division of Naval System, Stockholm, Sweden, 2006.

83. wiki, *Virtual Displacement*, http://en.wikipedia.org/wiki/Virtual_displacement.

84. Shames, I. H. and Dym, C. L., *Energy and Finite Element Methods in Structural Mechanics*, Taylor & Francis, 1985.

85. Chandrupatla, T. R. and Belegundu, A. D., *Introduction to Finite Elements in Engineering*, 3rd edition, Prentice Hall, 2002.

86. Soman, K., *Multibody Dynamics Using Matlab*, Master Thesis, Old Dominion University, 2008.

87. Haug, E. J., *Intermediate Dynamics*, Prentice Hall Publication, 1992.

88. Yoo, W. S., Kim, S. H. and Kim, O. J., "A Hybrid Scheme Using LU Decomposition and Projection Matrix for Dynamic Analysis of Constrained Multibody ", *International Journal of Automotive Technology*, Vol. 2, No. 3, pp. 117-122, 2001.

89. Wiki, *Butterworth filter*, http://en.wikipedia.org/wiki/Butterworth_filter

90. Riley, M. R., Haupt, K. D. and Jacobson, D.R., *A General Approach and Interim Criteria for Computing A$_{1/n}$ Accelerations Using Full-Scale High-Speed Craft Trials Data*, Technical Memorandum, Ship System and Integration and Design Department, NSWCCD-23-TM-2010/13

91. Garme, K. and Rosen, A., "Time-Domain Simulations and Full-Scale Trials on Plaining Craft in Waves", *International shipbuilding Progress*, Vol. 50, No. 3, pp. 177-208, 2003.

92. Rosen, A. and Garme, K., "Model Experiment Addressing the Impact Pressure Distribution on planning Craft In Waves", *International Journal of Small Craft Technology*, 2004.

93. Rosen, A., "Impact Pressure Distribution Reconstruction from Discrete Point Measurements ", *International shipbuilding Progress*, Vol. 52, No. 1, pp. 91-107, 2005.

94. Garme, K., Rosen, A. and Kuttenkeuler, J., "In Detail Investigation of Planing Pressure", Proceedings of the HYDRALAB III Joint User Meeting, Hannover, February, 2010.

95. Newmark, N. M., "A Method of Computation for Structural Dynamics", *Journal of Engineering Mechanics*, Vol. 85, pp. 67-94, 1959.

96. Krysl, P. and Endres, L., *Explicit Newmark/Verlet Algorithm for Time Integration of the Rotational Dynamics of Rigid Bodies*, University of California, San Diego, 2004.

97. Wiki, *Von Mises Stress*, http://en.wikipedia.org/wiki/Von_Mises_yield_criterion

APPENDIX 1

IN-LOOP INTEGRALS CALCULATION FOR BEAM ELEMENT

The Connecting Rod can be considered as a pure bending beam with axial deformation as shown in Fig. A1.1.
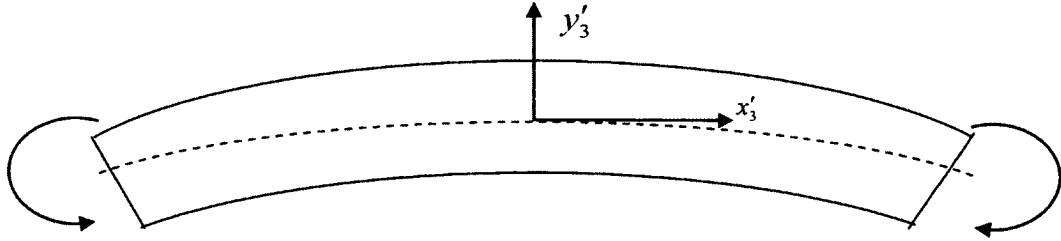
Figure A1.1 Bending of a Beam Element

The body-fixed coordinate system and degree of freedom of each node for the beam element are shown in Fig. A1.2. u_1 and u_2 are axial displacements of the endpoints, v_1 and v_2 are the transverse displacements, θ_1 and θ_2 are the slopes at the endpoints.
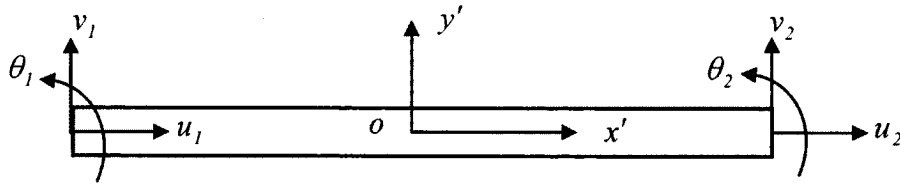
Figure A1.2 Beam Element Displacement Field at Local Coordinate System

Based upon the finite element model, the displacement of the beam element can be expressed as:

$$u(x) = u_0(x) - yv'(x)$$

where, $u(x)$ is displacement in x' direction, $v(x)$ is the displacement in y' direction, $u_0(x)$ is the elongation of the neutral axis, y is the vertical distance of a tension fiber on the edge from neutral axis and $v'(x)$ is the bending slope.

$$u_0 = N_1 u_1 + N_2 u_2 \text{ and } v = N_3 v_1 + N_4 \theta_1 + N_5 v_2 + N_6 \theta_2$$

where

$$N_1 = 1 - \xi; N_2 = \xi; N_3 = 1 - 3\xi^2 + 2\xi^3; N_4 = \ell_e \left(\xi - 2\xi^2 + \xi^3\right); N_5 = 3\xi^2 - 2\xi^3; N_6 = \ell_e \left(-\xi^2 + \xi^3\right)$$

where $\xi = x / l_e$

Based upon the chain rule, one has:

$$v'(x) = \frac{dv(x)}{dx} = \frac{dv}{d\xi} \frac{d\xi}{dx} = \left[\frac{dN_3}{d\xi} v_1 + \frac{dN_4}{d\xi} \theta_1 + \frac{dN_5}{d\xi} v_2 + \frac{dN_6}{d\xi} \theta_2 \right] / \ell_e$$

$$= \left[(-6\xi + 6\xi^2)v_1 + \ell_e (1 - 4\xi + 3\xi^2)\theta_1 + (6\xi - 6\xi^2)v_2 + \ell_e(-2\xi + 3\xi^2)\theta_2 \right] / \ell_e$$

From the above equations, one has:

$$u(x) = N_1 u_1 - \frac{y'}{\ell_e} \frac{dN_3}{d\xi} v_1 - \frac{y'}{\ell_e} \frac{dN_4}{d\xi} \theta_1 + N_2 u_2 - \frac{y'}{\ell_e} \frac{dN_5}{d\xi} v_2 - \frac{y'}{\ell_e} \frac{dN_6}{d\xi} \theta_2$$

$$= (1 - \xi)u_1 + \xi u_2 + y'(6\xi - 6\xi^2) / \ell_e v_1 + y'(-1 + 4\xi - 3\xi^2)\theta_1$$

$$+ y'(-6\xi + 6\xi^2) / \ell_e v_2 + y'(2\xi - 3\xi^2)\theta_2$$

Now the displacement vector of the flexible for the beam is given by,

$$e = \{u \quad v \quad w\}^T = \{u_0 - yv' \quad v \quad w\}^T = N q_e$$

where N is the shape function matrix given by:

$$N \equiv \begin{bmatrix} N_1 & -\dfrac{y'}{\ell_e} \dfrac{dN_3}{d\xi} & -\dfrac{y'}{\ell_e} \dfrac{dN_4}{d\xi} & N_2 & -\dfrac{y'}{\ell_e} \dfrac{dN_5}{d\xi} & --\dfrac{y'}{\ell_e} \dfrac{dN_6}{d\xi} \\ 0 & N_3 & N_4 & 0 & N_5 & N_6 \\ 0 & 0 & 0 & 0 & 0 & 0 \end{bmatrix}$$

$$= \begin{bmatrix} 1-\xi & y'(6\xi - 6\xi^2)/\ell_e & y'(-1 + 4\xi - 3\xi^2) & \xi & y'(-6\xi + 6\xi^2)/\ell_e & y'(2\xi - 3\xi^2) \\ 0 & 1 - 3\xi^2 + 2\xi^3 & \ell_e\left(\xi - 2\xi^2 + \xi^3\right) & 0 & 3\xi^2 - 2\xi^3 & \ell_e\left(\xi^3 - \xi^2\right) \\ 0 & 0 & 0 & 0 & 0 & 0 \end{bmatrix}$$

$q_e = [u_1 \quad v_1 \quad \theta_1 \quad u_2 \quad v_2 \quad \theta_2]^T$ is the elastic displacement in the local coordinate,

Thus, the strain in x' direction is given by:

$$\varepsilon_x = \frac{d}{dx} u(x) = \frac{d}{dx} u_0(x) - y' \frac{d}{dx} v'(x) = u_0' - y'v''$$

where $u_0' = \dfrac{du_0}{d\xi} \dfrac{d\xi}{dx} = -u_1 / \ell_e + u_2 / \ell_e$ and $v'' = \dfrac{dv'}{dx} = \dfrac{dv'}{d\xi} \dfrac{d\xi}{dx}$

From the above equation, one has

$$v'' = \frac{dv'}{dx} = \frac{dv'}{d\xi}\frac{d\xi}{dx} = [(-6+12\xi)v_1 + \ell_e(-4+6\xi)\theta_1 + (6-12\xi)v_2 + \ell_e(-2+6\xi)\theta_2]/\ell_e^2$$

$$\varepsilon_x = u_0' - y'v''$$

$$= -u_1/\ell_e + u_2/\ell_e - y'[(-6+12\xi)v_1 + \ell_e(-4+6\xi)\theta_1 + (6-12\xi)v_2 + \ell_e(-2+6\xi)\theta_2]/\ell_e^2$$

$$= -\frac{u_1}{\ell_e} + \frac{y'(6-12\xi)}{\ell_e^2}v_1 + \frac{y'(4-6\xi)}{\ell_e}\theta_1 + \frac{u_2}{\ell_e} + \frac{y'(-6+12\xi)}{\ell_e^2}v_2 + \frac{y'(2-6\xi)}{\ell_e}\theta_2 \equiv Bq_e$$

where $B = \begin{bmatrix} -\dfrac{1}{\ell_e} & \dfrac{y'(6-12\xi)}{\ell_e^2} & \dfrac{y'(4-6\xi)}{\ell_e} & \dfrac{1}{\ell_e} & \dfrac{y'(-6+12\xi)}{\ell_e^2} & \dfrac{y'(2-6\xi)}{\ell_e} \end{bmatrix}$

According to Hooke's Law, $\sigma_x = E\varepsilon_x = EBq_e$

The strain energy stored in each element can be calculated as follows:

$$-\int_{\Omega_i}\sigma_x^T\delta\varepsilon_x dv = -\int_{\Omega_i}(EBq)^T(B\delta q)dv = -q_e^T\int_{V_i}E(B^TB)dv\delta q_e$$

$$B^TB =$$

$$\begin{bmatrix}
\dfrac{1}{\ell_e^2} & \dfrac{y'(12\xi-6)}{\ell_e^3} & \dfrac{y'(-4+6\xi)}{\ell_e^2} & \dfrac{-1}{\ell_e^2} & \dfrac{y'(6-12\xi)}{\ell_e^3} & \dfrac{y(6\xi-2)}{\ell_e^2} \\
 & \dfrac{y'^2(6-12\xi)^2}{\ell_e^4} & \dfrac{y'^2(6-12\xi)(4-6\xi)}{\ell_e^3} & \dfrac{y'(6-12\xi)}{\ell_e^3} & \dfrac{-y'^2(6-12\xi)^2}{\ell_e^4} & \dfrac{y'^2(6-12\xi)(2-6\xi)}{\ell_e^3} \\
 & & \dfrac{y'^2(4-6\xi)^2}{\ell_e^2} & \dfrac{y'(4-6\xi)}{\ell_e^2} & \dfrac{y'^2(4-6\xi)(12\xi-6)}{\ell_e^3} & \dfrac{y'^2(4-6\xi)(2-6\xi)}{\ell_e^2} \\
 & & & \dfrac{1}{\ell_e^2} & \dfrac{y'(12\xi-6)}{\ell_e^3} & \dfrac{y'(2-6\xi)}{\ell_e^2} \\
 & \text{sym} & & & \dfrac{y'^2(6-12\xi)^2}{\ell_e^4} & \dfrac{y'^2(12\xi-6)(2-6\xi)}{\ell_e^3} \\
 & & & & & \dfrac{y'^2(2-6\xi)^2}{\ell_e^2}
\end{bmatrix}$$

Substituting into the integration equation, one has $-\int_{\Omega_i}\sigma_x^T\delta\varepsilon_x dv = -q_e^T K^e\delta q_e$

where

$$K^e = \begin{bmatrix}
\dfrac{EA}{\ell_e} & 0 & 0 & -\dfrac{EA}{\ell_e} & 0 & 0 \\
0 & \dfrac{12EI}{\ell_e^3} & \dfrac{6EI}{\ell_e^2} & 0 & -\dfrac{12EI}{\ell_e^3} & \dfrac{6EI}{\ell_e^2} \\
0 & \dfrac{6EI}{\ell_e^2} & \dfrac{4EI}{\ell_e} & 0 & -\dfrac{6EI}{\ell_e^2} & \dfrac{2EI}{\ell_e} \\
-\dfrac{EA}{\ell_e} & 0 & 0 & \dfrac{EA}{\ell_e} & 0 & 0 \\
0 & -\dfrac{12EI}{\ell_e^3} & -\dfrac{6EI}{\ell_e^2} & 0 & \dfrac{12EI}{\ell_e^3} & -\dfrac{6EI}{\ell_e^2} \\
0 & \dfrac{6EI}{\ell_e^2} & \dfrac{2EI}{\ell_e} & 0 & -\dfrac{6EI}{\ell_e^2} & \dfrac{4EI}{\ell_e}
\end{bmatrix}$$ is the stiffness matrix.

The following integration results will be used latter in calculating the integration terms:

$$\int_0^1 N_1 d\xi = \int_0^1 (1-\xi)d\xi = 1/2 \; ; \; \int_0^1 N_2 d\xi = \int_0^1 \xi d\xi = 1/2 \; ;$$

$$\int_0^1 N_3 d\xi = \int_0^1 (1-3\xi^2 +2\xi^3)d\xi = 1/2 \; ; \; \int_0^1 N_4 d\xi = \int_0^1 \ell_e(\xi - 2\xi^2 + \xi^3)d\xi = \ell_e/12$$

$$\int_0^1 N_5 d\xi = \int_0^1 (3\xi^2 - 2\xi^3)d\xi = 1/2 \; ; \; \int_0^1 N_6 d\xi = \int_0^1 \ell_e(\xi^3 - \xi^2)d\xi = -\ell_e/12$$

$$\int_0^1 \frac{dN_3}{d\xi}d\xi = \int_0^1 (-6\xi + 6\xi^2)d\xi = -1 \; ; \; \int_0^1 \frac{dN_4}{d\xi}d\xi = \int_0^1 \ell_e(1-4\xi+3\xi^2)d\xi = 0$$

$$\int_0^1 \frac{dN_5}{d\xi}d\xi = \int_0^1 (6\xi - 6\xi^2)d\xi = 1 \; ; \; \int_0^1 \frac{dN_6}{d\xi}d\xi = \int_0^1 \ell_e(3\xi^2 - 2\xi)d\xi = 0$$

$$\int_0^l \xi N_1 d\xi = \int_0^l N_1 N_2 d\xi = \int_0^l \xi(1-\xi)d\xi = 1/6 \; ; \; \int_0^l \xi N_2 d\xi = \int_0^l N_2^2 d\xi = \int_0^l \xi\xi d\xi = 1/3$$

$$\int_0^l \xi N_3 d\xi = \int_0^l N_2 N_3 d\xi = \int_0^l \xi(1-3\xi^2 + 2\xi^3)d\xi = 3/20 \; ;$$

$$\int_0^l \xi N_4 d\xi = \int_0^l N_2 N_4 d\xi = \int_0^l \ell_e \xi(\xi - 2\xi^2 + \xi^3)d\xi = \ell_e/30$$

$$\int_0^l \xi N_5 d\xi = \int_0^l N_2 N_5 d\xi = \int_0^l \xi(3\xi^2 - 2\xi^3)d\xi = 7/20 \; ;$$

$$\int_0^l \xi N_6 d\xi = \int_0^l N_2 N_6 d\xi = \int_0^l \ell_e \xi(\xi^3 - \xi^2)d\xi = -\ell_e/20$$

$$\int_0^l N_1^2 d\xi = \int_0^l (1-\xi)^2 d\xi = 1/3 \; ; \; \int_0^l N_1 N_3 d\xi = \int_0^l (1-\xi)(1-3\xi^2 + 2\xi^3)d\xi = 7/20$$

$$\int_0^l N_1 N_4 d\xi = \ell_e \int_0^l (1-\xi)(\xi - 2\xi^2 + \xi^3)d\xi = \ell_e/20 \; \int_0^l N_1 N_5 d\xi = \int_0^l (1-\xi)(3\xi^2 - 2\xi^3)d\xi = 3/20$$

$$\int_0^l N_1 N_6 d\xi = \ell_e \int_0^l (1-\xi)(-\xi^2 + \xi^3)d\xi = -\ell_e/30$$

$$\int_0^l N_3^2 d\xi = \int_0^l (1-3\xi^2 + 2\xi^3)^2 d\xi = 13/35$$

$$\int_0^l N_3 N_4 d\xi = \ell_e \int_0^l (1-3\xi^2 + 2\xi^3)(\xi - 2\xi^2 + \xi^3)d\xi = 11\ell_e/210$$

$$\int_0^l N_3 N_5 d\xi = \int_0^l (1-3\xi^2 + 2\xi^3)(3\xi^2 - 2\xi^3)d\xi = 9/70$$

$$\int_0^l N_3 N_6 d\xi = \ell_e \int_0^l (1-3\xi^2 + 2\xi^3)(-\xi^2 + \xi^3)d\xi = -13\ell_e/420$$

$$\int_0^l N_4^2 d\xi = \ell_e^2 \int_0^l (\xi - 2\xi^2 + \xi^3)^2 d\xi = \ell_e^2/105$$

$$\int_0^l N_4 N_5 d\xi = \ell_e \int_0^l (\xi - 2\xi^2 + \xi^3)(3\xi^2 - 2\xi^3)d\xi = 13\ell_e/420$$

$$\int_0^1 N_4 N_6 d\xi = \ell_e^2 \int_0^1 (\xi - 2\xi^2 + \xi^3)(-\xi^2 + \xi^3) d\xi = -\ell_e^2 / 140$$

$$\int_0^1 N_5^2 d\xi = \int_0^1 (3\xi^2 - 2\xi^3)(3\xi^2 - 2\xi^3) d\xi = 13/35$$

$$\int_0^1 N_5 N_6 d\xi = \ell_e \int_0^1 (3\xi^2 - 2\xi^3)(\xi^3 - \xi^2) d\xi = -11\ell_e / 210$$

$$\int_0^1 N_6^2 d\xi = \ell_e^2 \int_0^1 (-\xi^2 + \xi^3)(-\xi^2 + \xi^3) d\xi = \ell_e^2 / 105$$

$$\int_{\Omega_i} \frac{y'^2}{\ell_e^2} (\frac{dN_3}{d\xi})^2 dv = \frac{I_{zz}}{\ell_e} \int_0^1 (\frac{dN_3}{d\xi})^2 d\xi = \frac{I_{zz}}{\ell_e} \int_0^1 (-6\xi + 6\xi^2)^2 d\xi = \frac{6I_{zz}}{5\ell_e}$$

$$\int_{\Omega_i} \frac{y'^2}{\ell_e^2} \frac{dN_3}{d\xi} \frac{dN_4}{d\xi} dv = I_{zz} \int_0^1 (-6\xi + 6\xi^2)(1 - 4\xi + 3\xi^2) d\xi = \frac{I_{zz}}{10}$$

$$\int_{\Omega_i} \frac{y'^2}{\ell_e^2} \frac{dN_3}{d\xi} \frac{dN_5}{d\xi} dv = \frac{I_{zz}}{\ell_e} \int_0^1 (-6\xi + 6\xi^2)(6\xi - 6\xi^2) d\xi = \frac{-6I_{zz}}{5\ell_e}$$

$$\int_{\Omega_i} \frac{y'^2}{\ell_e^2} \frac{dN_3}{d\xi} \frac{dN_6}{d\xi} dv = I_{zz} \int_0^1 (-6\xi + 6\xi^2)(-2\xi + 3\xi^2) d\xi = \frac{I_{zz}}{10}$$

$$\int_{\Omega_i} \frac{y'^2}{\ell_e^2} (\frac{dN_4}{d\xi})^2 dv = I_{zz} \ell_e \int_0^1 (1 - 4\xi + 3\xi^2)^2 d\xi = \frac{2I_{zz}\ell_e}{15}$$

$$\int_{\Omega_i} \frac{y'^2}{\ell_e^2} \frac{dN_4}{d\xi} \frac{dN_5}{d\xi} dv = I_{zz} \int_0^1 (1 - 4\xi + 3\xi^2)(6\xi - 6\xi^2) d\xi = \frac{-I_{zz}}{10}$$

$$\int_{\Omega_i} \frac{y'^2}{\ell_e^2} \frac{dN_4}{d\xi} \frac{dN_6}{d\xi} dv = I_{zz} \ell_e \int_0^1 (1 - 4\xi + 3\xi^2)(-2\xi + 3\xi^2) d\xi = \frac{-I_{zz}\ell_e}{30}$$

$$\int_{\Omega_i} \frac{y'^2}{\ell_e^2} (\frac{dN_5}{d\xi})^2 dv = \frac{I_{zz}}{\ell_e} \int_0^1 (6\xi - 6\xi^2)(6\xi - 6\xi^2) d\xi = \frac{6I_{zz}}{5\ell_e}$$

$$\int_{\Omega_i} \frac{y'^2}{\ell_e^2} \frac{dN_5}{d\xi} \frac{dN_6}{d\xi} dv = I_{zz} \int_0^1 (6\xi - 6\xi^2)(3\xi^2 - 2\xi) d\xi = \frac{-I_{zz}}{10}$$

$$\int_{\Omega_i} \frac{y'^2}{\ell_e^2} (\frac{dN_6}{d\xi})^2 dv = I_{zz} \ell_e \int_0^1 (-2\xi + 3\xi^2)(-2\xi + 3\xi^2) d\xi = \frac{2I_{zz}\ell_e}{15}$$

The integration terms are calculated in detail as follows:

1. Global Stiffness matrix K

Assuming that the start and the end node number for an arbitrary element are i_1 and i_2, respectively, one has the global stiffness matrix as:

$$K(3i_1 - 2 : 3i_1 : 3i_1 - 2 : 3i_1) = K^e(1:3,1:3) \quad K(3i_1 - 2 : 3i_1 : 3i_2 - 2 : 3i_2) = K^e(1:3,4:6)$$

$$K(3i_2 - 2 : 3i_2 : 3i_1 - 2 : 3i_1) = K^e(4:6,1:3) \quad K(3i_2 - 2 : 3i_2 : 3i_2 - 2 : 3i_2) = K^e(4:6,4:6)$$

2. $I_N = \int_\Omega \rho N dv = \sum_{i=1}^{NE} \int_{\Omega_i} \rho N dv \Big|_{3 \times 3(NE+1)}$

At any arbitrary element, one has:

$$I_N^i = \int_{\Omega_i} N dv = \int_{\Omega_i} \rho \begin{bmatrix} N_1 & -\dfrac{y'}{\ell_e}\dfrac{dN_3}{d\xi} & -\dfrac{y'}{\ell_e}\dfrac{dN_4}{d\xi} & N_2 & -\dfrac{y'}{\ell_e}\dfrac{dN_5}{d\xi} & -\dfrac{y'}{\ell_e}\dfrac{dN_6}{d\xi} \\ 0 & N_3 & N_4 & 0 & N_5 & N_6 \\ 0 & 0 & 0 & 0 & 0 & 0 \end{bmatrix} dv$$

$$= \rho \int_{\Omega_i} \begin{bmatrix} N_1 & 0 & 0 & N_2 & 0 & 0 \\ 0 & N_3 & N_4 & 0 & N_5 & N_6 \\ 0 & 0 & 0 & 0 & 0 & 0 \end{bmatrix} dv = \frac{\rho A \ell_e}{12} \begin{bmatrix} 6 & 0 & 0 & 6 & 0 & 0 \\ 0 & 6 & \ell_e & 0 & 6 & -\ell_e \\ 0 & 0 & 0 & 0 & 0 & 0 \end{bmatrix}$$

where $A=bd$, is the area of the beam intersection, ℓ_e is the length of the element.

Summing up along the entire domain:

$$I_N(:,3(i-1)+1:3(i+1)) = I_N(:,3(i-1)+1:3(i+1)) + I_N^i$$

where $i=1,2,...$ NE. NE is the total number of the elements, I_N is a $3 \times 3(NE+1)$ matrix.

3. $I_{r'} = \int_\Omega \rho r' dv$

$$I_{r'} = \sum_{i=1}^{NE} \int_{\Omega_i} \rho \begin{bmatrix} x' \\ y' \\ z' \end{bmatrix} dv = \sum_{i=1}^{NE} \begin{bmatrix} \int_{\Omega_i} \rho(x'_e + \xi \ell_e) dv \\ 0 \\ 0 \end{bmatrix} = \sum_{i=1}^{NE} \rho A \ell_e \begin{bmatrix} x'_e + \ell_e / 2 \\ 0 \\ 0 \end{bmatrix}$$

If the origin is located at the center of gravity, $I_{r'} = 0$.

3.a) $I_{\tilde{r}} = \int_{\Omega} \rho \tilde{r} dv$

$$I_{\tilde{r}} = \begin{bmatrix} 0 & 0 & 0 \\ 0 & 0 & -I_{r'}(1) \\ 0 & I_{r'}(1) & 0 \end{bmatrix}$$

4. $I_e = \int_{\Omega} \rho e dv = \sum_{i=1}^{NE} \int_{\Omega_i} \rho e dv \bigg|_{3 \times 1}$

$I_e = \int_{\Omega} \rho e dv = \sum_{i=1}^{NE} \int_{\Omega_i} \rho N q^i dv$

$$= \frac{\rho A \ell_e}{12} \begin{bmatrix} 6 & 0 & 0 & 6 & 0 & 0 \\ 0 & 6 & \ell_e & 0 & 6 & -\ell_e \\ 0 & 0 & 0 & 0 & 0 & 0 \end{bmatrix} \begin{bmatrix} u_1^i \\ v_1^i \\ \theta_1^i \\ u_2^i \\ v_2^i \\ \theta_2^i \end{bmatrix} = \sum_{i=1}^{NE} \frac{\rho A \ell_e}{12} \begin{bmatrix} 6(u_1^i + u_2^i) \\ 6(v_1^i + v_2^i) + \ell_e(\theta_1^i - \theta_2^i) \\ 0 \end{bmatrix}$$

4.a) $I_{\tilde{e}} = \int_{\Omega} \rho \tilde{e} dv \bigg|_{3 \times 3}$

$$I_{\tilde{e}} = \begin{bmatrix} 0 & 0 & I_e(2) \\ 0 & 0 & -I_e(1) \\ -I_e(2) & I_e(1) & 0 \end{bmatrix}$$

5. $I_{\dot{e}} = \int_{\Omega} \rho \dot{e} dv \bigg|_{3 \times 1}$

$$\int_{\Omega} \rho \dot{e} dv = \sum_{i=1}^{NE} \int_{\Omega_i} N \dot{q}^i dv = \sum_{i=1}^{NE} \frac{\rho A \ell_e}{12} \begin{bmatrix} 6(\dot{u}_1^i + \dot{u}_2^i) \\ 6(\dot{v}_1^i + \dot{v}_2^i) + \ell_e(\dot{\theta}_1^i - \dot{\theta}_2^i) \\ 0 \end{bmatrix}$$

6. $I_{\tilde{r}\tilde{r}'} = \int_{\Omega} \rho \tilde{r} \tilde{r}' dv \bigg|_{3 \times 3}$

The result of the product of skew matrices is given as:

$$\widetilde{r}'\,\widetilde{r}' =$$

$$\begin{bmatrix} -y'^2 - z'^2 & x'y' & x'z' \\ & -x'^2 - z'^2 & y'z' \\ sym. & & -x'^2 - y'^2 \end{bmatrix} = \begin{bmatrix} -y'^2 - z'^2 & (x'_e + \xi\ell_e)y' & (x'_e + \xi\ell_e)z' \\ & -(x'_e + \xi\ell_e)^2 - z'^2 & y'z' \\ sym. & & -(x'_e + \xi\ell_e)^2 - y'^2 \end{bmatrix}$$

The mass moment of inertia at any arbitrary element is then integrated as

$$\int_{\Omega_i} \rho\widetilde{r}\,\widetilde{r}'\,dv = \iiint \rho\widetilde{r}\,\widetilde{r}'\,dxdydz = \ell_e \iiint \rho\widetilde{r}\,\widetilde{r}'\,d\xi dydz$$

$$= -\rho A\ell_e \begin{bmatrix} \dfrac{d^2 + b^2}{12} & 0 & 0 \\[3mm] 0 & x_e'^2 + x_e'\ell_e + \dfrac{1}{3}\ell_e^2 + \dfrac{1}{12}b^2 & 0 \\[3mm] 0 & 0 & x_e'^2 + x_e'\ell_e + \dfrac{1}{3}\ell_e^2 + \dfrac{1}{12}d^2 \end{bmatrix}$$

Summing up along the entire domain, one has:

$$I_{\widetilde{r}\widetilde{r}'} = \sum_{i=1}^{NE} -\frac{\rho A\ell_e}{12} \begin{bmatrix} d^2 + b^2 & 0 & 0 \\ 0 & 12x_e'^2 + 12x_e'\ell_e + 4\ell_e^2 + b^2 & 0 \\ 0 & 0 & 12x_e'^2 + 12x_e'\ell_e + 4\ell_e^2 + d^2 \end{bmatrix}$$

7. $I_{\widetilde{e}\widetilde{r}'} = \int_{\Omega} \rho\widetilde{e}\widetilde{r}'\,dv\Big|_{3\times3}$

$$\widetilde{e}\widetilde{r}' = \begin{bmatrix} 0 & -w & v \\ w & 0 & -u \\ -v & u & 0 \end{bmatrix}\begin{bmatrix} 0 & -z' & y' \\ z' & 0 & -x' \\ -y' & x' & 0 \end{bmatrix} = \begin{bmatrix} -wz'-vy' & vx' & wx' \\ uy' & -wz'-ux' & wy' \\ uz' & vz' & -vy'-ux' \end{bmatrix}$$

The integration of the above term over the sectional area results in the following matrix:

$$\int_{\Omega_i} \widetilde{e}\widetilde{r}'\,dv = \int_{\Omega_i} \begin{bmatrix} 0 & (x'_e + \xi\ell_e)v & 0 \\ y'u & -(x'_e + \xi\ell_e)u & 0 \\ 0 & 0 & -(x'_e + \xi\ell_e)u \end{bmatrix} dv$$

$$\int_{\Omega_i} (x'_e + \xi\ell_e)v\,dv = \int_{\Omega_i} (x'_e + \xi\ell_e)(N_3 v_1 + N_4\theta_1 + N_5 v_2 + N_6\theta_2)\,dv$$

$$= A\ell_e \int_0^1 x'_e (N_3 v_1 + N_4\theta_1 + N_5 v_2 + N_6\theta_2)\,d\xi + A\ell_e \int_0^1 \xi\ell_e(N_3 v_1 + N_4\theta_1 + N_5 v_2 + N_6\theta_2)\,d\xi$$

$$\int_{\Omega_i} (x'_e + \xi\ell_e)v\,dv = A\ell_e x'_e\left(\frac{v_1}{2} + \frac{\ell_e\theta_1}{12} + \frac{v_2}{2} - \frac{\ell_e\theta_2}{12}\right) + A\ell_e^2\left(\frac{3v_1}{20} + \frac{\ell_e\theta_1}{30} + \frac{7v_2}{20} - \frac{\ell_e\theta_2}{20}\right)$$

$$= A\ell_e / 60\left[(30x'_e + 9\ell_e)v_1 + (5x'_e + 2\ell_e)\ell_e\theta_1 + (30x'_e + 21\ell_e)v_2 - (5x'_e + 3\ell_e)\ell_e\theta_2\right]$$

$$\int_{\Omega_i} y'u\,dv = \int_{\Omega_i} y'\left(N_1 u_1 - \frac{y'}{\ell_e}\frac{dN_3}{d\xi}v_1 - \frac{y'}{\ell_e}\frac{dN_4}{d\xi}\theta_1 + N_2 u_2 - \frac{y'}{\ell_e}\frac{dN_5}{d\xi}v_2 - \frac{y'}{\ell_e}\frac{dN_6}{d\xi}\theta_2 \right)dv$$

$$= \int_{\Omega_i} y'\left(-\frac{y'}{\ell_e}\frac{dN_3}{d\xi}v_1 - \frac{y'}{\ell_e}\frac{dN_4}{d\xi}\theta_1 - \frac{y'}{\ell_e}\frac{dN_5}{d\xi}v_2 - \frac{y'}{\ell_e}\frac{dN_6}{d\xi}\theta_2 \right)dv$$

$$= -I_{zz}\int_0^1 \left(\frac{dN_3}{d\xi}v_1 + \frac{dN_4}{d\xi}\theta_1 + \frac{dN_5}{d\xi}v_2 + \frac{dN_6}{d\xi}\theta_2 \right)d\xi = I_{zz}(v_1 - v_2)$$

where $I_{zz} = \dfrac{bd^3}{12}$ is the moment inertia along the z' axis.

$$\int_{\Omega_i}(x_e' + \ell_e\xi)u\,dv = \int_{\Omega_i}(x_e' + \ell_e\xi)\left(N_1 u_1 - \frac{y}{\ell_e}\frac{dN_3}{d\xi}v_1 - \frac{y}{\ell_e}\frac{dN_4}{d\xi}\theta_1 + N_2 u_2 - \frac{y}{\ell_e}\frac{dN_5}{d\xi}v_2 - \frac{y}{\ell_e}\frac{dN_6}{d\xi}\theta_2 \right)dv$$

$$= \int_{\Omega_i}(x_e' + \ell_e\xi)(N_1 u_1 + N_2 u_2)\,dv = A\ell_e\left[\int_0^1 x_e'(N_1 u_1 + N_2 u_2)\,d\xi + \int_0^1 \ell_e\xi(N_1 u_1 + N_2 u_2)\,d\xi \right]$$

$$\int_{\Omega_i}(x_e' + \ell_e\xi)u\,dv = A\ell_e\left[(x_e'/2 + \ell_e/6)u_1 + (x_e'/2 + \ell_e/3)u_2 \right]$$

Summing up along the entire domain:

$$I_{\widetilde{er}'}(1,2) = \sum_{i=1}^{NE}\rho A\ell_e/60\left[(30x_e' + 9\ell_e)v_1 + (5x_e' + 2\ell_e)\ell_e\theta_1 + (30x_e' + 21\ell_e)v_2 - (5x_e' + 3\ell_e)\ell_e\theta_2 \right]$$

$$I_{\widetilde{er}'}(2,1) = \sum_{i=1}^{NE}\rho I_{zz}(v_1 - v_2)$$

$$I_{\widetilde{er}'}(2,2) = I_{\widetilde{er}'}(3,3) = \sum_{i=1}^{NE} -\frac{\rho A\ell_e}{6}\left[(3x_e' + \ell_e)u_1 + (3x_e' + 2\ell_e)u_2 \right]$$

7.a) $I_{\widetilde{re}} = \int_\Omega \rho \widetilde{r}\widetilde{e}\,dv\big|_{3\times3}$

Since $(\widetilde{er}')^T = \widetilde{r}'^T\widetilde{e}^T = \widetilde{r}\widetilde{e}$, One has: $I_{\widetilde{re}} = I_{\widetilde{er}'}^T$

8. $I_{\widetilde{er}'} = \int_\Omega \rho \widetilde{e}\widetilde{r}'\,dv\big|_{3\times3}$

$$\widetilde{e}\widetilde{r}' = \begin{bmatrix} 0 & 0 & \dot{v} \\ 0 & 0 & -\dot{u} \\ -\dot{v} & \dot{u} & 0 \end{bmatrix}\begin{bmatrix} 0 & -z' & y' \\ z' & 0 & -x' \\ -y' & x' & 0 \end{bmatrix} = \begin{bmatrix} -\dot{v}y' & \dot{v}x' & 0 \\ \dot{u}y' & -\dot{u}x' & 0 \\ \dot{u}z' & \dot{v}z' & -\dot{v}y'-\dot{u}x' \end{bmatrix}$$

$$\int_{\Omega_i} \widetilde{e}\widetilde{r}'dv = \int_{\Omega_i} \begin{bmatrix} 0 & \dot{v}x' & 0 \\ \dot{u}y' & -\dot{u}x' & 0 \\ 0 & 0 & -\dot{u}x' \end{bmatrix} dv$$

According to the results in the integration $I_{\widetilde{e}\widetilde{r}'}$:

$$I_{\widetilde{e}\widetilde{r}'}(1,2) = \sum_{i=1}^{NE} \frac{\rho A \ell_e}{60} \left[(30x'_e + 9\ell_e)\dot{v}_1 + (5x'_e + 2\ell_e)\ell_e\dot{\theta}_1 + (30x'_e + 21\ell_e)\dot{v}_2 - (5x'_e + 3\ell_e)\ell_e\dot{\theta}_2 \right]$$

$$I_{\widetilde{e}\widetilde{r}'}(2,1) = \sum_{i=1}^{NE} \rho I_{zz}(\dot{v}_1 - \dot{v}_2); \quad I_{\widetilde{e}\widetilde{r}'}(2,2) = I_{\widetilde{e}\widetilde{r}'}(3,3) = \sum_{i=1}^{NE} -\frac{\rho A \ell_e}{6} \left[(3x'_e + \ell_e)\dot{u}_1 + (3x'_e + 2\ell_e)\dot{u}_2 \right]$$

$9. I_{\widetilde{e}\widetilde{e}} = \int_{\Omega} \rho \widetilde{e}\widetilde{e} \, dv \big|_{3\times 3}$

$$\widetilde{e}\widetilde{e} = \begin{bmatrix} 0 & -w & v \\ w & 0 & -u \\ -v & u & 0 \end{bmatrix} \begin{bmatrix} 0 & -w & v \\ w & 0 & -u \\ -v & u & 0 \end{bmatrix} = \begin{bmatrix} -w^2 - v^2 & uv & uw \\ uv & -u^2 - w^2 & vw \\ uw & vw & -u^2 - v^2 \end{bmatrix}$$

Further, for a 2D problem, one has $w = 0$. As a result, the product $\widetilde{e}\widetilde{e}$ becomes

$$\widetilde{e}\widetilde{e} = \begin{bmatrix} -v^2 & uv & 0 \\ uv & -u^2 & 0 \\ 0 & 0 & -u^2 - v^2 \end{bmatrix}$$

Now, one can integrate each of those non-zero terms in the matrix separately to obtain

$$v^2 = (N_3v_1 + N_4\theta_1 + N_5v_2 + N_6\theta_2)(N_3v_1 + N_4\theta_1 + N_5v_2 + N_6\theta_2)$$

$$= (v_1^2 N_3^2 + 2v_1v_2N_3N_5 + v_2^2 N_5^2) + (2v_1\theta_1 N_3N_4 + 2v_1\theta_2 N_3N_6 + 2\theta_1 v_2 N_4N_5 + 2v_2\theta_2 N_5N_6)$$

$$+ (\theta_1^2 N_4^2 + 2\theta_1\theta_2 N_4N_6 + \theta_2^2 N_6^2)$$

$$\int_{\Omega_i} v^2 dv = A\ell_e \left(\frac{13}{35}v_1^2 + \frac{9}{35}v_1v_2 + \frac{13}{35}v_2^2 \right) + A\ell_e^2 \left(\frac{11}{105}v_1\theta_1 - \frac{13}{210}v_1\theta_2 + \frac{13}{210}v_2\theta_1 - \frac{11}{105}v_2\theta_2 \right)$$

$$+ A\ell_e^3 \left(\frac{1}{105}\theta_1^2 - \frac{1}{70}\theta_1\theta_2 + \frac{1}{105}\theta_2^2 \right)$$

$$uv = \left(N_1u_1 - \frac{y}{\ell_e}\frac{dN_3}{d\xi}v_1 - \frac{y}{\ell_e}\frac{dN_4}{d\xi}\theta_1 + N_2u_2 - \frac{y}{\ell_e}\frac{dN_5}{d\xi}v_2 - \frac{y}{\ell_e}\frac{dN_6}{d\xi}\theta_2 \right) \cdots$$

$$(N_3v_1 + N_4\theta_1 + N_5v_2 + N_6\theta_2)$$

$$\int_{\Omega_i} uv \, dv = \int_{\Omega_i} (N_1u_1 + N_2u_2)(N_3v_1 + N_4\theta_1 + N_5v_2 + N_6\theta_2) \, dv$$

$$= \int_{\Omega_i} N_1 u_1 (N_3 v_1 + N_4 \theta_1 + N_5 v_2 + N_6 \theta_2) dv + \int_{\Omega_i} N_2 u_2 (N_3 v_1 + N_4 \theta_1 + N_5 v_2 + N_6 \theta_2) dv$$

$$\int_{\Omega_i} uv \, dv = A\ell_e \left[u_1 \left(\frac{7}{20} v_1 + \frac{1}{20} \ell_e \theta_1 + \frac{3}{20} v_2 - \frac{1}{30} \ell_e \theta_2 \right) + u_2 \left(\frac{3}{20} v_1 + \frac{1}{30} \ell_e \theta_1 + \frac{7}{20} v_2 - \frac{1}{20} \ell_e \theta_2 \right) \right]$$

$$\int_{\Omega_i} u^2 \, dv = \int_{\Omega_i} \left(N_1 u_1 - \frac{y'}{\ell_e} \frac{dN_3}{d\xi} v_1 - \frac{y'}{\ell_e} \frac{dN_4}{d\xi} \theta_1 + N_2 u_2 - \frac{y'}{\ell_e} \frac{dN_5}{d\xi} v_2 - \frac{y'}{\ell_e} \frac{dN_6}{d\xi} \theta_2 \right)^2 dv$$

$$= \int_{\Omega_i} N_1 u_1 (N_1 u_1 + N_2 u_2) dv + \int_{\Omega_i} N_2 u_2 (N_1 u_1 + N_2 u_2) dv$$

$$+ \int_\Omega \left(\frac{y'^2}{\ell_e^2} (\frac{dN_3}{d\xi})^2 v_1^2 + \frac{y'^2}{\ell_e^2} \frac{dN_3}{d\xi} \frac{dN_5}{d\xi} 2 v_1 v_2 + \frac{y'^2}{\ell_e^2} (\frac{dN_5}{d\xi})^2 v_2^2 \right) dv$$

$$+ \int_\Omega \left(\frac{y'^2}{\ell_e^2} \frac{dN_3}{d\xi} \frac{dN_4}{d\xi} 2 v_1 \theta_1 + \frac{y'^2}{\ell_e^2} \frac{dN_3}{d\xi} \frac{dN_6}{d\xi} 2 v_1 \theta_2 + \frac{y'^2}{\ell_e^2} \frac{dN_4}{d\xi} \frac{dN_5}{d\xi} 2 v_2 \theta_1 + \frac{y'^2}{\ell_e^2} \frac{dN_5}{d\xi} \frac{dN_6}{d\xi} 2 v_2 \theta_2 \right) dv$$

$$+ \int_\Omega \left(\frac{y'^2}{\ell_e^2} (\frac{dN_4}{d\xi})^2 \theta_1^2 + \frac{y'^2}{\ell_e^2} \frac{dN_4}{d\xi} \frac{dN_6}{d\xi} 2 \theta_1 \theta_2 + \frac{y'^2}{\ell_e^2} (\frac{dN_6}{d\xi})^2 \theta_2^2 \right) dv$$

$$\int_{\Omega_i} u^2 \, dv = \frac{A\ell_e}{3} (u_1^2 + u_1 u_2 + u_2^2) + \frac{6 I_{zz}}{5 \ell_e} (v_1^2 - 2 v_1 v_2 + v_2^2)$$

$$+ \frac{I_{zz}}{10} (2 v_1 \theta_1 + 2 v_1 \theta_2 - 2 v_2 \theta_1 - 2 v_2 \theta_2) + \frac{I_{zz} \ell_e}{15} (2 \theta_1^2 - \theta_1 \theta_2 + 2 \theta_2^2)$$

$$I_{\tilde{e}\tilde{e}}(1,1) = \sum_{i=1}^{NE} -\frac{\rho A \ell_e}{210} \left[(78 v_1^2 + 54 v_1 v_2 + 78 v_2^2) + 22 \ell_e (v_1 \theta_1 - v_2 \theta_2) + 13 \ell_e (v_2 \theta_1 - v_1 \theta_2) \right.$$

$$+ \ell_e^2 (2 \theta_1^2 - 3 \theta_1 \theta_2 + 2 \theta_2^2) \Big]$$

$$I_{\tilde{e}\tilde{e}}(1,2) = I_{\tilde{e}\tilde{e}}(2,1) = \sum_{i=1}^{NE} \frac{\rho A \ell_e}{60} \left[u_1 (21 v_1 + 3 \ell_e \theta_1 + 9 v_2 - 2 \ell_e \theta_2) + u_2 (9 v_1 + 2 \ell_e \theta_1 + 21 v_2 - 3 \ell_e \theta_2) \right]$$

$$I_{\tilde{e}\tilde{e}}(2,2) = \sum_{i=1}^{NE} \left\{ -\frac{\rho A \ell_e}{3} (u_1^2 + u_1 u_2 + u_2^2) - \ldots \right.$$

$$\frac{\rho I_{zz}}{15 \ell_e} \left[18 (v_1 - v_2)^2 + 3 \ell_e (\theta_1 + \theta_2)(v_1 - v_2) + \ell_e^2 (2 \theta_1^2 - \theta_1 \theta_2 + 2 \theta_2^2) \right] \Big\}$$

$$I_{\tilde{e}\tilde{e}}(3,3) = I_{\tilde{e}\tilde{e}}(1,1) + I_{\tilde{e}\tilde{e}}(2,2)$$

$$10. \ I_{\tilde{e}\tilde{e}} = \int_\Omega \rho \tilde{e} \tilde{e} \, dv \Big|_{3 \times 3}$$

$$\tilde{e}\tilde{e} = \begin{bmatrix} 0 & 0 & \dot{v} \\ 0 & 0 & -\dot{u} \\ -\dot{v} & \dot{u} & 0 \end{bmatrix} \begin{bmatrix} 0 & 0 & v \\ 0 & 0 & -u \\ -v & u & 0 \end{bmatrix} = \begin{bmatrix} -\dot{v}v & \dot{v}u & 0 \\ \dot{u}v & -\dot{u}u & 0 \\ 0 & 0 & -\dot{u}u - \dot{v}v \end{bmatrix}$$

$$\dot{v}v = (N_3\dot{v}_1 + N_4\dot{\theta}_1 + N_5\dot{v}_2 + N_6\dot{\theta}_2)(N_3v_1 + N_4\theta_1 + N_5v_2 + N_6\theta_2)$$

$$= [\dot{v}_1v_1N_3^2 + (\dot{v}_1v_2 + \dot{v}_2v_1)N_3N_5 + \dot{v}_2v_2N_5^2]$$

$$+ [(\dot{v}_1\theta_1 + \dot{\theta}_1v_1)N_3N_4 + (\dot{v}_1\theta_2 + \dot{\theta}_2v_1)N_3N_6 + (\dot{\theta}_1v_2 + \dot{v}_2\theta_1)N_4N_5 + (\dot{v}_2\theta_2 + \dot{\theta}_2v_2)N_5N_6]$$

$$+ [\dot{\theta}_1\theta_1N_4^2 + (\dot{\theta}_1\theta_2 + \dot{\theta}_2\theta_1)N_4N_6 + \dot{\theta}_2\theta_2N_6^2]$$

$$\int_{\Omega_i}\dot{v}vdv = A\ell_e\left\{\left[\frac{13}{35}\dot{v}_1v_1 + \frac{9}{70}(\dot{v}_1v_2 + \dot{v}_2v_1) + \frac{13}{35}\dot{v}_2v_2\right]\right.$$

$$+ \left[\frac{11\ell_e}{210}(\dot{v}_1\theta_1 + \dot{\theta}_1v_1) - \frac{13\ell_e}{420}(\dot{v}_1\theta_2 + \dot{\theta}_2v_1) + \frac{13\ell_e}{420}(\dot{\theta}_1v_2 + \theta_1\dot{v}_2) - \frac{11\ell_e}{210}(\dot{\theta}_2v_2 + \dot{v}_2\theta_2)\right]$$

$$+ \left.\left[\frac{\ell_e^2}{105}\dot{\theta}_1\theta_1 - \frac{\ell_e^2}{140}(\dot{\theta}_1\theta_2 + \dot{\theta}_2\theta_1) + \frac{\ell_e^2}{105}\dot{\theta}_2\theta_2\right]\right\}$$

$$\int_{\Omega_i}\dot{v}udv = \int_{\Omega_i}\left[(N_3\dot{v}_1 + N_4\dot{\theta}_1 + N_5\dot{v}_2 + N_6\dot{\theta}_2)\cdot\right.$$

$$\left.\left(N_1u_1 - \frac{y'}{\ell_e}\frac{dN_3}{d\xi}v_1 - \frac{y'}{\ell_e}\frac{dN_4}{d\xi}\theta_1 + N_2u_2 - \frac{y'}{\ell_e}\frac{dN_5}{d\xi}v_2 - \frac{y'}{\ell_e}\frac{dN_6}{d\xi}\theta_2\right)\right]dv$$

$$= \int_{\Omega_i}(N_3\dot{v}_1 + N_4\dot{\theta}_1 + N_5\dot{v}_2 + N_6\dot{\theta}_2)(N_1u_1 + N_2u_2)dv$$

$$= \int_{\Omega_i}(N_3\dot{v}_1 + N_4\dot{\theta}_1 + N_5\dot{v}_2 + N_6\dot{\theta}_2)N_1u_1dv + \int_{\Omega_i}(N_3\dot{v}_1 + N_4\dot{\theta}_1 + N_5\dot{v}_2 + N_6\dot{\theta}_2)N_2u_2dv$$

$$= \int_{\Omega_i}(N_1N_3\dot{v}_1 + N_1N_4\dot{\theta}_1 + N_1N_5\dot{v}_2 + N_1N_6\dot{\theta}_2)u_1dv + \int_{\Omega_i}(N_2N_3\dot{v}_1 + N_2N_4\dot{\theta}_1 + N_2N_5\dot{v}_2 + N_2N_6\dot{\theta}_2)u_2dv$$

$$\int_{\Omega_i}\dot{v}udv = A\ell_e\left(\frac{7}{20}\dot{v}_1 + \frac{\ell_e}{20}\dot{\theta}_1 + \frac{3}{20}\dot{v}_2 - \frac{\ell_e}{30}\dot{\theta}_2\right)u_1 + A\ell_e\left(\frac{3}{20}\dot{v}_1 + \frac{\ell_e}{30}\dot{\theta}_1 + \frac{7}{20}\dot{v}_2 - \frac{\ell_e}{20}\dot{\theta}_2\right)u_2$$

Similarly, one has:

$$\int_{\Omega_i}\dot{u}vdv = \int_{\Omega_i}(N_1\dot{u}_1 + N_2\dot{u}_2)(N_3v_1 + N_4\theta_1 + N_5v_2 + N_6\theta_2)dv =$$

$$= A\ell_e\left[\dot{u}_1\left(\frac{7}{20}v_1 + \frac{\ell_e}{20}\theta_1 + \frac{3}{20}v_2 - \frac{\ell_e}{30}\theta_2\right) + \dot{u}_2\left(\frac{3}{20}v_1 + \frac{\ell_e}{30}\theta_1 + \frac{7}{20}v_2 - \frac{\ell_e}{20}\theta_2\right)\right]$$

$$\int_{\Omega_i}\dot{u}udv = \int_{\Omega_i}\left[\left(N_1\dot{u}_1 - \frac{y'}{\ell_e}\frac{dN_3}{d\xi}\dot{v}_1 - \frac{y'}{\ell_e}\frac{dN_4}{d\xi}\dot{\theta}_1 + N_2\dot{u}_2 - \frac{y'}{\ell_e}\frac{dN_5}{d\xi}\dot{v}_2 - \frac{y'}{\ell_e}\frac{dN_6}{d\xi}\dot{\theta}_2\right)\right.$$

$$\left.\cdot\left(N_1u_1 - \frac{y'}{\ell_e}\frac{dN_3}{d\xi}v_1 - \frac{y'}{\ell_e}\frac{dN_4}{d\xi}\theta_1 + N_2u_2 - \frac{y'}{\ell_e}\frac{dN_5}{d\xi}v_2 - \frac{y'}{\ell_e}\frac{dN_6}{d\xi}\theta_2\right)\right]dv$$

$$= \int_{\Omega_i} N_1 \dot{u}_1 (N_1 u_1 + N_2 u_2) dv + \int_{\Omega_i} N_2 \dot{u}_2 (N_1 u_1 + N_2 u_2) dv$$

$$+ \int_{\Omega_i} \left(\frac{y'^2}{\ell_e^2} (\frac{dN_3}{d\xi})^2 \dot{v}_1 v_1 + \frac{y'^2}{\ell_e^2} \frac{dN_3}{d\xi} \frac{dN_5}{d\xi} (\dot{v}_1 v_2 + \dot{v}_2 v_1) + \frac{y'^2}{\ell_e^2} (\frac{dN_5}{d\xi})^2 \dot{v}_2 v_2 \right) dv$$

$$\int_{\Omega_i} \left[\frac{y'^2}{\ell_e^2} \frac{dN_3}{d\xi} \frac{dN_4}{d\xi} (\dot{v}_1 \theta_1 + \dot{\theta}_1 v_1) + \frac{y'^2}{\ell_e^2} \frac{dN_3}{d\xi} \frac{dN_6}{d\xi} (\dot{v}_1 \theta_2 + \dot{\theta}_2 v_1) \right.$$

$$\left. \frac{y'^2}{\ell_e^2} \frac{dN_4}{d\xi} \frac{dN_5}{d\xi} (\dot{v}_2 \theta_1 + \dot{\theta}_1 v_2) + \frac{y'^2}{\ell_e^2} \frac{dN_5}{d\xi} \frac{dN_6}{d\xi} (\dot{v}_2 \theta_2 + \dot{\theta}_2 v_2) \right] dv$$

$$+ \int_{\Omega_i} \left(\frac{y'^2}{\ell_e^2} (\frac{dN_4}{d\xi})^2 \dot{\theta}_1 \theta_1 + \frac{y'^2}{\ell_e^2} \frac{dN_4}{d\xi} \frac{dN_6}{d\xi} (\dot{\theta}_1 \theta_2 + \dot{\theta}_2 \theta_1) + \frac{y'^2}{\ell_e^2} (\frac{dN_6}{d\xi})^2 \dot{\theta}_2 \theta_2 \right) dv$$

$$\int_{\Omega_i} \dot{u} u \, dv = A\ell_e (\dot{u}_1 u_1 / 3 + \dot{u}_1 u_2 / 6) + A\ell_e (\dot{u}_2 u_1 / 6 + \dot{u}_2 u_2 / 3)$$

$$+ \frac{6 I_{zz}}{5 \ell_e} \left[\dot{v}_1 v_1 - (\dot{v}_1 v_2 + \dot{v}_2 v_1) + \dot{v}_2 v_2 \right]$$

$$+ \frac{I_{zz}}{10} \left[(\dot{v}_1 \theta_1 + \dot{\theta}_1 v_1) + (\dot{v}_1 \theta_2 + \dot{\theta}_2 v_1) - (\dot{v}_2 \theta_1 + \dot{\theta}_1 v_2) - (\dot{v}_2 \theta_2 + \dot{\theta}_2 v_2) \right]$$

$$+ \frac{I_{zz} \ell_e}{30} \left[4 \dot{\theta}_1 \theta_1 - (\dot{\theta}_1 \theta_2 + \dot{\theta}_2 \theta_1) + 4 \dot{\theta}_2 \theta_2 \right]$$

$$I_{\tilde{e}\tilde{e}}(1,1) =$$

$$\sum_{i=1}^{NE} -\frac{\rho A \ell_e}{420} \left[(156 \dot{v}_1 v_1 + 54(\dot{v}_1 v_2 + v_1 \dot{v}_2) + 156 \dot{v}_2 v_2) + 22 \ell_e [(\dot{v}_1 \theta_1 + v_1 \dot{\theta}_1) - (\dot{v}_2 \theta_2 + v_2 \dot{\theta}_2)] \right.$$

$$\left. + 13 \ell_e [(v_2 \dot{\theta}_1 + \dot{v}_2 \theta_1) - (\dot{v}_1 \theta_2 + v_1 \dot{\theta}_2)] + \ell_e^2 (4 \dot{\theta}_1 \theta_1 - 3 \dot{\theta}_1 \theta_2 - 3 \theta_1 \dot{\theta}_2 + 4 \dot{\theta}_2 \theta_2) \right]$$

$$I_{\tilde{e}\tilde{e}}(1,2) = \sum_{i=1}^{NE} \frac{\rho A \ell_e}{60} \left[u_1 (21 \dot{v}_1 + 3 \ell_e \dot{\theta}_1 + 9 \dot{v}_2 - 2 \ell_e \dot{\theta}_2) + u_2 (9 \dot{v}_1 + 2 \ell_e \dot{\theta}_1 + 21 \dot{v}_2 - 3 \ell_e \dot{\theta}_2) \right]$$

$$I_{\tilde{e}\tilde{e}}(2,1) = \sum_{i=1}^{NE} \frac{\rho A \ell_e}{60} \left[\dot{u}_1 (21 v_1 + 3 \ell_e \theta_1 + 9 v_2 - 2 \ell_e \theta_2) + \dot{u}_2 (9 v_1 + 2 \ell_e \theta_1 + 21 v_2 - 3 \ell_e \theta_2) \right]$$

$$I_{\tilde{e}\tilde{e}}(2,2) = \sum_{i=1}^{NE} -\frac{\rho A \ell_e}{6} (2 \dot{u}_1 u_1 + \dot{u}_1 u_2 + \dot{u}_2 u_1 + 2 \dot{u}_2 u_2) - \sum_{i=1}^{NE} \frac{\rho I_{zz}}{30 \ell_e} \{ 36 (\dot{v}_1 - \dot{v}_2)(v_1 - v_2) \right.$$

$$\left. + 3 \ell_e [(\dot{v}_1 - \dot{v}_2)(\theta_1 + \theta_2) + (v_1 - v_2)(\dot{\theta}_1 + \dot{\theta}_2)] + \ell_e^2 [4 \dot{\theta}_1 \theta_1 - \dot{\theta}_1 \theta_2 - \dot{\theta}_2 \theta_1 + 4 \dot{\theta}_2 \theta_2] \}$$

$$I_{\tilde{e}\tilde{e}}(3,3) = I_{\tilde{e}\tilde{e}}(1,1) + I_{\tilde{e}\tilde{e}}(2,2)$$

11. $I_{\tilde{r}' \tilde{\omega}' N} = \int_{\Omega} \rho \tilde{r}' \tilde{\omega}' N dv \big|_{3 \times 3(NE+1)}$

Since $\tilde{r}' \tilde{\omega}' = \omega'^T r' - r'^T \omega'$

$$I_{\tilde{r}'\bar{\omega}'N} = \int_\Omega \rho \tilde{r}'\bar{\omega}'N dv = \int_\Omega \rho \left(\omega' r'^T - r'^T \omega'\right) N dv = \omega' \int_\Omega \rho r'^T N dv - \int_\Omega \rho r'^T \omega'N dv$$

$$r'^T N = \begin{bmatrix} x' \\ y' \\ z' \end{bmatrix}^T \begin{bmatrix} N_1 & -\dfrac{y'}{\ell_e}\dfrac{dN_3}{d\xi} & -\dfrac{y'}{\ell_e}\dfrac{dN_4}{d\xi} & N_2 & -\dfrac{y'}{\ell_e}\dfrac{dN_5}{d\xi} & -\dfrac{y'}{\ell_e}\dfrac{dN_6}{d\xi} \\ 0 & N_3 & N_4 & 0 & N_5 & N_6 \\ 0 & 0 & 0 & 0 & 0 & 0 \end{bmatrix}$$

$$= \begin{bmatrix} x'N_1 & -x'\dfrac{y'}{\ell_e}\dfrac{dN_3}{d\xi}+y'N_3 & -x'\dfrac{y'}{\ell_e}\dfrac{dN_4}{d\xi}+y'N_4 & x'N_2 & -x'\dfrac{y'}{\ell_e}\dfrac{dN_5}{d\xi}+y'N_5 & -x'\dfrac{y'}{\ell_e}\dfrac{dN_6}{d\xi}+y'N_6 \end{bmatrix}$$

After integration of the above term over y' and z' for any arbitrary element, one has:

$$\int_{\Omega_i} r'^T N\, dv = \int_{\Omega_i} \left[(x'_e + \xi \ell_e)N_1 \quad 0 \quad 0 \quad (x'_e + \xi \ell_e)N_2 \quad 0 \quad 0\right] dv$$

$$= \frac{\rho A\ell_e}{6}\left[(3x'_e + \ell_e) \quad 0 \quad 0 \quad (3x'_e + 2\ell_e) \quad 0 \quad 0\right]$$

$$I^i_{r'^T N} \equiv \rho \int_{\Omega_i} r'^T N\, dv = \frac{\rho A\ell_e}{6}\left[(3x'_e + \ell_e) \quad 0 \quad 0 \quad (3x'_e + 2\ell_e) \quad 0 \quad 0\right]$$

$$r'^T \omega'N = \begin{bmatrix} x' \\ y' \\ z' \end{bmatrix}^T \begin{bmatrix} 0 \\ 0 \\ \omega'_z \end{bmatrix} \begin{bmatrix} N_1 & -\dfrac{y'}{\ell_e}\dfrac{dN_3}{d\xi} & -\dfrac{y'}{\ell_e}\dfrac{dN_4}{d\xi} & N_2 & -\dfrac{y'}{\ell_e}\dfrac{dN_5}{d\xi} & -\dfrac{y'}{\ell_e}\dfrac{dN_6}{d\xi} \\ 0 & N_3 & N_4 & 0 & N_5 & N_6 \\ 0 & 0 & 0 & 0 & 0 & 0 \end{bmatrix}$$

$$= z'\omega'_z \begin{bmatrix} N_1 & -\dfrac{y'}{\ell_e}\dfrac{dN_3}{d\xi} & -\dfrac{y'}{\ell_e}\dfrac{dN_4}{d\xi} & N_2 & -\dfrac{y'}{\ell_e}\dfrac{dN_5}{d\xi} & -\dfrac{y'}{\ell_e}\dfrac{dN_6}{d\xi} \\ 0 & N_3 & N_4 & 0 & N_5 & N_6 \\ 0 & 0 & 0 & 0 & 0 & 0 \end{bmatrix}$$

After integration of the above matrix over y' and z', one has $\int_{\Omega_i} r'^T \omega'N dv = 0$.

Finally, $I_{\tilde{r}'\bar{\omega}'N} = \int_\Omega \rho \tilde{r}'\bar{\omega}'N dv = \int_\Omega \rho \left(\omega' r'^T - r'^T \omega'\right) N dv = \omega' \int_\Omega \rho r'^T N dv = \omega' \cdot I_{r'^T N}$

where

$$I_{r'^T N}\left(:,3(i-1)+1:3(i+1)\right) = \sum_{i=1}^{NE} I^i_{r'^T N}$$

12. $I_{\tilde{e}\bar{\omega}'N} = \int_\Omega \rho \tilde{e}\bar{\omega}'N dv\Big|_{3\times3(NE+1)}$

Since $\tilde{e}\bar{\omega}' = \omega'e^T - e^T\omega'$

$$I_{\tilde{e}\bar{\omega}'N} = \int_\Omega \rho \left(\omega'e^T - e^T\omega'\right) N dv = \omega' \int_\Omega \rho e^T N dv - \int_\Omega \rho e^T \omega'N dv$$

$$e^T N = q^T N^T N$$

$$N^T N = \begin{bmatrix} N_1 & 0 & 0 \\ -\dfrac{y'}{\ell_e}\dfrac{dN_3}{d\xi} & N_3 & 0 \\ -\dfrac{y'}{\ell_e}\dfrac{dN_4}{d\xi} & N_4 & 0 \\ N_2 & 0 & 0 \\ -\dfrac{y'}{\ell_e}\dfrac{dN_5}{d\xi} & N_5 & 0 \\ -\dfrac{y'}{\ell_e}\dfrac{dN_6}{d\xi} & N_6 & 0 \end{bmatrix} \begin{bmatrix} N_1 & -\dfrac{y'}{\ell_e}\dfrac{dN_3}{d\xi} & -\dfrac{y'}{\ell_e}\dfrac{dN_4}{d\xi} & N_2 & -\dfrac{y'}{\ell_e}\dfrac{dN_5}{d\xi} & -\dfrac{y'}{\ell_e}\dfrac{dN_6}{d\xi} \\ 0 & N_3 & N_4 & 0 & N_5 & N_6 \\ 0 & 0 & 0 & 0 & 0 & 0 \end{bmatrix} = $$

$$\begin{bmatrix} N_1^2 & -\dfrac{y'}{\ell_e}N_1\dfrac{dN_3}{d\xi} & -\dfrac{y'}{\ell_e}N_1\dfrac{dN_4}{d\xi} & N_1 N_2 & -\dfrac{y'}{\ell_e}N_1\dfrac{dN_5}{d\xi} & -\dfrac{y'}{\ell_e}N_1\dfrac{dN_6}{d\xi} \\ & \dfrac{y'^2}{\ell_e^2}(\dfrac{dN_3}{d\xi})^2+N_3^2 & \dfrac{y'^2}{\ell_e^2}\dfrac{dN_3}{d\xi}\dfrac{dN_4}{d\xi}+N_3 N_4 & -\dfrac{y'N_2}{\ell_e}\dfrac{dN_3}{d\xi} & \dfrac{y'^2}{\ell_e^2}\dfrac{dN_3}{d\xi}\dfrac{dN_5}{d\xi}+N_3 N_5 & \dfrac{y'^2}{\ell_e^2}\dfrac{dN_3}{d\xi}\dfrac{dN_6}{d\xi}+N_3 N_6 \\ & & \dfrac{y'^2}{\ell_e^2}(\dfrac{dN_4}{d\xi})^2+N_4^2 & -\dfrac{y'N_2}{\ell_e}\dfrac{dN_4}{d\xi} & \dfrac{y'^2}{\ell_e^2}\dfrac{dN_4}{d\xi}\dfrac{dN_5}{d\xi}+N_4 N_5 & \dfrac{y'^2}{\ell_e^2}\dfrac{dN_4}{d\xi}\dfrac{dN_6}{d\xi}+N_4 N_6 \\ & & & N_2^2 & -\dfrac{y'N_2}{\ell_e}\dfrac{dN_5}{d\xi} & -\dfrac{y'N_2}{\ell_e}\dfrac{dN_6}{d\xi} \\ & \text{sym} & & & \dfrac{y'^2}{\ell_e^2}(\dfrac{dN_5}{d\xi})^2+N_5^2 & \dfrac{y'^2}{\ell_e^2}\dfrac{dN_5}{d\xi}\dfrac{dN_6}{d\xi}+N_5 N_6 \\ & & & & & \dfrac{y'^2}{\ell_e^2}(\dfrac{dN_6}{d\xi})^2+N_6^2 \end{bmatrix}$$

$$I^i_{N^T N} = \int_{\Omega_i} N^T N\, dv$$

$$= \begin{bmatrix} \dfrac{A\ell_e}{3} & 0 & 0 & \dfrac{A\ell_e}{6} & 0 & 0 \\ & \dfrac{6I_{zz}}{5\ell_e}+\dfrac{13A\ell_e}{35} & \dfrac{I_{zz}}{10}+\dfrac{11A\ell_e^2}{210} & 0 & \dfrac{-6I_{zz}}{5\ell_e}+\dfrac{9A\ell_e}{70} & \dfrac{I_{zz}}{10}-\dfrac{13A\ell_e^2}{420} \\ & & \dfrac{2I_{zz}\ell_e}{15}+\dfrac{A\ell_e^3}{105} & 0 & -\dfrac{I_{zz}}{10}+\dfrac{13A\ell_e^2}{420} & -\dfrac{I_{zz}\ell_e}{30}-\dfrac{A\ell_e^3}{140} \\ & & & \dfrac{A\ell_e}{3} & 0 & 0 \\ & \text{sym} & & & \dfrac{6I_{zz}}{5\ell_e}+\dfrac{13A\ell_e}{35} & -\dfrac{I_{zz}}{10}-\dfrac{11A\ell_e^2}{210} \\ & & & & & \dfrac{2I_{zz}\ell_e}{15}+\dfrac{A\ell_e^3}{105} \end{bmatrix}$$

$$\int_{\Omega_i} e^T N dv = q^{i^T} \int_{\Omega_i} N^T N dv = q^{i^T} \cdot I^i_{N^T N} \equiv I^i_{e^T N}$$

$$= \begin{bmatrix} \dfrac{\rho A \ell_e}{6}(2u_1 + u_2) \\[2mm] \dfrac{\rho A \ell_e}{420}(156v_1 + 22\ell_e\theta_1 + 54v_2 - 13\ell_e\theta_2) + \dfrac{\rho I_{zz}}{10\ell_e}\left[12(v_1 - v_2) + \ell_e(\theta_1 + \theta_2)\right] \\[2mm] \dfrac{\rho A \ell_e^2}{420}(22v_1 + 4\ell_e\theta_1 + 13v_2 - 3\ell_e\theta_2) + \dfrac{\rho I_{zz}}{30}\left(3(v_1 - v_2) + 4\ell_e\theta_1 - \ell_e\theta_2\right) \\[2mm] \dfrac{\rho A \ell_e}{6}(u_1 + 2u_2) \\[2mm] \dfrac{\rho A \ell_e}{420}(54v_1 + 13\ell_e\theta_1 + 156v_2 - 22\ell_e\theta_2) - \dfrac{\rho I_{zz}}{10\ell_e}\left[12(v_1 - v_2) + \ell_e(\theta_1 + \theta_2)\right] \\[2mm] -\dfrac{\rho A \ell_e^2}{420}(13v_1 + 3\ell_e\theta_1 + 22v_2 - 4\ell_e\theta_2) + \dfrac{\rho I_{zz}}{30}\left[3(v_1 - v_2) - \ell_e\theta_1 + 4\ell_e\theta_2\right] \end{bmatrix}^T$$

$$e^T \omega' N = \begin{bmatrix} u \\ v \\ 0 \end{bmatrix}^T \begin{bmatrix} 0 \\ 0 \\ \omega'_z \end{bmatrix} \begin{bmatrix} N_1 & -\dfrac{y'}{\ell_e}\dfrac{dN_3}{d\xi} & -\dfrac{y'}{\ell_e}\dfrac{dN_4}{d\xi} & N_2 & -\dfrac{y'}{\ell_e}\dfrac{dN_5}{d\xi} & -\dfrac{y'}{\ell_e}\dfrac{dN_6}{d\xi} \\ 0 & N_3 & N_4 & 0 & N_5 & N_6 \\ 0 & 0 & 0 & 0 & 0 & 0 \end{bmatrix} = 0$$

Finally, $I_{\widetilde{e}\widetilde{\omega}'N} = \omega' \int_\Omega \rho e^T N dv = \omega' \cdot I_{e^T N}$

where $I_{e^T N}(:,3(i-1)+1 : 3(i+1)) = \displaystyle\sum_{i=1}^{NE} I^i_{e^T N}$

13. $I_{\widetilde{r}'N} = \int_\Omega \rho \widetilde{r}' N dv \Big|_{3\times 3(NE+1)}$

$$\widetilde{r}'N = \begin{bmatrix} 0 & -z' & y' \\ z' & 0 & -x' \\ -y' & x' & 0 \end{bmatrix} \begin{bmatrix} N_1 & -\dfrac{y'}{\ell_e}\dfrac{dN_3}{d\xi} & -\dfrac{y'}{\ell_e}\dfrac{dN_4}{d\xi} & N_2 & -\dfrac{y'}{\ell_e}\dfrac{dN_5}{d\xi} & -\dfrac{y'}{\ell_e}\dfrac{dN_6}{d\xi} \\ 0 & N_3 & N_4 & 0 & N_5 & N_6 \\ 0 & 0 & 0 & 0 & 0 & 0 \end{bmatrix}$$

$$= \begin{bmatrix} 0 & -z'N_3 & -z'N_4 & 0 & -z'N_5 & -z'N_6 \\[2mm] z'N_1 & -\dfrac{y'z'}{\ell_e}\dfrac{dN_3}{d\xi} & -\dfrac{y'z'}{\ell_e}\dfrac{dN_4}{d\xi} & z'N_2 & -\dfrac{y'z'}{\ell_e}\dfrac{dN_5}{d\xi} & -\dfrac{y'z'}{\ell_e}\dfrac{dN_6}{d\xi} \\[2mm] -y'N_1 & \dfrac{y'^2}{\ell_e}\dfrac{dN_3}{d\xi}+x'N_3 & \dfrac{y'^2}{\ell_e}\dfrac{dN_4}{d\xi}+x'N_4 & -y'N_2 & \dfrac{y'^2}{\ell_e}\dfrac{dN_5}{d\xi}+x'N_5 & \dfrac{y'^2}{\ell_e}\dfrac{dN_6}{d\xi}+x'N_6 \end{bmatrix}$$

$$\int_{\Omega_i} \tilde{r}\,'N dv =$$

$$\int_0^1 \begin{bmatrix} 0 & 0 & 0 & 0 & 0 & 0 \\ 0 & 0 & 0 & 0 & 0 & 0 \\ 0 & I_{zz}\dfrac{dN_3}{d\xi}+A\ell_e x'N_3 & I_{zz}\dfrac{dN_4}{d\xi}+A\ell_e x'N_4 & 0 & I_{zz}\dfrac{dN_5}{d\xi}+A\ell_e x'N_5 & I_{zz}\dfrac{dN_6}{d\xi}+A\ell_e x'N_6 \end{bmatrix} d\xi$$

$$\int_0^1 \left(I_{zz}\frac{dN_3}{d\xi}+A\ell_e x'N_3 \right)d\xi = \int_0^1 \left[I_{zz}\frac{dN_3}{d\xi}+A\ell_e (x_e'+\zeta\ell_e)N_3 \right]d\xi = -I_{zz}+A\ell_e\left(\frac{x_e'}{2}+\frac{3\ell_e}{20} \right)$$

$$\int_0^1 \left(I_{zz}\frac{dN_4}{d\xi}+A\ell_e x'N_4 \right)d\xi = A\ell_e\left(\ell_e x_e'/12+\ell_e^2/30\right)$$

$$\int_0^1 \left(I_{zz}\frac{dN_5}{d\xi}+A\ell_e x'N_5 \right)d\xi =I_{zz}+A\ell_e\left(x_e'/2+7\ell_e/20\right)$$

$$\int_0^1 \left(I_{zz}\frac{dN_6}{d\xi}+A\ell_e x'N_6 \right)d\xi =-A\ell_e\left(\ell_e x_e'/12+\ell_e^2/20\right)$$

$$I_{\tilde{r}N}^i(3,2)=-\rho I_{zz}+\rho A\ell_e/20(10x_e'+3\ell_e);\ I_{\tilde{r}N}^i(3,3)=\rho A\ell_e/60\left(5\ell_e x_e'+2\ell_e^2\right)$$

$$I_{\tilde{r}N}^i(3,5)=\rho I_{zz}+\rho A\ell_e/20(10x_e'+7\ell_e);\ I_{\tilde{r}N}^i(3,6)=-\rho A\ell_e/60\left(5\ell_e x_e'+3\ell_e^2\right)$$

$$I_{\tilde{r}N}(:,3(i-1)+1:3(i+1))=I_{\tilde{r}N}(:,3(i-1)+1:3(i+1))+I_{\tilde{r}N}^i$$

14. $I_{\tilde{e}N} = \int_\Omega \rho\tilde{e}N dv\Big|_{3\times 3(NE+1)}$

The product of integrands in a two dimensional problem is given by:

$$\tilde{e}N = \begin{bmatrix} 0 & 0 & v \\ 0 & 0 & -u \\ -v & u & 0 \end{bmatrix} \begin{bmatrix} N_1 & -\dfrac{y'}{\ell_e}\dfrac{dN_3}{d\xi} & -\dfrac{y'}{\ell_e}\dfrac{dN_4}{d\xi} & N_2 & -\dfrac{y'}{\ell_e}\dfrac{dN_5}{d\xi} & -\dfrac{y'}{\ell_e}\dfrac{dN_6}{d\xi} \\ 0 & N_3 & N_4 & 0 & N_5 & N_6 \\ 0 & 0 & 0 & 0 & 0 & 0 \end{bmatrix}$$

$$= \begin{bmatrix} 0 & 0 & 0 & 0 & 0 & 0 \\ 0 & 0 & 0 & 0 & 0 & 0 \\ -vN_1 & \dfrac{y'v}{\ell_e}\dfrac{dN_3}{d\xi}+uN_3 & \dfrac{y'v}{\ell_e}\dfrac{dN_4}{d\xi}+uN_4 & -vN_2 & \dfrac{y'v}{\ell_e}\dfrac{dN_5}{d\xi}+uN_5 & \dfrac{y'v}{\ell_e}\dfrac{dN_6}{d\xi}+uN_6 \end{bmatrix}$$

$$\int_{\Omega_i}\tilde{e}N dv = A\ell_e\int_0^1 \begin{bmatrix} 0 & 0 & 0 & 0 & 0 & 0 \\ 0 & 0 & 0 & 0 & 0 & 0 \\ -vN_1 & uN_3 & uN_4 & -vN_2 & uN_5 & uN_6 \end{bmatrix} d\xi$$

$$\int_{\Omega_i} vN_1 dv = A\ell_e \int_0^l (N_3 v_1 + N_4 \theta_1 + N_5 v_2 + N_6 \theta_2) N_1 d\xi$$

$$= A\ell_e \left(\int_0^l N_1 N_3 v_1 d\xi + \int_0^l N_1 N_4 \theta_1 d\xi + \int_0^l N_1 N_5 v_2 d\xi + \int_0^l N_1 N_6 \theta_2 d\xi \right)$$

$$= A\ell_e (7v_1 / 20 + \ell_e \theta_1 / 20 + 3v_2 / 20 - \ell_e \theta_2 / 30)$$

$$\int_{\Omega_i} vN_2 dv = A\ell_e \int_0^l (N_3 v_1 + N_4 \theta_1 + N_5 v_2 + N_6 \theta_2) N_2 d\xi$$

$$= A\ell_e \left(\int_0^l N_2 N_3 v_1 d\xi + \int_0^l N_2 N_4 \theta_1 d\xi + \int_0^l N_2 N_5 v_2 d\xi + \int_0^l N_2 N_6 \theta_2 d\xi \right)$$

$$= A\ell_e (3v_1 / 20 + \ell_e \theta_1 / 30 + 7v_2 / 20 - \ell_e \theta_2 / 20)$$

$$\int_{\Omega_i} uN_3 dv = \int_{\Omega_i} \left(N_1 u_1 - \frac{y'}{\ell_e} \frac{dN_3}{d\xi} v_1 - \frac{y'}{\ell_e} \frac{dN_4}{d\xi} \theta_1 + N_2 u_2 - \frac{y'}{\ell_e} \frac{dN_5}{d\xi} v_2 - \frac{y'}{\ell_e} \frac{dN_6}{d\xi} \theta_2 \right) N_3 dv$$

$$= \int_{\Omega_i} (N_1 u_1 + N_2 u_2) N_3 dv = A\ell_e (7u_1 / 20 + 3u_2 / 20)$$

$$\int_{\Omega_i} uN_4 dv = \int_{\Omega_i} \left(N_1 u_1 - \frac{y}{\ell_e} \frac{dN_3}{d\xi} v_1 - \frac{y}{\ell_e} \frac{dN_4}{d\xi} \theta_1 + N_2 u_2 - \frac{y}{\ell_e} \frac{dN_5}{d\xi} v_2 - \frac{y}{\ell_e} \frac{dN_6}{d\xi} \theta_2 \right) N_4 dv$$

$$= \int_{\Omega_i} (N_1 u_1 + N_2 u_2) N_4 dv = A\ell_e^2 (u_1 / 20 + u_2 / 30)$$

$$\int_{\Omega_i} uN_5 dv = \int_{\Omega_i} \left(N_1 u_1 - \frac{y'}{\ell_e} \frac{dN_3}{d\xi} v_1 - \frac{y'}{\ell_e} \frac{dN_4}{d\xi} \theta_1 + N_2 u_2 - \frac{y'}{\ell_e} \frac{dN_5}{d\xi} v_2 - \frac{y'}{\ell_e} \frac{dN_6}{d\xi} \theta_2 \right) N_5 dv$$

$$= \int_{\Omega_i} (N_1 u_1 + N_2 u_2) N_5 dv = A\ell_e (3u_1 / 20 + 7u_2 / 20)$$

$$\int_{\Omega_i} uN_6 dv = \int_{\Omega_i} \left(N_1 u_1 - \frac{y'}{\ell_e} \frac{dN_3}{d\xi} v_1 - \frac{y'}{\ell_e} \frac{dN_4}{d\xi} \theta_1 + N_2 u_2 - \frac{y'}{\ell_e} \frac{dN_5}{d\xi} v_2 - \frac{y'}{\ell_e} \frac{dN_6}{d\xi} \theta_2 \right) N_6 dv$$

$$= \int_{\Omega_i} (N_1 u_1 + N_2 u_2) N_6 dv = -A\ell_e^2 (u_1 / 30 + u_2 / 20)$$

$$I_{\tilde{e}N}^i(3,1) = -\frac{\rho A \ell_e}{60} (21v_1 + 3\ell_e \theta_1 + 9v_2 - 2\ell_e \theta_2); \quad I_{\tilde{e}N}^i(3,2) = \frac{\rho A \ell_e}{20} (7u_1 + 3u_2)$$

$$I_{\tilde{e}N}^i(3,3) = \frac{\rho A \ell_e^2}{60} (3u_1 + 2u_2); \quad I_{\tilde{e}N}^i(3,4) = -\frac{\rho A \ell_e}{60} (9v_1 + 2\ell_e \theta_1 + 21v_2 - 3\ell_e \theta_2)$$

$$I_{\tilde{e}N}^i(3,5) = \frac{\rho A \ell_e}{20} (3u_1 + 7u_2); \quad I_{\tilde{e}N}^i(3,6) = -\frac{\rho A \ell_e^2}{60} (2u_1 + 3u_2)$$

$$I_{\tilde{e}N}(:,3(i-1)+1:3(i+1)) = I_{\tilde{e}N}(:,3(i-1)+1:3(i+1)) + I_{\tilde{e}N}^i$$

$15. I_{\tilde{e}N} = \int_{\Omega} \rho \tilde{e} N dv \Big|_{3\times3(NE+1)}$

$$\tilde{e}N = \begin{bmatrix} 0 & 0 & \dot{v} \\ 0 & 0 & -\dot{u} \\ -\dot{v} & \dot{u} & 0 \end{bmatrix} \begin{bmatrix} N_1 & -\dfrac{y'}{\ell_e}\dfrac{dN_3}{d\xi} & -\dfrac{y'}{\ell_e}\dfrac{dN_4}{d\xi} & N_2 & -\dfrac{y'}{\ell_e}\dfrac{dN_5}{d\xi} & -\dfrac{y'}{\ell_e}\dfrac{dN_6}{d\xi} \\ 0 & N_3 & N_4 & 0 & N_5 & N_6 \\ 0 & 0 & 0 & 0 & 0 & 0 \end{bmatrix}$$

$$= \begin{bmatrix} 0 & 0 & 0 & 0 & 0 & 0 \\ 0 & 0 & 0 & 0 & 0 & 0 \\ -N_1\dot{v} & \dfrac{y'\dot{v}}{\ell_e}\dfrac{dN_3}{d\xi}+N_3\dot{u} & \dfrac{y'\dot{v}}{\ell_e}\dfrac{dN_4}{d\xi}+N_4\dot{u} & -N_2\dot{v} & \dfrac{y'\dot{v}}{\ell_e}\dfrac{dN_5}{d\xi}+N_5\dot{u} & \dfrac{y'\dot{v}}{\ell_e}\dfrac{dN_6}{d\xi}+N_6\dot{u} \end{bmatrix}$$

$$\int_{\Omega_i}\tilde{e}Ndv = \int_{\Omega_i} \begin{bmatrix} 0 & 0 & 0 & 0 & 0 & 0 \\ 0 & 0 & 0 & 0 & 0 & 0 \\ -N_1\dot{v} & N_3\dot{u} & N_4\dot{u} & -N_2\dot{v} & N_5\dot{u} & N_6\dot{u} \end{bmatrix} dv$$

According to the results in the integration $I_{\tilde{e}N}$:

$$I_{\tilde{e}N}^i(3,1) = -\frac{\rho A\ell_e}{60}(21\dot{v}_1 + 3\ell_e\dot{\theta}_1 + 9\dot{v}_2 - 2\ell_e\dot{\theta}_2); \quad I_{\tilde{e}N}^i(3,2) = \frac{\rho A\ell_e}{20}(7\dot{u}_1 + 3\dot{u}_2)$$

$$I_{\tilde{e}N}^i(3,3) = \frac{\rho A\ell_e^2}{60}(3\ddot{u}_1 + 2\dot{u}_2); \quad I_{\tilde{e}N}^i(3,4) = -\frac{\rho A\ell_e}{60}(9\dot{v}_1 + 2\ell_e\dot{\theta}_1 + 21\dot{v}_2 - 3\ell_e\dot{\theta}_2)$$

$$I_{\tilde{e}N}^i(3,5) = \frac{\rho A\ell_e}{20}(3\dot{u}_1 + 7\dot{u}_2); \quad I_{\tilde{e}N}^i(3,6) = -\frac{\rho A\ell_e^2}{60}(2\dot{u}_1 + 3\dot{u}_2)$$

$$I_{\tilde{e}N}(:,3(i-1)+1:3(i+1)) = I_{\tilde{e}N}(:,3(i-1)+1:3(i+1)) + I_{\tilde{e}N}^i$$

$16. I_{N^TN} = \int_{\Omega} \rho N^T N dv \Big|_{3(NE+1)\times3(NE+1)}$

$$I_{N^TN}(3(i-1)+1:3(i+1),3(i-1)+1:3(i+1))$$

$$= I_{N^TN}(3(i-1)+1:3(i+1),3(i-1)+1:3(i+1)) + I_{N^TN}^i$$

where $I_{N^TN}^i$ has been defined in the term of $I_{\tilde{e}\tilde{\omega}N}$.

APPENDIX 2

PRE-ODE INTEGRALS CALCULATION FOR BEAM ELEMENT

0. $\psi^T K \psi = diag(\lambda)$

wherer λ is the eigen values, which can be obtained from mode analysis directly.

1. $I_{N\psi} = \int_{\Omega} \rho N \psi dv$

$$\int_{\Omega_i} \rho N \psi dv = I_N^i \cdot \psi_{ik} = \frac{\rho A \ell_e}{12} \begin{bmatrix} 6\left(\psi_{ik}^1 + \psi_{ik}^4\right) \\ 6\left(\psi_{ik}^2 + \psi_{ik}^5\right) + \ell_e\left(\psi_{ik}^3 - \psi_{ik}^6\right) \\ 0 \end{bmatrix}$$

$$I_{N\psi}(:,k) = \sum_{i=1}^{NE} \frac{\rho A \ell_e}{12} \begin{bmatrix} 6\left(\psi_{ik}^1 + \psi_{ik}^4\right) \\ 6\left(\psi_{ik}^2 + \psi_{ik}^5\right) + \ell_e\left(\psi_{ik}^3 - \psi_{ik}^6\right) \\ 0 \end{bmatrix}$$

1.1). $I_e = \int_{\Omega} \rho e dv$

$$\int_{\Omega_i} \rho e_i dv = \sum_{k=1}^{Nm} a_k \int_{\Omega_i} N \psi(3(i-1)+1:3(i+1),k) dv \equiv \sum_{k=1}^{Nm} a_k \int_{\Omega_i} N dv \psi_{ik} \equiv \sum_{k=1}^{Nm} a_k \cdot I_N^i \psi_{ik}$$

$$I_e = \sum_{k=1}^{Nm} a_k \cdot I_{N\psi}$$

1.2) $I_{\dot{e}} = \int_{\Omega} \rho \dot{e} dv$

$$\dot{e} = N \psi \dot{a} = \sum_{k=1}^{Nm} \dot{a}_k \cdot N \psi_k$$

$$I_{\dot{e}} = \int_{\Omega} \rho \dot{e} dv = \sum_{k=1}^{Nm} \dot{a}_k \cdot I_{N\psi}$$

1.3) $I_{\tilde{e}} = \int_{\Omega} \tilde{e} dv$

$$I_{\tilde{e}} = \begin{bmatrix} 0 & 0 & I_e(2) \\ 0 & 0 & -I_e(1) \\ -I_e(2) & I_e(1) & 0 \end{bmatrix}$$

2. $I_{r'} = \int_\Omega \rho r' dv$: same as integration within ODE

2.1) $I_{\tilde{r}} = \int_\Omega \rho \tilde{r} dv$

3. $I_{\tilde{r}\tilde{r}'} = \int_\Omega \rho \tilde{r} \tilde{r}' dv$: same as integration within ODE

4. $I_{\tilde{e}\tilde{r}'} = \int_\Omega \rho \tilde{e} \tilde{r}' dv$

$$\tilde{e} = \sum_{k=1}^{Nm} a_k \cdot \begin{bmatrix} 0 & -\psi_{wk} & \psi_{vk} \\ \psi_{wk} & 0 & -\psi_{uk} \\ -\psi_{vk} & \psi_{uk} & 0 \end{bmatrix} \equiv \sum_{k=1}^{Nm} a_k \cdot \tilde{\psi}_N$$

$$\tilde{\psi}_N \cdot \tilde{r}' = \begin{bmatrix} 0 & -\psi_{wk} & \psi_{kv} \\ \psi_{wk} & 0 & -\psi_{uk} \\ -\psi_{vk} & \psi_{uk} & 0 \end{bmatrix} \begin{bmatrix} 0 & -z' & y' \\ z' & 0 & -x' \\ -y' & x' & 0 \end{bmatrix}$$

$$= \begin{bmatrix} -z'\psi_{wk} - y'\psi_{kv} & x'\psi_{vk} & x'\psi_{wk} \\ y'\psi_{uk} & -z'\psi_{wk} - x'\psi_{uk} & y'\psi_{wk} \\ z'\psi_{uk} & z'\psi_{vk} & -x'\psi_{uk} - y'\psi_{vk} \end{bmatrix}$$

The integration of the above term over area results in the following matrix.

$$\int_{\Omega_i} \tilde{e}\tilde{r}' dv = \sum_{k=1}^{Nm} a_k \int_{\Omega_i} \begin{bmatrix} 0 & (x_e' + \xi\ell_e)\psi_v & 0 \\ y'\psi_u & -(x_e' + \xi\ell_e)\psi_u & 0 \\ 0 & 0 & -(x_e' + \xi\ell_e)\psi_u \end{bmatrix} dv$$

$$\int_{\Omega_i} \rho(x_e' + \ell_e\xi)\psi_u dv$$

$$= \int_{\Omega_i} \rho(x_e' + \ell_e\xi)\left(N_1\psi_{ik}^1 - \frac{y'}{\ell_e}\frac{dN_3}{d\xi}\psi_{ik}^2 - \frac{y'}{\ell_e}\frac{dN_4}{d\xi}\psi_{ik}^3 + N_2\psi_{ik}^4 - \frac{y'}{\ell_e}\frac{dN_5}{d\xi}\psi_{ik}^5 - \frac{y'}{\ell_e}\frac{dN_6}{d\xi}\psi_{ik}^6 \right) dv$$

$$= \int_{\Omega_i} \rho(x_e' + \ell_e\xi)\left(N_1\psi_{ik}^1 + N_2\psi_{ik}^4 \right) dv = \rho A\ell_e \left[\int_0^1 x_e'\left(N_1\psi_{ik}^1 + N_2\psi_{ik}^4 \right)d\xi + \int_0^1 \ell_e\xi\left(N_1\psi_{ik}^1 + N_2\psi_{ik}^4 \right)d\xi \right]$$

$$= \rho A\ell_e \left[\left(\frac{1}{2}x_e' + \frac{1}{6}\ell_e \right)\psi_{ik}^1 + \left(\frac{1}{2}x_e' + \frac{1}{3}\ell_e \right)\psi_{ik}^4 \right] \equiv I_{xu}^i$$

$$\int_{\Omega_i} \rho y' \psi_u dv = \int_{\Omega_i} \rho y' \left(N_1 \psi_{ik}^1 - \frac{y'}{\ell_e}\frac{dN_3}{d\xi}\psi_{ik}^2 - \frac{y'}{\ell_e}\frac{dN_4}{d\xi}\psi_{ik}^3 + N_2\psi_{ik}^4 - \frac{y'}{\ell_e}\frac{dN_5}{d\xi}\psi_{ik}^5 - \frac{y'}{\ell_e}\frac{dN_6}{d\xi}\psi_{ik}^6 \right) dv$$

$$= -\rho I_{zz}\int_0^1 \left(\frac{dN_3}{d\xi}\psi_{ik}^2 + \frac{dN_4}{d\xi}\psi_{ik}^3 + \frac{dN_5}{d\xi}\psi_{ik}^5 + \frac{dN_6}{d\xi}\psi_{ik}^6 \right)d\xi = \rho I_{zz}(\psi_{ik}^2 - \psi_{ik}^5) \equiv I_{yu}^i$$

$$\int_{\Omega_i} \rho(x_e' + \xi\ell_e)\psi_v dv = \int_{\Omega_i} \rho(x_e' + \xi\ell_e)\left(N_3\psi_{ik}^2 + N_4\psi_{ik}^3 + N_5\psi_{ik}^5 + N_6\psi_{ik}^6 \right)dv$$

$$= \rho A\ell_e \int_0^1 x_e'\left(N_3\psi_{ik}^2 + N_4\psi_{ik}^3 + N_5\psi_{ik}^5 + N_6\psi_{ik}^6 \right)d\xi$$

$$+ \rho A\ell_e \int_0^1 \xi\ell_e\left(N_3\psi_{ik}^2 + N_4\psi_{ik}^3 + N_5\psi_{ik}^5 + N_6\psi_{ik}^6 \right)d\xi$$

$$= \rho A\ell_e \left[\left(\frac{x_e'}{2} + \frac{3\ell_e}{20} \right)\psi_{ik}^2 + \left(\frac{x_e'}{12} + \frac{\ell_e}{30} \right)\ell_e\psi_{ik}^3 + \left(\frac{x_e'}{2} + \frac{7\ell_e}{20} \right)\psi_{ik}^5 - \left(\frac{x_e'}{12} + \frac{\ell_e}{20} \right)\ell_e\psi_{ik}^6 \right] \equiv I_{xv}^i$$

$$I_{\widetilde{er}'} = \sum_{i=1}^{Nm} a_k \cdot I_{\widetilde{er}'k}$$

$$\text{where } I_{\widetilde{er}'k} = \sum_{i=1}^{NE} \begin{bmatrix} 0 & I_{xv}^i & 0 \\ I_{yu}^i & -I_{xu}^i & 0 \\ 0 & 0 & -I_{xu}^i \end{bmatrix}$$

4.1) $I_{\widetilde{r}\widetilde{e}} = \int_\Omega \rho\widetilde{r}'\widetilde{e}dv$

Since $(\widetilde{e}\widetilde{r}')^T = \widetilde{r}'^T\widetilde{e}^T = \widetilde{r}\widetilde{e}$, One has: $I_{\widetilde{r}\widetilde{e}} = I_{\widetilde{er}'}^T$

4.2) $I_{\widetilde{er}'} = \int_\Omega \rho\widetilde{e}\widetilde{r}'dv$

Since $\dot{e} = N\psi\dot{a} = \sum_{i=1}^{Nm} N\psi_k \dot{a}_k = \sum_{i=1}^{Nm} \dot{a}_k \cdot N\psi_k$, one has:

$$I_{\widetilde{er}'} = \int_\Omega \rho\widetilde{e}\widetilde{r}'dv = \sum_{k=1}^{Nm} \dot{a}_k \sum_{i=1}^{NE} \int_{\Omega_i} \rho\widetilde{\psi}_N \widetilde{r}'dv = \sum_{k=1}^{Nm} \dot{a}_k I_{\widetilde{er}'k}$$

4.3) $I_{\widetilde{r}'\widetilde{\omega}'N\psi} = \int_V \rho\widetilde{r}'\widetilde{\omega}'N\psi dv$

Since $\widetilde{r}'\widetilde{\omega}' = \omega'r'^T - r'^T\omega'$

$$I_{\widetilde{r}'\widetilde{\omega}'N\psi} = \int_\Omega \rho\widetilde{r}'\widetilde{\omega}'N\psi dv = \int_\Omega \rho(\omega'r'^T - r'^T\omega')N\psi dv = \omega'\int_\Omega \rho r'^T N\psi dv - \int_\Omega \rho r'^T \omega'N\psi dv$$

For any arbitrary element, one has:

$$\psi_N(k) = \begin{bmatrix} \psi_{uk} \\ \psi_{vk} \\ 0 \end{bmatrix}_{k=1,2,\cdots,Nm}$$

$$r'^T \psi_N(k) = \begin{bmatrix} x' & y' & z' \end{bmatrix} \begin{bmatrix} \psi_{uk} \\ \psi_{vk} \\ 0 \end{bmatrix} = x'\psi_{uk} + y'\psi_{vk}$$

$$I^i_{r'^T N\psi}(k) = \left(I^i_{xu} + I^i_{yv} \right)$$

$$\int_\Omega \rho r'^T N\psi dv = I_{r'^T N\psi}$$

where $I_{r'^T N\psi}(k) = \sum\limits_{i=1}^{NE} \left(I^i_{xu} + I^i_{yv} \right)$

$$r'^T \omega' \psi_N(k) = \begin{bmatrix} x' \\ y' \\ z' \end{bmatrix}^T \begin{bmatrix} 0 \\ 0 \\ \omega'_z \end{bmatrix} \begin{bmatrix} \psi_{uk} \\ \psi_{vk} \\ 0 \end{bmatrix} = \omega'_z z' \begin{bmatrix} \psi_{uk} \\ \psi_{vk} \\ 0 \end{bmatrix} = \omega'_z \begin{bmatrix} z'\psi_{uk} \\ z'\psi_{vk} \\ 0 \end{bmatrix}$$

$$\int_{\Omega_i} \rho r'^T \omega' N\psi_{ik} dv = 0$$

$$I_{\tilde{r}'\tilde{\omega}'N\psi} = \omega' I_{r'^T N\psi}$$

4.4) $I_{\tilde{r}'N\psi} = \int_V \rho \tilde{r}' N\psi dv$

$$\tilde{r}' \psi_N(k) = \begin{bmatrix} 0 & -z' & y' \\ z' & 0 & -x' \\ -y' & x' & 0 \end{bmatrix} \begin{bmatrix} \psi_u \\ \psi_v \\ 0 \end{bmatrix} = \begin{bmatrix} -z'\psi_v \\ z'\psi_u \\ -y'\psi_u + x'\psi_v \end{bmatrix}$$

$$I_{\tilde{r}'N\psi}(:,k) = \sum\limits_{i=1}^{NE} \begin{bmatrix} 0 \\ 0 \\ -I_{yui} + I_{xvi} \end{bmatrix}$$

5. $I_{\tilde{e}\tilde{e}} = \int_\Omega \rho \tilde{e}\tilde{e} dv$

$$\tilde{e}\tilde{e} = \begin{bmatrix} 0 & -w & v \\ w & 0 & -u \\ -v & u & 0 \end{bmatrix} \begin{bmatrix} 0 & -w & v \\ w & 0 & -u \\ -v & u & 0 \end{bmatrix} = \begin{bmatrix} -v^2 - w^2 & vu & wu \\ & -u^2 - w^2 & wv \\ sym. & & -u^2 - v^2 \end{bmatrix}$$

Let $u = \sum_{k=1}^{Nm} \psi_u^k a_k = \psi_u^T \boldsymbol{a}$, $v = \sum_{k=1}^{Nm} \psi_v^k a_k = \psi_v^T \boldsymbol{a}$ and $w = \sum_{k=1}^{Nm} \psi_w^k a_k = \psi_w^T \boldsymbol{a}$ where Nm

is the number of mode shapes used to approximate the displacement field, ψ_u^k, ψ_v^k and

ψ_w^k are the x, y and z components of the kth eigenfunction. $a_k(t)$ is the corresponding

modal coordinate. One then has $uv = (\psi_u^T \boldsymbol{a})^T (\psi_v^T \boldsymbol{a}) = \boldsymbol{a}^T (\psi_u \psi_v^T) \boldsymbol{a}$. In doing so, one can

obtain the mass moment of inertia term, $I_{\tilde{e}\tilde{e}}$ as:

$$I_{\tilde{e}\tilde{e}} = \int_V \rho \tilde{e}\tilde{e}\, dv = \rho \int_V \begin{bmatrix} -\boldsymbol{a}^T(\psi_v\psi_v^T + \psi_w\psi_w^T)\boldsymbol{a} & \boldsymbol{a}^T\psi_u\psi_v^T\boldsymbol{a} & \boldsymbol{a}^T\psi_u\psi_w^T\boldsymbol{a} \\ & -\boldsymbol{a}^T(\psi_u\psi_u^T + \psi_w\psi_w^T)\boldsymbol{a} & \boldsymbol{a}^T\psi_v\psi_w^T\boldsymbol{a} \\ sym. & & -\boldsymbol{a}^T(\psi_u\psi_u^T + \psi_v\psi_v^T)\boldsymbol{a} \end{bmatrix} dv$$

$$= \begin{bmatrix} -\boldsymbol{a}^T\int_V\rho(\psi_v\psi_v^T + \psi_w\psi_w^T)dv\boldsymbol{a} & \boldsymbol{a}^T\int_V\rho\psi_u\psi_v^T dv\boldsymbol{a} & \boldsymbol{a}^T\int_V\rho\psi_u\psi_w^T dv\boldsymbol{a} \\ & -\boldsymbol{a}^T\int_V\rho(\psi_u\psi_u^T + \psi_w\psi_w^T)dv\boldsymbol{a} & \boldsymbol{a}^T\int_V\rho\psi_v\psi_w^T dv\boldsymbol{a} \\ sym. & & -\boldsymbol{a}^T\int_V\rho(\psi_u\psi_u^T + \psi_v\psi_v^T)dv\boldsymbol{a} \end{bmatrix}$$

For 2D beam, the displacement along z vanished, w=0, one has:

$$I_{\tilde{e}\tilde{e}} = \begin{bmatrix} -\boldsymbol{a}^T\int_V\rho(\psi_v\psi_v^T)dv\boldsymbol{a} & \boldsymbol{a}^T\int_V\rho\psi_u\psi_v^T dv\boldsymbol{a} & 0 \\ & -\boldsymbol{a}^T\int_V\rho(\psi_u\psi_u^T)dv\boldsymbol{a} & 0 \\ sym. & -\boldsymbol{a}^T\int_V\rho(\psi_u\psi_u^T + \psi_v\psi_v^T)dv\boldsymbol{a} \end{bmatrix}$$

Each term in the above equation can be calculated separately, the details are as follow:

$$I_{UU}^i(m,n) = \int_{\Omega_i} \psi_u^m \psi_u^n dv$$

$$= \int_{\Omega_i} N_1\psi_{im}^1 (N_1\psi_{in}^1 + N_2\psi_{in}^4)dv + \int_{\Omega_i} N_2\psi_{im}^4 (N_1\psi_{in}^1 + N_2\psi_{in}^4)dv$$

$$+ \int_{\Omega_i}\left[\frac{y'^2}{\ell_e^2}(\frac{dN_3}{d\xi})^2 \psi_{im}^2\psi_{in}^2 + \frac{y'^2}{\ell_e^2}\frac{dN_3}{d\xi}\frac{dN_5}{d\xi}(\psi_{im}^2\psi_{in}^5 + \psi_{im}^5\psi_{in}^2) + \frac{y'^2}{\ell_e^2}(\frac{dN_5}{d\xi})^2 \psi_{im}^5\psi_{in}^5 \right]dv$$

$$\int_{\Omega_i}\frac{y'^2}{\ell_e^2}\frac{dN_3}{d\xi}\frac{dN_4}{d\xi}(\psi_{im}^2\psi_{in}^3 + \psi_{im}^3\psi_{in}^2) + \frac{y'^2}{\ell_e^2}\frac{dN_3}{d\xi}\frac{dN_6}{d\xi}(\psi_{im}^2\psi_{in}^6 + \psi_{im}^6\psi_{in}^2)$$

$$+ \frac{y'^2}{\ell_e^2}\frac{dN_4}{d\xi}\frac{dN_5}{d\xi}(\psi_{im}^3\psi_{in}^5 + \psi_{im}^5\psi_{in}^3) + \frac{y'^2}{\ell_e^2}\frac{dN_5}{d\xi}\frac{dN_6}{d\xi}(\psi_{im}^5\psi_{in}^6 + \psi_{im}^6\psi_{in}^5)\right]dv$$

$$+ \int_{\Omega_i}\left[\frac{y'^2}{\ell_e^2}(\frac{dN_4}{d\xi})^2 \psi_{im}^3\psi_{in}^3 + \frac{y'^2}{\ell_e^2}\frac{dN_4}{d\xi}\frac{dN_6}{d\xi}(\psi_{im}^3\psi_{in}^6 + \psi_{im}^6\psi_{in}^3) + \frac{y'^2}{\ell_e^2}(\frac{dN_6}{d\xi})^2 \psi_{im}^6\psi_{in}^6 \right]dv$$

$$I_{uu}^i(m,n) = \frac{\rho A \ell_e}{6}\left[2\psi_{im}^1\psi_{in}^1 + (\psi_{im}^1\psi_{in}^4 + \psi_{im}^4\psi_{in}^1) + 2\psi_{im}^4\psi_{in}^4\right]$$

$$+ \frac{6\rho I_{zz}}{5\ell_e}\left[\psi_{im}^2\psi_{in}^2 - (\psi_{im}^2\psi_{in}^5 + \psi_{im}^5\psi_{in}^2) + \psi_{im}^5\psi_{in}^5\right]$$

$$+ \frac{\rho I_{zz}}{10}\left[(\psi_{im}^2\psi_{in}^3 + \psi_{im}^3\psi_{in}^2) + (\psi_{im}^2\psi_{in}^6 + \psi_{im}^6\psi_{in}^2) - (\psi_{im}^3\psi_{in}^5 + \psi_{im}^5\psi_{in}^3) - (\psi_{im}^5\psi_{in}^6 + \psi_{im}^6\psi_{in}^5)\right]$$

$$+ \frac{\rho I_{zz}\ell_e}{30}\left[4\psi_{im}^3\psi_{in}^3 - (\psi_{im}^3\psi_{in}^6 + \psi_{im}^6\psi_{in}^3) + 4\psi_{im}^6\psi_{in}^6\right]$$

$$= \frac{\rho A\ell_e}{6}\left[2\psi_{im}^1\psi_{in}^1 + (\psi_{im}^1\psi_{in}^4 + \psi_{im}^4\psi_{in}^1) + 2\psi_{im}^4\psi_{in}^4\right] + \frac{\rho I_{zz}}{30\ell_e}\left\{36\left(\psi_{im}^2 - \psi_{im}^5\right)\left(\psi_{in}^2 - \psi_{in}^5\right) +\right.$$

$$+ 3\ell_e\left[\left(\psi_{im}^2 - \psi_{im}^5\right)\left(\psi_{in}^3 + \psi_{in}^6\right) + \left(\psi_{im}^3 + \psi_{im}^6\right)\left(\psi_{in}^2 - \psi_{in}^5\right)\right] + \ell_e^2\left(4\psi_{im}^3\psi_{in}^3 - \psi_{im}^3\psi_{in}^6 - \psi_{im}^6\psi_{in}^3 + 4\psi_{im}^6\psi_{in}^6\right)\right\}$$

$$I_{UV}^i(m,n) = \int_{\Omega_i}\psi_u^m\psi_v^n\,dv = \int_{\Omega_i}\left(N_1\psi_{im}^1 + N_2\psi_{im}^4\right)\left(N_3\psi_{in}^2 + N_4\psi_{in}^3 + N_5\psi_{in}^5 + N_6\psi_{in}^6\right)dv$$

$$= \int_{\Omega_i}\psi_{im}^1\left(N_1N_3\psi_{in}^2 + N_1N_4\psi_{in}^3 + N_1N_5\psi_{in}^5 + N_1N_6\psi_{in}^6\right)dv$$

$$+ \int_{\Omega_i}\psi_{im}^4\left(N_2N_3\psi_{in}^2 + N_2N_4\psi_{in}^3 + N_2N_5\psi_{in}^5 + N_2N_6\psi_{in}^6\right)dv$$

$$I_{UV}^i(m,n) = \int_{\Omega_i}\psi_u^m\psi_v^n\,dv = \frac{\rho A\ell_e}{60}\left[\psi_{im}^1\left(21\psi_{in}^2 + 3\ell_e\psi_{in}^3 + 9\psi_{in}^5 - 2\ell_e\psi_{in}^6\right)\right.$$

$$+ \psi_{im}^4\left(9\psi_{in}^2 + 2\ell_e\psi_{in}^3 + 21\psi_{in}^5 - 3\ell_e\psi_{in}^6\right)\right]$$

$$I_{VV}^i(m,n) = \int_{\Omega_i}\psi_v^m\psi_v^n\,dv = \frac{\rho A\ell_e}{420}\left[156\psi_{im}^2\psi_{in}^2 + 54\left(\psi_{im}^2\psi_{in}^5 + \psi_{im}^5\psi_{in}^2\right) + 156\psi_{im}^5\psi_{in}^5\right.$$

$$+ 22\ell_e\left[\left(\psi_{im}^2\psi_{in}^3 + \psi_{im}^3\psi_{in}^2\right) - \left(\psi_{im}^5\psi_{in}^6 + \psi_{im}^6\psi_{in}^5\right)\right] + 13\ell_e\left[\left(\psi_{im}^3\psi_{in}^5 + \psi_{im}^5\psi_{in}^3\right) - \left(\psi_{im}^2\psi_{in}^6 + \psi_{im}^6\psi_{in}^2\right)\right]$$

$$+ \ell_e^2\left[4\psi_{im}^3\psi_{in}^3 - 3\left(\psi_{im}^3\psi_{in}^6 + \psi_{im}^6\psi_{in}^3\right) + 4\psi_{im}^6\psi_{in}^6\right]\right]$$

5.1) $I_{\tilde{e}\tilde{e}} = \int_\Omega \rho\tilde{e}\tilde{e}\,dv$

$$\tilde{e}\tilde{e} = \begin{bmatrix} 0 & -\dot{w} & \dot{v} \\ \dot{w} & 0 & -\dot{u} \\ -\dot{v} & \dot{u} & 0 \end{bmatrix}\begin{bmatrix} 0 & -w & v \\ w & 0 & -u \\ -v & u & 0 \end{bmatrix} = \begin{bmatrix} -(\dot{v}v + \dot{w}w) & u\dot{v} & u\dot{w} \\ \dot{u}v & -(\dot{u}u + \dot{w}w) & v\dot{w} \\ \dot{u}w & \dot{v}w & -(\dot{v}v + \dot{u}u) \end{bmatrix}$$

Similarly, $I_{\tilde{e}\tilde{e}}$ can be defined as follows:

$$I_{\tilde{e}\tilde{e}} =$$

$$\rho \begin{bmatrix} -\dot{a}^T \int_\Omega \left(\psi_v \psi_v^T + \psi_w \psi_w^T \right) dv a & a^T \int_\Omega \psi_u \psi_v^T dv \dot{a} & a^T \int_\Omega \psi_u \psi_w^T dv \dot{a} \\ \dot{a}^T \int_\Omega \psi_u \psi_v^T dv a & -\dot{a}^T \int_\Omega \left(\psi_u \psi_u^T + \psi_w \psi_w^T \right) dv a & a^T \int_\Omega \psi_v \psi_w^T dv \dot{a} \\ \dot{a}^T \int_\Omega \psi_u \psi_w^T dv a & \dot{a}^T \int_\Omega \psi_v \psi_w^T dv a & -\dot{a}^T \int_\Omega \left(\psi_u \psi_u^T + \psi_v \psi_v^T \right) dv a \end{bmatrix}$$

$$= \begin{bmatrix} -\dot{a}^T \left(I_{VV} + I_{WW} \right) a & a^T I_{UV} \dot{a} & a^T I_{UW} \dot{a} \\ \dot{a}^T I_{UV} a & -\dot{a}^T \left(I_{WW} + I_{UU} \right) a & a^T I_{VW} \dot{a} \\ \dot{a}^T I_{UW} a & \dot{a}^T I_{VW} a & -\dot{a}^T \left(I_{VV} + I_{UU} \right) a \end{bmatrix}$$

For 2D beam, one has:

$$I_{\tilde{e}\tilde{e}} = \begin{bmatrix} -\dot{a}^T VV a & a^T UV \dot{a} & 0 \\ \dot{a}^T UV a & -\dot{a}^T UU a & 0 \\ 0 & 0 & -\dot{a}^T \left(VV + UU \right) a \end{bmatrix}$$

5.2) $I_{\tilde{e}\tilde{\omega}'N\psi} = \int_V \rho \tilde{e} \tilde{\omega}' N\psi dv$

Since $\tilde{e}\tilde{\omega}' = \omega' e^T - e^T \omega'$

$$I_{\tilde{e}\tilde{\omega}'N\psi} = \int_\Omega \rho \left(\omega' e^T - e^T \omega' \right) N\psi dv = \int_\Omega \rho \omega' e^T N\psi dv - \int_\Omega \rho e^T \omega' N\psi dv$$

$$= \omega' \int_\Omega \rho e^T N\psi dv - \int_\Omega \rho e^T \omega' N\psi dv$$

$$\int_{\Omega_i} \rho e^T N\psi dv = \int_{\Omega_i} \rho e^T N\psi_{ij} dv = \sum_{k=1}^{Nm} a_k \int_{\Omega_i} \rho \psi_{Nk}^T \psi_{Nj} dv$$

$$= \sum_{k=1}^{Nm} a_k \int_{\Omega_i} \rho \left(\psi_{uk} \psi_{uj} + \psi_{vk} \psi_{vj} \right) dv = \sum_{k=1}^{Nm} a_k \cdot \left(I_{UU} + I_{VV} \right)$$

$$e^T \omega' = \sum_{k=1}^{Nm} a_k \cdot \psi_N^T \omega' = \sum_{k=1}^{Nm} a_k \cdot \begin{bmatrix} \psi_{uk} \\ \psi_{vk} \\ 0 \end{bmatrix}^T \begin{bmatrix} 0 \\ 0 \\ \omega'_z \end{bmatrix} = 0$$

$$\int_{\Omega_i} \rho e^T \omega' N\psi dv = 0$$

$$I_{\tilde{e}\tilde{\omega}'N\psi} = \omega' \sum_{k=1}^{Nm} a_k \cdot \left(I_{UU} + I_{VV} \right)$$

If the mode shape is normalized, then $I_{\tilde{e}\tilde{\omega}'N\psi} = \omega' a^T$

$$5.3)\ I_{\psi^T N^T N\psi} = \int_V \rho\psi^T N^T N\psi dv$$

$$\psi_{ik}^T N^T N\psi_{im} = \begin{bmatrix} \psi_{uk} \\ \psi_{vk} \\ 0 \end{bmatrix}^T \begin{bmatrix} \psi_{uj} \\ \psi_{vj} \\ 0 \end{bmatrix} = \psi_{uk}\psi_{uj} + \psi_{vk}\psi_{vj}$$

$$I_{\psi^T N^T N\psi} = (I_{UU} + I_{VV})$$

If mode shape is normalized, then $I_{\psi^T N^T N\psi} = \int_V \rho\psi^T N^T N\psi dv = I$

$$6.\ I_{\tilde{e}N\psi} = \int_V \rho\tilde{e}N\psi dv$$

For any arbitrary element:

$$\tilde{e} = \sum_{k=1}^{Nm} a_k \cdot \begin{bmatrix} 0 & 0 & \psi_{vk} \\ 0 & 0 & -\psi_{uk} \\ -\psi_{vk} & \psi_{uk} & 0 \end{bmatrix} \quad N\psi = \begin{bmatrix} \psi_{u1} & \psi_{u2} & \cdots & \psi_{uNm} \\ \psi_{v1} & \psi_{v2} & \cdots & \psi_{vNm} \\ 0 & 0 & \cdots & 0 \end{bmatrix}$$

$$\int_{\Omega_i} \rho\tilde{e}N\psi(j)dv = \sum_{k=1}^{Nm} a_k \int_{\Omega_i} \rho \begin{bmatrix} 0 & 0 & \psi_{vk} \\ 0 & 0 & -\psi_{uk} \\ -\psi_{vk} & \psi_{uk} & 0 \end{bmatrix} \begin{bmatrix} \psi_{uj} \\ \psi_{vj} \\ 0 \end{bmatrix} dv = \sum_{k=1}^{Nm} a_k \int_{\Omega_i} \rho \begin{bmatrix} 0 \\ 0 \\ -\psi_{vk}\psi_{uj} + \psi_{uk}\psi_{vj} \end{bmatrix} dv$$

According to the integration I_{uv}^i in I_{UV}, one has:

$$I_{VU}^i = \rho A\ell_e \left[\psi_{ij}^1 \left(\frac{7}{20}\psi_{ik}^2 + \frac{1}{20}\ell_e\psi_{ik}^3 + \frac{3}{20}\psi_{ik}^5 - \frac{1}{30}\ell_e\psi_{ik}^6 \right) \right.$$

$$\left. + \psi_{ij}^4 \left(\frac{3}{20}\psi_{ik}^2 + \frac{1}{30}\ell_e\psi_{ik}^3 + \frac{7}{20}\psi_{ik}^5 - \frac{1}{20}\ell_e\psi_{ik}^6 \right) \right]$$

$$I_{\tilde{e}N\psi}(:,k) = \sum_{k=1}^{Nm} a_k \cdot \sum_{i=1}^{NE} \begin{bmatrix} 0 \\ 0 \\ -I_{VU}^i + I_{UV}^i \end{bmatrix}$$

$$6.1)\ I_{\tilde{e}N\psi} = \int_V \rho\tilde{e}N\psi dv$$

Similarly, one has:

$$I_{\tilde{e}N\psi} = \int_V \rho\tilde{e}N\psi dv = \sum_{k=1}^{Nm} \dot{a}_k \cdot \sum_{i=1}^{NE} \begin{bmatrix} 0 \\ 0 \\ -I_{\psi_{vk}\psi_{uj}}^i + I_{\psi_{uk}\psi_{vj}}^i \end{bmatrix}$$

APPENDIX 3

INTEGRAL CALCULATION FOR TRIANGULAR ELEMENT

For the iso-parametric constant strain triangular (CST) element, the elastic displacement and coordinates within the element both can be approximated using the same polynomial function. The elastic displacement is defined as follows:

$$e = \begin{pmatrix} u \\ v \\ w \end{pmatrix} = \begin{Bmatrix} \xi u_1 + \eta u_2 + \zeta u_3 \\ \xi v_1 + \eta v_2 + \zeta v_3 \\ \xi w_1 + \eta w_2 + \zeta w_3 \end{Bmatrix} = Nq_f = \sum_{k=1}^{Nm} N\psi_k a_k$$

where (u_1, v_1, w_1), (u_2, v_2, w_2) and (u_3, v_3, w_3) are the components of displacements at the vertices of the triangle element of concern.

$$N = \begin{bmatrix} \xi & 0 & 0 & \eta & 0 & 0 & \zeta & 0 & 0 \\ 0 & \xi & 0 & 0 & \eta & 0 & 0 & \zeta & 0 \\ 0 & 0 & \xi & 0 & 0 & \eta & 0 & 0 & \zeta \end{bmatrix} \equiv [\xi I_3 \quad \eta I_3 \quad \zeta I_3]$$ is the shape function matrix in

which I_3 is a $3X3$ identity matrix, ξ, η and ζ are area coordinates, ψ_k is the kth mode shape value. a_k is the corresponding modal coordinate of the mode shape.

1. $I_{N\psi} = \int_V \rho N\psi dv$

Assuming that the node numbers of the ith element are N_1, N_2, N_3, the mode vector of the kth mode for the ith element ψ_{ik} is defined as follows:

$$\psi_{ik} = \begin{Bmatrix} \psi_k(3N_1 - 2) \\ \psi_k(3N_1 - 1) \\ \psi_k(3N_1) \\ \psi_k(3N_2 - 2) \\ \psi_k(3N_2 - 1) \\ \psi_k(3N_2) \\ \psi_k(3N_3 - 2) \\ \psi_k(3N_3 - 1) \\ \psi_k(3N_3) \end{Bmatrix} = \begin{bmatrix} \psi_{ik}^1 \\ \psi_{ik}^2 \\ \vdots \\ \psi_{ik}^9 \end{bmatrix}$$

where $k=1, 2, ..., Nm$, Nm is the number of total mode shapes.

For any arbitrary element, one has:

$$N\psi_{ik} \equiv \psi_N = \begin{bmatrix} \xi I_3 & \eta I_3 & \zeta I_3 \end{bmatrix} \begin{bmatrix} \psi_{ik}^1 \\ \psi_{ik}^2 \\ \vdots \\ \psi_{ik}^9 \end{bmatrix} = \begin{bmatrix} \xi\psi_{ik}^1 + \eta\psi_{ik}^4 + \zeta\psi_{ik}^7 \\ \xi\psi_{ik}^2 + \eta\psi_{ik}^5 + \zeta\psi_{ik}^8 \\ \xi\psi_{ik}^3 + \eta\psi_{ik}^6 + \zeta\psi_{ik}^9 \end{bmatrix} \equiv \begin{bmatrix} \psi_u^k \\ \psi_v^k \\ \psi_w^k \end{bmatrix}$$

$$\int_{\Omega_i} N\psi_{ik}\,dv = \int_{\Omega_i} \begin{bmatrix} \psi_u^k \\ \psi_v^k \\ \psi_w^k \end{bmatrix} dv = \int_{\Omega_i} \begin{bmatrix} \xi\psi_{ik}^1 + \eta\psi_{ik}^4 + \zeta\psi_{ik}^7 \\ \xi\psi_{ik}^2 + \eta\psi_{ik}^5 + \zeta\psi_{ik}^8 \\ \xi\psi_{ik}^3 + \eta\psi_{ik}^6 + \zeta\psi_{ik}^9 \end{bmatrix} dv$$

In Chapter 6, one has the integration of area coordinates as follows:

$$\int_{A_i} \xi\,dA = \int_{A_i} \eta\,dA = \int_{A_i} \zeta\,dA = \frac{A}{3}; \quad \int_{A_i} \xi^2\,dA = \int_{A_i} \eta^2\,dA = \int_{A_i} \zeta^2\,dA = \frac{A}{6};$$

$$\int_{A_i} \xi\eta\,dA = \int_{A_i} \xi\zeta\,dA = \int_{A_i} \eta\zeta\,dA = \frac{A}{12}$$

With the help of such integrations:

$$\int_{\Omega_i} N\psi_{ik}\,dv = \frac{\rho A_i t_i}{3} \begin{bmatrix} \psi_{ik}^1 + \psi_{ik}^4 + \psi_{ik}^7 \\ \psi_{ik}^2 + \psi_{ik}^5 + \psi_{ik}^8 \\ \psi_{ik}^3 + \psi_{ik}^6 + \psi_{ik}^9 \end{bmatrix} \equiv I_{N\psi}^{ik}$$

where A_i is the area of the triangular element, t_i is the thickness of the triangle element along the local z direction of body fixed coordinate.

Summing up along the entire domain:

$$I_{N\psi}(:,k) = \sum_{i=1}^{NE} I_{N\psi}^{ik}$$

where NE is number of total elements, $I_{N\psi}$ is a $3 \times Nm$ matrix,

1.1) $I_e = \int_V \rho e\,dv$

$$I_e = \int_V \rho e\,dv = \sum_{i=1}^{NE} \sum_{k=1}^{Nm} a_k \int_{\Omega_i} \rho N\psi_{ik}\,dv = \sum_{k=1}^{Nm} a_k \sum_{i=1}^{NE} \int_{\Omega_i} \rho N\psi_{ik}\,dv = \sum_{k=1}^{Nm} a_k I_{N\psi}$$

1.2) $I_{\dot{e}} = \int_V \rho\dot{e}\,dv$

$$I_{\dot{e}} = \sum_{i=1}^{NE} \sum_{k=1}^{Nm} \dot{a}_k \int_{\Omega_i} \rho N\psi_{ik}\,dv = \sum_{k=1}^{Nm} \dot{a}_k I_{N\psi}$$

1.3) $I_{\tilde{e}} = \int_V \rho \tilde{e}\, dv$

$$I_{\tilde{e}} = \begin{bmatrix} 0 & -I_e(3) & I_e(2) \\ I_e(3) & 0 & -I_e(1) \\ -I_e(2) & I_e(1) & 0 \end{bmatrix}$$

2. $I_{r'} = \int_V \rho r'\, dv$

$$\int_{\Omega_i} \rho r'\, dv = \int_{\Omega_i} \rho \begin{bmatrix} x' \\ y' \\ z' \end{bmatrix} dv, \quad \int_{\Omega_i} z'\, dv = \int_{A_i} \int_{\bar{z}-\frac{t_i}{2}}^{\bar{z}+\frac{t_i}{2}} z'\, dz\, dA = \int_{A_i} \left.\frac{z'^2}{2}\right|_{\bar{z}-\frac{t_i}{2}}^{\bar{z}+\frac{t_i}{2}} dA = \int_{A_i} t_i \bar{z}\, dA = t_i \int_{A_i} \bar{z}\, dA$$

$$\int_{\Omega_i} r'\, dv = \int_{\Omega_i} \begin{Bmatrix} x' \\ y' \\ z' \end{Bmatrix} dv = t_i \int_{A_i} \begin{Bmatrix} x' \\ y' \\ \bar{z} \end{Bmatrix} dA$$

For an iso-paramatic element, the coordinates and displacements of any triangle with thickness t in 3D space can be expressed as follows:

$$\begin{Bmatrix} x' \\ y' \\ \bar{z} \end{Bmatrix} = \begin{Bmatrix} \xi x_1 + \eta x_2 + \zeta x_3 \\ \xi y_1 + \eta y_2 + \zeta y_3 \\ \xi z_1 + \eta z_2 + \zeta z_3 \end{Bmatrix} = \begin{bmatrix} \xi I_3 & \eta I_3 & \zeta I_3 \end{bmatrix} \begin{bmatrix} x_1 \\ y_1 \\ z_1 \\ x_2 \\ y_2 \\ z_2 \\ x_3 \\ y_3 \\ z_3 \end{bmatrix}$$

where (x_1, y_1, z_1), (x_2, y_2, z_2) and (x_3, y_3, z_3) are the vertices coordinates of the triangle of concern, which are given by the meshed finite element model.

$$I_{r'} = \sum_{i=1}^{NE} \int_{\Omega_i} \rho r'\, dv$$

$$= \sum_{i=1}^{NE} t_i \int_{A_i} \rho \begin{Bmatrix} x' \\ y' \\ \bar{z} \end{Bmatrix} dA = \sum_{i=1}^{NE} t_i \int_{A_i} \rho \begin{Bmatrix} \xi x_1 + \eta x_2 + \zeta x_3 \\ \xi y_1 + \eta y_2 + \zeta y_3 \\ \xi z_1 + \eta z_2 + \zeta z_3 \end{Bmatrix} dA = \sum_{i=1}^{NE} \frac{\rho A_i t_i}{3} \begin{bmatrix} x_1 + x_2 + x_3 \\ y_1 + y_2 + y_3 \\ z_1 + z_2 + z_3 \end{bmatrix}$$

2.1) $I_{\tilde{r}'} = \int_V \rho \tilde{r}' dv$

$$I_{\tilde{r}'} = \begin{bmatrix} 0 & -I_{r'}(3) & I_{r'}(2) \\ I_{r'}(3) & 0 & -I_{r'}(1) \\ -I_{r'}(2) & I_{r'}(1) & 0 \end{bmatrix}$$

3. $I_{\tilde{r}\tilde{r}'} = \int_V \rho \tilde{r} \tilde{r}' dv$

$$\tilde{r}\tilde{r}' = \begin{bmatrix} 0 & -z' & y' \\ z' & 0 & -x' \\ -y' & x' & 0 \end{bmatrix}\begin{bmatrix} 0 & -z' & y' \\ z' & 0 & -x' \\ -y' & x' & 0 \end{bmatrix} = \begin{bmatrix} -y'^2 - z'^2 & x'y' & x'z' \\ & -x'^2 - z'^2 & y'z' \\ sym & & -x'^2 - y'^2 \end{bmatrix}$$

$$\int_{\Omega_i} \rho x'z' dv_i = \int_{A_i} x' \int_{\bar{z}-\frac{t_i}{2}}^{\bar{z}+\frac{t_i}{2}} \rho z' dz dx dy = \int_{A_i} \rho x' t_i \bar{z} dx dy = t_i \int_{A_i} \rho x' \bar{z} dx dy$$

$$= t_i \int_{A_i} \rho (\xi x_1 + \eta x_2 + \zeta x_3)(\xi z_1 + \eta z_2 + \zeta z_3) dx dy$$

$$= \frac{\rho A_i t_i}{12} [(2x_1 z_1 + x_1 z_2 + x_1 z_3) + (x_2 z_1 + 2x_2 z_2 + x_2 z_3) + (x_3 z_1 + x_3 z_2 + 2x_3 z_3)]$$

$$= \frac{\rho A_i t_i}{12} [(x_1 + x_2 + x_3)(z_1 + z_2 + z_3) + x_1 z_1 + x_2 z_2 + x_3 z_3] \equiv I_{xz}^i$$

Similarly:

$$\int_{\Omega_i} \rho z'^2 dv_i = \int_{A_i} \int_{\bar{z}-t_i/2}^{\bar{z}+t_i/2} \rho z'^2 dz dx dy = \int_{A_i} v \frac{z'^3}{3}\Big|_{\bar{z}-t_i/2}^{\bar{z}+t_i/2} dx dy = \int_{A_i} \rho \left(\bar{z}^2 t_i + \frac{t_i^3}{12} \right) dx dy$$

$$= t_i \int_{A_i} \rho \bar{z}^2 dx dy + \frac{t_i^3}{12} \int_{A_i} \rho dx dy = \frac{\rho A_i t_i}{6}(z_1^2 + z_2^2 + z_3^2 + z_1 z_2 + z_1 z_3 + z_2 z_3) + \frac{\rho A_i t_i^3}{12} \equiv I_{zz}^i$$

$$\int_{\Omega_i} \rho x'y' dv_i == \frac{\rho A_i t_i}{12} [(x_1 + x_2 + x_3)(y_1 + y_2 + y_3) + x_1 y_1 + x_2 y_2 + x_3 y_3] \equiv I_{xy}^i$$

$$\int_{\Omega_i} \rho yz dv_i = \frac{\rho A_i t_i}{12} [(y_1 + y_2 + y_3)(z_1 + z_2 + z_3) + y_1 z_1 + y_2 z_2 + y_3 z_3] \equiv I_{yz}^i$$

$$\int_{\Omega_i} \rho x'^2 dv_i = \frac{\rho A_i t_i}{12} [(x_1 + x_2 + x_3)^2 + x_1^2 + x_2^2 + x_3^2] \equiv I_{xx}^i$$

$$\int_{\Omega_i} \rho y'^2 dv_i = \frac{\rho A_i t_i}{12} [(y_1 + y_2 + y_3)^2 + y_1^2 + y_2^2 + y_3^2] \equiv I_{yy}^i$$

$$I_{\vec{r}\vec{r}'} = \sum_{i=1}^{NE} \begin{bmatrix} -I_{yy}^i - I_{zz}^i & I_{xy}^i & I_{xz}^i \\ & -I_{xx}^i - I_{zz}^i & I_{yz}^i \\ sym & & -I_{xx}^i - I_{yy}^i \end{bmatrix}$$

4. $I_{\vec{e}\vec{r}'} = \int_V \rho \vec{e} \vec{r}' dv$

For any arbitrary element:

$$e = N\psi_i a = \sum_{k=1}^{Nm} a_k \cdot N\psi_{ik} \equiv \sum_{k=1}^{Nm} a_k \cdot \begin{bmatrix} \psi_{uk} \\ \psi_{vk} \\ \psi_{wk} \end{bmatrix}, \text{ then}$$

$$\tilde{e} = \sum_{k=1}^{Nm} a_k \cdot \begin{bmatrix} 0 & -\psi_{wk} & \psi_{vk} \\ \psi_{wk} & 0 & -\psi_{uk} \\ -\psi_{vk} & \psi_{uk} & 0 \end{bmatrix} \equiv \sum_{k=1}^{Nm} a_k \cdot \tilde{\psi}_N$$

$$\tilde{\psi}_N \cdot \tilde{r}' = \begin{bmatrix} 0 & -\psi_{wk} & \psi_{kv} \\ \psi_{wk} & 0 & -\psi_{uk} \\ -\psi_{vk} & \psi_{uk} & 0 \end{bmatrix} \begin{bmatrix} 0 & -z' & y' \\ z' & 0 & -x' \\ -y' & x' & 0 \end{bmatrix}$$

$$= \begin{bmatrix} -z'\psi_{wk} - y'\psi_{kv} & x'\psi_{vk} & x'\psi_{wk} \\ y'\psi_{uk} & -z'\psi_{wk} - x'\psi_{uk} & y'\psi_{wk} \\ z'\psi_{uk} & z'\psi_{vk} & -x'\psi_{uk} - y'\psi_{vk} \end{bmatrix}$$

According to the terms in the integration $I_{\vec{r}\vec{r}'}$, one has:

$$\int_{\Omega_i} \rho x' \psi_u dv = \frac{\rho A_i t_i}{12} \left[(x_1 + x_2 + x_3)(\psi_{ik}^1 + \psi_{ik}^4 + \psi_{ik}^7) + x_1\psi_{ik}^1 + x_2\psi_{ik}^4 + x_3\psi_{ik}^7 \right] \equiv I_{xu}^i$$

$$\int_{\Omega_i} \rho y' \psi_u dv = \frac{\rho A_i t_i}{12} \left[(y_1 + y_2 + y_3)(\psi_{ik}^1 + \psi_{ik}^4 + \psi_{ik}^7) + y_1\psi_{ik}^1 + y_2\psi_{ik}^4 + y_3\psi_{ik}^7 \right] \equiv I_{yu}^i$$

$$\int_{\Omega_i} \rho z' \psi_u dv = \frac{\rho A_i t_i}{12} \left[(z_1 + z_2 + z_3)(\psi_{ik}^1 + \psi_{ik}^4 + \psi_{ik}^7) + z_1\psi_{ik}^1 + z_2\psi_{ik}^4 + z_3\psi_{ik}^7 \right] \equiv I_{zu}^i$$

$$\int_{\Omega_i} \rho x' \psi_v dv = \frac{\rho A_i t_i}{12} \left[(x_1 + x_2 + x_3)(\psi_{ik}^2 + \psi_{ik}^5 + \psi_{ik}^8) + x_1\psi_{ik}^2 + x_2\psi_{ik}^5 + x_3\psi_{ik}^8 \right] \equiv I_{xv}^i$$

$$\int_{\Omega_i} \rho y' \psi_v dv = \frac{\rho A_i t_i}{12} \left[(y_1 + y_2 + y_3)(\psi_{ik}^2 + \psi_{ik}^5 + \psi_{ik}^8) + y_1\psi_{ik}^2 + y_2\psi_{ik}^5 + y_3\psi_{ik}^8 \right] \equiv I_{yv}^i$$

$$\int_{\Omega_i} \rho z' \psi_v dv = \frac{\rho A_i t_i}{12} \left[(z_1 + z_2 + z_3)(\psi_{ik}^2 + \psi_{ik}^5 + \psi_{ik}^8) + z_1\psi_{ik}^2 + z_2\psi_{ik}^5 + z_3\psi_{ik}^8 \right] \equiv I_{zv}^i$$

$$\int_{\Omega_i} \rho x' \psi_w dv = \frac{\rho A_i t_i}{12} \left[(x_1 + x_2 + x_3)(\psi_{ik}^3 + \psi_{ik}^6 + \psi_{ik}^9) + x_1 \psi_{ik}^3 + x_2 \psi_{ik}^6 + x_3 \psi_{ik}^9 \right] \equiv I_{xw}^i$$

$$\int_{\Omega_i} \rho y' \psi_w dv = \frac{\rho A_i t_i}{12} \left[(y_1 + y_2 + y_3)(\psi_{ik}^3 + \psi_{ik}^6 + \psi_{ik}^9) + y_1 \psi_{ik}^3 + y_2 \psi_{ik}^6 + y_3 \psi_{ik}^9 \right] \equiv I_{yw}^i$$

$$\int_{\Omega_i} \rho z' \psi_w dv = \frac{\rho A_i t_i}{12} \left[(z_1 + z_2 + z_3)(\psi_{ik}^3 + \psi_{ik}^6 + \psi_{ik}^9) + z_1 \psi_{ik}^3 + z_2 \psi_{ik}^6 + z_3 \psi_{ik}^9 \right] \equiv I_{zw}^i$$

$$I_{\widetilde{er}'k}(:,3(k-1)+1:3k) = \sum_{i=1}^{NE} \int_{\Omega_i} \rho \widetilde{\psi}_N \widetilde{r}' dv = \sum_{i=1}^{NE} \begin{bmatrix} -I_{zw}^i - I_{yv}^i & I_{xv}^i & I_{xw}^i \\ I_{yu}^i & -I_{zw}^i - I_{xu}^i & I_{yw}^i \\ I_{zu}^i & I_{zv}^i & -I_{xu}^i - I_{yv}^i \end{bmatrix}$$

$$I_{\widetilde{er}'} = \sum_{k=1}^{Nm} a_k \sum_{i=1}^{NE} \int_{\Omega_i} \rho \widetilde{N} \widetilde{\psi}_{ik} \widetilde{r}' dv = \sum_{k=1}^{Nm} a_k \cdot I_{\widetilde{er}'k}(:,3(k-1)+1:3k)$$

4.1) $I_{\widetilde{r}\widetilde{e}} = \int_V \rho \widetilde{r}\widetilde{e} dv$

Since $(\widetilde{r}\widetilde{e})^T = \widetilde{e}^T \widetilde{r}'^T = \widetilde{e}\widetilde{r}'$, one has: $I_{\widetilde{r}\widetilde{e}} = I_{\widetilde{er}'}^T$

4.2) $I_{\widetilde{er}'} = \int_V \rho \widetilde{e}\widetilde{r}' dv = \sum_{i=1}^{NE} \sum_{k=1}^{Nm} \dot{a}_k \int_{\Omega_i} \rho \widetilde{\psi}_N \widetilde{r}' dv = \sum_{k=1}^{Nm} \dot{a}_k \sum_{i=1}^{NE} \int_{\Omega_i} \rho \widetilde{\psi}_N \widetilde{r}' dv$

$$I_{\widetilde{er}'} = \sum_{k=1}^{Nm} \dot{a}_k \cdot I_{\widetilde{er}'k}(:,3(k-1)+1:3k)$$

4.3) $I_{\widetilde{r}'\widetilde{\omega}'N\psi} = \int_V \rho \widetilde{r}' \widetilde{\omega}' N\psi dv$

Since $\widetilde{r}'\widetilde{\omega}' = \omega' r'^T - r'^T \omega'$

$$I_{\widetilde{r}'\widetilde{\omega}'N\psi} = \int_V \rho \widetilde{r}' \widetilde{\omega}' N\psi dv = \int_V \rho (\omega' r'^T - r'^T \omega') N\psi dv = \omega' \int_V \rho r'^T N\psi dv - \int_V \rho r'^T \omega' N\psi dv$$

For an arbitrary element,

$$\int_{\Omega_i} \rho r'^T N\psi dv$$

$$= \int_{\Omega_i} \rho \begin{bmatrix} x' \\ y' \\ z' \end{bmatrix}^T \begin{bmatrix} \psi_{u1} & \psi_{u2} & \cdots & \psi_{uNm} \\ \psi_{v1} & \psi_{v2} & \cdots & \psi_{vNm} \\ \psi_{w1} & \psi_{w2} & \cdots & \psi_{vNm} \end{bmatrix} dv = \begin{bmatrix} I_{xu}^{1i} + I_{yv}^{1i} + I_{zw}^{1i} & \cdots & I_{xu}^{Nmi} + I_{yv}^{Nmi} + I_{zw}^{Nmi} \end{bmatrix}$$

$$r'^T \omega' \psi_N(k)$$

$$= \begin{bmatrix} x' \\ y' \\ z' \end{bmatrix}^T \begin{bmatrix} \omega'_x \\ \omega'_y \\ \omega'_z \end{bmatrix} \begin{bmatrix} \psi_{uk} \\ \psi_{vk} \\ \psi_{wk} \end{bmatrix} = \left(\omega'_x x' + \omega'_y y' + \omega'_z z' \right) \begin{bmatrix} \psi_{uk} \\ \psi_{vk} \\ \psi_{wk} \end{bmatrix} = \omega'_x \begin{bmatrix} x' \psi_{uk} \\ x' \psi_{vk} \\ x' \psi_{wk} \end{bmatrix} + \omega'_y \begin{bmatrix} y' \psi_{uk} \\ y' \psi_{vk} \\ y' \psi_{wk} \end{bmatrix} + \omega'_z \begin{bmatrix} z' \psi_{uk} \\ z' \psi_{vk} \\ z' \psi_{wk} \end{bmatrix}$$

$$\int_{\Omega_i} \rho r'^T \omega' N \psi_{ik} dv = \omega'_x \begin{bmatrix} I^i_{xu} \\ I^i_{xv} \\ I^i_{xw} \end{bmatrix} + \omega'_y \begin{bmatrix} I^i_{yu} \\ I^i_{yv} \\ I^i_{yw} \end{bmatrix} + \omega'_z \begin{bmatrix} I^i_{zu} \\ I^i_{zv} \\ I^i_{zw} \end{bmatrix}$$

$$I_{\tilde{r}\tilde{\omega}'N\psi} = \omega' I_{r'^T N\psi} - \omega'_x I_{r'^T N\psi x} - \omega'_y I_{r'^T N\psi y} - \omega'_z I_{r'^T N\psi z}$$

where $I_{r'^T N\psi}(:,k) = \sum_{i=1}^{NE} I^i_{xu} + I^i_{yv} + I^i_{zw}$, $I_{r'^T N\psi x}(:,k) = \sum_{i=1}^{NE} \begin{bmatrix} I^i_{xu} \\ I^i_{xv} \\ I^i_{xw} \end{bmatrix}$, $I_{r'^T N\psi y}(:,k) = \sum_{i=1}^{NE} \begin{bmatrix} I^i_{yu} \\ I^i_{yv} \\ I^i_{yw} \end{bmatrix}$,

$$I_{r'^T N\psi z}(:,k) = \sum_{i=1}^{NE} \begin{bmatrix} I^i_{zu} \\ I^i_{zv} \\ I^i_{zw} \end{bmatrix}$$

4.4) $I_{\tilde{r}'N\psi} = \int_V \rho \tilde{r}' N \psi dv$

$$\tilde{r}' \psi_N(k) = \begin{bmatrix} 0 & -z' & y' \\ z' & 0 & -x' \\ -y' & x' & 0 \end{bmatrix} \begin{bmatrix} \psi_u \\ \psi_v \\ \psi_w \end{bmatrix} = \begin{bmatrix} -z' \psi_v + y' \psi_w \\ z' \psi_u - x' \psi_w \\ -y' \psi_u + x' \psi_v \end{bmatrix}$$

$$I_{\tilde{r}'N\psi}(:,k) = \sum_{i=1}^{NE} \begin{bmatrix} -I^i_{zv} + I^i_{yw} \\ I^i_{zu} - I^i_{xw} \\ -I^i_{yu} + I^i_{xv} \end{bmatrix}$$

5. $I_{\tilde{e}\tilde{e}} = \int_V \rho \tilde{e}\tilde{e} dv$

$$\tilde{e}\tilde{e} = \begin{bmatrix} 0 & -w & v \\ w & 0 & -u \\ -v & u & 0 \end{bmatrix} \begin{bmatrix} 0 & -w & v \\ w & 0 & -u \\ -v & u & 0 \end{bmatrix} = \begin{bmatrix} -(v^2 + w^2) & vu & wu \\ uv & -(u^2 + w^2) & wv \\ uw & vw & -(u^2 + v^2) \end{bmatrix}$$

Let $u = \sum_{k=1}^{Nm} \psi^k_u a_k = \psi^T_u a$, $v = \sum_{k=1}^{Nm} \psi^k_v a_k = \psi^T_v a$ and $w = \sum_{k=1}^{Nm} \psi^k_w a_k = \psi^T_w a$ where Nm is the

number of mode shapes used to approximate the displacement field, ψ_u^k, ψ_v^k and ψ_w^k are

the x, y and z components of the kth eigenfunction. $a_k(t)$ is the corresponding modal

coordinate. One then has $uv = \left(\psi_u^T a\right)^T \left(\psi_v^T a\right) = a^T \left(\psi_u \psi_v^T\right) a$. In doing so, one can obtain the

mass moment of inertia term, $I_{\tilde{e}\tilde{e}}$ as:

$$I_{\tilde{e}\tilde{e}} = \int_V \rho \tilde{e}\tilde{e}\,dv = \rho \int_V \begin{bmatrix} -a^T\left(\psi_v\psi_v^T + \psi_w\psi_w^T\right)a & a^T\psi_u\psi_v^T a & a^T\psi_u\psi_w^T a \\ & -a^T\left(\psi_u\psi_u^T + \psi_w\psi_w^T\right)a & a^T\psi_v\psi_w^T a \\ sym. & & -a^T\left(\psi_u\psi_u^T + \psi_v\psi_v^T\right)a \end{bmatrix}dv$$

$$= \begin{bmatrix} -a^T\int_V \rho\left(\psi_v\psi_v^T + \psi_w\psi_w^T\right)dva & a^T\int_V \rho\psi_u\psi_v^T dva & a^T\int_V \rho\psi_u\psi_w^T dva \\ & -a^T\int_V \rho\left(\psi_u\psi_u^T + \psi_w\psi_w^T\right)dva & a^T\int_V \rho\psi_v\psi_w^T dva \\ sym. & & -a^T\int_V \rho\left(\psi_u\psi_u^T + \psi_v\psi_v^T\right)dva \end{bmatrix}$$

Each term in the above equation can be calculated separately. The details are as follows:

$$I_{UU} \equiv \rho\int_\Omega \psi_u\psi_u^T dv$$

$$= \int_\Omega \begin{Bmatrix} \psi_u^1 \\ \psi_u^2 \\ \vdots \\ \psi_u^{Nm} \end{Bmatrix}\begin{pmatrix} \psi_u^1 & \psi_u^2 & \cdots & \psi_u^{Nm} \end{pmatrix}dv = \rho\int_\Omega \begin{bmatrix} \psi_u^1\psi_u^1 & \psi_u^1\psi_u^2 & \cdots & \psi_u^1\psi_u^{Nm} \\ & \psi_u^2\psi_u^2 & \cdots & \psi_u^2\psi_u^{Nm} \\ & & \ddots & \vdots \\ sym. & & & \psi_u^{Nm}\psi_u^{Nm} \end{bmatrix}dv$$

$$I_{UU}^i(m,n) = \int_{\Omega_i} \psi_u^m\psi_u^n dv = \int_{\Omega_i} \left(\xi\psi_{im}^1 + \eta\psi_{im}^4 + \varsigma\psi_{im}^7\right)\left(\xi\psi_{in}^1 + \eta\psi_{in}^4 + \varsigma\psi_{in}^7\right)dv$$

$$= \frac{tA_i}{12}\left[(\psi_{im}^1 + \psi_{im}^4 + \psi_{im}^7)(\psi_{in}^1 + \psi_{in}^4 + \psi_{in}^7) + \psi_{im}^1\psi_{in}^1 + \psi_{im}^4\psi_{in}^4 + \psi_{im}^7\psi_{in}^7\right]$$

$$I_{UV} \equiv \rho\int_\Omega \psi_u\psi_v^T dvdv$$

$$= \int_\Omega \begin{Bmatrix} \psi_u^1 \\ \psi_u^2 \\ \vdots \\ \psi_u^{Nm} \end{Bmatrix}\begin{pmatrix} \psi_v^1 & \psi_v^2 & \cdots & \psi_v^{Nm} \end{pmatrix}dv = \rho\int_\Omega \begin{bmatrix} \psi_u^1\psi_v^1 & \psi_u^1\psi_v^2 & \cdots & \psi_u^1\psi_v^{Nm} \\ & \psi_u^2\psi_v^2 & \cdots & \psi_u^2\psi_v^{Nm} \\ & & \ddots & \vdots \\ sym. & & & \psi_u^{Nm}\psi_v^{Nm} \end{bmatrix}$$

$$I_{UV}^i(m,n) = \int_{\Omega_i} \psi_u^m\psi_v^n dv = \int_{\Omega_i} \left(\xi\psi_{im}^1 + \eta\psi_{im}^4 + \varsigma\psi_{im}^7\right)\left(\xi\psi_{in}^2 + \eta\psi_{in}^5 + \varsigma\psi_{in}^8\right)dv$$

$$= \frac{tA_i}{12}\left[(\psi_{im}^1 + \psi_{im}^4 + \psi_{im}^7)(\psi_{in}^2 + \psi_{in}^5 + \psi_{in}^8) + \psi_{im}^1\psi_{in}^2 + \psi_{im}^4\psi_{in}^5 + \psi_{im}^7\psi_{in}^8\right]$$

$$I_{UW} \equiv \rho\int_\Omega \psi_u\psi_w^T dv$$

$$= \int_\Omega \left\{ \begin{array}{c} \psi_u^1 \\ \psi_u^2 \\ \vdots \\ \psi_u^{Nm} \end{array} \right\} \left(\psi_w^1 \quad \psi_w^2 \quad \cdots \quad \psi_w^{Nm} \right) dv = \rho \int_\Omega \begin{bmatrix} \psi_u^1 \psi_w^1 & \psi_u^1 \psi_w^2 & \cdots & \psi_u^1 \psi_w^{Nm} \\ & \psi_u^2 \psi_w^2 & \cdots & \psi_u^2 \psi_w^{Nm} \\ & & \ddots & \vdots \\ sym. & & & \psi_u^{Nm} \psi_w^{Nm} \end{bmatrix} dv$$

$$I_{UW}^i(m,n) = \int_{\Omega_i} \psi_u^m \psi_w^n dv = \int_{\Omega_i} \left(\xi \psi_{im}^1 + \eta \psi_{im}^4 + \varsigma \psi_{im}^7 \right) \left(\xi \psi_{in}^3 + \eta \psi_{in}^6 + \varsigma \psi_{in}^9 \right) dv$$

$$= \frac{tA_i}{12} \left[(\psi_{im}^1 + \psi_{im}^4 + \psi_{im}^7)(\psi_{in}^3 + \psi_{in}^6 + \psi_{in}^9) + \psi_{im}^1 \psi_{in}^3 + \psi_{im}^4 \psi_{in}^6 + \psi_{im}^7 \psi_{in}^9 \right]$$

$$I_{VV} \equiv \rho \int_\Omega \psi_v \psi_v^T dv$$

$$= \int_\Omega \left\{ \begin{array}{c} \psi_v^1 \\ \psi_v^2 \\ \vdots \\ \psi_v^{Nm} \end{array} \right\} \left(\psi_v^1 \quad \psi_v^2 \quad \cdots \quad \psi_v^{Nm} \right) dv = \rho \int_\Omega \begin{bmatrix} \psi_v^1 \psi_v^1 & \psi_v^1 \psi_v^2 & \cdots & \psi_v^1 \psi_v^{Nm} \\ & \psi_v^2 \psi_v^2 & \cdots & \psi_v^2 \psi_v^{Nm} \\ & & \ddots & \vdots \\ sym. & & & \psi_v^{Nm} \psi_v^{Nm} \end{bmatrix} dv$$

$$I_{VV}^i(m,n) = \int_{\Omega_i} \psi_v^m \psi_v^n dv = \int_{\Omega_i} \left(\xi \psi_{im}^2 + \eta \psi_{im}^5 + \varsigma \psi_{im}^8 \right) \left(\xi \psi_{in}^2 + \eta \psi_{in}^5 + \varsigma \psi_{in}^8 \right) dv$$

$$= \frac{tA_i}{12} \left[(\psi_{im}^2 + \psi_{im}^5 + \psi_{im}^8)(\psi_{in}^2 + \psi_{in}^5 + \psi_{in}^8) + \psi_{im}^2 \psi_{in}^2 + \psi_{im}^5 \psi_{in}^5 + \psi_{im}^8 \psi_{in}^8 \right]$$

$$I_{VW} \equiv \rho \int_\Omega \psi_v \psi_w^T dv$$

$$= \int_\Omega \left\{ \begin{array}{c} \psi_v^1 \\ \psi_v^2 \\ \vdots \\ \psi_v^{Nm} \end{array} \right\} \left(\psi_w^1 \quad \psi_w^2 \quad \cdots \quad \psi_w^{Nm} \right) dv = \rho \int_\Omega \begin{bmatrix} \psi_v^1 \psi_w^1 & \psi_v^1 \psi_w^2 & \cdots & \psi_v^1 \psi_w^{Nm} \\ & \psi_v^2 \psi_w^2 & \cdots & \psi_v^2 \psi_w^{Nm} \\ & & \ddots & \vdots \\ sym. & & & \psi_v^{Nm} \psi_w^{Nm} \end{bmatrix} dv$$

$$I_{VW}^i(m,n) = \int_{\Omega_i} \psi_v^m \psi_w^n dv = \int_{\Omega_i} \left(\xi \psi_{im}^2 + \eta \psi_{im}^5 + \varsigma \psi_{im}^8 \right) \left(\xi \psi_{in}^3 + \eta \psi_{in}^6 + \varsigma \psi_{in}^9 \right) dv$$

$$= \frac{tA_i}{12} \left[(\psi_{im}^2 + \psi_{im}^5 + \psi_{im}^8)(\psi_{in}^3 + \psi_{in}^6 + \psi_{in}^9) + \psi_{im}^2 \psi_{in}^3 + \psi_{im}^5 \psi_{in}^6 + \psi_{im}^8 \psi_{in}^9 \right]$$

$$I_{WW} \equiv \rho \int_\Omega \psi_w \psi_w^T dv$$

$$= \int_\Omega \left\{ \begin{array}{c} \psi_w^1 \\ \psi_w^2 \\ \vdots \\ \psi_w^{Nm} \end{array} \right\} \left(\psi_w^1 \quad \psi_w^2 \quad \cdots \quad \psi_w^{Nm} \right) dv = \rho \int_\Omega \begin{bmatrix} \psi_w^1 \psi_w^1 & \psi_w^1 \psi_w^2 & \cdots & \psi_w^1 \psi_w^{Nm} \\ & \psi_u^2 \psi_w^2 & \cdots & \psi_w^2 \psi_w^{Nm} \\ & & \ddots & \vdots \\ sym. & & & \psi_w^{Nm} \psi_w^{Nm} \end{bmatrix} dv$$

$$I_{WW}^i(m,n) = \int_{\Omega_i} \psi_w^m \psi_w^n dv = \int_{\Omega_i} \left(\xi\psi_{im}^3 + \eta\psi_{im}^6 + \varsigma\psi_{im}^9\right)\left(\xi\psi_{in}^3 + \eta\psi_{in}^6 + \varsigma\psi_{in}^9\right)dv$$

$$= \frac{tA_i}{12}\left[(\psi_{im}^3 + \psi_{im}^6 + \psi_{im}^9)(\psi_{in}^3 + \psi_{in}^6 + \psi_{in}^9) + \psi_{im}^3\psi_{in}^3 + \psi_{im}^6\psi_{in}^6 + \psi_{im}^9\psi_{in}^9\right]$$

5.1). $I_{\tilde{e}\tilde{e}} = \int_V \rho\tilde{e}\tilde{e}\,dv$

$$\tilde{e}\tilde{e} = \begin{bmatrix} 0 & -\dot{w} & \dot{v} \\ \dot{w} & 0 & -\dot{u} \\ -\dot{v} & \dot{u} & 0 \end{bmatrix}\begin{bmatrix} 0 & -w & v \\ w & 0 & -u \\ -v & u & 0 \end{bmatrix} = \begin{bmatrix} -(\dot{v}v + \dot{w}w) & u\dot{v} & u\dot{w} \\ \dot{u}v & -(\dot{u}u + \dot{w}w) & v\dot{w} \\ \dot{u}w & \dot{v}w & -(\dot{v}v + \dot{u}u) \end{bmatrix}$$

Similarly, $I_{\tilde{e}\tilde{e}}$ can be defined as follows:

$$I_{\tilde{e}\tilde{e}} =$$

$$\rho\begin{bmatrix} -\dot{a}^T\int_\Omega\left(\psi_v\psi_v^T + \psi_w\psi_w^T\right)dv a & a^T\int_\Omega\psi_u\psi_v^T dv\dot{a} & a^T\int_\Omega\psi_u\psi_w^T dv\dot{a} \\ \dot{a}^T\int_\Omega\psi_u\psi_v^T dv a & -\dot{a}^T\int_\Omega\left(\psi_u\psi_u^T + \psi_w\psi_w^T\right)dv a & a^T\int_\Omega\psi_v\psi_w^T dv\dot{a} \\ \dot{a}^T\int_\Omega\psi_u\psi_w^T dv a & \dot{a}^T\int_\Omega\psi_v\psi_w^T dv a & -\dot{a}^T\int_\Omega\left(\psi_u\psi_u^T + \psi_v\psi_v^T\right)dv a \end{bmatrix}$$

$$= \begin{bmatrix} -\dot{a}^T\left(I_{VV} + I_{WW}\right)a & a^T I_{UV}\dot{a} & a^T I_{UW}\dot{a} \\ \dot{a}^T I_{UV}a & -\dot{a}^T\left(I_{WW} + I_{UU}\right)a & a^T I_{VW}\dot{a} \\ \dot{a}^T I_{UW}a & \dot{a}^T I_{VW}a & -\dot{a}^T\left(I_{VV} + I_{UU}\right)a \end{bmatrix}$$

5.2) $I_{\tilde{e}\tilde{\omega}'N\psi} = \int_V \rho\tilde{e}\tilde{\omega}'N\psi\,dv$

Since $\tilde{e}\tilde{\omega}' = \omega'e^T - e^T\omega'$

$$I_{\tilde{e}\tilde{\omega}'N\psi} = \int_\Omega\rho\left(\omega'e^T - e^T\omega'\right)N\psi\,dv = \int_\Omega\rho\omega'e^T N\psi\,dv - \int_\Omega\rho e^T\omega'N\psi\,dv$$

$$= \omega'\int_\Omega\rho e^T N\psi\,dv - \int_\Omega\rho e^T\omega'N\psi\,dv$$

$$\int_{\Omega_i}\rho e^T N\psi\,dv = \int_{\Omega_i}\rho e^T N\psi_{ij}\,dv = \sum_{k=1}^{Nm}a_k\int_{\Omega_i}\rho\psi_{Nk}^T\psi_{Nj}\,dv$$

$$= \sum_{k=1}^{Nm}a_k\int_{\Omega_i}\rho\left(\psi_{uk}\psi_{uj} + \psi_{vk}\psi_{vj} + \psi_{wk}\psi_{wj}\right)dv = \sum_{k=1}^{Nm}a_k\cdot\left(I_{UU} + I_{VV} + I_{WW}\right)$$

If the mode shape is normalized, then $\left(I_{UU} + I_{VV} + I_{WW}\right) = I$

$$e^T\omega' = \sum_{k=1}^{Nm}a_k\cdot\psi_N^T\omega' = \sum_{k=1}^{Nm}a_k\cdot\begin{bmatrix} \psi_{uk} \\ \psi_{vk} \\ \psi_{wk} \end{bmatrix}^T\begin{bmatrix} \omega'_x \\ \omega'_y \\ \omega'_z \end{bmatrix} = \sum_{k=1}^{Nm}a_k\cdot\left(\omega'_x\psi_{uk} + \omega'_y\psi_{vk} + \omega'_z\psi_{wk}\right)$$

$$\int_{\Omega_i} \rho e^T \omega' N \psi dv = \int_{\Omega_i} \rho e^T \omega' N \psi_{ij} dv$$

$$= \omega'_x \sum_{k=1}^{Nm} a_k \int_{\Omega_i} \psi_{uk} \begin{bmatrix} \psi_{uj} \\ \psi_{vj} \\ \psi_{wj} \end{bmatrix} dv + \omega'_y \sum_{k=1}^{Nm} a_k \int_{\Omega_i} \psi_{vk} \begin{bmatrix} \psi_{uj} \\ \psi_{vj} \\ \psi_{wj} \end{bmatrix} dv + \omega'_z \sum_{k=1}^{Nm} a_k \int_{\Omega_i} \psi_{wk} \begin{bmatrix} \psi_{uj} \\ \psi_{vj} \\ \psi_{wj} \end{bmatrix} dv$$

$$I_{e^T \omega' N \psi x}(:,j,k) = \sum_{i=1}^{NE} \begin{bmatrix} I^i_{UU} \\ I^i_{UV} \\ I^i_{UW} \end{bmatrix}, \quad I_{e^T \omega' N \psi y}(:,j,k) = \sum_{i=1}^{NE} \begin{bmatrix} I^i_{VU} \\ I^i_{VV} \\ I^i_{VW} \end{bmatrix}, \quad I_{e^T \omega' N \psi z}(:,j,k) = \sum_{i=1}^{NE} \begin{bmatrix} I^i_{WU} \\ I^i_{WV} \\ I^i_{WW} \end{bmatrix}$$

where $j,k=1, 2, .., Nm$

$$I^i_{WV} \equiv \int_{v_i} \psi_{wk} \psi_{vj} dv = \int_{v_i} \left(\xi \psi^3_{ik} + \eta \psi^6_{ik} + \varsigma \psi^9_{ik} \right)\left(\xi \psi^2_{ij} + \eta \psi^5_{ij} + \varsigma \psi^8_{ij} \right) dv$$

$$= \frac{tA_i}{12} \left[(\psi^3_{ik} + \psi^6_{ik} + \psi^9_{ik})(\psi^2_{ij} + \psi^5_{ij} + \psi^8_{ij}) + \psi^3_{ik} \psi^2_{ij} + \psi^6_{ik} \psi^5_{ij} + \psi^9_{ik} \psi^8_{ij} \right]$$

$$I^i_{WU} \equiv \int_{v_i} \psi_{wk} \psi_{uj} dv = \int_{v_i} \left(\xi \psi^3_{ik} + \eta \psi^6_{ik} + \varsigma \psi^9_{ik} \right)\left(\xi \psi^1_{ij} + \eta \psi^4_{ij} + \varsigma \psi^7_{ij} \right) dv$$

$$= \frac{tA_i}{12} \left[(\psi^3_{ik} + \psi^6_{ik} + \psi^9_{ik})(\psi^1_{ij} + \psi^4_{ij} + \psi^7_{ij}) + \psi^3_{ik} \psi^1_{ij} + \psi^6_{ik} \psi^4_{ij} + \psi^9_{ik} \psi^7_{ij} \right]$$

$$I^i_{VU} \equiv \int_{\Omega_i} \psi_{vk} \psi_{uj} dv = \int_{\Omega_i} \left(\xi \psi^2_{ik} + \eta \psi^5_{ik} + \varsigma \psi^8_{ik} \right)\left(\xi \psi^1_{ij} + \eta \psi^4_{ij} + \varsigma \psi^7_{ij} \right) dv$$

$$= \frac{tA_i}{12} \left[(\psi^2_{ik} + \psi^5_{ik} + \psi^8_{ik})(\psi^1_{ij} + \psi^4_{ij} + \psi^7_{ij}) + \psi^2_{ik} \psi^1_{ij} + \psi^5_{ik} \psi^4_{ij} + \psi^8_{ik} \psi^7_{ij} \right]$$

I^i_{UV}, I^i_{UW}, and I^i_{VW} have been defined in the term of $I_{\tilde{e}\tilde{e}}$.

$$\int_{\Omega} \rho e^T \omega' N \psi dv = \omega'_x \sum_{k=1}^{Nm} a_k I_{e^T \omega' N \psi x} + \omega'_y \sum_{k=1}^{Nm} a_k I_{e^T \omega' N \psi y} + \omega'_z \sum_{k=1}^{Nm} a_k I_{e^T \omega' N \psi z}$$

$$I_{\tilde{e}\tilde{\omega}'N\psi} = \omega' \sum_{k=1}^{Nm} a_k \cdot (I_{UU} + I_{VV} + I_{WW}) - \omega'_x \sum_{k=1}^{Nm} a_k I_{e^T \omega' N \psi x} - \omega'_y \sum_{k=1}^{Nm} a_k I_{e^T \omega' N \psi y} - \omega'_z \sum_{k=1}^{Nm} a_k I_{e^T \omega' N \psi z}$$

If the mode shape is normalized, then

$$I_{\tilde{e}\tilde{\omega}'N\psi} = \omega' a^T - \omega'_x \sum_{k=1}^{Nm} a_k I_{e^T \omega N \psi x} - \omega'_y \sum_{k=1}^{Nm} a_k I_{e^T \omega N \psi y} - \omega'_z \sum_{k=1}^{Nm} a_k I_{e^T \omega N \psi z}$$

$$5.3) I_{\psi^T N^T N \psi} = \int_V \rho \psi^T N^T N \psi dv$$

$$\psi_{ik}{}^T N^T N \psi_{im} = \begin{bmatrix} \psi_{uk} \\ \psi_{vk} \\ \psi_{wk} \end{bmatrix}^T \begin{bmatrix} \psi_{uj} \\ \psi_{vj} \\ \psi_{wj} \end{bmatrix} = \psi_{uk}\psi_{uj} + \psi_{vk}\psi_{vj} + \psi_{wk}\psi_{wj}$$

$$I_{\psi^T N^T N \psi} = (I_{UU} + I_{VV} + I_{WW})$$

If the mode shape is normalized, then $I_{\psi^T N^T N \psi} = \int_V \rho \psi^T N^T N \psi dv = I$

6. $I_{\tilde{e}N\psi} = \int_V \rho \tilde{e} N \psi dv$

$$\tilde{e} = \sum_{k=1}^{Nm} a_k \cdot \begin{bmatrix} 0 & -\psi_{wk} & \psi_{vk} \\ \psi_{wk} & 0 & -\psi_{uk} \\ -\psi_{vk} & \psi_{uk} & 0 \end{bmatrix}, \quad \psi_N \equiv N\psi = \begin{bmatrix} \psi_{u1} & \psi_{u2} & \cdots & \psi_{uNm} \\ \psi_{v1} & \psi_{v2} & \cdots & \psi_{vNm} \\ \psi_{w1} & \psi_{w2} & \cdots & \psi_{wNm} \end{bmatrix}$$

$$\int_{\Omega_i} \rho \tilde{e} \, \psi_N^j dv = \sum_{k=1}^{Nm} a_k \int_{\Omega_i} \rho \begin{bmatrix} 0 & -\psi_{wk} & \psi_{vk} \\ \psi_{wk} & 0 & -\psi_{uk} \\ -\psi_{vk} & \psi_{uk} & 0 \end{bmatrix} \begin{bmatrix} \psi_{uj} \\ \psi_{vj} \\ \psi_{vj} \end{bmatrix} dv$$

$$= \sum_{k=1}^{Nm} a_k \int_{\Omega_i} \rho \begin{bmatrix} -\psi_{wk}\psi_{vj} + \psi_{vk}\psi_{wj} \\ \psi_{wk}\psi_{uj} - \psi_{uk}\psi_{wj} \\ -\psi_{vk}\psi_{uj} + \psi_{uk}\psi_{vj} \end{bmatrix} dv = \sum_{k=1}^{Nm} a_k \begin{bmatrix} -I_{WV}^i + I_{VW}^i \\ I_{WU}^i - I_{UW}^i \\ -I_{VU}^i + I_{UV}^i \end{bmatrix}$$

I_{UV}^i, I_{UW}^i, I_{VW}^i are defined in $I_{\tilde{e}\tilde{e}}$, I_{VU}^i, I_{WU}^i, I_{WV}^i have been defined in the term of $I_{\tilde{e}\tilde{\omega}N\psi}$

$$I_{\tilde{e}N\psi}(:,j,k) = \sum_{k=1}^{Nm} a_k \cdot \sum_{i=1}^{NE} \begin{bmatrix} -I_{WV}^i + I_{VW}^i \\ I_{WU}^i - I_{UW}^i \\ -I_{VU}^i + I_{UV}^i \end{bmatrix}$$

6.1) $I_{\dot{\tilde{e}}N\psi} = \int_V \rho \dot{\tilde{e}} N \psi dv$

Similarly:

$$I_{\dot{\tilde{e}}N\psi}(:,j,k) = \int_V \rho \dot{\tilde{e}} N \psi dv = \sum_{k=1}^{Nm} \dot{a}_k \cdot \sum_{i=1}^{NE} \begin{bmatrix} -I_{WV}^i + I_{VW}^i \\ I_{WU}^i - I_{UW}^i \\ -I_{VU}^i + I_{UV}^i \end{bmatrix}$$

VITA

The author was born in 1978 in northeastern China. He graduated from Xi'an Highway University in 2002 with a Bachelor of Engineering in Vehicle Engineering. In 2005, he completed his Master's of Engineering in Vehicle Engineering at the Shanghai Jiao Tong University. The author worked in the automobile industry at Shanghai General Motor Co. Ltd for two and a half years after graduation in 2005. He was responsible for the Vehicle Interior Noise and Vibration finite element analysis and test.